Scaling of a tree: How *Picea sitchensis* development, neighborhood forest density, and forest structure influence canopy complexity in Olympic rainforests

Russell D. Kramer

A dissertation

submitted in partial fulfillment of the

requirements for the degree of

Doctor of Philosophy

University of Washington

2019

Reading Committee:

Jerry F. Franklin, Chair

Stephen C. Sillett

Patrick C. Tobin

Van R. Kane

Program Authorized to Offer Degree:

School of Environmental and Forest Sciences

University of Washington

Abstract

Scaling of a tree: How *Picea sitchensis* development, neighborhood forest density, and forest structure influence canopy complexity in Olympic rainforests

Russell D. Kramer

Chair of the Supervisory Committee:
Dr. Jerry F. Franklin
School of Environmental and Forest Sciences

Picea sitchensis is dominant tree in coastal forest ecosystems whose large appendages provide canopy habitat for epiphytes, mammals, and birds. Growth and development of *P. sitchensis* is described across three scales—tree, neighborhood, and landscape—to illustrate ways this species can accelerate old-growth structure in young forests. We climbed, cored, and three-dimensionally mapped 60 *P. sitchensis* from 14 to 495-cm diameter, 10 to 94-m tall, and 18 to 390 yr age and developed predictive equations of aboveground biomass and leaf area with > 90 % accuracy. Both *Pseudotsuga menziesii* and *Sequoia sempervirens* are radically out-grown by *P. sitchensis*, which becomes heavier (155 ± 9 Mg) than any living *P. menziesii* and almost half as heavy as any living *S. sempervirens* in < 500 yr. Measurements of 30-m plots around 36 *P. sitchensis* trees were used to quantify neighborhood-scale competition on habitat-related appendage development. Appendage diameters and crown volume decrease ~20 % per 25 % increase in neighborhood density, and dense neighborhoods retard development > 15-cm-daimeter appendages by > 100 yr relative to unencumbered trees. Compared to *P. menziesii, P. sitchensis* accumulates crown complexity twice as fast, yet lives only half as long. At landscape-scale, *P. sitchensis*-dominated valleys were contrasted with upland *P. menziesii*-dominated

forests based on LiDAR of the Hoh River watershed on the Olympic Peninsula. Valley bottom forests differ from upland forests by consisting of small patches of tall trees (11 %), dense shorter trees (19 %), and gaps (7.4 %) dispersed in a matrix of open forest with scattered large trees (63 %). In contrast, upland forests consist of larger patches of tall (13 %), dense (58 %), and open forest (27 %) with fewer gaps (2.1 %). Valley-associated disturbances increase the amount of open-canopy forest, while upland processes increase closed-canopy tall forests, dense shorter forests, and aggregation of forest patches. The largest trees (top 10 %) are twice as densely distributed in valley-bottom (0.05 tree ha^{-1}) compared to upland (0.02 tree ha^{-1}) forests. Arrangement of tall *P. sitchensis* within a matrix of more open conditions in valley-bottoms versus large blocks of tall *P. menziesii* in upland forests accounts for this major landscape-scale difference in canopy structure. The integrated management implications relevant to *P. sitchensis* are: (1) *P. sitchensis* is valuable for management to accelerate old-growth structure because of its rapid growth but should be included with longer lived species, (2) competition within 30-m strongly depresses large appendage growth so some trees should be left with ≥ 30-m growing space, and (3) forest treatments emulate a matrix of open-canopy forest with of scattered tall trees interspersed with pockets of dense tall trees to create optimal conditions for growing the largest and most complex individuals.

TABLE OF CONTENTS

LIST OF FIGURES

LIST OF TABLES

ACKNOWLEDGEMENTS

Funding for this research was generously provided by Kenneth L. Fisher through a gift to the University of Washington, by Humboldt State University, and by the Save the Redwoods League. We thank Carly Marshall, Stephen Calkins, Tristan O'Mara, Natalie Kramer, Stephanie Kramer, John Kramer, Amber Noble, Riley Plumb, Luke Semler, James Luce, John Woods, Mathew Aghai, Sean Jeronimo, Miles LeFevre, Caileigh Shoot, Nathan Berner, Heather Bjortvedt, Noah Zimmerman, Mikolaj Miazo, Jessica Jemison, Caitlin Littlefield, Hannah Stapleton, Catherine Kuhn, Rebecca Bradley, and Dan Menten for their help in the field. Allyson Carroll provided expert tree ring crossdating advice while Bob McGaughey, Bryce Bartl-Geller, Johnathan Kane, and Bill Kruse assisted with LiDAR processing and sampling. Olympic National Park, Olympic National Forest, Six Rivers National Forest, and Washington State Department of Natural resources provided permits as access to study sites. Notably, Roger Hoffman, Joel Nowak, Kimberly Roper, Dan Donato, Kathy Potter, and Pat Manley assisted in the permitting process. I thank Greg Ettl for lab space, and Van Kane and Patrick Tobin for helpful comments on this manuscript. Bob Van Pelt, Steve Sillett, and Jerry Franklin have been invaluable sounding boards as these ideas developed. Finally, I thank my family for helping me make it all happen.

INTRODUCTION

In temperate forests throughout the world the ecological importance of large trees is well established (Lindenmayer, 2016; Lindenmayer et al., 2014; Lutz et al., 2012; Sillett and Van Pelt, 2007), yet relative contributions of one of its largest species, *Picea sitchensis*, remains relatively unknown. In the Pacific Northwest, the largest species in decreasing order are *Sequoia sempervirens*, *Pseudotsuga menziesii*, and *Picea sitchensis* (hereafter *S. sempervirens*, *P. menziesii*, and *P. sitchensis*). Crown complexity in the form of large and highly-branched appendages are particularly important as substrate for epiphytes (Ellyson and Sillett, 2003) and supporting platforms for rare or endangered amphibians, mammals, and birds (Burger et al., 2010; Carey, 1996; Forsman and Swingle, 2007; Hamer and Nelson, 1995; Spickler et al., 2006). Crown structure of large *S. sempervirens* and *P. menziesii* are well-studied (e.g. Sillett, 1999; Sillett et al., 2000; Van Pelt and Sillett, 2008), while that of *P. sitchensis* is not. The distinct ecology of *P. sitchensis* as a fast growing, shade-tolerant canopy-dominant (Franklin and Dyrness, 1988) makes it a uniquely important contributor to forest-wide crown complexity. Preference for high moisture and tolerance to ocean salt spray define its distribution (Cordes, 1972). In relatively dry California and Oregon it is restricted to a narrow belt along the coast where summer fog alleviates moisture stress (Burns and Honkala, 1990) and presumably because *S. sempervirens* is excluded by ocean aerosols. In Washington and southern British Columbia *P. sitchensis* reaches up inland valleys, and in wet Northern British Columbia and Alaska it becomes the dominant overstory tree with a range up to 210 km wide (Burns and Honkala, 1990). Because of its shade tolerance and ability to germinate on decayed logs, *Picea* reproduces in shade cast by larger trees, thus is present in climax forests (Mckee et al., 1982). Thick

protective bark of other large trees never evolved in *P. sitchensis* because fire is rare or nearly non-existent (Gavin et al., 2003; Harcombe et al., 2004). Compared to *P. menziesii* and *S. sempervirens, P. sitchensis* is ill-defended against fungi (Kimmey, 1956; Kramer et al., 2018). Root and heart rots predispose *P. sitchensis* to windthrow (Hennon, 1995; Wagener and Davidson, 1954), which provide both nurse-log seedbeds for future trees and light access through canopy gaps. In productive coastal valley bottoms spruce becomes an unrivaled dominant tree routinely exceeding 85-m height and averaging > 120-cm diameter within two and a half centuries (Cordes, 1972; Fonda, 1974; Mckee et al., 1982). Therefore, valley bottom forests host the largest and most habitat-rich *P. sitchensis* trees and offer a perfect opportunity to study their development.

Valley-bottom *P. sitchensis*-forest density is highly variable, making it an ideal system to quantify effects of forest heterogeneity on crown development of large *P. sitchensis* at tree and forest scale. Such valley bottoms are shaped by past glacial and alluvial processes, creating steep-walled flat-bottomed valleys with upper terraces out of the river's reach and lower flood plains reworked by the migrating river (Latterell et al., 2006; Thackray, 2001). Due to proximity to water, *P. sitchensis* forests are highly influenced by water tables. Areas bordering mountain slopes and depressions of abandoned river channels may be flooded most of the winter and have summer soil moisture 54 % above field capacity (Cordes, 1972). Such conditions limit rooting depth to just 40–50 cm and dominant tree density to 12 trees per hectare (TPH, Cordes, 1972). Optimal conditions occur on well-drained floodplain sites and on terraces, where tree roots penetrate as deep as 75-150 cm (Cordes, 1972). In floodplains versus on terraces, dominant tree density is lower (19 vs 28 TPH), proportion of other shade tolerant species higher (5–15 % versus 10–25% basal area or volume), and *P. sitchensis* diameter larger (90 versus 120-178 cm),

respectively (Cordes, 1972; Mckee et al., 1982). Although generally canopy is more open in valley-bottom than upland forests (Fonda, 1974), patches of valley-bottom forest developing on bars excised by the moving river can have high tree density (Latterell et al., 2006; Van Pelt et al., 2006). Conditions ranging from open canopy forest to high tree density result in widely ranging tree development. Understanding repercussions of such variable density on development of the largest trees and their distribution across the landscape has strong implications for ecological forest management.

The unique ecology of *P. sitchensis* should be integrated into objectives for sustaining ecological integrity in native and non-native forests where it grows. Ecological forest management represents a wide gradient of practices with the common goal of providing continuity of ecological values through time (Franklin et al., 2018). Continuity is achieved with various levels of forest retention, so describing functional relationships between *P. sitchensis* ecology, forest structure, and individual tree development is integral for refining retention targets. Accelerating old-growth attributes in North American *P. menziesii* plantations and creating biodiverse forest in Britain and Ireland where *P. sitchensis* is heavily planted is of growing interest (Bauhus et al., 2009; Carey, 2007; Deal et al., 2014; Franklin and Johnson, 2012). Thus far most studies of retention focus on ground-level responses of micro-climate (Aubry et al., 2009), regeneration (Zhu et al., 2014), shrub growth (Alaback, 1982), ground-dwelling animals (Baker et al., 2016; Carey and Wilson, 2001), and growth response of remaining trees (Cissel et al., 1999; Looney et al., 2018; Newton and Cole, 2015; Palik et al., 2014). Recommendations for ecologically managing spruce are not specific (e.g. Deal et al., 2014) or specific targets have to be inferred from general descriptions of forest structure in old-growth settings (Fonda, 1974; Mckee et al., 1982; Van Pelt et al., 2006), assuming those

structures provide the same values for a wide suite of goals. For recommendations to benefit management more easily, they should be specific to particular responses so they can be integrated with other management objectives and site-specific anomalies.

This study explores *P. sitchensis* crown development at tree, neighborhood, and watershed scale in three chapters. Each lays groundwork for the next and builds upon the previous. Primarily I seek to understand the capacity of *P. sitchensis* to produce canopy structure relevant to arboreal habitat in valley-bottom forests where *P. sitchensis* reaches its maximum potential size. A common theme throughout, and one I attempt to bring to a cohesive whole in the conclusion, is application of my findings to forest management for accelerating habitat development in young forests. Chapter provides codified methods for quantifying all major aboveground tissue components of even the largest trees with *in situ* three-dimensional mapping. This chapter compares *P. sitchensis* development with two co-occurring canopy-dominant species (*S. sempervirens* and *P. menziesii*), and establishes maximum *P. sitchensis* size and age limits. Chapter two expands upon chapter one by integrating crown-level measurements and tree age with plots of neighborhood forest density. Here I show the relative effects of neighborhood forest density and age on the development of specific habitat-related appendages in terms of appendage type, how long they take to form, and compare these with appendage development in *P. menziesii*. Chapter three contrasts patterns of forest structure in *P. sitchensis*-dominated valley bottoms with *P. menziesii*-dominated upland forest and relates structural pattern to per-hectare provision of the largest and most complex trees. Here I highlighted are how patterns of tall dense trees within a matrix of open-canopy contribute uniquely to growing these critically important habitat trees across ~9,700 ha.

The general and specific objectives of this research are to:

(1) Describe the potential of *P. sitchensis* to provide and accelerate development of complex crown-structures in forested ecosystems.
    a. Develop equations for predicting whole-tree aboveground quantities and age
    b. Describe effects of forest density on development of complex crown structure
    c. Describe how landscape-level patterns of canopy structure contribute to provision of the largest trees.
(2) Interpret findings into guidelines for incorporating *P. sitchensis* into ecological forest management.

Two of my chapters are published as stand-alone articles in the peer-reviewed journals, while the third is in preparation for publication. All three have been copied into this dissertation with only minor edits to the section, table, figure, and appendix names and use of species names for consistency. During first reference to species in each chapter or appendix the full species name is used and then referred to using the first genus letter followed by species name during subsequent use. Because appendices F, G, and H are excel or PDFs they are not included in this document and can be found in conjunction with the published articles. Additionally, I have consolidated abstracts for the three chapters into one for the entire dissertation. Chapter one, titled: "Quantifying aboveground components of *Picea sitchensis* for allometric comparisons among tall conifers in North American rainforests" is published in Forest Ecology and Management volume 430, 2018. Chapter two, titled: "Neighborhood competition mediates crown development of Picea sitchensis in Olympic rainforests: Implications for restoration management" is also published in Forest Ecology and Management volume 441, 2019. Chapter three, tentatively titled: "Effects of disturbance and species composition on canopy structure of Olympic rainforests" is formatted for submission to Landscape Ecology by June 30th 2019. Because I

formatted each chapter for publication you will notice citation of previous published chapters in subsequent ones and repetition of background information and discussion concepts. I hope this does not distract from reading the document as a whole. And now I turn over the story to *Picea sitchensis*…

Chapter 1. TREE SCALE

Quantifying aboveground components of *Picea sitchensis* for allometric comparisons among tall conifers in North American rainforests

Kramer et al., 2018. Forest Ecology and Management. 430, 59-77.

1.1 INTRODUCTION

Accurate quantification of aboveground tree components such as leaves, bark, cambium, and wood is the basis for understanding the dynamics of forest biomass. Carbon accounting is a major goal of forest scientists and managers (Fahey et al., 2010), especially in replanted areas with rapid rates of carbon accumulation (Poorter et al., 2016) and in older forests where terrestrial carbon stores are high (Luyssaert et al., 2008). Equations predicting biomass and carbon are extrapolations with unknown accuracy unless derived from trees spanning the full range of sizes in a population, yet the maximum size of trees used to make such equations is often limited by how feasible they are to dissect. Quantifying carbon sequestration additionally requires integrating tree growth in the context of species-level differences in decay-resistance, vulnerability to fire, and consequent longevity (Franklin et al., 2002; Sillett et al., 2015ab; Sillett et al., 2018b).

Determining biomass and ages of large trees in old-growth forests is particularly challenging. While tree-level dissection is accurate and accounts for biomass separation into trunk, branches, and leaves (e.g. Bormann, 1990; Harrison et al., 2009), this method has disadvantages with increasing tree size. Branches are damaged in the falling process, destroying information about within-crown structure, and it is now socially unacceptable to kill the largest trees. Ground-based LiDAR scanning is able to produce impressive models of tree structure

(Côté et al., 2011; Hackenberg et al., 2014) but is unable to distinguish leaves, bark, sapwood, heartwood, and deadwood necessary for accurate biomass accounting at the tree-level unless combined with destructive sampling. Remotely sensed methods for scaling biomass to large areas are subsuming many ground-based techniques because of their relative affordability at large scales and high resolution (Kane et al., 2010; Lisein et al., 2013; Tanago et al., 2017; Zolkos et al., 2013). Remote methods rely on correlations between area-based metrics and ground plots (Kane et al., 2010; Lefsky et al., 1999), tree survey type data from tree segmentation (Lamb et al., 2017; Yao et al., 2011), or structural units centered on canopy dominant vegetation (Jeronimo et al., 2018). In all cases it is necessary to anchor the results of any scaling requiring accurate (as opposed to precise relative) estimates of biomass with ground-truthing to calibrate and validate such models (Goetz et al., 2009; Nelson et al., 2017).

An alternative approach to dissecting whole trees, and the one we promote in this study, is to climb and measure them directly. Crown mapping includes climbing and intensively measuring trees to create three-dimensional (3D) models of their structure. These maps along with extracted increment cores at multiple heights along the main trunk provides the empirical basis for computing tree component quantities and age. The term ‘crown mapping’ is preferred to ‘tree mapping’ even though we are mapping whole trees, because the latter is confused with mapping tree locations in ground-based plots. Although labor-intensive, crown mapping has been used to generate allometric equations for *Sequoiadendron giganteum*, *Sequoia sempervirens*, *Pseudotsuga menziesii*, and *Eucalyptus regnans* trees spanning the full size range (Sillett et al., 2015ab; Sillett et al., 2018b; Van Pelt and Sillett, 2008). Crown mapping further improves estimates of carbon by accommodating differences in wood density along trunks and between trunks and branches (Sillett et al., 2010; Wassenberg et al., 2015), and relatively

portable equipment promotes sampling across a broad geographic range. Due to advances in equipment, climbing techniques, and standard methodologies, all portions of a tree crown can be safely accessed and quantified by trained technicians (Anderson et al., 2015; Jepson, 2000, **166**).

Picea sitchensis (hereafter *P. sitchensis*) is an ideal species with which to demonstrate this methodology because it is a dominant structural element in many coastal forests (Franklin and Dyrness, 1988; Van Pelt et al., 2006) and no published allometrics yet span its full size range up to > 90 m tall and > 400 cm diameter (Chin and Sillett, 2017; Van Pelt, 2001). Native to the northwest coast of North America from Alaska to California, *P. sitchensis* grows in forest receiving over 500 to under 65 cm of annual rainfall (Burns and Honkala, 1990). A suite of traits indicate that *P. sitchensis* has evolved a "grow-fast-die-young" strategy. First, it is relatively shade tolerant, capable of reproducing in gaps under its own canopy (Taylor, 1990), and its foliar morphology is geared towards maximizing photosynthesis with increasing light. Unlike other tall conifers, individual *P. sitchensis* leaves are twice as wide and have more stomata in well-illuminated upper crowns compared to the deeply shaded lower crowns of tall trees, and mesophyll cells are uniquely organized to promote rapid gas exchange (Chin and Sillett, 2017). Second, wood defense investment is low in *P. sitchensis*, whose heartwood is pale and vulnerable to many decay fungi, including *Phaeolus schweinitzii*, *Porodaedalea pini*, and *Armillaria mellea* (Hennon, 1995; Kimmey, 1956, *personal observation*). Third, *P. sitchensis* does not produce thick bark, averaging just 3 cm thick below 10 m height on trees > 60 m tall (this study) and is consequently not resistant to fire. Growing in rainforests with long fire return intervals, its primary disturbance agents are wind (Greene et al., 1992), fungi (Hennon, 1995), and avulsion by stream channels (Van Pelt et al., 2006). The combination of efficient photosynthesis and low investments in decay and fire resistance may be why *P. sitchensis* trees

can gain 1 m^3 yr^{-1} for more than a century, and area-based annual production is among the highest of any conifer (Ford, 1982; Van Pelt et al., 2006).

Producing estimates of tree-level components for allometric equations is just one application of crown mapping. Extending the applications to a broader range of species and scientific inquiry requires a critical mass of scientists with diverse perspectives. Thus far, consistent use of this method is limited to a closely linked group of researchers (**Appendix 1.A**), partially due to lack of a detailed and comprehensive set of methods. The primary goal of this study is to present crown mapping in an easy-to-use form and demonstrate its use by creating allometric equations for *P. sitchensis*. Although crown mapping is mostly used in larger trees, it is generalizable and adaptable to any tree species (**Appendix 1.B**). We have three specific objectives: 1) to provide a user-friendly guide to our current crown mapping methodology, including a new programmatic tool for error checking and visualizing 3D data, 2) to develop allometric equations for predicting aboveground components of *P. sitchensis* based on 60 intensively measured trees spanning the full size range of the species, and 3) to validate this approach for tall forests via comparison to previously published allometrics for this species.

1.2 METHODS

1.2.1 *Overview*

Crown mapping consists of modeling all aboveground external and internal components of the tree by combining low-impact external measurements with minimal extractive sampling of branches and increment cores. The basic principal behind crown mapping is to locate positions and associated diameters of tree components in 3D Cartesian coordinate space, calculate or predict the volumes and surface areas of these components, and then to sum them for each tree. Like trees themselves, these methods are modular and can be used selectively depending on

research objectives once the overarching concepts are clear (**Figure 1.1**). For the remainder of this study, we refer to the tree components of heartwood, sapwood, bark, cambium, and leaves collectively as **tissues** and to their separation into component portions as **tissue components** recognizing that plant anatomists may define them differently (Esau, 1965). This terminology allows us to compartmentalize the tree hierarchically into **components** such as trunks and appendages and their breakdown into tissues. We first present generalized methods and then specific methods for *P. sitchensis.*

Crown mapping relies on the repeating nature of genetically programmed tree architecture (Tomlinson, 1983). It quantifies trees in terms of main trunks and segmented appendages treated one way, while branches with a simple architecture are treated another way (**Figure 1.2**, **Table 1.1**). Trunks and segments are modeled as conic frusta whose volumes and surface areas are calculated directly. In contrast, branches are tabulated with their location, diameter, and orientation, which are then used to predict separation into tissue components using allometric equations developed by dissecting a sample of branches. Obtaining tree-level tissue masses and leaf quantities requires additional subsampling of trunks and appendages with increment cores and branch dissection to measure their density (kg m^{-3}) and specific leaf area and number (m^2 kg^{-1}, # kg^{-1}). From these data, we can create tissue-level scalars and height-dependent equations (e.g. wood density, leaf area) to apply to each tree component.

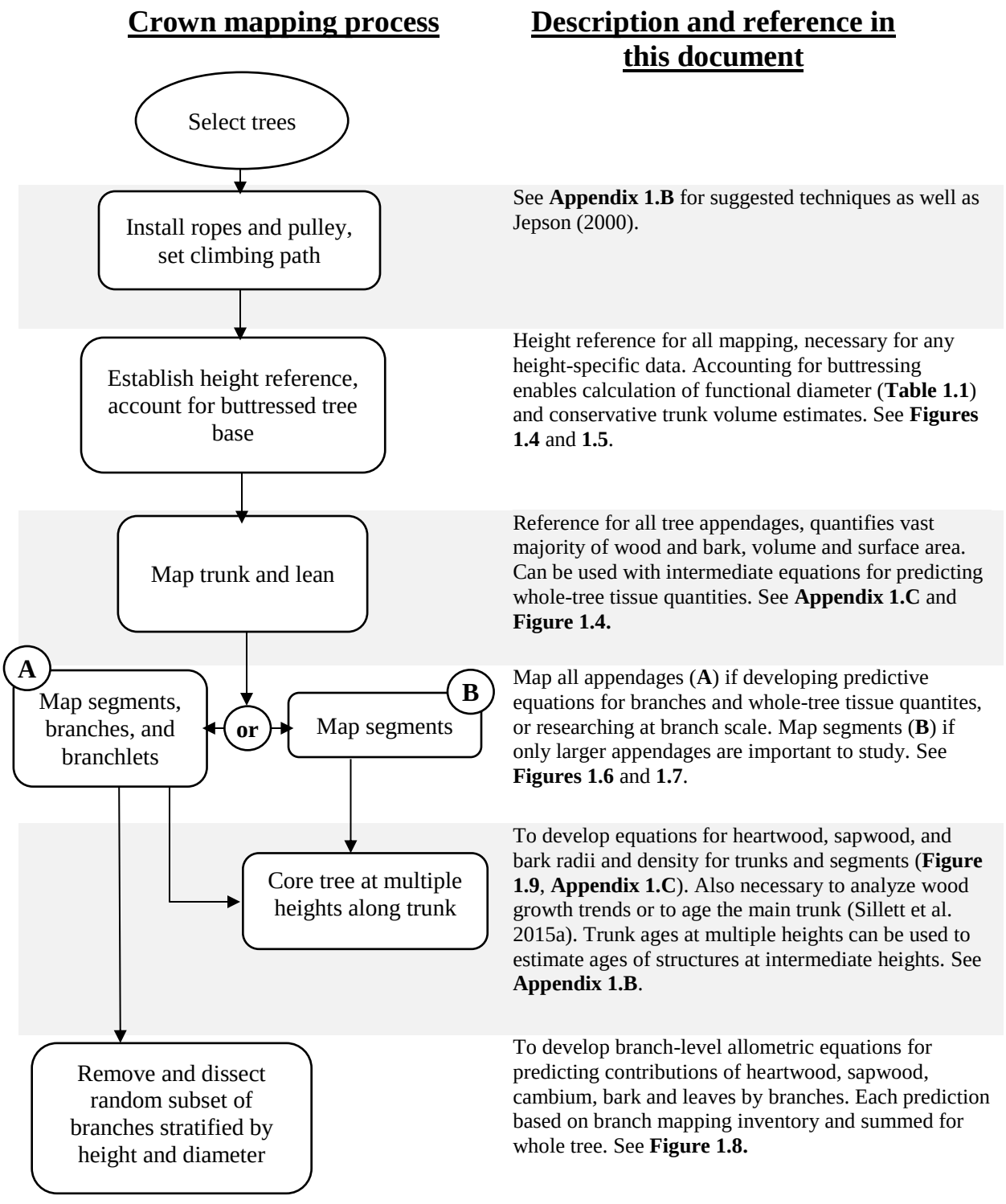

Figure 1.1. Crown mapping is a modular process. Researchers can select aspects of crown mapping (**left**) depending on desired objectives (**right**). References to supporting materials and figures are in **bold**. Data templates are provided on GitHub at (https://gihub.com/northcoastmountainrat/Sitchensis).

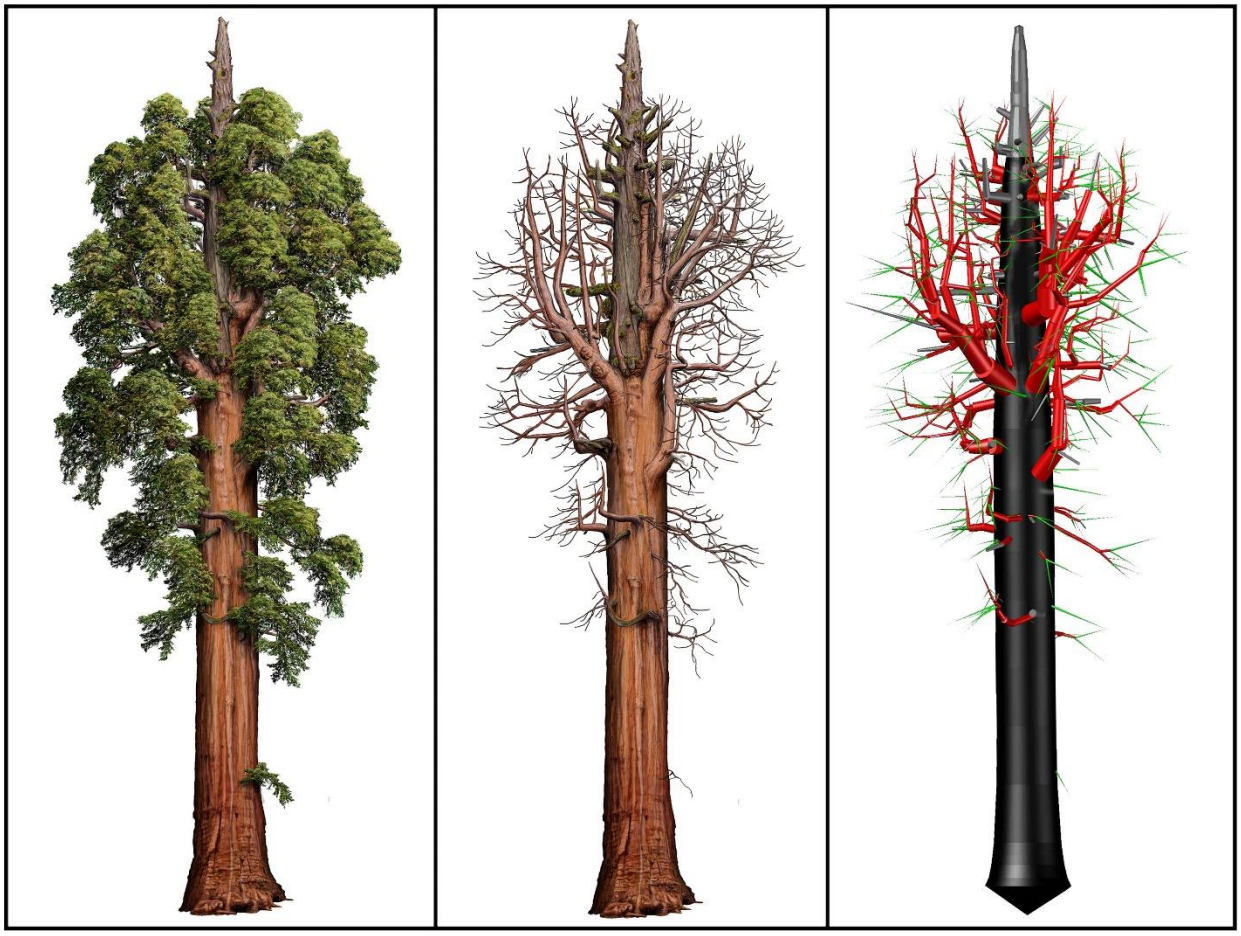

Figure 1.2. Crown mapping data represent the underlying sizes and location of the tree trunk and appendages. It is helpful to visualize a tree (**left**) stripped of leaves (**middle**) and then partitioned into different appendage types (**right**). This tree is the second largest *S. giganteum* (tree 32 in Sillett et al, 2015b) showing its underlying structure, and mapping of simple conic shapes to represent the main trunk (black), segments (red frusta), branches (green cones), and dead tree portions (gray). Illustration by Robert Van Pelt.

To determine the location of tree structures it is easier to collect cylindrical or polar coordinates and convert to Cartesian with the help of the program *SITCHENSIS* (see below, **Figure 1.3**). Partitioning the tree into components, mapping their locations, and summing them at the tree-level is conceptually simple, but its implementation is not. There are many specific terms and measurements (**Table 1.2**) attributed to tree components, making it potentially confusing. Data templates are available in the GitHub distribution of *SITCHENSIS* (see *Error*

checking and 3D geometry) to aid data collection and input. The following sections describe the most efficient approach to mapping each tree component.

Table 1.1. Common terms and definitions used in this study. In angiosperms, the distinction between trunk, limb, and branch segments applies less reliably.

Term	Definition
Frustum	Shape of a cone with the top cut off parallel to the base, thus having different top and base diameters
Diameter wrap	Location where a diameter measurement is taken or the physical process of measuring a diameter with a tape
Model conforming	Repeated species-specific growth pattern that applies to tree-crown or branch form (Halle et al., 1978; Tomlinson, 1983)
Main trunk	Central trunk from the ground up to the treetop. In spreading trees or those with multiple tops the main trunk is the central-most trunk up to the height it forks and is no longer central.
Trunk section	Frustum of main trunk between two diameter measurements and the length between them
Branches	Repeated unit tree uses to array foliage with no sign of substantial departure from model-conforming development (e.g. severe kinks or breaks), minimum size determined subjectively on a per species-basis
Branchlets	Repeated unit similar to branches but below a species-specific diameter threshold
Segment	Portions of tree appendages defined by abrupt changes in diameter or direction indicating an event causing a departure from model-conforming branch or trunk development
Trunk segment	In conifers these are appendage segments with an angle greater than 45° above horizontal. Trunk segments are not sections of the main trunk but separate near-vertical appendages.
Limb segment	In conifers these are segments with an angle of less than 45° above horizontal between the main trunk and a subsequent trunk segment.
Branch segment	In conifers these are segments with an angle less than 45° above horizontal that do not give rise to a trunk segment.
Node	Locations of the base and top of segments, nodes are shared between sequential segments (**Figure 1.6**).
Coordinate system	System for mapping locations of tree components relative to the tree origin using coordinates, either Cartesian, Cylindrical, or Polar (**Figure 1.3**)
Reference	Named location with surveyed coordinates to which locations of tree components are measured
Tree origin	Center of the trunk (pith) at average ground level around the tree
Foliar unit	Visually distinguishable units of wood and foliage representative of a model-conforming branch of a given diameter
DTB	Diameter at the top of buttress, measured at the height where trunk cross-section becomes mostly round
f-DBH	Function diameter at breast height: cross sectional area at breast height converted to the diameter of a circle with equivalent area
Foliage centroid	Perceived volumetric center of a branch's foliage

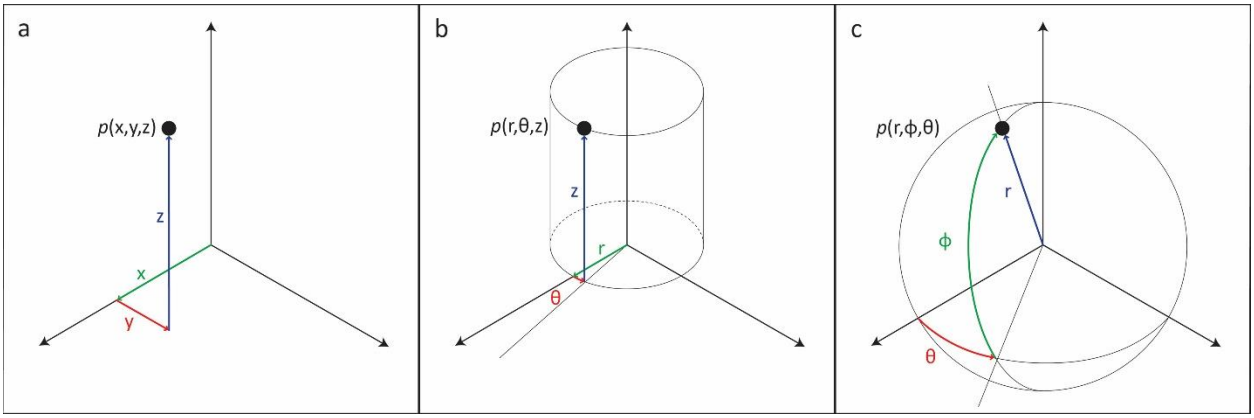

Figure 1.3. Cartesian coordinates use known distances along three orthogonal axes (**a**), cylindrical coordinates use a distance, angle, and height (**b**), and polar coordinates use a distance and two angles (**c**) to location points in space. Crown mapping uses all threes systems, which are converted to Cartesian for rectifying 3D geometry.

1.2.2 *Main trunk measurements*

The basis for all crown mapping is the center, or pith, of the tree at ground level and is henceforth called the **origin**. The origin has the Cartesian coordinates of (0,0,0), and the main trunk is mapped as a collection of vertically stacked conic frusta above it. Conic frusta of the main trunk are called trunk **sections**. The position of all subsequent segments and branches are referenced to the trunk or to other positions in the tree that have been referenced to the main trunk, so it is imperative to correctly measure the trunk's shape and lean.

The first step is to establish a height reference in the tree relative to average ground level. Start by wrapping a level diameter tape measure (tape) around the tree above any extreme buttressing. Next, measure the height of this tape wrap above the highest and lowest points of the surrounding ground just outside of debris piled against the tree base and record the average as the height of the tape wrap. Ascend to the treetop and lower a fiberglass tape measure (**Appendix 1.C**), fixing it in place when average ground level on the vertical tape is matched to the tape wrap (**Figure 1.4**). Use two-way radios in tall trees so a person on the ground can communicate

this to the climber. These steps vertically align the zero mark on the vertical tape with the origin. If the vertical tape on a leaning tree is far from the tree base, stand at the tape and sight though a clinometer adjusting your vertical position until the zero-degree mark in the clinometer aligns with the tape wrap on the main trunk and then align the vertical tape accordingly. If the tree will be remapped in the future, tag it at a specific height so the tape can easily be reset in the same position. On larger trees, it is worthwhile to set one or more additional tapes aligned to the original to reduce the time it takes to make height measurements from various positions in the tree.

Table 1.2. Description of measurements made during crown mapping.

Data collected	Units	Description
Name	-	Unique name for tree component
Type	-	Categorical for segments: branch, limb, or trunk
Origin	-	For branches: M if from main trunk, node name if from segment end, or segment name if from between nodes
Epicormic/Original	-	Categorical for segments or branches as defined by Ishii and Wilson (2001)
Live/Dead	-	Categorical for branches
Height	m	Height of measurement above ground
Diameter	cm	Circumference/π, past the collar on branches, seek the waist on trunks and segments
Distance	m	Distance to a tree location from a surveyed reference
Azimuth	degrees	Angle to a location from a reference with respect to North
Reference	-	Surveyed point as a reference for distance and azimuth measurements
Slope	degrees	Slope from branch base to center of foliage volume, or if dead to branch tip
% dead	-	Visual estimate of percent dead for main trunk and segments
Branchlet counts	integer	Size class count of branchlets for main trunk sections or on segments
Path length	m	Length along branch stem out to a predetermined diameter cutoff
Bark thickness	mm	Distance from cambium diameter wrap, may include air space (**Figure 1.9**)
Sapwood thickness	cm	Distance from heartwood boundary to cambium
Wet wood length	cm	Length of tree core excluding bark for scaling dry-measured ring widths to wet
Notes	-	Treetop, tag height, height of buttressing, past breaks, forking for branches, anomalies, special habitat

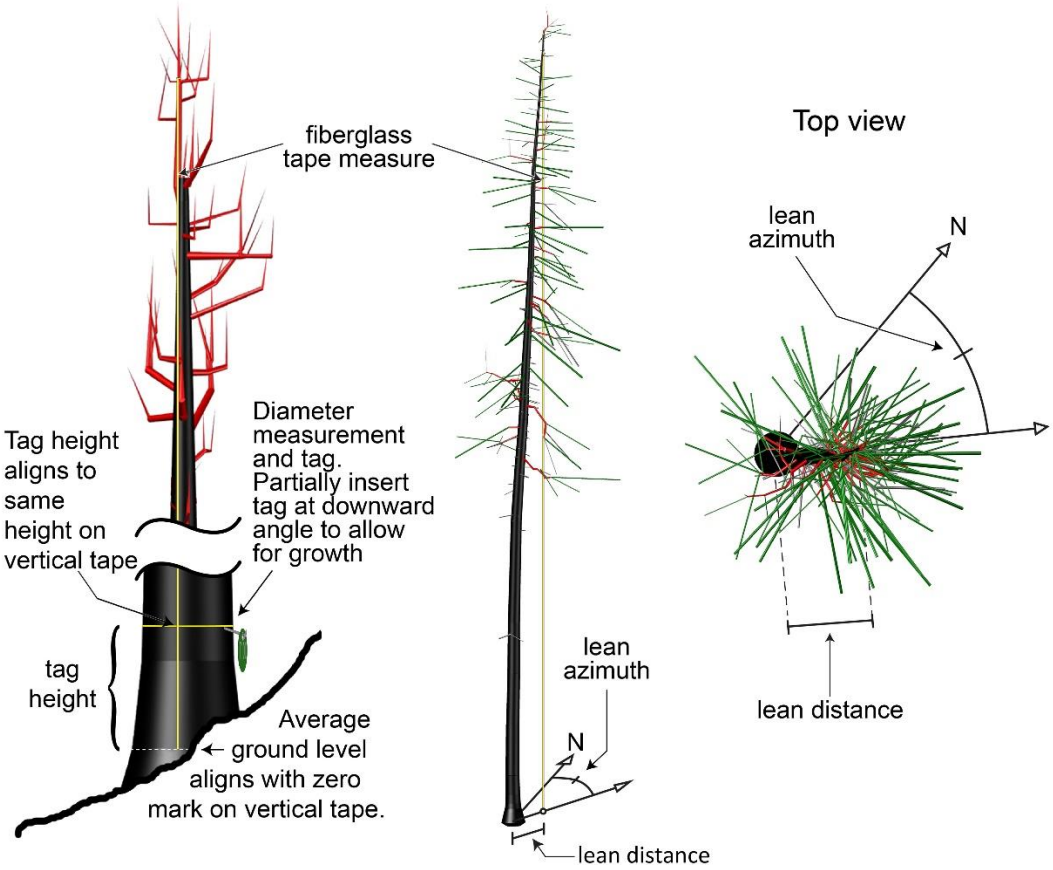

Figure 1.4. Basics of crown mapping. Left side shows vertical tape set to average ground level. Center demonstrates mapping lean using a vertical tape as a reference. Right shows lean angle and distance on ground.

Once the vertical tape(s) are in place, proceed to measure the trunk diameter at regular intervals no greater than 5 m apart. Always measure diameters at the narrowest point possible—the waist—if there are trunk irregularities. Measure diameter more frequently near the base and top of the tree and other places where the trunk shape changes rapidly. For leaning trunks, measure an azimuth and distance from the treetop to the tree origin. Walk around the tree until it leans directly toward the viewer and has no apparent lean. Note the tree lean azimuth, and then walk 90 degrees around the tree to where the lean is most pronounced. Stand away from the tree and use a compass to align with the treetop. The distance from the point on the ground directly beneath the treetop and the origin is the tree lean distance (**Figure 1.4**). Record the tree lean

azimuth and distance in association with highest measurement of the trunk. These measurements will be used by *SITCHENSIS* to interpolate the x, y position of the trunk for all other trunk sections between the treetop and the ground.

Moderate tree leans, kinks or bows, and the leans of multiple diverging tops are best measured from within the tree in one of two ways. The first is to hang a vertical weighted line from the top of the tree insuring it does not deflect off any branches. To save time, use one of the vertical reference tapes previously affixed. Note the azimuth and distance of the weighted line to the origin. A distance and azimuth measurement to this reference at each trunk diameter measurement provides the information to calculate the x and y coordinates of the trunk's lean (**Figure 1.4**). Alternatively, place a target such as a survey reflector at a visible surveyed location from the origin and use it as a reference. Measure the azimuth and horizontal distance from this target using a compass and laser rangefinder. Enter these data on the "custom references" tab of the Excel data template for *SITCHENSIS.*

1.2.3 *Footprint*

Trunk diameter at breast height (1.37 m) is generally a good metric for predicting various aspects of a whole tree, but this relationship weakens in trees with irregular bases or highly buttressed roots (Van Pelt, 2007). A tape wrap around complex tree bases includes air voids, swellings, and irregularities, which overestimates the cross-sectional area. To correct for this, create a footprint map and extract the cross-sectional area of the tree at breast height, then calculate the diameter of a circle with equivalent area. This tree attribute is called the functional diameter at breast height (*f*-DBH) and is more useful in equations for calculating tree-level metrics such as leaf area than diameter at breast height (Sillett et al., 2015a). Three techniques

for creating footprints are described in Van Pelt et al. (2016, Appendix C therein) as well as in Dean et al. (2018). Here we give a brief overview.

A footprint map is a topographic representation of the tree base with cross-sectional contours at specific heights. Create contours by measuring trunk-face locations relative to references. Use tape wraps at specific heights, surveyed points around the tree, or common points in multiple photographs as references. In the first instance, reference diameter wraps are assumed round and locations inwards from the tape wrap to the surface of the tree are measured at known azimuths to augment the circle's shape. In the second instance, the distance and azimuth to the trunk surface at key inner and outer locations at height contours are measured from three or more surveyed locations. A final technique called photogrammetry (or *structure from motion*) uses common features from scores of overlapping photographs to create at 3D point cloud, which is the basis for a 3D mesh. Critically, the photographs *must* have >70% overlap and a scale such as a meter stick propped against the tree. The mesh is then scaled and cross-sections are extracted from it (**Figure 1.5**). The third technique is the most efficient and is preferred but difficult in cases where the trunk is obscured by vegetation.

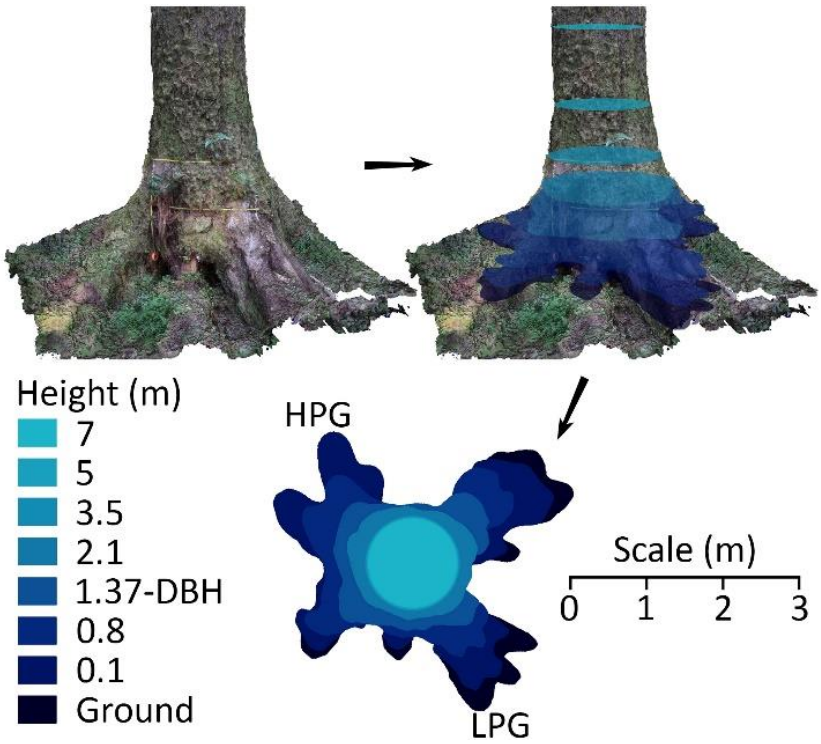

Figure 1.5. The easiest and most accurate method to map a tree footprint is to create a scaled 3D mesh with photographs (**upper-left**) from which to extract cross-sections (**upper-right**). The final footprint (**bottom**) represents an accurate topographic map of a buttressed tree base. HPG and LPG are high point of ground, and low point of ground, respectively.

1.2.4 *Segment measurements*

Segments represent tree components other than the main trunk that additionally are not model-conforming branches for a given species. Angiosperms and conifers conform to 23 architectural models that are a particular configuration of trunks and branches reflecting growth habit (Tomlinson, 1983). Angiosperms typically have dichotomous and continually forking stems that lead to terminal branches, while conifers typically consist of a monopodial trunk with radially arranged horizontal branches. Many exceptions exist, and both phyla may reiterate their typical architectural model (trunk and branch arrangement) when injured. Series of segments compose large tree appendages, reiterations, or the forked trunks proximal to branches in angiosperms. In both angiosperms and conifers, segments are defined along an appendage by

abrupt changes in direction or diameter representing past injury in the tree's life. It is also helpful to partition very large branches that are beyond the size of those dissected to create whole-branch predictive equations (see *Branch dissection*) into a system of segments giving rise to smaller branches. In conifers, segments are classified into three categories based on their orientation. Branch segments are those < 45° from horizontal. Trunk segments are those that are > 45° from horizontal and often resemble a normal trunk with branches typical of the species. Limb segments are those giving rise to trunks, are < 45° from horizontal, and are often buttressed where they attach to the tree. In angiosperms, segment types are usually not distinctly different in appearance, however for the *SITCHENSIS* calculation program it is convenient to categorize them based on their slope.

To partition a tree appendage into segments, first visualize its skeletonized version with joints representing changes in direction or diameter. Segments are the sections between joints and the joints are called **nodes** (**Figure 1.6**). Node locations are mapped using cylindrical coordinates referenced to the main trunk or to other nodes that have been referenced to the main trunk. Each node is defined by a height taken from the vertical tape, a distance and azimuth from the reference, and a diameter at each end. For short segments (<40 cm) or locations where the main trunk is obstructed from view, it is acceptable to reference nodes to other nodes instead of the main trunk, but to reduce error propagation reference to the main trunk whenever practicable.

Tree structures have diameters, thus distances must explicitly state weather they are measured from and to the face or pith of the reference or target structure. In the final 3D model, the coordinates refer to the 'pith-to-pith' distances between locations. It is useful to adopt the convention of always measuring distances between trunks and nodes from face of reference to pith of target and distances between nodes from pith of reference to pith of target. Sometimes it

is convenient to make measurements from ‘pith-to-face’ or ‘face-to-face’ between adjacent trunks. Any deviations from the convention must be noted for that segment. *SITCHENSIS* corrects distances later by adding the appropriate reference trunk or node radius at the target node height. If a reference trunk has no diameter measurement at a target height, *SITCHENSIS* calculates it by interpolating between measured trunk diameters.

Each node is named as it is mapped. Node names need not be sequential as long as they are *unique* within a tree. Conic frusta represent segments defined by their endpoint node names and diameter at each end. Like in trunks, measure diameters at natural waist locations near the segment ends to avoid buttressing. For short segments, measure only one diameter at the midpoint and model them as cylinders. Adjacent diameters of connected segments usually differ, resulting in connected segments sharing node locations but not diameters. For consistency, segment **base** measurements refer to those proximal to the trunk and **top** measurements refer to those distal to the trunk along an appendage *regardless of which is above or below the other or closer to the trunk*. Each segment is named based on its base and top nodes, thus segment names are also unique. Segments arising from the main trunk are given the base node designation ‘M.’ The result is an efficient naming convention that reveals the actual hierarchical connections between tree components (**Figure 1.6**).

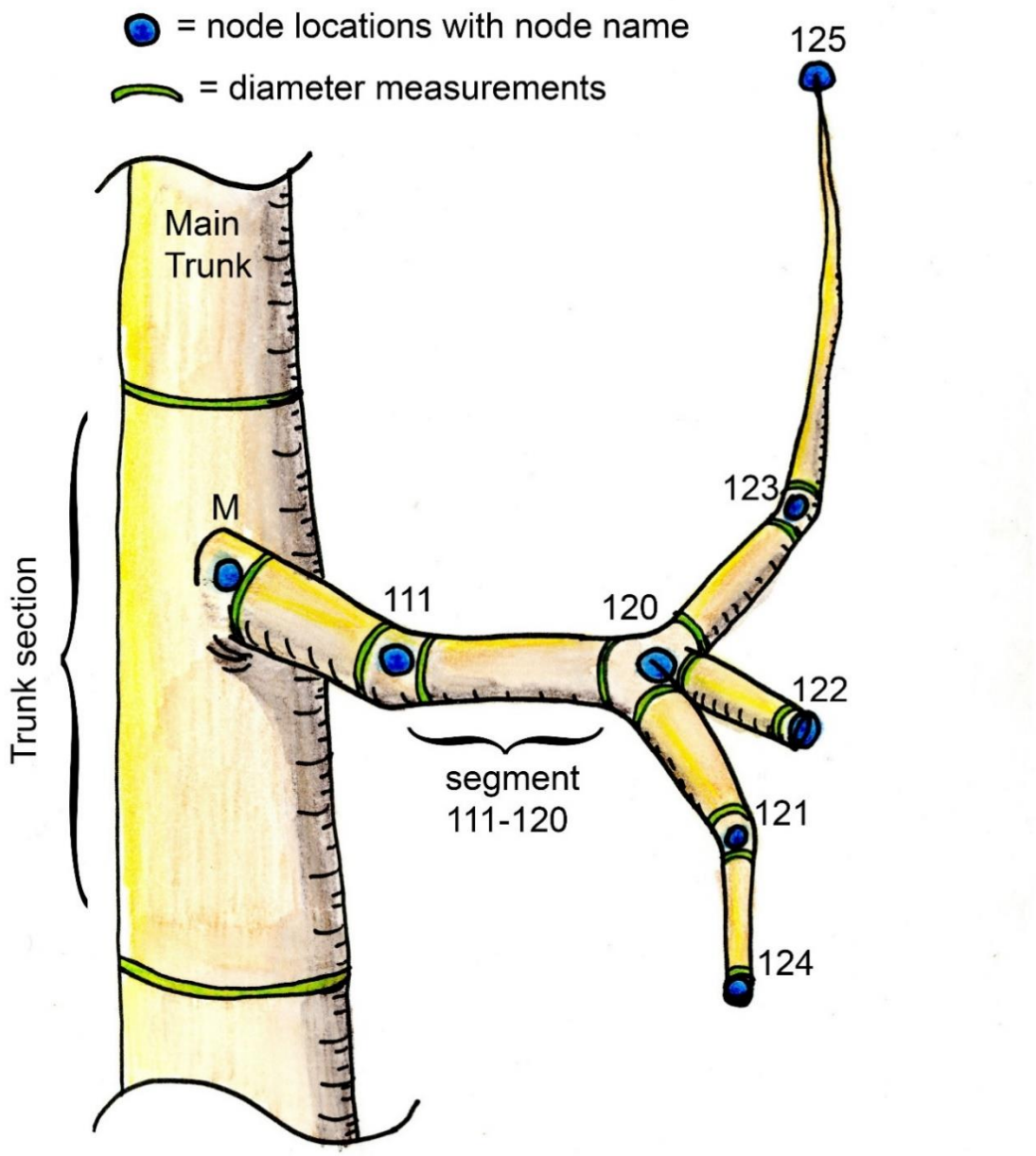

Figure 1.6. A sketch of a main trunk section with a tree appendage stripped of branches to show underlying segments. The trunk is divided into sections between diameter measurements. Nodes have unique names and are referenced to the main trunk or other nodes with cylindrical coordinates. Segments are named as connections between nodes (e.g. segment 111-120). This appendage consists of segments M-111, 111-120, 120-121, 121-124, 120-122, 120-123, and 123-125 each with unique base (proximal) and top (distal) diameters. Note that the trifurcation at node 120 is documented by having three segments arising from 120 (segments 120-121, 120-122, and 120-123).

1.2.5 *Branch measurements*

Branches are different from segments in that all foliage originates from them and they conform to a genetically determined architectural model (Tomlinson, 1983). Branch data map the dimensions, location, and number of branches on a tree and provide variables (**Table 1.2**) for predicting whole-branch tissue quantities with allometric equations. Always measure branch diameter past the branch collar to insure a conservative and repeatable measurement. Depending on the tree species, define a minimum branch diameter where anything smaller are defined as **branchlets** (**Table 1.1**). Simply tally branchlets by their trunk section or segment of origin. Branches originate from the main trunk, segment nodes, and along segments between nodes. To assign a branch location on a trunk, include the name of the trunk (main trunk or trunk-segment name) as the branch origin (**Table 1.2**) and measure the branch base height and azimuth from the center to the surface of the trunk (**Figure 1.7**). A branch arising from a node receives the node name for its origin, the node height for its height, and no origin azimuth. Those arising from the middle of segments (mid-segment branches) are a special case addressed in the next section. The branch top location is determined by recording the horizontal distance the branch extends (extension), the azimuth from reference, and slope to the perceived centroid of the foliage volume (**Table 1.2**). If the branch is dead, measure the azimuth and slope to the dead branch tip as well as the estimated tip diameter. If the branch slopes > 45° then record the vertical offset of the foliage centroid from the branch base instead of slope because very small changes in slope result in extreme changes in modeled branch length at high angles. Record the length of branch stem out to a pre-determined species-specific diameter cutoff (path length) for each branch as a predictor variable to account for extra wood in forked branches. Finally, if investigating reproduction, include a fruit or cone count on a random 5-10 % of the branches.

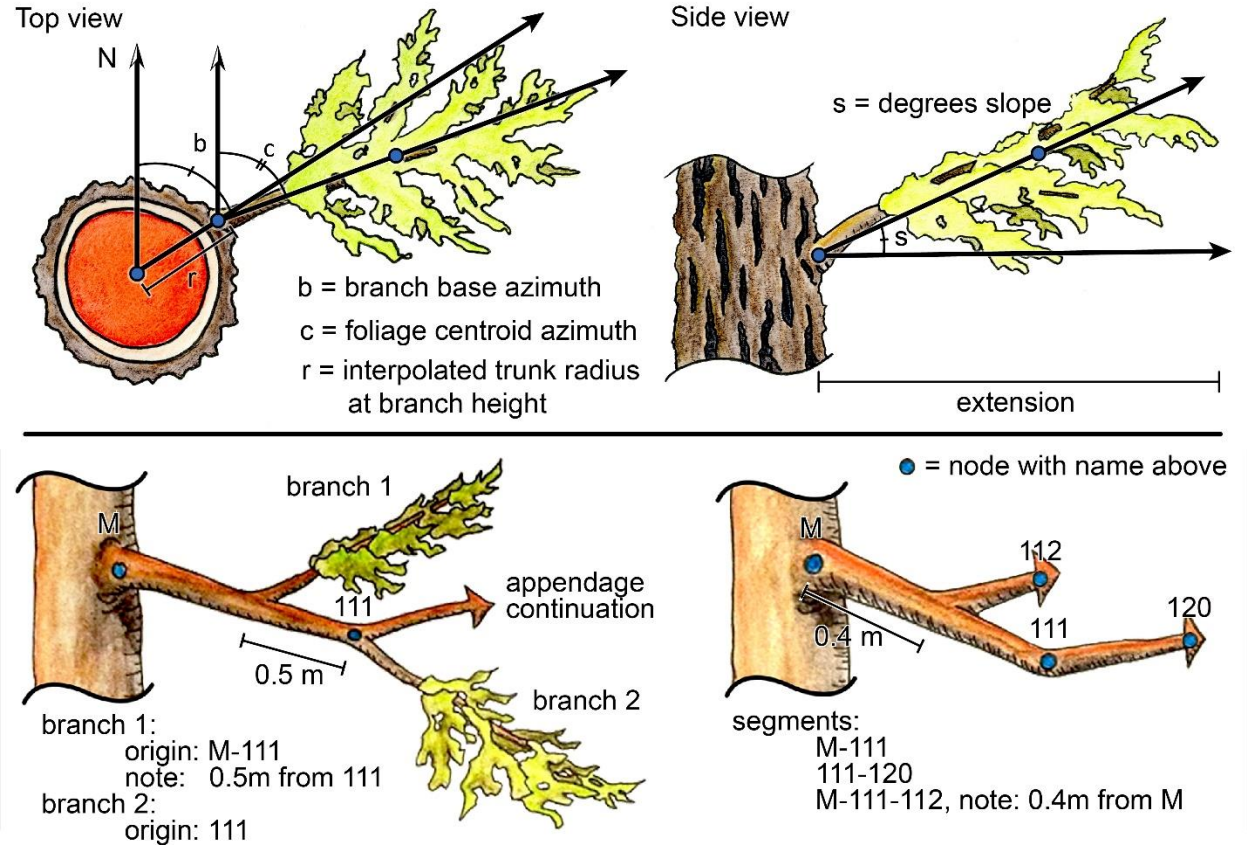

Figure 1.7. Measurements specific to branches and mid-segment appendages. Letters **b** and **r** locate branch base on the surface of its parent trunk, while **c**, **s** and **extension** locate the top of the branch relative to its base. Mid-segment segments acquire a base name of the parent segment. Branches acquire an origin name of the parent segment. The distance along parent segment to a mapped node provides *SITCHENSIS* the information to calculate the mid-segment appendage base coordinates.

Two general methods exist for calculating whole-branch tissue quantities—wood, cambium, bark, and leaves—that require slightly different data. The first uses whole-branch equations. This technique works well in species where appendages do not clearly exhibit conveniently sized foliar units (**Table 1.1**), such as *P. sitchensis*. Foliar units are visually distinguishable units of branch wood and foliage representative of a model-conforming branch of a given diameter. For these trees, it is appropriate to use allometric equations based on a subset of branch dissections to predict tissue quantities of all remaining mapped branches. To quantify

whole-branch tissues using equations, pool the branch inventory for all mapped trees and stratify them by height and diameter. Randomly select at least 40 branches across strata to insure a representative sample. Subsequently dissect, measure, dry, and weigh all branch tissues—wood, bark, and leaves—to develop branch-level equations for different tissue components using standard mapping data (**Table 1.3**) as predictor variables (see *Branch dissection*).

Table 1.3. Measurements recorded when crown mapping the main trunk, segments, or branches.

	Tree components			
Data collected	Main Trunk	Segments	Branches	Notes
Name		x	x	M for main trunk, hyphenated base and top node name for segments, sequential numerical name for branches
Type		x		Branch, limb, or trunk segment type
Origin		x	x	Same as base node name for segments for branches
Epicormic/Original			x	
Live/Dead			x	
Height	x	x	x	At section boundaries for main trunk, base and top for segments and branches
Diameter	x	x	x	Same as height, top diameter of unbroken branches is zero
Distance (extension)	x	x	x	At section boundaries for main trunk, base and top nodes for segments, and base of branches, branch top distance = extension (**Figure 1.7**).
Azimuth(s)	x	x	x	Same as distance except base of branch called origin azimuth and top called centroid azimuth
Reference	x	x	x	Origin for main trunk, main trunk at given height for segments and branch bases, branch base for branch top
Slope			x	Slope of top referenced to base of branch
% dead	x	x	x	Proportion of missing cambium and foliage, used for damaged or dying branches outside of normal variability
Branchlet counts	x	x		Captured in equations or foliar unit counts in branches (**Table 1.2**)
Path length			x	Accounts for added variability due to branch forking in some species
Bark thickness	x		x	From cores on the main trunk and cross-sections from harvested branches
Sapwood thickness	x		x	Same as above
Wet wood length	x			Measured as soon as core is extracted

The second method for quantifying branch tissues works well in species such as *P. menziesii*, *S. giganteum*, and many angiosperms where appendages are collections of obvious repeating foliar units (**Table 1.1**) of similar size. It is convenient to define a **foliar unit** of a certain diameter that can be counted to the nearest 0.1 for each branch so that most branches

have multiple foliar units while small branches have less than one. For example, in *Eucalyptus globulus* a foliar unit is equivalent to a model-conforming 5-cmdiameter branch with a foliage volume of approximately 1.5 m^3. For further clarification and application of foliar units to three different tree species, see Van Pelt and Sillett (2008), Sillett et al. (2010), and Sillett et al. (2015b). Reduce subjectivity in foliar unit counts by agreeing on a standard foliar unit size and then periodically calibrating between observers. A benefit of using foliar units is that they are usually much smaller than entire branches, which can be quite large (> 30 cm diameter) and dangerous to collect. Lastly, a subset of branches receives detailed measurements of the path length (**Table 1.2**) between 1-cm diameter increments out to the foliar unit diameter cutoff and are combined with measurements of bark and heartwood thickness at 1-cm diameter increments from either fallen or dissected branches. These more detailed data are used to predict the amount of bark, cambium, and wood in all other mapped branches. Based on experience, whole-branch regressions are superior, except in cases where foliar units are obvious and discrete.

Foliar units or branchlets (**Table 1.1**) from segments or main trunk sections are smaller than a predetermined species-specific branch diameter cutoff. These are tallied rather than individually measured to account for leaves, bark, and wood. If following the foliar unit method, estimate how many foliar units or what proportion of a foliar unit each trunk section of segment has in sum. Otherwise, tally branchlets in two or more diameter classes for each trunk section or segment. The linkage between specific tree parts and foliar unit or branchlet counts is important since leaf mass and area relationships commonly change with height (Ishii et al., 2008; Sillett et al., 2015b). During branch dissections, a set of foliar units or branchlets are removed in sufficient quantities to compute multipliers of key tissue components using the same method as for branch dissections (see *Branch dissection*).

1.2.6 *Mid-segment measurements*

Segmenting appendages at nodes cannot accurately model them in two distinct cases. In the first case, a segment spans a long distance and curves or tapers substantially between nodes. For these, record supplemental measurements of height, distance, azimuth, and a reference one or more places along the segment. Supplemental measurements are added to the segment data later, before entering into *SITCHENSIS*. The second case is when there is another smaller segment or branch arising between segment nodes without disrupting its natural diameter taper. These are mid-segment segments or branches. The only difference in data collection is the base name and location of these segments, or the name of mid-segment branch origins. For example, if a mid-segment segment arises from M-111 and terminates at node 112, it is named M-111-112, and a similar mid-segment branch receives the origin of M-111. The only information to collect for the base is the distance along M-111 from either M or 111, and *SITCHENSIS* will calculate the base x, y, and z coordinates by interpolating between M and 111 (**Figure 1.7**).

1.2.7 *Branch dissection*

Dissecting a random subsample of branches, foliar units, and branchlets allows quantification of tissue components. From these data, we create whole-branch equations for all other mapped branches and multipliers for foliar units and branchlets (see *Size calculations*). Branch-level equations and multipliers for *S. sempervirens, S. giganteum, E. regnans, P. menziesii,* and *P. sitchensis* already exist (Sillett et al., 2015b, 2010, Sillett et al., 2018b, **Appendix 1.D**), but it is necessary to create new equations for other species.

Remove selected branches from the tree with a hand saw by cutting just beyond the branch collar and insure no loss of material (**Appendix 1.C**). Once on the ground, cut the branch stems at 1-cm diameter intervals and sort into piles for each size class. Average paired

measurements of bark thickness (hereafter bark radius) and heartwood diameter for a subset of cut ends from each size class. Calculate sapwood as the remainder so that the sum of heartwood, sapwood, and bark radii equal the total radius (i.e., half the diameter). Next, model each size class as a continuous conic frustum with a length equal to the total length of all its pieces and girth represented by its end diameters. For example, if a 5.6 cm diameter branch is dissected the largest size class is modeled as a conic frustum with a large diameter of 5.6 and a small diameter of 5.0 cm. The next smallest size class has a large diameter of 5.0 and a small diameter of 4.0 cm. Bark and sapwood are modeled as successive shells around a frustum of heartwood.

To convert branch-stem tissue volumes to masses, carefully measure the fresh dimensions of a subset of cross-sections from each size-class pile. Dissect cross-sections into bark and wood tissue components while fresh (much easier than when dry) then dry these at 101° C until mass stabilizes. Weigh each dissected tissue to calculate dry-mass-to-fresh-volume density (**Figure 1.8)**. Use these data to create density equations based on stem diameter and height and predict each size-class density using the geometric mean of size class end diameters.

In many species, the smallest twigs are the attachment point for all leaves and are often green and photosynthetic, such as in *E. regnans* and *Sequoia*. Separate green from brown woody twigs and cut at 1-cm-diameter increment locations if they are larger than whole centimeters. This results in stems either less or greater than 1 cm. The brown end of the green-brown transition becomes the small-end diameter of the smallest brown-barked twigs. Quantify green stems > 1-cm-diameter the same way as brown-barked stems. Estimate green twig components < 1-cm diameter with mass scalars. Weigh all of each twig class and a subset while fresh, then dissect, dry, and weight the subset to obtain tissue quantities—areas, volumes, masses—of wood, cambium, and bark for a given unit of dry mass. To calculate leaf area and number, pluck leaves

from another subset of the twigs, scan on a flatbed scanner, then analyze with ImageJ (Abràmoff et al., 2004) for count and silhouette area. Dry and weigh the leaves and use these numbers to calculate specific leaf area and count (m^2 kg^{-1} and # kg^{-1}). Finally, scale tissue values of subsets to the fresh mass of the whole branch.

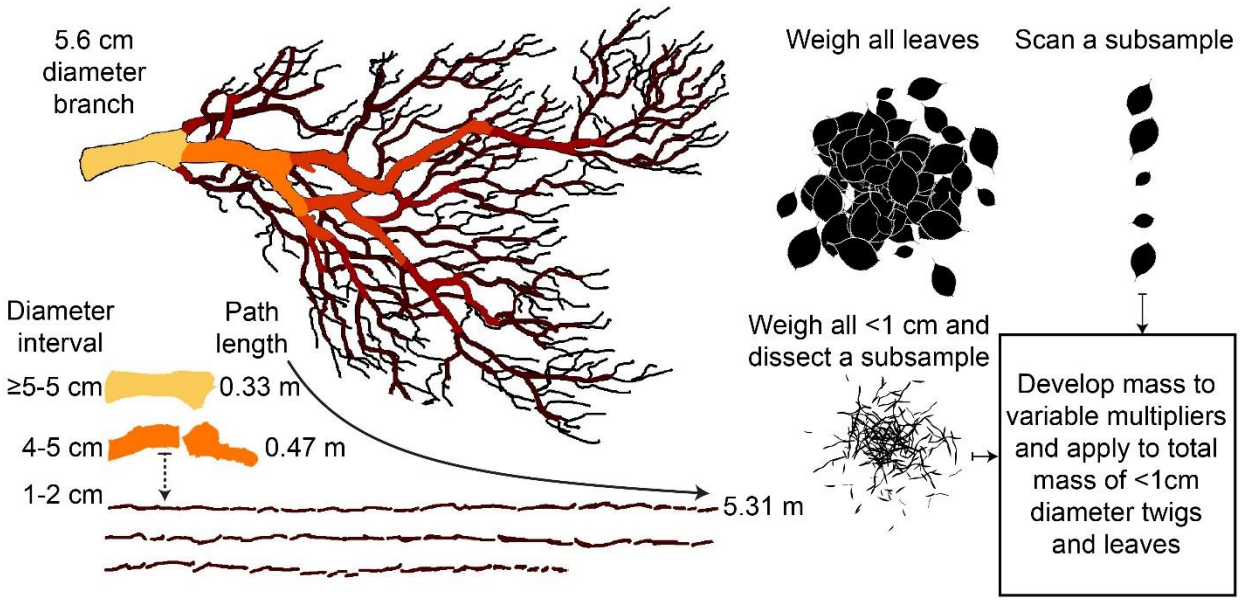

Figure 1.8. Branches are dissected to quantify whole-branch tissues. Stems are excised at 1-cm diameter intervals and the path length of each size class is measured. The volume of each stem size class is calculated as conic frusta with base and top diameter equal to largest and smallest diameter for each size class. Bark and heartwood for each end are acquired via paired measurements of a sample from each diameter interval. Leaves and small twigs are calculated via mass multipliers from subsamples. Figure adapted from drawing by Robert Van Pelt.

1.2.8 *Coring and bark measurements*

Increment cores are mandatory to quantify tissue components of the tree trunks hidden from view, obtain wood density for converting wood volumes to masses, and to quantify growth increments. Extract cores at multiple heights along the trunk to account for taper in bark and sapwood thickness and changing wood density with height. Cores at multiple heights also enable estimates of tree age from cores too short to reach the trunk pith. Sillett et al. (2015b, 2018b) and

Appendix 1.E provide detailed descriptions of aging large trees using cores from multiple heights. At each core height, measure the trunk diameter with a tape wrap to link internal data with external predictors. It is best to take cores at the same heights (preferably every 10 m) for all mapped trees. See **Appendix 1.C** for more details about coring at multiple heights.

Immediately after core extraction, measure the fresh sapwood thickness, full fresh core wood length. It is sometimes preferable to wait for heartwood compounds to oxidize to make the distinction between sapwood and heartwood more distinct. In some species, (e.g., *E. regnans*) it is necessary to apply a stain such as Methyl Orange to delineate this boundary (Sillett et al., 2010). Measure the sapwood and core length again when dry in the lab to account for ring width shrinkage if you intend to do any wood volume growth analyses. Take additional short cores from multiple heights containing portions of both sapwood and heartwood to obtain wood density data for these tissues. Separate the core into pure sapwood and heartwood portions avoiding the transition zone of heartwood deposition and immediately seal them in labeled airtight tubes. Determine the fresh volume by Archimedes principal then oven-dry them at 101°C and weigh to obtain the fresh-volume-to-dry-mass density. Process cores further in the lab using standard dendrochronology techniques to obtain ring-width series for growth and age analyses (**Appendix 1.E**).

Total trunk diameter is measured with a tape wrap including declivities in the bark, which can bias bark mass computations. Measure bark radius by inserting the core extraction spoon into the hole at a slight angle, sliding it along one surface until the sapwood-bark boundary is clearly felt, and then mark the spoon where it crosses the tape wrap. Bark radius is the length from the tip of the spoon to the mark (**Figure 1.9**). This technique results in a bark radius that includes air, thus to convert bark volume to true bark mass the volume of bark samples dried and weighed in

the lab must be based on the fresh sample outer dimensions. Some species such as *S. giganteum* have deeply furrowed bark > 30 cm thick (Sillett et al., 2015b). In these cases, it is essential to collect, measure, and weigh bark samples from a wide range of trunk diameters to account for bark mass. Whenever possible do this from freshly fallen trees.

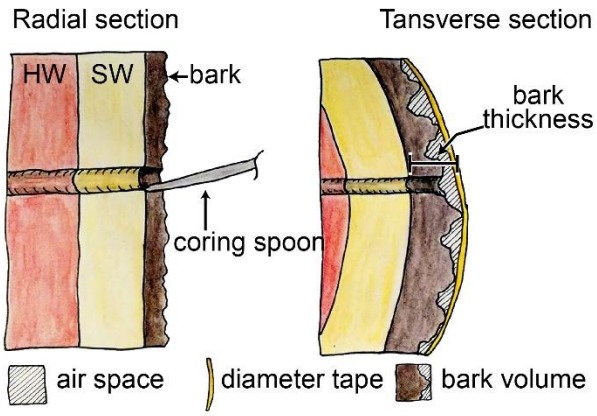

Figure 1.9. Quantifying bark via tree coring. Insert a coring spoon and feel for bark-wood boundary, mark spoon at bark surface and measure (**left**). The downward angle on the spoon is exaggerated to show technique. Bark must be measured relative to diameter wrap to account for air space included in diameter wrap (**right**). Volume of density samples must also include airspace to avoid over-estimating bark mass. HW = heartwood, SW = sapwood.

1.2.9 *Ground-based predictors*

Creating allometric equations requires ground-based parameters as predictors of tree-level tissue quantities. For each tree, the height to crown base, defined as the height where branches extend one third of the way around trunk circumference, and four to eight crown radii, measured from the extent of the crown to the origin from the cardinal or sub-cardinal directions, are measured from the ground to create the predictor variable of crown volume. All distances are measured with a laser range-finder (Laser Technology Inc.), while crown extents were located by vertically aligning a clinometer at 90˚ to the outer crown. Crown volumes area calculated as simple geometric solids best representing the crown of a particular species based on crown depth

and average crown radius. For example paraboloids well represent *P. sitchensis* crowns and ellipsoids the older crowns *Sequoia.*

1.2.10 *Error checking and 3D geometry*

Before crown mapping data are used to calculate any study variables, they are error-checked and geometrically rectified into Cartesian coordinates. This complicated process is greatly simplified by the *SITCHENSIS* program and a calculation template (**Appendix F** of published article). The program is documented and housed on GitHub (https://github.com/northcoastmountainrat/Sitchensis), a centralized online repository for sharing and developing open source programs. In the GitHub repository, there is a "Wiki" link with instructions for installing, testing, and using *SITCHENSIS*, a template for standardizing inputs, and a Jupyter notebook (Kluyver et al., 2016) demonstrating its utility. Briefly, *SITCHENSIS* uses raw field data to screen for errors, produce visualizations of the data, and outputs calculated Cartesian coordinates of tree trunks, segments, and branches.

1.2.11 *Size calculations*

Simplify tree size calculations by breaking them into two stages. Stage one involves calculating tissue volumes and masses of the main trunk and segments from the tree geometry and requires developing equations from bark, sapwood, and heartwood radius data. During stage two, apply branch-level equations to the branch inventory, and apply multipliers to foliar units or branchlets. The modularity of tree mapping means the data can be summarized in any manner that suits a particular study. For example, to calculate horizontal surfaces that can be accumulate arboreal soils, filter appendages by slope and diameter, and calculate the upper surface area of all of these appendages.

Calculate the volume and surface area of trunk sections and segments directly from the 3D geometry of node locations and diameters that describe conic frusta. Model internal tissues such as sapwood and heartwood as successive shells by subtracting the inner volume from outer layers. Predict the thickness of bark and sapwood at each end of trunk sections and segments from equations based on the branch dissection and core data. Due to uncertainty in these thicknesses, it is important to include the standard error in these predictions and carry them forward in the calculations of tissue volumes and surface areas. Likewise, when converting volumes to masses apply the uncertainty in tissue density to the uncertainty in the volume.

Predict branch components based on the equations developed from branch dissection data and *in situ* measurements. For species with foliar unit counts for each branch, the branch is the sum of its tissue components larger than the foliar unit cutoff diameter and contributions from its foliar units. Using the detailed subset of branches collected during mapping, contributions of all tissue components of branch stems larger than the foliar unit cutoff are used to predict quantities in the remaining branches. Apply the foliar unit multipliers to the count and sum for each branch. For species where foliar units are not used, simply apply whole-branch equations to the total branch inventory. Common important predictor variables include branch height, relative height (branch height/tree height), branch diameter, and path length (**Table 1.2**) out to a given diameter. The branch total is the sum of predictions for each branch ± the sum of the standard error for each.

Recall that branchlets are counted in diameter classes specific to trunk sections and segments. A simple approach to creating multipliers for branchlets is to first develop tissue-level equations as a function of the diameter of dissected branchlets and then apply them to midpoint diameters of size classes. This technique develops a multiplier with a standard error for

converting branchlet or foliar-unit counts to their resulting tissue components. It is appropriate to develop height-dependent multipliers based on foliar units collected from a range of heights, especially for leaf-level quantities, which vary significantly with height in tall trees (England and Attiwill, 2006; Koch et al., 2004).

1.2.12 *Methods for Picea sitchensis*

Four datasets were utilized to ensure that the resulting predictive equations could be applied to *P. sitchensis* trees of any size. Dataset 1 was the most southerly and included eight trees, four from the Arcata Community Forest in Arcata, California and four from the Redwood Experimental Forest in Klamath, California (**Table 1.4**). These trees were climbed and mapped from 2013-2015 and ranged from 90 to 330 cm *f*-DBH and from 50 to 94 m tall. Five of these trees were cored twice at a minimum of 10, 30, 50, and 70 m. They included relatively young model-conforming trees as well as two individuals with structurally complex crowns.

Table 1.4. Basic regional conditions for 60 crown mapped trees. Summer is defined as the driest and hottest 3 months of the year and winter as the wettest and coldest. Temperature is abbreviated as T. Columns for dataset and tree number refer to those in **Figure 1.10** and **Appendix G** of published article. Values are 30-yr means from the PRISM Climate Group. The Olympics region refers to river valleys on the western Olympic Peninsula.

Region state	Dateset (trees)	Winter mean T Dec. - Feb. (°C)	Summer mean T Jul. - Sept. (°C)	Total rainfall (cm)	Summer Rainfall Jul.-Sept. (cm)	Geomorphic position
Klamath, CA	1, 4 (7, 21, 47, 52, 57)	8.2	15.2	195	5	Alluvial flats
Arcata, CA	1 (13, 15, 22, 30)	9.0	14.9	121	3	Wet hillslopes to flats
Olympics, WA	2, 3, 4 (all except 57)	4.5	16.1	319	24	Alluvial flats, toe slopes, and upland swales

Dataset 2 was a subset from a study of riparian forest development along the Queets River on the Olympic Peninsula in Washington (Van Pelt et al., 2006, **Table 1.4**). It included 11 trees from a broad range of sizes. The smallest tree was 14 cm *f*-DBH and 10 m tall, while the

largest was 161 cm *f*-DBH and 64 m tall. Most of these trees exhibited simple, model-conforming crown structure. The methodology when these trees were mapped was less refined than our current one for very large appendages; the largest trees had branches much larger than those dissected to create the whole-branch equations. The largest of these trees were subsequently remapped during 2017, segmenting large branches, and incorporated into dataset 3. One large tree deemed unsafe to climb in 2017 was included in dataset 4 (see below), but only with its main trunk data.

Dataset 3 included 36 trees mapped in 2016 and 2017 from river valleys along the western Olympic Mountains (**Table 1.4**). Tree selection was based primarily on a stratified random selection from various forest densities and heights > 60 m but also included opportunistic sampling of particularly complex trees. It encompassed the full range of structural complexity, forest density, and tree ages past approximately 150 yr. LiDAR was used to calculate a forest density metric called canopy relief ratio (mean height – min height)/(max height – min height) based on 30 m plots around all trees > 60 m tall. All 36 of these trees were cored twice at DTB, 10, 30, 50, and 70 m. The final dataset included suppressed as well as dominant trees ranging from 72 to 395 cm diameter and 55 to 90 m tall.

Dataset 4 was included as an anchor for the large end of the equations by including five very large trees. It included the three largest known before they toppled or started collapsing from decay and two other partially mapped trees (Van Pelt, 2001). All trees were either climbed and trunk mapped, or the trunk was measured from the ground using a reticle on the lens of a scope to capture diameter at multiple heights above ground. The reticle method utilizes distance and angle to a trunk location and a conversion factor calibrated for each reticle mark to measure horizontal distances tangent to the observer. These caliper-like measurements are taken at

perpendicular angles for each height on the trunk to account for elliptical trunk cross-sections. All were footprint mapped to obtain *f*-DBH and a conservative trunk volume. The three largest trees of this set were substantially bigger than any other tree in the previous three datasets. Four of these trees were from western slope Olympic river valleys and one was from the Redwood Experimental Forest in California which was also the only cored tree in this dataset (**Table 1.4**).

In addition to the methods described above, several additional steps were taken to map *P. sitchensis* trees. Decay was ubiquitous in older *P. sitchensis* stands, and many trees had evidence of decay in tree cores and from basidiocarps, mostly from *P. pini*. In the case of one of the largest trees, the data were collected before the trees collapsed due to heart rot by *P. schweinitzii* (R. Van Pelt *personal observation*). One tree had an exposed wound, and a few had broken tops. Because internal scanning of trunk decay was impractical we crudely estimated decay volume as a paraboloid five times taller than the estimated decay diameter (Van Pelt et al. 2016). Decay diameter was measured directly from tree cores, or for uncored and collapsed trees, as 70% of the total diameter based on visual estimation from photographs. Mass of the main trunk was decremented by mass lost to decayed wood volume by reducing heartwood density from 439 kg m^{-3} (**Appendix 1.D**) to 324 kg m^{-3} using 0.74 relative density loss for decay-class III *P. sitchensis* wood (Harmon et al., 2008). Cull factors reported for *P. sitchensis* in Alaska > 270 cm diameter were 12% of cubic trunk volume and included defects related and unrelated to decay (Kimmey, 1956). Our estimates for the largest trees averaged 7.6% and may be underestimates.

We dissected 40 branches and 16 branchlets from 7 trees to develop whole-branch equations and branchlet multipliers for predicting tissue components of all branches and branchlets on the 60 trees. Branches were chosen with a stratified random procedure so that all representative diameters and heights were included. Dissected branches ranged from 10.1 to

88.4 m height and from 2.5 to 16.6 cm diameter. All 40 branches were included to create intermediate whole-branch equations. Branchlet multipliers were created by applying equations based on the 15 smallest dissected branches (2.5 to 7.0 cm diameter) and 16 additional branches dissected for only leaf mass and area to the midpoint diameters of branchlet size classes. Branchlets were counted in categories of 0-2 cm and 2-4 cm in diameter. The smallest branchlets were > 0 cm diameter and we represented these by the average of the smallest diameter twig tips from the branch dissection (0.25 cm). The multipliers were thus based on predictive equations (N = 16, 31 branches) applied to midpoint diameters of $\sqrt{(0.25 * 2)}$ and $\sqrt{(2 * 4)}$ for each branchlet category.

In order to predict branches larger than were safe to remove and > 16.6 cm diameter, eight additional segmented appendages were incorporated into the data as follows. All segment data were filtered to obtain a set of large appendages. These were truncated to only model-conforming appendages based on field notes indicating lack of injury and data indicating lack of abrupt diameter or direction changes. They ranged from 35 to 65 m height and 20.5 to 39.2 cm diameter. The intermediate equations from above (N = 40 branches) were applied to all branches arising from each appendage and the result added to segment and branchlet tissue contributions to each appendage. Appendage totals were added into the branch data set, which was used to create final whole-branch predictive equations (**Table 1.5**). These equations were applied to all mapped branches and summed for each tree.

Table 1.5. Equations to predict whole-branch tissue components for *P. sitchensis* as power functions of basal diameter (diam) using 40 dissected branches and 8 additional segmented appendages (N = 48). These can be applied to branches ranging from 2 – 40 cm diameter. Minimum, mean, and maximum of dependent variables are provided for reference to the root mean square error (RMSE).

Dependent variable	Form	***a***	***b***	R^2	RMSE	min	mean	max
Total mass (kg)	$\boldsymbol{a}$*diam$^{\boldsymbol{b}}$	6.983E-02	2.503E+00	0.984	1.57E+01	8.00E-01	6.13E+01	6.50E+02
Total volume (m^3)	$\boldsymbol{a}$*diam$^{\boldsymbol{b}}$	1.468E-04	2.416E+00	0.985	2.31E-02	1.00E-03	1.00E-01	1.00E+00
Wood volume (m^3)	$\boldsymbol{a}$*diam$^{\boldsymbol{b}}$	6.033E-05	2.598E+00	0.985	1.84E-02	1.00E-03	7.20E-02	8.04E-01
Heartwood volume (m^3)	$\boldsymbol{a}$*diam$^{\boldsymbol{b}}$	1.108E-05	2.919E+00	0.981	1.22E-02	0.00E+00	3.50E-02	4.76E-01
Bark area (m^2)	$\boldsymbol{a}$*diam$^{\boldsymbol{b}}$	3.770E-01	1.548E+00	0.906	7.19E+00	6.01E-01	1.92E+01	1.07E+02
Cambium area (m^2)	$\boldsymbol{a}$*diam$^{\boldsymbol{b}}$	2.212E-01	1.585E+00	0.913	4.61E+00	3.84E-01	1.26E+01	7.13E+01
Leaf mass (kg)	$\boldsymbol{a}$*diam$^{\boldsymbol{b}}$	1.126E-01	1.484E+00	0.919	1.44E+00	1.06E-01	3.87E+00	2.58E+01
Leaf area (m^2)	$\boldsymbol{a}$*diam$^{\boldsymbol{b}}$	4.892E-01	1.508E+00	0.922	6.72E+00	2.66E-01	1.79E+01	1.22E+02
Millions of leaves	$\boldsymbol{a}$*diam$^{\boldsymbol{b}}$	2.483E-02	1.519E+00	0.915	3.73E-01	9.00E-03	9.31E-01	6.45E+00

Tree data were first screened for errors using the visualizations from *SITCHENSIS* (**Figure 1.10**) before quantities of all tree tissues were summed to obtain tree-level estimates and then used to create tree-level equations. These equations were created by linearizing each independent variable with respect to each dependent variable with a power function and then including the transformed and sometimes untransformed variables in a stepwise a linear model selection process in JMP (version 13, SAS Institute Inc.). Models were selected based on parsimony by selecting for the least number of parameters, goodness of fit by examining residual plots for systematic patterns, and variability explained by examining R^2. Only models with precise (S_E < half the mean) coefficient estimates were retained. The coefficients of the power transformation and the linear fit were combined to produce equations for untransformed variable inputs. First, we fit intermediate models for all tree tissue quantities based on main trunk and crown volume (N = 55 trees, **Appendix 1.D**) and used them to predict tissue quantities and standard errors for the five large trees in dataset four. To incorporate additional measurement error, the average proportional standard error from all 55 original trees for each tissue quantity was added to the standard error from the models. The predicted values of the five trees from the

fourth dataset were then appended to the original data before creating the final predictive equations based on 60 trees.

Final allometric equations were developed and fitted with all data sets combined using methods described above and three ground-based predictors: *f*-DBH, DTB, and crown volume. Two sets of models were retained—the best possible set of equations and a set based only on lower trunk diameters (*f*-DBH and DTB). To insure the addition of the largest trees did not overly leverage the equations, predicted values versus the most important predictor (DTB) were plotted with the prediction error of dataset 4 trees. We evaluated whether the slopes of these equations differed by duplicating the data for the 55 original trees from datasets 1-3, assigning a dummy variable to indicate datasets (i.e., 1-3 or 1-4), and then fitting a model include an interaction term between DTB, *f*-DBH, and the dummy variable and examining its *P*-value. Plots and R^2 based on linear equations between predictions and actual measurements were used to assess goodness of fit, and residual plots were examined for non-random patterns. Finally, the results of our allometric equations were compared to those previously published to examine the effects of including the largest possible trees in the dataset (Bormann, 1990; Chojnacky et al., 2014; Jenkins et al., 2004, 2003). To make the results comparable between our equations using DTB and *f*-DBH and published equations using only DBH we predicted total and leaf dry mass using a DTB series and associated *f*-DBH predicted from all trees with both measurements ($f\text{-DBH} = 0.5744 * \text{DTB}^{1.1737}$, $R^2 = 0.919$, N = 44) for our equations, then we used the *f*-DBH of this series as DBH for predicting with published equations. This approach conservatively estimates masses using other published equations because *f*-DBH averages 92% DBH over our tree sample (**Appendix 1.D** Table 9 therein).

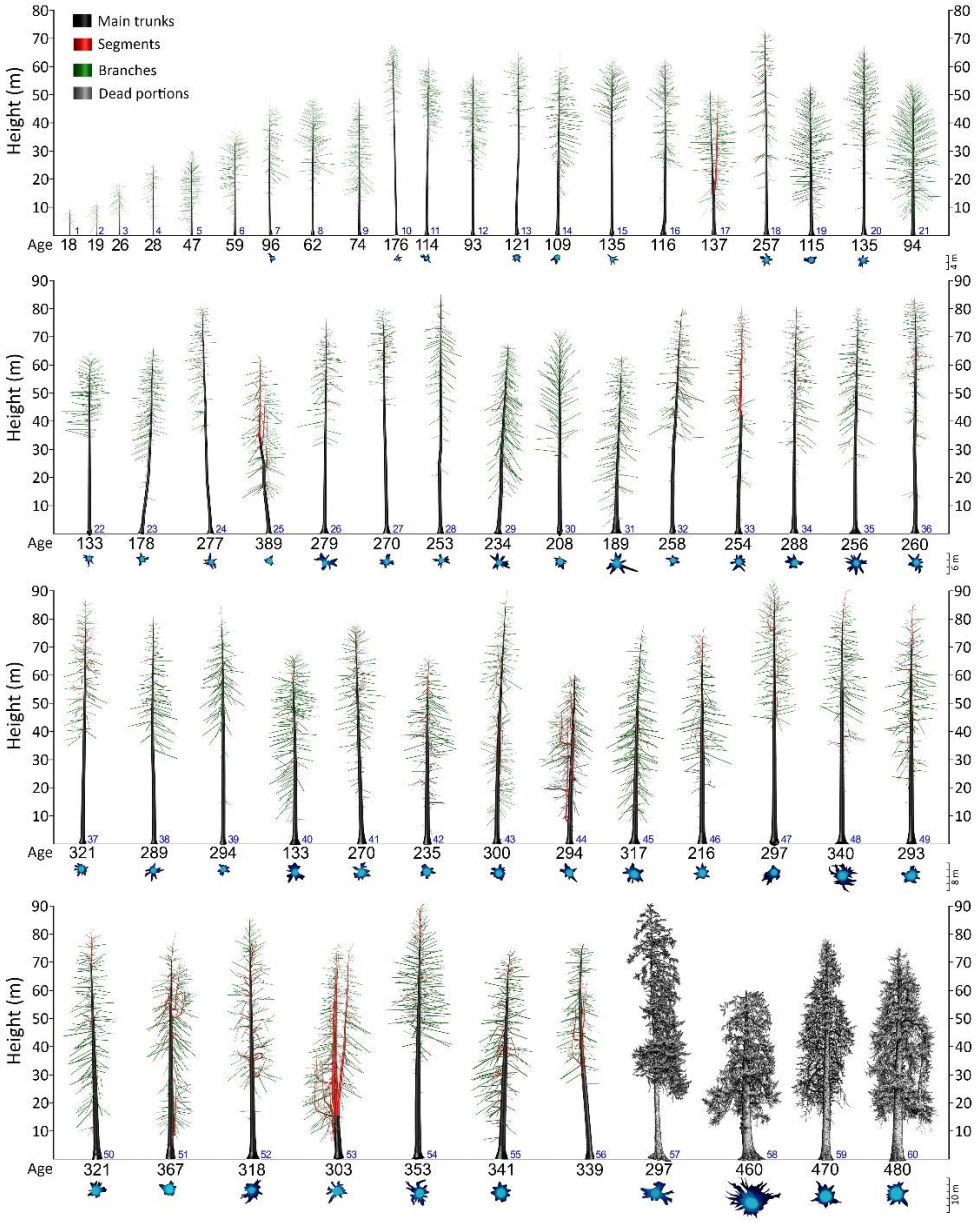

Figure 1.10. Crown structure of 60 *P. sitchensis* trees ranked by total mass and depicted as scale models showing trunks and appendages in orthographic view. Main trunks and segments are portrayed as conic frusta using end diameters. Branches are displayed as cylinders with thickness equal to basal diameter. Blue numbers to lower right of each model correspond to trees in **Table 1.4** and **Appendix G** of published article. Beneath tree models, cross sections of main trunks (if available) are shown to scale indicated by short vertical bar on right (ticks at 2-m intervals) with colors indicating different heights above the ground, basal cross section being darkest. Trees 56-60 are from dataset 4 and ranked by total mass separately. Scale illustrations of partially mapped trees by Robert Van Pelt are based on field measurements and photographs.

1.3 RESULTS

Tree mapping, branch dissection, and increment coring allowed us to quantify aboveground volumes, areas, and masses of bark, cambium, sapwood, heartwood, and leaves in 60 *P. sitchensis* trees. This combined dataset included trees ranging in total mass from 0.054 ± 0.006 to 155 ± 9 Mg, thus spanning four orders of magnitude. Leaf dry mass ranged from 10 ± 2 to 1260 ± 215 kg per tree with a mean of 435 ± 45 kg. In addition, it included some of the tallest (up to 94 m) and largest living *P. sitchensis* trees (up to 495 cm *f*-DBH). The trees also spanned a wide range of relative crown size with voluminous and diminutive crowns across the height distribution. For example, crown volumes of trees > 80 m tall ranged from 2271 to 10884 m^3, trees 60 to 80 m tall ranged from 389 to 15115 m^3, and trees 40 to 60 m tall ranged from 621 to 14662 m^3, representing 5- to 24-fold differences within each height class. Like other metrics, trunk shapes also varied widely with the diameter to height ratio (cm m^{-1}) ranging from 1.0 to 5.2.

Tracking standard error from beginning to end in bark and sapwood thickness, as well as leaf mass, showed that tree-level estimates of fully-mapped trees were precise (**Appendix G,** published article). In aboveground dry mass, the total standard error ranged from 3 to 6%, except in the two smallest trees, which were 14 and 18 cm *f*-DBH and had 10 and 7% error, respectively. Leaf mass estimates were best in fully mapped trees with error ranging from 5 to 15% in all but the smallest two trees that had 28 and 21% error, respectively. For all other tissue quantities, the average error ranged from < 1 to 10%. However, the average of the errors for the same two small trees mentioned above ranged from 1.4 to 65% and were highest in heartwood, bark, and cambium quantities due to errors in wood radii equations (**Appendix 1.D**). Excluding

these variables, error ranged from 1.3 to 25% and averaged 8.5%, the highest of which were from branch-level estimates due to error in whole-branch equations (**Table 1.5**).

The tissue quantities of the five partially mapped trees in dataset 4 were predicted with an equation based on main trunk and crown volumes. Of all fully-mapped trees, trunk wood mass ranged from 40 to 84% of total mass in trees < 100 cm DTB, 69 to 88% in trees > 100 and < 200 cm DTB, and from 74 to 82% in trees > 200 cm DTB. The five partially mapped trees ranged from 197 to 318 cm DTB, thus measured trunk volume converted to bark and wood mass likely accounted for > 75% of their total (**Appendix G**, published article). Consequently, the standard error around each total mass estimate was only 6 to 8%. The standard error of all combined tree-tissue predictions from allometric equations ranged from 4 to 25% of the mean, while standard error on the mean ranged from 3 to 16% (not shown). Comparing equations fit with and without the additional data showed that they were slightly but not significantly higher for total dry mass (P = 0.08 and 0.19 for slopes on DTB and *f*-DBH) and reduced but not significantly (P = 0.17 and 0.22 for slopes on DTB and *f*-DBH) for leaf mass (**Figure 1.11**).

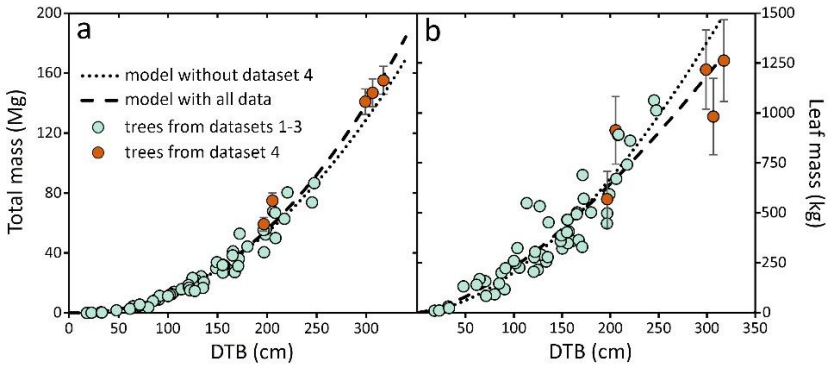

Figure 1.11. Models of dry aboveground total and leaf mass showing effects of adding large trees from dataset 4. Added trees (dark circles) are predicted with intermediate equations (**Appendix 1.D**) of main trunk and crown volume developed from trees in datasets 1-3. Whiskers on added trees represent 1 standard error. Dashed and dotted lines are equations fitted with and without added trees, respectively. Total (**a**) and leaf mass (**b**) are predicted using diameter at top of buttress (DTB) and diameter at breast height corrected for non-circularity (*f*-DBH).

Allometric equations from the 60 mapped individuals accurately modeled tree-level tissue quantities (**Figure 1.12, Appendix G**, **H**, published article). The dominant parameters in the best models included DTB, *f*-DBH, and crown volume. The best equations typically included both DTB and *f*-DBH with DTB being more important than *f*-DBH. Leaf and cambium-surface-area models invariably included crown volume as the most important predictor followed by a measure of trunk size, thus accounting for relative crown size. The only equations explaining less than 90% of the variability in any dependent parameter were those predicting either sapwood or leaves, which also showed slight systematic residual patterns in the diameter-based set of equations (**Appendix 1.D**, Table 8 therein, **Appendix H**, published article).

Equations in this study compared to those of previous research were similar up to ~100 cm beyond their published diameter range for total mass while being more conservative overall for leaf mass (**Figure 1.13**). The Jenkins (2003, 2004) equations are generalized for all spruce species, the Chojnacky (2014) total mass equation for low specific gravity (< 0.35) is the one recommended for *P. sitchensis* based on pseudodata from 8 separate equations including Bormann (1990), and the Bormann equations are specific to *P. sitchensis* from naturally regenerated stands in Alaska. The leaf mass equations for Bormann (1990) and Chojnacky (2014) are the identical. The generalized spruce equation for total mass (Jenkins 2003, 2004) more closely aligned than did spruce-specific equations of Bormann (1990) and Chojnacky et al. (2014), which both diverged at ~150 cm diameter. The maximum tree-diameters reported for these equations were 78 and 283 cm respectively. Predicted leaf mass diverged at much smaller diameters than did total mass at ~50 cm for the identical Bormann (1990) and Chojnacky (2014) equations and close to the reported diameter limit of 78 cm for Jenkins (**Figure 1.13**).

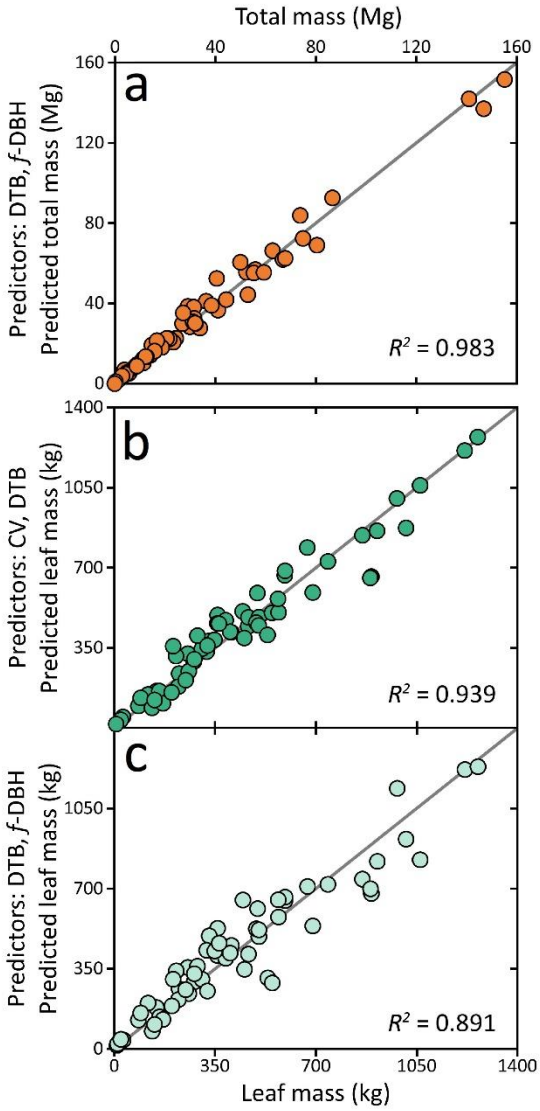

Figure 1.12. Actual vs. predicted values for aboveground total (**a**) and leaf (**b** and **c**) mass. The best model for total mass (**a**, **Table 1.6**) includes the predictors DTB and *f*-DBH and is the same as that presented in **Appendix 1.D**. The best leaf mass model (**b**) includes DTB in addition to crown volume (CV). The next best model for leaf mass (**c**) includes only DTB and *f*-DBH. Grey line is 1 to 1. Other tree-level tissue predictions are similarly well-defined (**Appendix H**, published article).

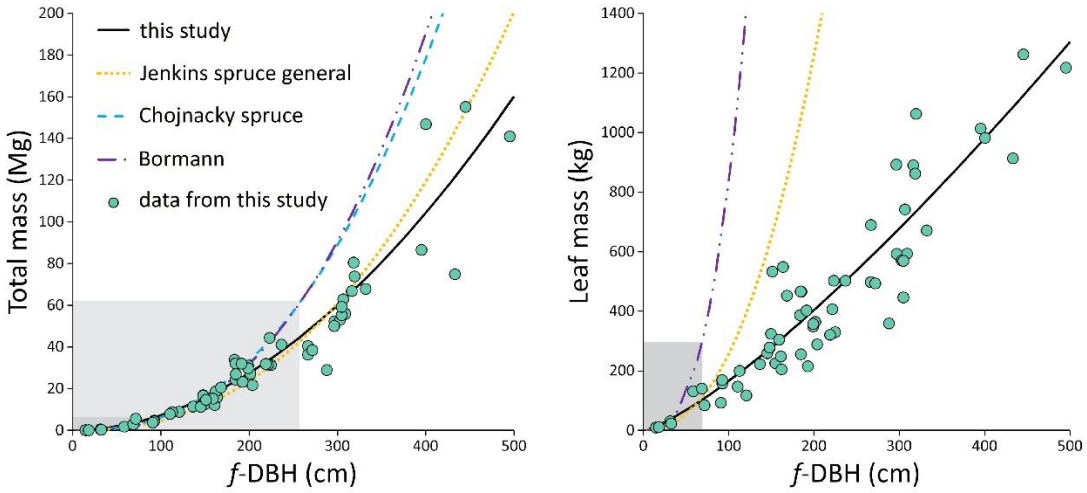

Figure 1.13. Data from this study plotted with allometric predictions from Jenkins (2004), Chojnacky (2014), and Bormann (1990). Light and dark grey boxes show the range of diameters and predictions reported in Jenkins (≤ 250 cm DBH) and Bormann (≤ 78 cm DBH), respectively. Jenkins leaf mass is calculated from product of the predicted leaf ratio from an equation based on trees ≤ 78 cm DBH and total mass. Chojnacky predicted leaf mass is the same model as Bormann and not shown.

1.4 DISCUSSION

The methodology presented in this paper is the culmination of > 40 yr of development (**Appendix 1.A**). Pioneering researchers ascended trees using rudimentary mountain climbing techniques. Despite this, they were able to crown map several large individuals. Sample sizes remained low for the next two decades, but climbing methods improved. Further methods development has been mostly limited to one group of researchers (but see Nakanishi et al., 2016, 2013) since the early 2000s with sample sizes per species ranging from the mid-20s to a maximum of 97 (**Appendix 1.A)**. These techniques are now efficient and repeatable, and obtaining a robust sample size is feasible in one or two field seasons.

Climbing *P. sitchensis* trees, mapping external structure, then modeling internal structure with data from increment cores and branch dissections demonstrates one application of the

methodology, which takes advantage of spatially explicit information. For example, trunk bark thickness changes with diameter as well as height and is often different than bark on branches. Likewise, trunk wood density changes with height and between trunks and appendages, and this variability is incorporated into the final tree quantities (Wassenberg et al., 2015; Sillett et al., 2018b). A conservative approach is taken at all steps, for example, by measuring branch diameters past the branch collar and by decreasing main trunk mass due to evident decay. This—in combination with tracking standard errors for predicted quantities through to their summation of tree totals—results in reliable tree-level estimates. The estimates of tree tissues are less precise for the smallest individuals, but the smallest trees also provide the least contributions to total forest biomass. To obtain equivalent accuracy for small trees or shrubs, researchers can increase dissection and diameter cut-off resolution with < 1-cm sampling while using the same general approach.

The tool *SITCHENSIS* vastly improves processing time from field data collection to final analysis. The 3D geometry (**Figure 1.10**) that is rectified in seconds otherwise takes a skilled technician a day or more to complete. In addition, the program rapidly locates errors, eliminates errors due to manual data manipulation, and recalculates the 3D geometry after errors are located with the click of a button. This program is now housed on the centralized repository GitHub, which facilitates and documents its future improvements by the authors or other researchers. Planned improvements include the ability to apply published equations to the 3D data to produce final, tree-level quantities.

Equations produced from these data are applicable to nearly all forest-grown *P. sitchensis* trees for three reasons. First, the dataset includes nearly all possible tree conditions present in a natural forest. Represented are small, medium, and large trees with various levels of crown

structural complexity, social position (dominant, intermediate, suppressed), and stand density (trees ha^{-1}). Second, equations are anchored by the largest trees of the species. Adding these trees to the data ensures that the equations are valid for trees up to and including the largest in any forest (**Figure 1.11**). Third, equations include crown volume rather than height as a predictor. Although height is a better predictor than crown volume in some cases, the relationship between height and many of the variables is nearly exponential (results not shown). If applied to forests further north in the range where large yet shorter trees grow (Farr and Harris, 1979; Peterson et al., 1997), they would under-predict biomass. Short trees with deep and wide crowns **(Figure 1.10**, trees 19, 21) and tall trees with short narrow crowns (**Figure 1.10**, trees 10, 27) also exist, making crown volume a better size predictor than height.

We recommend using the equations by first predicting quantities in all but one tissue component and then subtracting to obtain the remainder. Solving by subtraction insures that the total predictions are always the sum of all tissues. For example, to obtain the quantity of branch wood (which is nearly twice as dense as trunk wood, **Appendix 1.D**), subtract the contribution by all trunk wood from total wood. The sapwood equations are not as predictive as others and show some systematic residual patterns (**Table 1.6**, **Appendix H**, published article), so we recommend subtracting heartwood and bark from total volume to obtain sapwood volume. We assume that bark density is the same for branches and trunks in *P. sitchensis*, so equations are only supplied for total bark. Trees in this dataset are from natural forest environments and include only four individuals < 30 m tall and < 50 cm *f*-DBH, so our equations should not be used for krummholz trees from fringe environments where crown morphology is sculpted primarily by wind (Peterson et al., 1997) or in plantations with trees < 30 m tall or < 50 cm *f*-DBH.

Table 1.6. Best equations for predicting tree-level tissue components for *P. sitchensis* > 40 m tall and > 30 cm *f*-DBH based on $N = 60$ trees. DTB is diameter at top of buttress (cm), *f*-DBH is functional diameter at breast height (cm), CV is crown volume (m^3) modeled as a paraboloid. Reference to trunks is to main trunk + reiterated trunks (if any). Predictors are listed in order of importance. RMSE is root mean square error in units of dependent variable. See **Appendix G** of published article to relate RMSE to variable scales.

Dependent variable	Form	***a***	***b***	***c***	***d***	R^2	RMSE
Total mass (kg)	$a*DTB^b + c*f\text{-}DBH^d$	2.818E-01	2.256E+00	2.279E-01	1.917E+00	0.983	4.55E+03
Bark mass (kg)	$a*DTB^b + c*CV$	9.596E-02	1.965E+00	1.953E-01	—	0.958	5.11E+02
All trunks wood mass (kg)	$a*DTB^b + c*f\text{-}DBH^d$	2.814E-01	2.216E+00	2.278E-01	1.871E+00	0.976	4.22E+03
All trunks sapwood mass (kg)	$a*DTB^b + c*CV^d$	6.757E+00	1.154E+00	1.104E+01	5.723E-01	0.885	6.65E+02
All trunks heartwood mass (kg)	$a*DTB^b + c*f\text{-}DBH^d$	1.179E-01	2.360E+00	9.477E-02	1.995E+00	0.976	4.01E+03
Total volume (m^3)	$a*DTB^b + c*f\text{-}DBH^d$	7.536E-04	2.240E+00	5.648E-04	1.888E+00	0.980	1.12E+01
Bark volume (m^3)	$a*DTB^b + c*CV$	3.428E-04	1.901E+00	5.270E-04	—	0.960	1.27E+00
All trunks wood volume (m^3)	$a*DTB^b + c*f\text{-}DBH^d$	7.101E-04	2.214E+00	5.770E-04	1.870E+00	0.977	1.04E+01
All trunks sapwood volume (m^3)	$a*DTB^b + c*CV^d$	1.673E-02	1.162E+00	2.783E-02	5.769E-01	0.887	1.73E+00
All trunks heartwood volume (m^3)	$a*DTB^b + c*f\text{-}DBH^d$	2.909E-04	2.362E+00	2.345E-04	1.997E+00	0.976	9.88E+00
Cambium (m^2)	$a*CV^b + c*DTB^d$	9.132E-01	8.006E-01	2.603E-01	1.546E+00	0.960	1.88E+02
Leaf mass (kg)	$a*CV^b + c*DTB^d$	4.087E-01	7.868E-01	8.678E-02	1.495E+00	0.939	7.54E+01
Leaf area (m^2)	$a*CV^b + c*DTB^d$	1.709E+00	7.964E-01	3.515E-01	1.514E+00	0.939	3.44E+02
Millions of leaves	$a*CV^b + c*DTB^d$	8.500E-02	8.012E-01	1.718E-02	1.523E+00	0.939	1.80E+01

None of the three parameters in our best allometric equations are typically used to predict tree-level quantities, which usually rely solely on DBH (Jenkins et al., 2004). Crown volume requires the measurement of crown radii and depth, a difficult task, especially in dense forests where the treetop is hard to see. Although the height of the DTB measurement is inherently subjective, it is consistently more useful than measurements of *f*-DBH. This case is similar to redwoods and highly buttressed tropical trees (Nölke et al., 2015, Sillett et al., 2010) but unlike that of *P. menziesii* or *E. regnans* (Sillett et al., 2015a, Sillett et al., 2018b). The fact that DTB is a better predictor than *f*-DBH is likely because *P. sitchensis* often germinates on logs and stumps and then encapsulates this dead wood in an unevenly buttressed base (Van Pelt, 2007). Many of the equations include a term for *f*-DBH in addition to DTB, hinting that more massive trees require more buttressing to support higher moment forces in wind (Crook et al., 1997; Ennos, 1993). Recognizing that crown volume is excessively time consuming to measure in some

applications, we provide another set of less accurate equations (minimum R^2 = 0.882) based on fewer measurements as well as equations to convert between *f*-DBH and DTB using measured DBH, *f*-DBH, DTB or buttress height (**Appendix 1.D**).

Comparisons of our allometric equations to those from previous research show that the new equations provide conservative predictions of tree mass for large trees and highlight the importance of anchoring equations with the largest trees possible in forests where they are being used. This is especially true as tree diameter increases. In our sample, DBH averaged 9% larger than *f*-DBH used to compare these equations. If DBH were used instead of *f*-DBH, biomass predictions would diverge even sooner. Equations are generally good within a range of trunk diameters and forest conditions sampled with uncertainty increasing outside this scope (Means et al., 1994), but in some instances it is difficult to determine the actual scope of equations. For example, the total mass equations of Jenkins (2003, 2004) and Chojnacky (2014) are the sum of trunk mass from trees ≤ 283 cm DBH and crown mass from smaller trees (≤ 78 cm DBH) or averages across equations from studies dominated by small trees. This may be why the total mass values from Chojnacky (2014) diverged before the recommended diameter limit of 283 cm when compared to our spruce data that contained small and large trees in many forest conditions. Leaf mass from Jenkins (2003, 2004) is based on a predicted ratio of total mass and its diversion at ~80 cm implies that the proportion of leaf mass in primarily young trees of previous work is greater than that of older trees sampled in this study. Such high leaf mass in young trees has repercussions for estimating standing biomass, rates of biomass accumulation, leaf area index, and by extension critical ecological processes like low summer stream flows moderated by transpiration (Perry and Jones, 2016; Sillett et al. 2018b; Smith and Long, 2001).

The rate of biomass accumulation in *P. sitchensis* is best appreciated in comparison with co-occurring conifers *P. menziesii* and *Sequoia*. These species were quantified with the same methodology (Sillett et al., 2015b, Sillett et al. 2018b) presented here in addition to having age estimates. To compare the three species, we estimated ages of all *P. sitchensis* trees in this study (**Appendix 1.E**), which includes the oldest reported age (480 yr) for *P. sitchensis*. This age likely represents an upper age limit for the species given that one of the three largest trees (all > 400 yr) has collapsed and another is shedding large portions weakened by fungi (*personal observation*). Comparison trees comprise 15 *P. menziesii* from low elevation rainforests on the western Olympic Peninsula and 93 *Sequoia* from old-growth forests spanning its geographic distribution in California. The *P. menziesii* range from 80 to 620 yr old and 92 to 429 cm *f*-DBH (Sillett et al., 2018b), and the *S. sempervirens* range from 110 to 2510 yr old and 2 to 681 cm *f*-DBH (Sillett et al., 2015b).

Picea sitchensis attains biomass similar to *P. menziesii* but much less than *Sequoia* (**Figure 1.14ab**) and differs by provisioning substantially greater biomass to crowns and leaves with higher rates of accumulation. Although the largest *P. sitchensis* tree (155 Mg) is 30% heavier than the largest living *P. menziesii,* the largest known *P. menziesii* likely weighed 212 Mg (Sillett et al., 2018b). However, similar total mass is not reflected in crown or leaf mass, where *P. sitchensis* is 230% and 79% heavier than *P. menziesii,* respectively. More investment in crown mass by *P. sitchensis* makes sense given that its average branch (wood + bark) density is 620 kg m^{-3} compared to 501 and 479 kg m^{-3} for *P. menziesii* and *Sequoia,* respectively (**Appendix 1.D**, Sillett et al., 2018b; Sillett et al., 2015a). Despite attaining only 31% of *S. sempervirens* total mass, *P. sitchensis* leaf mass reaches 77% of *Sequoia*. For a given size, *P. sitchensis* leaves weigh more than either of the other two conifers. It has a higher crown-mass-to-

total-mass ratio (14 vs. 8 and 11%, $P < 0.001$) and a higher average leaf mass density (leaf mass/crown volume, 0.13 vs. 0.08 and 0.07 kg m^{-3}, $P < 0.001$) than *P. menziesii* and *Sequoia*. *Picea sitchensis* supports similar amounts of leaves as the other conifers nearly twice its mass and age (**Figure 1.14f**, **Table 1.7**). The high leaf-mass-to-total-mass ratio is reflected in growth rates that enable *P. sitchensis* to attain nearly 1.7 and 1.5 times the total mass of *P. menziesii* and *S. sempervirens* in 300 yr (**Figure 1.14ab**, **Table 1.7**). Notably *P. sitchensis* accumulates biomass at similar rates to *P. menziesii* and *S. sempervirens* for the first century before accelerating over its lifespan (**Figure 1.14a-f, Table 1.7**).

Table 1.7. Biomass accumulation with tree age in *P. sitchensis* (PISI), *P. menziesii* (PSME), and *S. sempervirens* (SESE) based on equations from **Figure 1.14** (see **Appendix 1.D**).

	Total mass (Mg)			Crown mass (Mg)			Leaf mass (kg)		
Age	PISI	PSME	SESE	PISI	PSME	SESE	PISI	PSME	SESE
50	0.7	2.1	3.8	0.0	0.1	0.2	66	44	59
100	3.6	5.6	8.6	0.3	0.4	0.5	154	82	102
200	18.1	15.4	19.6	2.2	1.2	1.4	357	153	176
300	47.0	27.7	31.7	6.6	2.2	2.5	584	221	243
400	92.4	41.9	44.6	14.7	3.5	3.8	828	287	305
500	156.1	57.9	58.2	27.2	5.0	5.2	1085	351	364

Faster biomass accumulation of *P. sitchensis* compared to *P. menziesii* and *S. sempervirens* is attributable to different life history strategies. *Picea sitchensis* is a shade tolerant tree in productive and highly dynamic forests inhabited by other tall conifers (Hennon, 1995; Van Pelt et al., 2006). Consequently it must grow rapidly to utilize canopy gaps before they close and outpace co-occurring conifers to maintain access to sunlight. Several traits promote rapid growth of *P. sitchensis*. It carries some of the highest leaf masses reported for species, and its leaf anatomy is organized to maximize photosynthesis (Chin and Sillett, 2017). Both *P. menziesii* and *Sequoia* invest in thick bark allowing them to survive fires (Ryan and Reinhardt, 1988; Sillett et al., 2015b; Starker, 1934), while *P. sitchensis* does not. Additionally *Sequoia* converts

50-90% annual wood production into extremely decay-resistant heartwood, conferring immunity to all but a few fungi (Kimmey, 1958; Kimmey and Hornibrook, 1952; Sillett et al., 2015b) and allowing them to reach millennial ages. *Picea sitchensis* and *P. menziesii* do not invest as much in decay-resistant heartwood and are thus both susceptible to common heart rot fungi ultimately responsible for their demise (Harvey, 1962; Hennon, 1995), but *P. menziesii* likely invests more in defense than *P. sitchensis* because it can live at least twice as long (Sillett et al., 2018b). Delayed biomass acceleration of *P. sitchensis* relative to *P. menziesii* in Olympic rainforests (**Table 1.7**) can be explained by forest developmental processes. Unlike *P. sitchensis*, relatively shade-intolerant *P. menziesii* establishes primarily after high-severity fires, forming dense cohorts competing for light (Huff, 1995). In contrast, *P. sitchensis* often establishes concurrently with deciduous and nitrogen-fixing *Alnus rubra* (hereafter *A. rubra*) on alluvial terraces where many of our trees were sampled (Van Pelt et al., 2006). These *A. rubra* typically disappear in forest development after 80-100 yr, freeing *P. sitchensis* from light competition and providing a nitrogen boost.

In conclusion, the methodology presented in this study can do more than produce accurate tree-level quantities and robust allometric equations. Our findings have implications for managers seeking to increase old-growth characteristics via development of large trees with complex crowns (Franklin and Johnson 2018; Sillett et al., 2018a). Because *P. sitchensis* grows so fast relative to other dominant conifers and becomes one of the largest structural elements in the forest, it has early potential to provide arboreal habitats for old-growth associated species, especially epiphytes (Ellyson and Sillett, 2003). The utility of crown mapping can be increased by changing the scales of analyses. Fine-scale questions can take advantage of spatially explicit crown mapping data, for example, by examining structural development and habitat provisioning

of individual trees (Ishii et al., 2018; Williams and Sillett, 2007) or separating growth responses of trunks and branches using repeated measurements (Ishii et al., 2017; Sillett et al., 2018a, 2010). Large-scale questions can utilize detailed crown mapping data to link individual trees to remote sensing techniques such as LiDAR. Large trees provide most of forest biomass and habitat (Bastin et al., 2015; Lutz et al., 2012; Sillett and Van Pelt, 2007) and are easily detected with LiDAR. However, individual "trees" segmented from LiDAR actually constitute a larger structural unit composed of a dominant tree and its subordinates (Jeronimo et al., 2018). This limitation may actually be an advantage by refocusing the unit of measurement to groups of trees and linking to ground plots centered on individual overstory trees for scaling to the landscape with remote sensing.

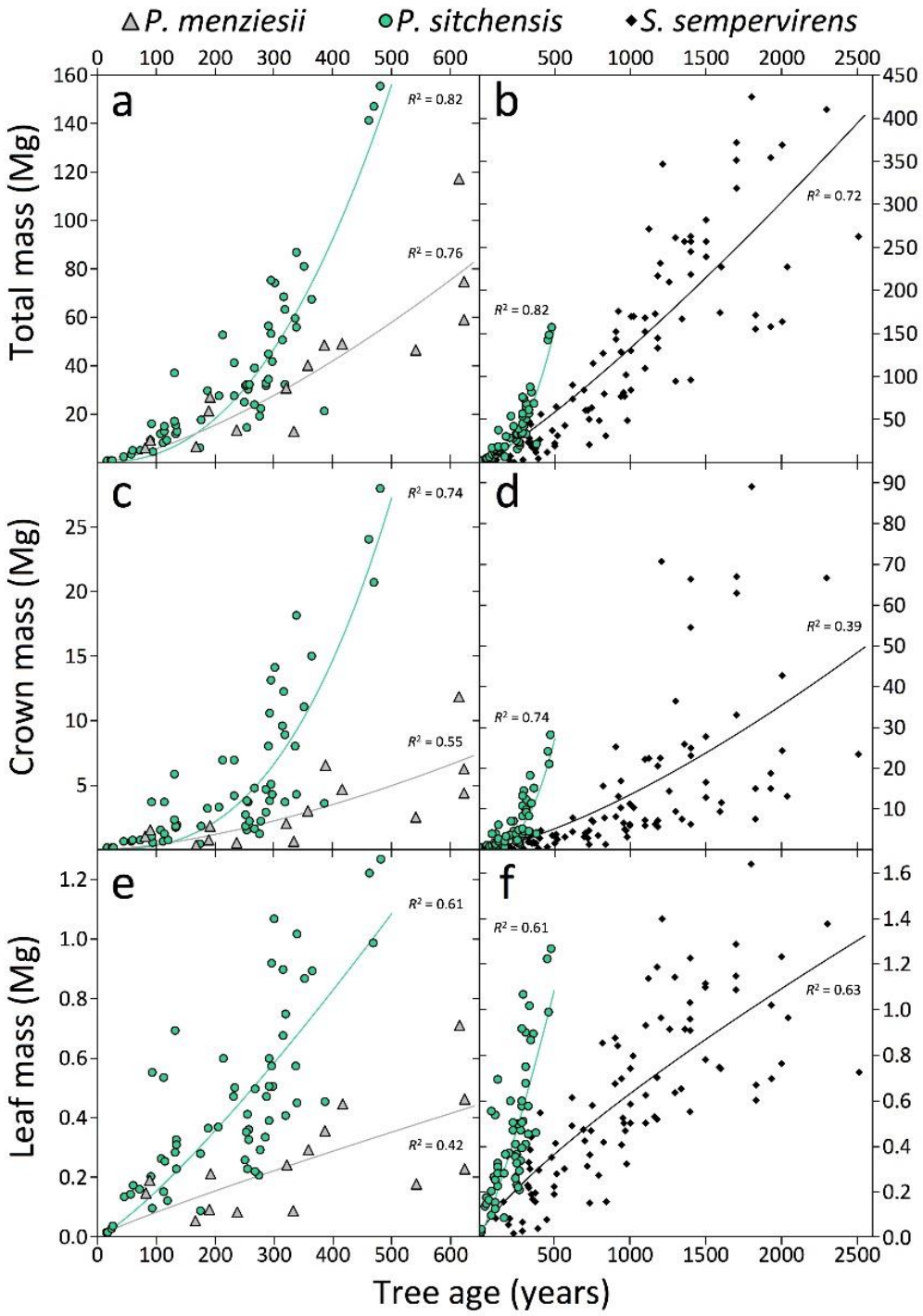

Figure 1.14. Biomass accumulation of *P. sitchensis* compared to *P. menziesii* (**left**) and *S. sempervirens* (**right**) showing aboveground total mass (**a**, **b**), crown mass (**c**, **d**), and leaf mass (**e**, **f**). Best power functions fitting mass data for each species (**Appendix 1.D**) are shown along with corresponding R^2. Data for *P. menziesii* from Sillett et al., 2018b, and data for *S. sempervirens* from Sillett et al., 2015b.

Chapter 2. NEIGHBORHOOD SCALE

Neighborhood competition mediates crown development of *Picea sitchensis* in Olympic rainforests: Implications for restoration management

Kramer et al., 2019. Forest Ecology and Management. 441, 127-143.

2.1 INTRODUCTION

Large trees are rarer and more structurally and ecologically important than small trees in forested ecosystems (Bauhus et al., 2009; Lindenmayer, 2016; Lutz et al., 2018, but see Fajardo et al., 2018). However, the ecological benefits ascribed to large trees are largely due to structural characteristics they accumulate with age such as increased heartwood, dead wood in the crown, and large appendages (Lindenmayer et al., 2014; Sheridan et al., 2013; Van Pelt et al., 2016). In the US and elsewhere societal interests in restoring and sustaining complex forest ecosystems with old-growth characteristics are broadening management objectives on public lands to include enhancing biodiversity and sustaining threatened and endangered species (Franklin et al., 2018; Skillen, 2015). Silviculturalists are responding with attempts to accelerate development of large trees and provide spatial heterogeneity through variable density thinning and variable retention harvests. The importance of large trees to biodiversity and increasing use of variable density treatments motivates the need to understand how forest density affects crown development in large trees.

Rich communities of arboreal plants and animals provide an important supplement to ground-based biodiversity, yet an explicit link between forest density and development of tree crowns has not been made. Critical to arboreal habitats are specific large and complex within-

crown structures lacking in young trees. Large appendages support communities of epiphytic lichens, bryophytes, and vascular plants as well as formation of canopy soils with high water-holding capacity (Burger et al., 2010; McCune et al., 2000; Nadkarni, 1981; Sillett and Van Pelt, 2007). Complex trees provide refugia for epiphytes when neighboring trees are logged, thus facilitating recolonization by dispersal-limited species (Ishii et al., 2018; Sillett et al., 2000). Recognition of the importance of tree structure for a variety of plants and animals including the threatened marbled murrelet (Brown et al., 2018; Carey et al., 1996; Forsman and Swingle, 2007; Hamer and Nelson, 1995; Hershey et al., 1998; Progar and Schowalter, 2002; Wunder et al., 1996) has inspired tree-level manipulations to improve habitat value of mature tree crowns (Sillett et al., 2018a). Since forest density controls crown size, it must also affect growth of appendages that provide critical habitats.

The current conceptual framework of crown development in tall conifers is generally applicable yet lacks incorporation of forest density. It essentially consists of three phases, here referred to as the canopy attainment phase, the crown building phase, and the decadent phase. The first is dominated by genetically predetermined architecture called *model-conforming development* (*sensu* Hallé et al., 1978), during which trees rapidly gain height and initiate original branches, defined as those produced from the treetop apical meristem. Apical dominance and apical control via hormones produced by the apical meristem inhibit bud break and reduce growth of lower branches, respectively (Cline, 1997), thus branches increase in age and generally in size with decreasing height to create a conical crown (Tomlinson, 1983). Shade in the lower crown slows growth or kills branches, forcing the crown base to rise (crown lift). During this phase and coincident with density-dependent tree mortality, some epicormic branches—those produced by the vascular cambium—arise to take advantage of shifting light

availability in the lower crown (Ishii et al., 2002), producing characteristic fans of branches and non-radial angles of attachment (Ishii and Ford, 2001; Pike et al., 1977). Crown structure amassed during canopy attainment sets the stage for further development.

A tree's crown-building phase is dominated by spatially-aggregated mortality and reiteration of model-conforming branches or secondary trunks in response to injury (Ishii et al., 2007; Van Pelt and Sillett, 2008). This is the longest phase and, therefore, most influenced by forest density. It begins when tree height growth and production of new original branches slows. During this phase roughly half of branches die, creating optimized vertical foliage spacing (Ishii and McDowell, 2002; Van Pelt and Sillett, 2008). The remaining long-lived branches continue to enlarge and develop. Trunks and branches are inevitably wounded over time and respond by reiterating structure as either epicormic branches or new trunks architecturally similar to a model-conforming tree (Van Pelt and Sillett, 2008). Repeated injury and reiteration leads to segmented appendages with abrupt changes in direction, diameter, and forks as well as broom-like appendages with fans of epicormic branches arising from a break (Kramer et al., 2014). Injury of the treetop and branches also promotes limb formation, here defined as a branch giving rise to a reiterated trunk (Sillett et al., 2018a). Limbs increase habitat because they become larger than branches, creating wider platforms (Sillett and Van Pelt, 2007; Van Pelt and Sillett, 2008). How these reiterative processes are affected by forest density remains unclear.

Onset and duration of the decadent phase are fundamentally determined by a species' decay-resistance. Since tree physiology does not fundamentally change with age (Lanner and Connor, 2001; Mencuccini et al., 2007, 2005), and age has little (if any) negative effect on tree-level growth after accounting for crown structure in the two largest species (Sillett et al., 2015b), the decadent phase is dominated by physical collapse due to decay. Many trees experience

periods when biomass declines even as growth continues, probably due to loss of crown portions through injury (Sheil et al., 2017; Sillett et al., 2015a). Once a tree is structurally compromised, it begins to shed appendages and portions of the main trunk, interrupting the crown-building process. Because model-conforming development is bereft of important habitat-related crown structures, and decadent trees are difficult to access safely, this study focuses on how forest density effects the crown-building phase.

Picea sitchensis is the focus of this study because it is a rapidly growing and large species whose ecology makes it especially responsive to neighborhood density. After 300 yr of development, *P. sitchensis* is 170% and 150% more massive than *Pseudotsuga menziesii* or *Sequoia sempervirens* and has 260% and 240% more leaf mass, respectively. It can also rival them in size, reaching > 90 m tall and > 400 cm trunk diameter (Kramer et al., 2018). *Picea sitchensis* coexists with other large dominant conifers by maximizing photosynthesis and growth at the expense of drought and decay resistance. Accordingly, *P. sitchensis* responds in basal area growth more to reductions in neighborhood density than *Tsuga heterophylla*, *P. menziesii*, or *Thuja plicata* (Roberts and Harrington, 2008). It is also relatively shade tolerant, able to reproduce in small gaps and survive under forest canopy (Maas-Hebner et al., 2005; Taylor, 1990) and thus can reach old age in a wide variety of light conditions.

Here we quantify structural development of *P. sitchensis* in Olympic rainforests during the crown-building phase, providing an explicit link between neighborhood density and specific within-crown structures in large trees. Four specific objectives are to: 1) identify effects of neighborhood density on timing, abundance, and size of specific appendage types at given tree ages; 2) provide a conceptual framework for crown development that incorporates neighborhood density; and 3) compare developmental aspects of *P. sitchensis* with the more frequently

managed *P. menziesii* and incorporate this with knowledge of how density effects crown development to provide management guidelines for accelerating development of large complex tree crowns in forests managed for old-growth characteristics.

2.2 METHODS

Apex *P. sitchensis* development is reached in British Columbia, Washington, Oregon, and California in inland river valleys and coastal regions with mild temperatures and a mesic climate (Burns and Honkala, 1990, **Table 2.1**). The primary study areas were in low lying glaciated river valleys on the Olympic Peninsula in Washington State (**Figure 2.1**). These valleys run from east to west and are backed by the Olympic Mountains, thus intercepting storm systems from the Pacific Ocean and receiving > 100 cm of annual precipitation, which almost exclusively falls outside of the summer months. Other study trees come from California, where they experience a similar climate regime (**Table 2.1**). In the primary study locations, a combination of fire (rare), expanding wind gaps, and migrating river channel disturbances in Olympic rainforests create a wide range of neighborhood densities from which to sample (Harcombe et al., 2004; Taylor, 1990; Van Pelt et al., 2006).

Table 2.1. Regional temperature and moisture regime for all 55 trees used in this study. The 36 trees from the Olympics region are crown- and plot- mapped, while the remainder are only crown-mapped. Summer is defined as the driest and hottest 3 months of the year (July to September) and winter as the wettest and coldest (December to February). Values are 30-yr means from the PRISM Climate Group for temperature (T) and rainfall (PRISM, 2018).

Region, state	*N*	Winter T °C	Summer T °C	Annual rain cm	Summer rain cm	Geomorphic position
Klamath, CA	4	8.2	15.2	195	5	Alluvial flats
Arcata, CA	4	9.0	14.9	121	3	Hillslopes to flats
Olympics, WA	47	4.5	16.1	289 – 428	24	Alluvial flats, upland swales

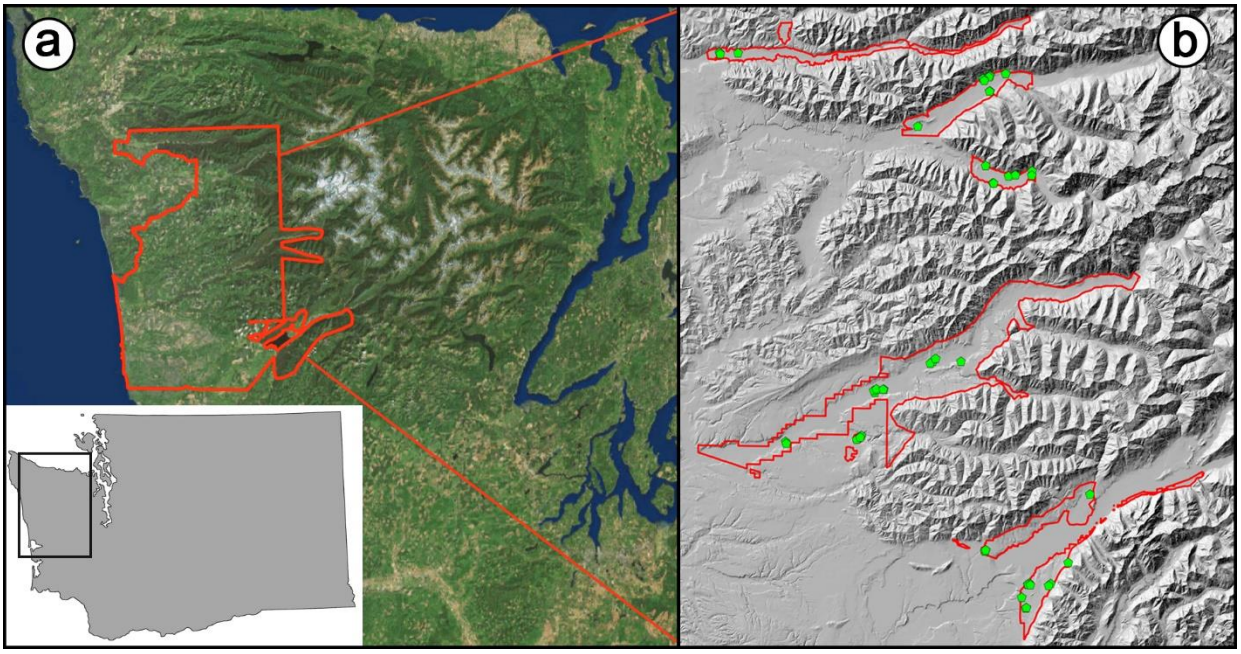

Figure 2.1. Map of the study region with inset showing the Olympic Peninsula in Washington State, USA. Panel (**a**) shows the region with LiDAR coverage used for sampling in orange outline, while (**b**) shows a digital elevation model with alluvial valley bottoms with LiDAR coverage and in old-growth forests in red. Sample trees are in green. Note some trees overlap each other at this scale.

2.1 Sampling design

The main objective of this study was to describe *P. sitchensis* crown development after the model-conforming phase, because trees generally do not display complex structure until that time. If we define this transition by the stabilization of crown lift, then the minimum tree height should be ~55 m. The height at which naturally established *P. menziesii* crowns cease to lift (Winter et al., 2002) was 50-55 m, similar to the height at which large appendages supporting soils and epiphytes were present in old-growth *S. sempervirens* forests (Sillett and Van Pelt, 2007). We had four specific sampling objectives. These were to: 1) include sites across the four major river valleys in the western Olympic Mountains; 2) sample trees > 60 m tall; 3) sample areas representing the full range of naturally occurring neighborhood densities; and 4) include trees with wide variation in crown structural complexity.

Existing point clouds from aerial light detection and ranging (LiDAR) scanning of the western Olympic Peninsula (PSLC, 2018) as well as a custom acquisition allowed us to limit the potential sample area. Overstory tree heights extracted from the point cloud with FUSION software (McGaughey, 2009) and GIS data layers in ArcMap (ESRI, 2014) limited potential study trees to those > 60 m tall, ≤ 10 km from a road, and ≤ 2 km from a trail in the Bogachiel, Hoh, Queets, and Quinault river valleys. During preliminary field excursions, *P. sitchensis* was only observed on alluvial terraces and upland swales. Accordingly, the sample area was further limited to valley bottoms and toe slopes from a LiDAR-derived digital elevation model in ArcMap (**Figure 2.1**). The resulting population encompassed 112,832 trees distributed over 1,946 ha, including *P. sitchensis* up to 91.7 m tall. A random ~15% sample was selected to represent the full range of tall tree heights and neighborhood densities in the population.

The ~12,000 trees from the previous step were then stratified by height and neighborhood density using LiDAR-based metrics to represent the desired sampling space. Tree height and canopy-relief ratio—(max-mean)/(max-min) of return heights—within 30 m around each tree were calculated using the cloud metrics tool in FUSION to represent a two-dimensional sampling space. The 30-m distance was based on a preliminary analysis of tree crown size in relation to metrics calculated at different plot diameters from LiDAR data (**Appendix 2.A**). Canopy relief ratio was selected from a suite of default FUSION output variables to represent neighborhood density based on visual inspection of random clipped plots (**Appendix 2.A**). Variability in neighborhood density around target trees was divided into five equal levels. Tree height growth slows with age, so tree ages range more widely within taller tree-height classes than shorter ones. A decreasing height interval based on *P. sitchensis* height-growth curves was used to stratify the sample to select trees among even age classes (60, 74, 83, and 90 m,

Appendix 2.A). Overlaying the 15% sample with these strata resulted in 13 populated bins, allowing up to three study trees in densely populated strata, two in less-densely populated strata, and enough leeway to select additional trees > 90 m if they were found (**Appendix 2.A**).

Selected trees were mapped onto this stratification to insure a well-distributed sample of 36 target individuals. Selection proceeded in three ways. The first four trees were re-sampled from a previous study of alluvial forest development (Van Pelt et al., 2006), because they were already safely rigged for climbing. Heights and neighborhood densities of these trees were back-calculated and plotted onto the sampling space. Digital LiDAR-canopy-height maps were overlain with a random selection of ~4,000 trees labelled by height and neighborhood density classes for field verification. Candidate trees were visited in each drainage to insure they were *P. sitchensis*, did not show outward signs of decay such as rot or basidiocarps making them unsafe to climb, and not having evidence of recent major disturbance (e.g., many fallen neighbors). If suitable, they were plotted onto the sampling space and removed from the target tree list. Lastly, because we had no LiDAR metrics to estimate crown structural complexity, especially complex trees were opportunistic selected (N = 5). As with the first four trees, heights and neighborhood densities were back-calculated and added to the sampling space. This process resulted in a regionally dispersed, yet locally aggregated sample of 36 trees (**Figure 2.1**, **2.2**).

2.2.1 *Field methods*

Field work proceeded in stages, allowing us to error-check data during collection. During the first stage, all selected individuals were climbed and strung with a loop of 3-mm-diameter black cord through a pulley at the top (**Appendix 1.C**). On the next visit, 30-m-radius plots were installed around each tree in which Cartesian coordinates relative to trunk center, diameter at the top of buttressing (DTB), lean distance and azimuth, height for trees < 30 m tall, and species of

all trees were recorded along with a temporary tag number. Trunk DTB and the height above average ground level of this measurement were recorded rather than more commonly measured diameter at breast height (DBH, 1.37 m) because many *P. sitchensis* and *T. heterophylla* trees germinated on logs and then engulfed them to reach mineral soil, creating highly buttressed bases (Van Pelt, 2007). Therefore, DTB was more representative of overall tree size (Kramer et al., 2018). If DTB was below DBH, such as in small trees, DBH was used instead. After this initial ground-work, cord in the central tree was replaced with a static climbing rope, and the tree was crown-mapped (Kramer et al., 2018) to determine locations, numbers, and sizes of all appendages. From the central treetop, all remaining treetops were located based on their ground-location measurements, and height was measured relative to a vertical tape using the vertical distance routine on a laser rangefinder (LaserTech™). These heights were later corrected for each tree's vertical displacement at ground level relative to the central tree. Finally, each tree including the central tree was systematically revisited to measure crown radius in four cardinal directions and crown base height. During this revisit all trees were checked for species and diameter errors, and all tree tags were removed.

Plot design—Concentric circular plots were installed around each study tree to quantify the density of potential competitors. All trees above a diameter threshold were measured using the following criteria of distance (m) from central tree and diameter (cm): $\leq$ 10 m and $\geq$ 5 cm, $\leq$ 17 m and $\geq$ 50 cm, $\leq$ 25 m and $\geq$ 75 cm, and $\leq$ 30 m and $\geq$ 100 cm, respectively (**Appendix 2.A**). Thresholds were determined using plot data from three *P. menziesii* forests previously sampled in the study region (Sillett et al., 2018b), by examining the distance various diameter and height trees were that cast shadows up to the average crown base height (30 m) on the center tree during the growing season (**Appendix 2.A**).

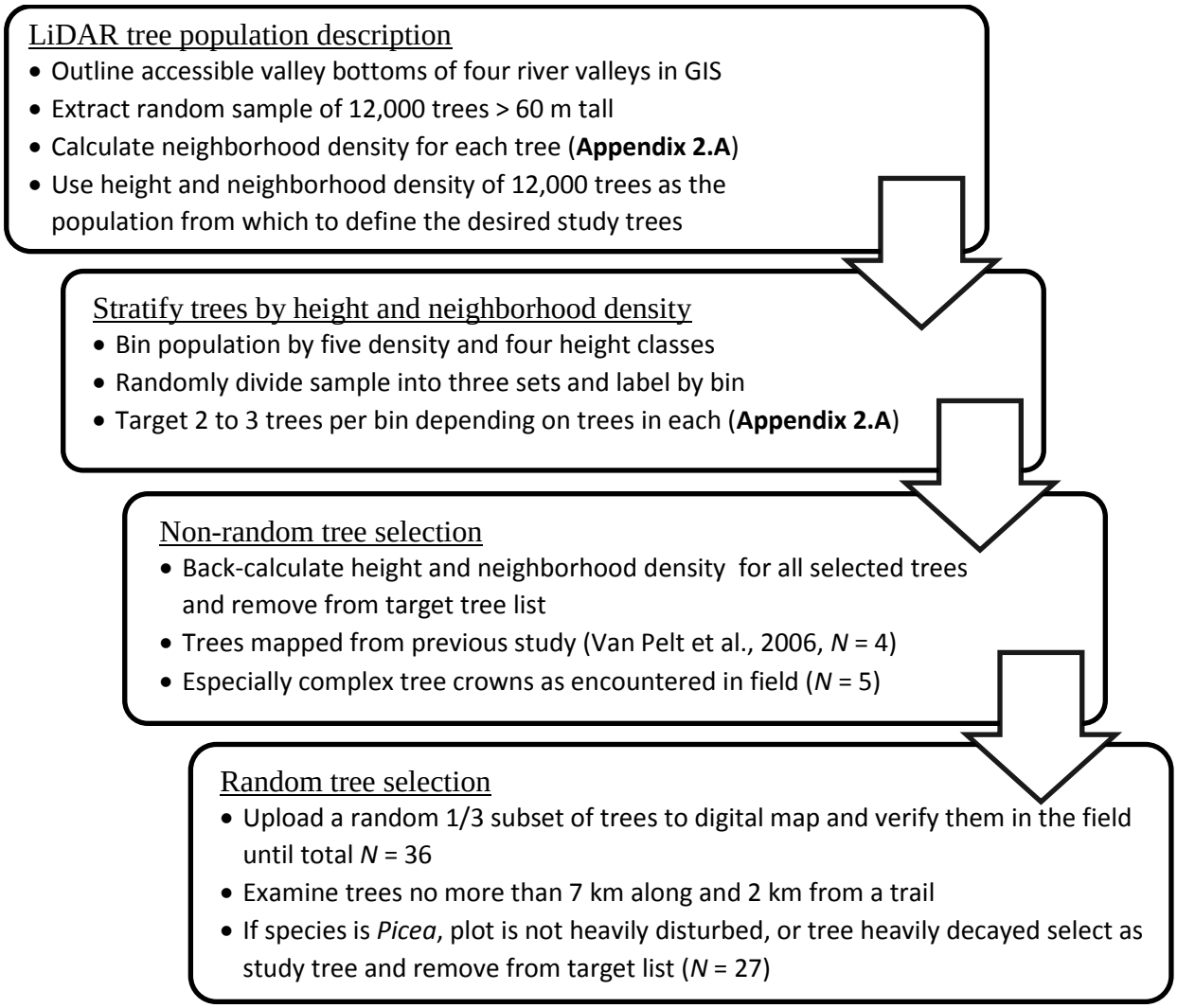

Figure 2.2 Sampling design to include the full range of naturally occurring neighborhood densities, tree heights > 60 m, and simple to complex crowns incorporated LiDAR-based methods in conjunction with field-based reconnaissance. More detail about the sampling design is in **Appendix 2.A**.

Within-tree measurements— To quantify crown complexity, three-dimensional structure of the main trunk and all appendages > 4 cm diameter was mapped as described previously (Kramer et al., 2018). To summarize, trunk lean distance, lean azimuth, and diameter were measured at ≤ 5 m height intervals. All model-conforming branches ≥ 4 cm diameter measured for height above ground, diameter, horizontal extension, azimuth, slope, classification as epicormic or original, percent dead, and name of origin (e.g., main trunk or node, see below). A

model-conforming branch adhered to the genetically determined architectural model (Tomlinson, 1983); in *P. sitchensis* this was a long single or evenly forked stem with small branchlets attached. Appendages with abrupt changes in direction or diameter indicative of past injury and those > 25 cm diameter were partitioned into segments giving rise to model-conforming branches. The height, diameter, distance from trunk, and azimuth from trunk center were recorded for proximal and distal segment ends (nodes) as well as percent dead, segment type (branch, limb, or trunk), and classification as epicormic or original. Lastly, on a random subset of appendages, paired diameters of moss mats and their supporting structure were taken (N = 332) to determine the minimum branch diameter necessary to create the ~14 cm platform diameter required for nesting by the threatened marbled murrelet (Hamer and Nelson, 1995).

A set of two increment cores were extracted at the top of buttress, 10, 30, 50, and 70 m along the main trunk as well as above and below any breaks indicated by distinct diameter reductions or direction changes. If the trunk was small enough to core and reach cambium on the opposite side, only one core was extracted. Upon extraction, we measured the wet-wood length of the first 154 cores, sapwood and bark thickness, and recorded azimuth, height, and tree diameter at each core location. These measurements were used to develop wood shrinkage scalars and estimates of internal tree tissue volumes as described previously (Kramer et al., 2018).

2.2.2 *Metric calculation*

Plot-level variables were designed to summarize neighborhood competition between trees and to determine if simple metrics could substitute for those already published, and thereby be more useful to managers. We included two standard forestry metrics of tree density (basal area and trees per hectare), two published metrics predictive of tree growth response (horizontal angle

and distance-dependent crown volume; Contreras et al., 2011; Coonen and Sillett, 2015), modifications of these (e.g., azimuth-weighted horizontal angle and basal area of trees ≥ 80% of study-tree diameter), as well as 12 simplified metrics (**Appendix 2.A**). Distance-dependent crown volume was the amount of neighbor tree crown volume in a 60° inverted cone extending from the crown base of the focal tree, horizontal angle was the amount of horizontal angle around the center tree blocked from view by neighboring trunks, while azimuth-weighted horizontal angle weighted the contributions of trees increasing from northeast to southwest (**Appendix 2.A**).

Within-tree calculations— Field data were used to calculate Cartesian coordinates of all crown structures as well as their volumes, masses, and surface areas. Prior to calculation, models for each tree were screened using *SITCHENSIS* (https://github.com/northcoastmountainrat/Sitchensis; Kramer et al., 2018), a programmatic tool for 3D rendering of tree structures. Typical data quality problems were evident in disjointed appendage renderings or obvious diameter discrepancies of connected tree parts due to faulty data entry. After screening, final coordinates, diameters at ends of appendage segments and branch bases and percent dead data were exported from *SITCHENSIS* for whole-tree summaries. These consisted of computing wood and bark volumes and surface areas of trunk sections and appendage segments as conic frusta. Volumes were converted to masses using tissue-specific dry-mass-to-fresh-volume ratios (Kramer et al., 2018). For branches, a diameter-specific equation was applied to the whole-branch inventory to estimate whole-branch volumes and masses based on 48 dissected branches of varying height and diameter (Kramer et al., 2018). Branch, segment, and trunk quantities were then summed for each tree to compute aboveground quantities of leaves, bark, cambium, sapwood, and heartwood.

All tree cores were prepared in the lab before being analyzed with standard dendrochronological techniques. Dry cores were glued into grooved wooden slats and length of each core was measured to develop a scalar for converting dry wood radius to fresh as 1.02501 x dry (R^2 = 0.9998, N = 154). Cores were then sanded with progressively finer sandpaper (80 to 1100 grit) until annual rings were easily distinguishable. Cores were cross-dated and marked under a dissection scope, scanned at 1200 dpi, and measured with CooRecorder (Cybis Technologies). Crossdating was confirmed using detrended ring-width plots with a 30-yr cubic smoothing spline in CDendro (Cybis Technologies) and COFECHA (Grissino-Mayer, 2001). This was first done within each tree before checking the cumulative tree chronologies against a master chronology that included all previously cross-dated trees. Raw ring widths for each tree were then consolidated for analysis of trunk and appendage ages. Estimating trunk age at multiple heights including at ground-level with cores from along the trunk that do not reach pith has been described previously (Sillett et al., 2018b; Kramer et al., 2018). A description of trunk and appendage age estimation is also included in **Appendix 2.A**.

Whole-tree summaries— Macro-characteristics of tree size and amount of available horizontal surfaces were first calculated for each tree to examine the increase of these metrics across the chronosequence irrespective of neighborhood density (**Table 2.2**). Crown volume was calculated as a paraboloid based on crown depth and average crown radius, total mass was computed as the sum of all aboveground components, and crown mass was total mass minus main-trunk mass. Horizontal surfaces were calculated as 1/3 the surface area of all appendages if their average slope was within 30˚ from horizontal for > 4 and > 10 cm diameter stems. If segment end diameters spanned one of these thresholds, the geometric mean of its end diameters provided a cutoff value for whether or not to include the segment. Separate equations were

applied to branches to predict surface area (m^2) of > 4 or > 10 cm diameter portions (> 4: SA = 0.050 x (diameter – 4)$^{1.668}$, N = 45, R^2 = 0.68; > 10: SA = 0.073 x (diameter – 10)$^{1.539}$, N = 22, R^2 = 0.75). All appendage horizontal surface areas were then summed and divided by the crown projected area (π x crown radius^2) to compute the horizontal surface index (HSI).

Counts of ten specific within-crown structures and appendage diameters relevant to development and canopy habitat were summarized for each tree (**Table 2.2**). Epicormic and forked appendages were chosen to represent the first expected deviations from model-conforming development. These were followed by large appendages defined as > 10, > 15, and > 20 cm diameter. The lower limit was chosen based on the minimum diameter stem capable of supporting a moss mat large enough (~14 cm) for murrelet nesting (branch diameter = 1.37 x (dry moss + branch diameter)$^{0.748}$, N = 332, R^2 = 0.71, **Appendix 2.B**). Clusters of large appendages, brooms, and fans were all typified by concentrations of stems (**Figure 2.3bce**, **Table 2.2**) and supported large quantities of moss and direct observations of animal use during mapping (**Appendix 2.B**). Brooms were distinguished from fans by a concentration of stems originating from the location of a break > 1 m from the trunk on a single appendage, whereas fans were defined by multiple distinct branches arising from the main trunk or from short appendages < 1 m from it in a fan shape (**Figure 2.3c**). Trunk reiterations and limbs were chosen because they are associated with large platforms and are the most conspicuous element of complex tree crowns (**Figure 2.3afg**, **Table 2.2**). Last, to account for appendage diameter shifts with neighborhood density, the mean diameter and the 90th percentile diameter of all appendages were calculated for each tree.

Table 2.2. Tree-level dependent and independent variables for describing effects of neighborhood density on crown development.

Variable	Units	Description
Dependent variables for analyses of macro-characteristics		
Crown volume	m^3	1/3 x π x (crown radius)^2 x (crown depth)^2
Total mass	Mg	Sum of trunk, branch and leaf mass (Kramer et al. 2018)
Horizontal surface area index (HSI)	—	Calculated at > 4 and > 10 cm for appendages with average slope between –30 and 30°, 1/3 surface area of appendages/projected crown area
Percent crown mass	%	Crown mass/Total mass * 100
Height	m	Tape measured tree height
Crown base height (CBH)	m	Height at which live appendages extend 1/3 around the trunk
Dependent variables for assessing operative neighborhoods		
Trunk form	cm/m	DTB/Height
Crown ratio	—	(Tree height – CBH)/Tree height
Crown radius	m	Average of 4 cardinal radii from trunk center to crown edge
Dependent variables of within-tree structure		
Epicormic appendages	count	Branches arising from vascular cambium, younger than tree at branch height and often attached at acute angles to trunk (Ishii et al. 2002)
Forking	index	Forking score summed at appendage-level, based on notes for branches (forked = 1, highly forked = 2, very highly forked = 3) and structure for attached segments (# of unique distal nodes – 1)
Large appendages	count	Appendages from main trunk > 10, 15, and 20 cm diameter
Clusters	count	≥ 2 appendages from main trunk > 10 cm diameter, within 0.8 m vertical, 0.4 m horizontal, and 45° azimuth
Brooms	count	Appendages with ≥ 3 branches from a common point > 1 m from the trunk (**Figure 2.3**)
Fans	count	Clusters of ≥ 3 appendages, < 1 m from the trunk, < 5° apart, and within 0.3 m vertical distance
Reiterated trunks	count	Reiterated trunks from main trunk or from appendage
Limbs	count	Appendage giving rise to a reiterated trunk
Mean appendage diameter	cm	Mean diameter of all appendages for each tree
90th percentile appendage diameter	cm	Diameter of 90th percentile diameter for each tree
Dependent variables for describing developmental framework		
Surface area of appendage types	m^2	Surface area predicted for all crown components > 4 cm diameter, b = model-conforming branch, B = segmented appendage, L = segmented appendage giving rise to reiterated trunk, T = reiterated trunk from trunk of limb, D = dead of any type
Independent variables for describing tree development		
Age	yr	Intercept of linear model of height and age for aged trunk heights using tree cores
Density	—	Linear combination of forest density metrics, scaled from 0–1 (**Table 2.5)**
Appendage damage index (ADI)	—	Sum of damage rating on each appendage, see **Appendix 2.A** for rating heuristic
Top damage index (TDI)	—	Sum of ratio of top break and tree DTB for all observed breaks

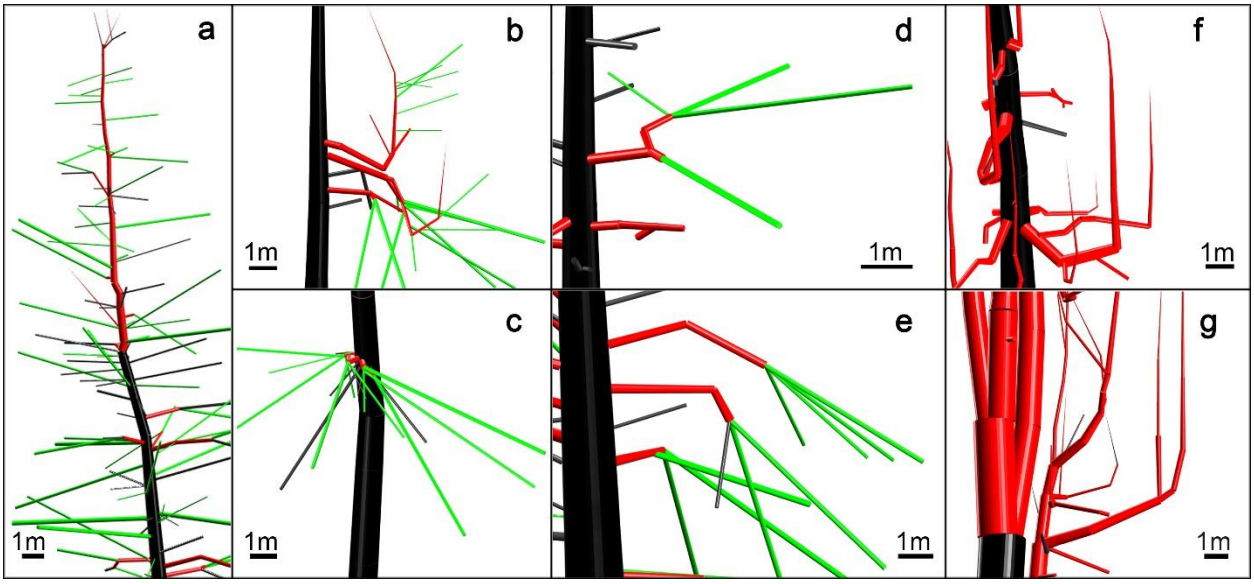

Figure 2.3. Field data are rectified into 3D models to visualize their structure as a composite of multiple conic frusta. Magnified views of specific crown structures in **Table 2.2** are isolated from models to demonstrate unique characteristics: (**a**) treetop replacement with kinks at subsequent breaks, (**b**) appendage cluster, (**c**) fan, (**d**) segmented branch, (**e**) brooms, (**f** and **g**) limb and trunk systems with branches removed for clarity. Trunks are black, segments red, model-conforming branches green, and dead gray.

Some structure types most likely resulted from injury to the main trunk, such as trunk reiterations (Sillett et al., 2018a), or to appendages, such as brooms. We developed a top damage index (TDI) and appendage damage index (ADI) to account for such injuries. TDI was the sum of all mapped main trunk-break-diameter-to-DTB ratios for each tree to represent cumulative damage. For example, in **Figure 2.3a**, past break diameters are at locations of connections between main trunk (black) and reiterated trunk (red) and at each obvious kink along reiterated trunks. Diameter at each location was divided by DTB and all ratios were summed to obtain tree-level TDI. ADI was the sum of a damage rating for each appendage. Appendages were defined as all branches and segments attached to each other and arising from the main trunk (**Figure 2.3d**) or as un-segmented branches arising from the main trunk (green cylinders attached to trunk **Figure 2.3a**). The rating was based on notes of damage to all live segments and branches of an

appendage such as “cracked” and “broken and recovered.” An appendage was also considered damaged if its distal diameter was > 0 cm with nothing attached or no more than one branch attached with a > 50˚ change in direction from the segment trajectory. In these cases, the damage rating was increased according to the ratio of its end diameter and diameter of the segmented appendage base (see **Appendix 2.A** for full rating heuristic). To avoid circularity between these damage indices and dependent variables, no reiterated trunks that were not a continuation of the main trunk were included in TDI, likewise, information parsed from structure and notes to formulate ADI were not used to distinguish each appendage type (**Table 2.2**, **Appendix 2.A**).

Choosing the scale with which to define a conceptual model of crown development was finding a balance between too little detail to be meaningful and so much data as to be impractical. Summarizing solely by counts of appendages or mean appendage size ignored how complex individual appendages were, while examining each specific appendage (e.g., brooms, fans, clusters) was unnecessarily complex. The developmental model was defined by tree-level surface area of appendages > 4 cm diameter in five broad structure classes. The classes were model-conforming branches (b), branch segments without reiterated trunks (B), limbs (L), reiterated trunks (T), and dead of any category (D).

2.2.3 *Analysis*

A supplementary dataset of 19 crown-mapped *P. sitchensis* trees, 11 from a previous study along the Queets river (Van Pelt et al., 2006), 4 near Arcata, California, and 4 near Klamath, California (Kramer et al., 2018) were added to expand the sample size from 36 to 55 for analyses not including neighborhood density. Ages of these trees were estimated using the same method as above but with the full wood radius treated as unaged for 14 un-cored trees. Of the 19 added trees, 9 were smaller and 11 were younger than any in the 36-tree dataset. The

smallest tree (ranked by total mass) was 18 yr old and 10.0 m tall, and the largest was 297 yr old and 90.6 m tall.

All analyses were performed with the statistical programming language R (R core team, 2018). Parametric models (i.e., those not incorporating loess smoothing) were checked for violations of assumptions by examining normal probability plots, heteroscedasticity, leverage, and non-random residual patterns. Appropriate transformations and distributions using generalized linear models were chosen for non-normally distributed dependent variables or for relationships showing excessive leverage or systematic lack of fit (**Table 2.3**).

Table 2.3. Modeling overview showing dependent and independent variables, statistical techniques, and dataset for each step. For description of tree-level variables see **Table 2.2** and for plot-level variables see Table 4 of **Appendix 2.A**. Steps are highlighted gray.

Dependent variables	Independent variables	Method and distribution	*N*
Overall trends ignoring density			
Crown volume, total mass, HSI, crown mass, height	Age	Quadratic loess smoothing using a span parameter of 0.75	55
Tree-level presence/absence of: > 10, 15, and 20 cm diameter, forked, clusters of large, broomed, epicormic spray, limb, and trunk appendages	Age	Linear regression, Binomial	55
Describing operative neighborhoods			
Trunk form, crown radius, crown ratio	Plot-level metrics calculated at 5-m radii intervals (**Appendix 2.C**)	Linear regression, compared via AICc, Normal	36
Density effects on macro-features			
Crown volume, total mass, HSI, crown mass, height, CBH	Age + Density and Total mass + Density, Tree height + Density for CBH	Linear regression, Lognormal	36
Density defects on within-crown features			
Quantity of: > 15 and 20 cm diameter, forked, clusters of large, broomed, epicormic spray, limb, and trunk appendages	Age + Density + TDI + ADI	Hurdle model, Poisson	36
Presence/absence of same variables as above	Age + Density + TDI + ADI	Hurdle model, Binomial	36
Mean appendage diameter, 90^{th} percentile appendage diameter, count > 10 cm diameter	Age + Density + TDI + ADI	Linear regression, Normal	36
Describing conceptual model of development			
Surface area of appendage types b, B, L, T, and D	Age + Density + TDI + ADI	Linear regression, Gamma	36

Baseline for development—Analysis of tree development irrespective of neighborhood density utilized the 55-tree dataset to provide a reference for the effects of density. Patterns of crown development were described using plots of tree age against the loess-smoothed values of six macro-features (**Table 2.3**) to create locally-weighted estimates based on the quadratic fit of a 75% span of the data. Additionally, expected tree-age thresholds for presence of specific habitat-related structures were modeled with logistic regression and a binomial distribution (estimated dispersion < 1) after converting structural quantities to presence-absence data (**Table 2.3**). From these fitted models, tree age at which the probability of having a particular structure was 0.5 was calculated as $-a/b$ based on solving the algebraic logistic function of $\log(p/(1-p)) = a + (b \times \text{Age})$ for Age. This value was interpreted as the tree-age threshold for the presence of that structure.

Quantifying neighborhood density— Determining which neighborhood density variables influenced tree development and at what scale was a two-stage process using the 36-tree dataset. We chose the response variables of trunk form, crown radius, and crown ratio (**Table 2.2**, **2.3**) to evaluate the effectiveness of 20 possible metrics (**Appendix 2.C**), because all three responded to increasing neighborhood density in previous work (Rouvinen and Kuuluvainen, 1997; Sumida et al., 2013; Thorpe et al., 2010). In stage 1, 20 linear models for each dependent variable based on each density metric calculated at a 30-m radius. These were winnowed by ranking them using Akaike's information criterion corrected for small sample sizes (AIC_c), retaining only the top five models from each set, then selecting only those that occurred in two of the three sets resulting in four models. These density metrics were used in stage 2 for determining the most influential radius for *P. sitchensis* neighborhoods. In stage 2, the top density metrics were recalculated at 5-m intervals from 10–30 m and used to predict trunk form, crown radius, and

crown ratio. Again, the relative AIC_c ranking of models within each dependent variable was examined to determine which neighborhood distance was most influential.

A composite metric of neighborhood density was extracted from the data with a principal component analysis. Input variables were scaled, centered, and transformed so that each had equal influence and so that skew and kurtosis were < 3 to reduce leveraging effects of a single variable. This analysis included the four density metrics identified above as well as three metrics related to forest development, including the standard deviation of basal area, dead basal area, and basal area of shade-tolerant species. The principal component explaining the most variability in the data and most heavily weighted by the four previously identified variables was scaled between 0 and 1 and used to represent neighborhood density (hereafter Density in figures and tables) in all subsequent analyses.

Neighborhood effects on tree crowns—Expectations from modeling basic developmental trends were modified by incorporating neighborhood density to examine its effects on crown development. Neighborhood density was only quantified in the 36-tree dataset, so these trees were used for all subsequent analyses. Crown volume, total mass, HSI > 4 and > 10 cm diameter, percent crown mass, and height were modeled with linear regressions based on tree age and neighborhood density. Crown base height (CBH) was also modeled but instead of using tree age and density, we used height and density because CBH was unaffected by age within the range of our sample. All response variables were natural-log transformed except CBH to normalize right-skewed distributions. The tree age predictor was also natural-log transformed to create a power relationship to dependent variables except in the crown volume model, where it was allowed to have an exponential relationship. Because models of transformed variables can return unreliable

R^2, in all cases predicted and then back-transformed values and actual values were used to calculate R^2.

A common approach described in this paragraph was taken in all subsequent analyses unless otherwise noted. A set of multiple models derived from combinations of predictors (**Table 2.3**) were compared by ranking them according to AIC_c weights, which were computed as ratios of each model likelihood to the sum of all likelihoods. Models with small changes (≤ 1) in likelihood and changes in AIC_c close to 2 and only differing by the addition a new parameter relative to a simpler model were removed from the model set, and AIC_c weights were recalculated (Burnham and Anderson, 2002 p. 131). The highest-ranked model in which all coefficients were significant was then retained for making inferences. As with previous analyses, R^2 was calculated based on predicted and actual response variables in cases where models used a link function (see below).

Effects of tree age, neighborhood density, and injury on within-crown structure were assessed by comparing regression models of crown structure presence, abundance, and diameter (**Table 2.2**). Presence and abundance of crown structures were evaluated using hurdle models to account for zero-inflated data (i.e., more zeros than expected because zeros were due to more than one process) with the pscl package in R. The full hurdle model comprised a logistic regression to account for structure presence or absence and a Poisson regression with a log link to model positive structure counts. Since dispersion parameter was < 1, these were modeled with binomial rather than quasi- binomial and Poisson distributions. Both logistic and Poisson models were selected using AIC_c from a set of models in the same manner as previously described. Comparison models used different combinations of tree age, neighborhood density, TDI, and ADI as predictors (**Appendix 2.C**). The logistic portion of these models allowed us to examine

the shift in tree-age thresholds due to neighborhood density in structures for which age and density were both important. Likewise, mean appendage diameter and the 90th percentile appendage diameter were modeled with combinations of the same predictors via linear regression. Counts of > 10-cm-diameter appendages were present in all but one tree and were normally distributed, so they were also modeled via linear regression (**Table 2.3**).

Our empirically-based conceptual framework involved modeling surface areas of appendages in five types (b, B, L, T, and D, **Table 2.2**) and comparing outputs of these models at 20% and at 80% of maximum neighborhood density. Dependent variables were right-skewed and positive, so we used generalized linear models assuming a gamma distribution with a natural-log link function. We used independent variables of tree age, neighborhood density, ADI, and TDI and stepwise AIC_c regression to find the best predictive models. This framework was designed to express development as a linear function of tree age. Necessary increases of ADI and TDI with tree age were modeled with a log-log linear regression after adding 0.01 (to avoid the log of 0) to both damage indices to create a power functions of age. This step gave reasonable estimates of damage levels given tree age for predicting surface areas of components requiring ADI or TDI as input variables.

2.3 RESULTS

2.3.1 *Developmental trends irrespective of neighborhood density*

Structure is steadily and rapidly accumulated in *P. sitchensis* from 18 to 389 yr of age during which time trees transitioned to allocating more resources to appendages and less to height growth after ~200 yr. Based on trends from loess-smoothing of structural variables without considering neighborhood density, crown volume expanded from ~850 m^3 in the first 50 yr to ~2100 m^3 by the first century, and by 300 yr had doubled this again to approximately ~5300

m^3 (**Figure 2.4**). Likewise, aboveground mass increased from 3.2 Mg in 50 yr to 10, 22, and 45 Mg in 100, 200, and 300 yr, representing 320, 220, and 200% increases between these ages, respectively. Mass increase remained high through old age, and the increase was 134% between 300 and 380 yr. Horizontal surfaces > 4 cm diameter reached 47% and those > 10 cm diameter reached 17% of crown projected area (**Figure 2.4**). Average crown projected area of trees > 50 m tall was 167 m^2, and maximum was 392 m^2, thus appendages > 4 cm diameter provided 79 to 184 m^2 of horizontal surface area while stems > 10 cm diameter provided 29 to 67 m^2 of horizontal surface area in average and largest trees, respectively. Notably, the proportion of area in > 10 cm branches was negligible before trees reached 100 yr. In contrast to whole-tree mass, volume, and horizontal surface area, percent crown mass decreased from around 26% at 18 yr until a nadir of approximately 10% at 200 yr before reversing this trend and reaching 19% by 380 yr. The reversal in proportion of crown mass was roughly coincident with attenuation of height growth around 200 yr (**Figure 2.4**).

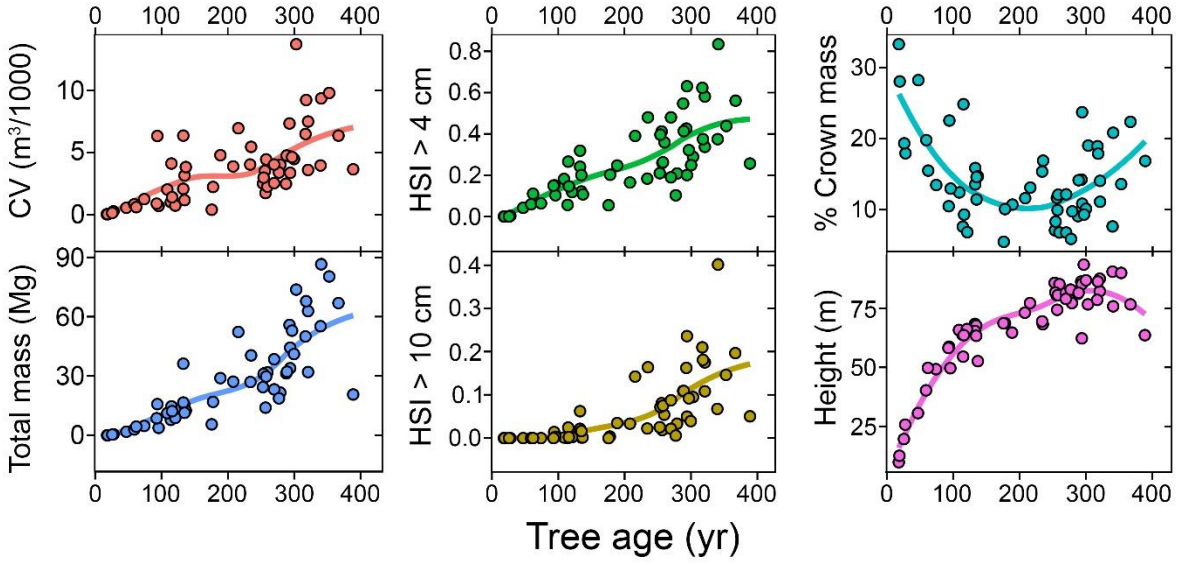

Figure 2.4. Whole-crown and tree-level attributes plotted against age for 55 crown-mapped *P. sitchensis* trees. Lines are quadratic loess-smoothed estimates using a span parameter on 0.75 in statistical program R. CV = crown volume and HSI = horizontal surface index (**Table 2.2**).

The largest and most important ecological structures (**Appendix 2.B**) first appeared in trees after ~150 yr and progressed steadily until 290 yr based on the full 55-tree sample. Intercepts on logistic threshold models were insignificant for epicormic appendages, counts of appendages > 10 cm diameter, and marginally significant for appendages with forks; however, in all models the coefficient on age was significant and positive (**Table 2.4**). For all remaining appendage types, intercepts and age were significant (**Table 2.4**). Precise coefficient estimates allowed us to calculate the tree age at which the probability of having a particular crown structure or not was 0.5. These calculations suggested a progression from the appearance of forked appendages after 80 yr, > 15 cm diameter and trunk appendages (including reiterated trunks from the main trunk) after 150 yr, large clustered appendages after 170 yr, brooms after 210 yr, > 20 cm diameter appendages after 218 yr, limbs after 260 yr, and, finally, fans after 290 yr (**Table 2.4**).

Table 2.4. Coefficient estimates for logistic models to predict presence of a structure based on age of 55 *P. sitchensis* trees. Thresholds are tree ages at which probability of having a structure is 0.5, calculated as – intercept/age coefficient. SE = standard error.

Appendage structure	Intercept	SE	*P*	Age	SE	*P*	Age threshold
Epicormic	–1.03	0.85	0.2240	0.019	0.007	0.0060	53
> 10 cm diameter	–1.69	1.07	0.1160	0.029	0.011	0.0092	57
Forked	–1.53	0.81	0.0597	0.019	0.006	0.0014	81
> 15 cm diameter	–3.19	0.94	0.0007	0.021	0.005	0.0001	151
Reiterated trunks	–2.29	0.78	0.0034	0.015	0.004	0.0001	152
Clusters of > 10 cm diameter	–2.81	0.85	0.0010	0.017	0.004	0.0001	170
Brooms	–7.33	2.08	0.0004	0.035	0.009	0.0001	209
> 20 cm diameter	–4.65	1.26	0.0002	0.021	0.005	0.0000	218
Limbs	–8.91	2.89	0.0020	0.034	0.011	0.0013	260
Fans	–3.39	1.03	0.0010	0.012	0.004	0.0029	290

2.3.2 *Describing operative neighborhoods*

Best descriptors of neighborhood density were heavily weighted towards the largest and closest trees within 25 m and had analogues with very simple neighborhood descriptors. Three sets of models, where each set used the same suite of neighborhood density variables calculated for a 30-m-radius plot, were evaluated for predicting trunk form, crown ratio, and crown radius. Top five models in each set explained and average of 55, 39, and 45% of the variability, respectively (**Appendix 2.C**). Counts of competitive trees, horizontal angle, SW-weighted horizontal angle, and competition-free distance were common metrics in the top five models of each set (**Appendix 2.C**). These were more important than standard metrics of basal area and TPH, each of which carried < 1% of total model weight in all model sets (**Appendix 2.C**). The SW-weighted horizontal index of neighborhood density in model sets to predict trunk form, crown ratio, and crown radius was 0.7, 0.2, and 1.3 times as likely as horizontal angle and always occurred in models cumulatively holding 90% of total AIC_c model weight. Top metrics computed at 5-m-radius intervals and compared to each other showed that the most influential neighborhood distance was 25 m for trunk form, 15 m for crown radius, and 30 m for crown ratio based on relative model rankings (**Appendix 2.C**). For all subsequent analyses, neighborhood density metrics were computed using a 25-m radius.

Three principal components describing the largest tree competitors, variability in tree sizes and dead wood, and basal area of shade tolerant species explained 87% of variability in the data. The first principal component (PC1) explained 53% of the variability and was evenly loaded (r = 0.49) by the four best neighborhood density variables identified in the previous analysis (**Table 2.5**). The second principal component (PC2) explained 23% of the variability and was heavily loaded by standard deviation of diameters as well as basal area of dead trees (r =

0.65). The third principal component (PC3) explained 11% of the variability and was highly correlated (r = –0.89) with basal area of shade tolerant species. Because PC1 explained a substantial amount of variability in trunk form ($P < 0.001$, $R^2 = 0.66$), crown radius ($P < 0.001$, $R^2 = 0.57$), and crown ratio ($P < 0.001$, $R^2 = 0.36$) while the other principal components did not (minimum $P > 0.23$, maximum $R^2 < 0.01$), it was used in all future analyses to represent neighborhood density. Higher density was associated with smaller DTB-to-height ratio, narrower crown width, and shorter crown depth.

Table 2.5. Principal components of plot-level variables. Correlations (r) of principal component (PC) are shown with strongest for each variable in bold. PC1 is used to represent neighborhood density in all subsequent analyses. Shade-tolerant species include *Tsuga heterophylla*, *Thuja plicata*, *Acer circinatum*, *Abies amabilis*, and *Abies grandis*. SD = standard deviation.

Variable	Transformation	Skew	Kurtosis	PC1	PC2	PC3
Competition-free distance (m)	square root	0.04	2.29	**–0.46**	0.14	0.02
Competitive trees (count)	square root	0.62	1.96	**0.50**	–0.12	0.12
Horizontal angle (°)	ln	–0.19	2.30	**0.50**	–0.17	0.10
SW-weighted horizontal angle (°)	ln	0.21	1.96	**0.48**	0.08	0.19
SD of basal area (m^2)	—	0.19	2.94	–0.06	**–0.65**	–0.09
Dead basal area (m^2)	—	0.47	2.63	0.08	**0.64**	0.37
Basal area of shade tolerants (m^2)	—	0.10	1.74	0.25	0.32	**–0.89**
Proportion of variance explained (R^2)	—	—	—	**0.53**	**0.23**	**0.11**

2.3.3 *Neighborhood density controls expression of crown complexity*

Macro characteristics—Neighborhood density strongly decreased all macro-characteristics describing basic patterns of development except for height, which increased slightly. Density and tree age alone explained from 41 to 73% of the variability in models predicting crown volume, total mass, horizontal appendage surfaces, percent crown mass, and

height (**Figure 2.5**, **Appendix 2.C**). In all variables except height, neighborhood density was more important than age and was negatively correlated with tree size. Holding tree age constant at 250 yr, models resulted in 34% reductions on crown volume, 26% reductions in total mass, 23% and 44% reductions in horizontal surfaces > 4 and > 10 cm diameter, respectively, and 25% reductions in percent of crown mass per 25% increase in neighborhood density. Conversely, height increased 3% per 25% increase in density. Reflecting the crown volume reduction, crown base height was significantly higher with higher density after accounting for tree height, increasing 2.2 m for each 10% increase in density (**Appendix 2.C**).

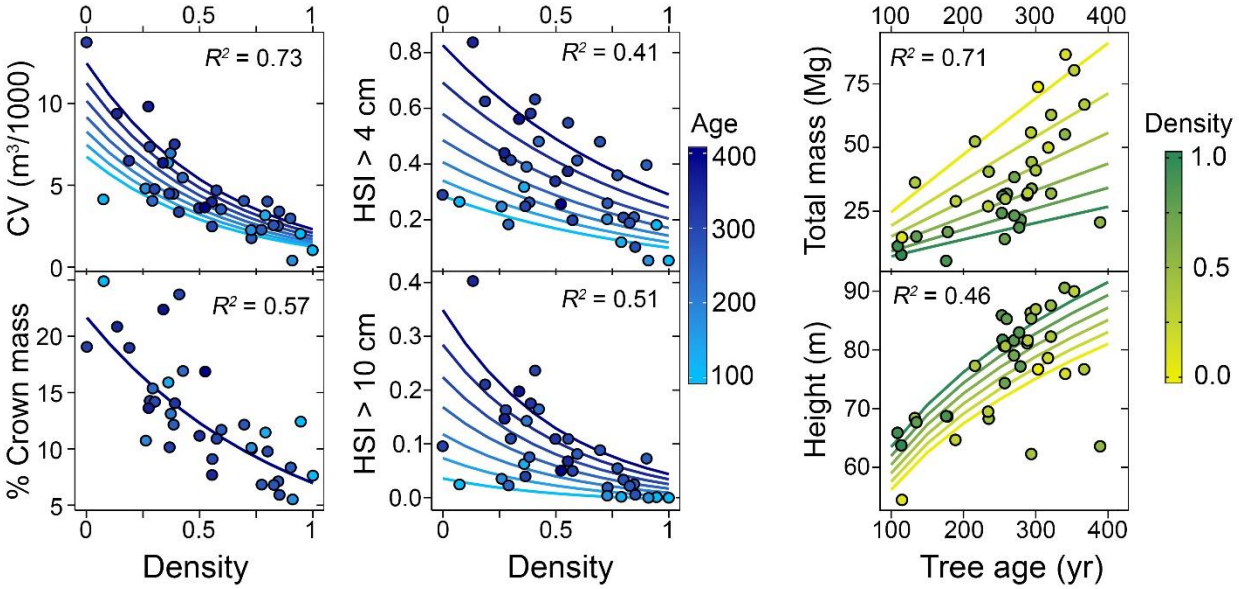

Figure 2.5. Whole-crown and tree-level attributes from 36 *P. sitchensis* trees with respect to age and neighborhood density. Density is on the x-axis when it is the dominant predictor. Models are presented in Table 5 of **Appendix 2.C**. Age is the dominant predictor for height and nearly even with density for total mass. CV = crown volume and HSI = horizontal surface index (**Table 2.2**). Outliers in height graph are broken-top trees discussed in **Appendix 2.D**.

Within-crown characteristics—The logistic portion of hurdle models for appendage abundance indicated that neighborhood density decreased and injury increased age thresholds for presence of within-crown structures in which they were important predictors. This set of models did not include epicormic, > 10-cm-diameter, or forked appendages because in the 55-tree dataset they occurred earlier in development than the youngest of the 36 trees (109 yr, **Table 2.4**). These models were unable to detect an additional effect of density on the presence of reiterated trunks, limbs, brooms, or fans (**Table 2.6**). Clusters of appendages were negatively associated with density and not at all with age (**Table 2.6**), having none beyond 70% of maximum density. In both > 15 and > 20 cm diameter appendage models, age was positively correlated (P = 0.020, 0.043), while density was negatively correlated (P = 0.048, 0.008) with structure presence, although the intercept was insignificant (P = 0.539, 0.649). Reiterated trunks were more likely to occur with higher ADI (P = 0.040), but the level of damage at which they occurred (intercept) was not well predicted (P = 0.780). Appendage damage index was collinear with age (r = 0.72) and appeared to displace it from the model because age was significant in the absence of damage (P = 0.034).

Tree age and injury were consistently positively correlated, and neighborhood density negatively correlated, with structure abundance across all types. Tree age had a positive effect on abundance of clusters as well as appendages > 15 and > 20 cm diameter, and density reduced abundance of clusters, > 10, > 15, and > 20 cm diameter appendages, and brooms (**Table 2.6**). The top break index was positively correlated with numbers of fans and trunk appendages, while density was not. The TDI alone was negatively correlated with numbers of > 15 and > 20 cm diameter appendages, but when in an interaction term with neighborhood density created a positive relationship (**Table 2.6**). This combination of singular and interacting TDI resulted in

more large appendages with higher TDI at neighborhood densities above 25% and fewer below 25% (**Appendix 2.C**). Lastly, numbers of trunk appendages also increased with increasing ADI, but the interaction between ADI and TDI was negative (**Table 2.6**). The negative interaction term served to slow the abundance increase with injury rather than decrease abundance of reiterated trunks (**Appendix 2.C**). Like abundance of structures, the mean and 90th percentile diameter of appendages generally increased with age and decreased with density (**Table 2.7**).

Table 2.6. Effect of each independent variable in best hurdle models for specific appendage counts using trees with quantified neighborhood density (N = 36). Logistic hurdle models with binomial distribution account for whether or not a structure occurs, while Poisson linear regression with model effects of neighborhood density, tree age, TDI, and ADI on abundance of each structure. Variables are listed in order of importance.

	Logistic		Poisson		Total
Dependent variable	Model	Link	Model	Link	R^2
> 10 cm diameter	—	none	– Density	none	0.52
> 15 cm diameter	+ Age – Density	logit	– Density + Age + (Density x TDI) – TDI	ln	0.62
> 20 cm diameter	– Density + Age	logit	– Density + Age + (Density x TDI) – TDI	ln	0.61
Clusters	– Density	logit	– Density + Age	ln	0.37
Brooms	+ Age	logit	– Density	ln	0.32
Fans	+ Age	logit	+ TDI	ln	0.40
Limbs	+ Age	logit	+ ADI	ln	0.39
Reiterated trunks	+ ADI	logit	+ ADI + TDI – (TDI x ADI)	ln	0.54

Table 2.7 Models predicting trunk and appendage diameters within the tree age range of the 36-tree sample (100–389 yr) demonstrate how neighborhood density alters crown development. Appendages are summarized as anything attached directly to main trunk, thus ignoring complexity of segmented appendages. Variables are presented in order of importance. All models P-values < 0.001.

Dependent variable	V1	V2	***a***	***b***	***c***	Form	R^2
Mean diameter (cm)	Age	Density	8.26E+00	1.80E-02	–5.05E+00	$\boldsymbol{a} + \boldsymbol{b}$V1 + $\boldsymbol{c}$V2	0.53
90th percentile diameter (cm)	Age	Density	1.16E+01	3.20E-02	–9.05E+00	$\boldsymbol{a} + \boldsymbol{b}$V1 + $\boldsymbol{c}$V2	0.61
Tree DTB (cm)	Density	Age	1.54E+02	–9.80E+01	2.21E-01	$\boldsymbol{a} + \boldsymbol{b}$V1 + $\boldsymbol{c}$V2	0.68

2.3.4 *Development of crown complexity in* Picea

The conceptual model of *P. sitchensis* appendage surface area development showed decreases in model-conforming branches (b) and dead (D), modest declines in branch segments (B), and no changes in limbs (L) and reiterated trunks (T) with neighborhood density; instead L and T surface area was largely a function of injury acquired with age. Although tree age was positively associated with surface areas of types b, B, and D, a decrease with neighborhood density was consistently the stronger relationship (**Table 2.8**). Surface area of type B segments also significantly increased with ADI. In contrast to types b, B, and D, surface areas of type L and T segments was strongly positively correlated to both ADI and TDI (**Table 2.8**) and uncorrelated with tree age. Models of ADI and TDI with tree age were significant (ADI = –0.01 + 9.49E-9 x $Age^{3.64}$, R^2 = 0.48; TDI = –0.01 + 1.37E-4 x $Age^{1.24}$, R^2 = 0.20). Although precision of these estimates was not high, they produced reasonable estimates of ADI and TDI. Measured medians of ADI and TDI, which were right-skewed, were 6.00 and 0.11 versus modeled medians of 4.01 and 0.11, respectively.

Table 2.8. Models of surface area > 4 cm diameter demonstrated effects of neighborhood density, damage (ADI and TDI), and tree age on different appendage types used in the conceptual model of the discussion. Surface area of each type is summed per tree, but not all trees had all appendage types, resulting in sample size variation. DV = dependent variable, b = model-conforming branch, B = segmented branch, L = limb, T = reiterated trunk, D = dead appendage. All coefficients significant at α = 0.05.

DV	V1	V2	V3	***a***	***b***	***c***	***d***	Form	*N*	R^2
b	Density	Age	—	1.91E+02	–2.29E+00	2.65E-03	—	$\boldsymbol{a}$ x $e^{\boldsymbol{b}V1}$ x $e^{\boldsymbol{c}V2}$	36	0.67
B	Density	ADI	Age	2.84E+00	–1.94E+00	3.04E-02	5.78E-03	$\boldsymbol{a}$ x $e^{\boldsymbol{b}V1}$ x $e^{\boldsymbol{c}V2}$ x $e^{\boldsymbol{d}V3}$	34	0.62
L	ADI	TDI	—	9.69E-01	5.21E-02	9.93E-01	—	$\boldsymbol{a}$ x $e^{\boldsymbol{b}V1}$ x $e^{\boldsymbol{c}V2}$	22	0.17
T	TDI	ADI	—	8.52E-01	2.73E+00	4.90E-02	—	$\boldsymbol{a}$ x $e^{\boldsymbol{b}V1}$ x $e^{\boldsymbol{c}V2}$	29	0.73
D	Density	Age	—	3.67E+01	–2.65E+00	6.56E-03	—	$\boldsymbol{a}$ x $e^{\boldsymbol{b}V1}$ x $e^{\boldsymbol{c}V2}$	36	0.37

2.4 DISCUSSION

Development of individual *P. sitchensis* generally adheres to the concept of an early model-conforming phase followed by a protracted crown-building phase (Tomlinson, 1983; Van Pelt and Sillett, 2008), explaining why trees can take a century or more to initiate complex crown structure yet still become very complex. Like other conifers, model-conforming *P. sitchensis* crown dynamics are dominated by fast height growth and cycling of young branches (Ishii and McDowell, 2002; Sillett et al., 2015b, 2018b). Therefore, the first substantive appendages do not occur until at least 100 yr despite *P. sitchensis's* rapid growth. Limb formation is also precluded during this phase because trunk breaks initiate reiteration from the break rather than from appendages to replace the treetop. Not until the attenuation of height growth coincident with the nadir in percent crown mass after approximately 200 yr (**Figure 2.4**, **Table 2.4**) do more complex appendages develop. Survival of large appendages after 150–220 yr (**Table 2.4**) likely drives a disproportionate accumulation of crown mass because branches produce wood 44% denser than trunk wood and large branches grow faster than small ones (Kramer et al. 2014; Kramer et al., 2018). Most complex appendages appear around or after this transition period. Examples include branch breaks that stimulate brooms after ~200 yr, reiterated trunks on damaged branches to create limbs after ~260 yr, and fans from the main trunk after ~290 yr (Ishii et al., 2002; Kramer et al., 2014; Van Pelt and Sillett, 2008, **Table 2.4**). We do not have crown-level data on trees in the last stage of life (> 400 yr), which is approximately when we believe *P. sitchensis* trees begin to undergo partial or complete collapse from decay. Unlike co-occurring dominant conifers such as *S. sempervirens* and *P. menziesii*, *P. sitchensis* invests little energy in fungal resistance, prompting early onset of decay and longevity < 500 yr (Kramer et al., 2018).

Many fallen *P. sitchensis* giants that appear outwardly healthy and vigorous exhibit extensive decay columns from *Phaeolus schweinitzii* (personal observations).

2.4.1 *Dominant effect of neighborhood density and injury*

Crown size ranges roughly four-fold due to density given tree age in *P. sitchensis* (**Figure 2.5**), demonstrating its responsiveness to neighborhood crowding. There is a > 20% reduction in all macro-scale tree size variables for each 25% increase in neighborhood density, except for height which actually increases slightly (**Figure 2.5**). This strong crown-level response to neighborhood density is reflected in proportionally similar diameter increment declines of *P. sitchensis* in British Columbia, where maximum shading reduces growth relative to minimum shading by 80% (Coates et al., 2009). Reduction in crown mass due to increased neighborhood density is partially responsible for the range of percent crown mass of 5 to 25% in trees from 100 to 400 yr (**Figure 2.5**).

Neighborhood density is also responsible for a > 100-yr range of when large within-crown structures first appear (**Table 2.9**) as well as 50 to 100% increases in their abundance and size (**Table 2.10**, **Appendix 2.C**). Relevant structures affected by density are large appendages in addition to appendage clusters and brooms (**Figure 2.3**, **Table 2.6**). Large limbs accumulate organic matter and epiphytes, while clusters and brooms create overlapping stems covered in moss that catch detritus and provide covered passageways and nest sites for arboreal animals (**Appendix 2.B**). The variability in time to form, number, and size are attributable to decreased appendage growth with less light in denser neighborhoods and, less obviously, to branch demographic processes modified by density.

Table 2.9. Effect of neighborhood density on tree age thresholds for > 15 and > 20 cm diameter appendages is demonstrated with model outputs from logistic regressions using density and age predictors (**Table 2.6**). Age thresholds at which the probability of structure presence is 0.5 are back-calculated for different density percentiles. Also shown are the translations of density to competition-free distance and competitive trees within a 25-m radius based on models in **Appendix 2.C** (N = 36, $P < 0.001$, and R^2 = 0.81 and 0.92, respectively).

Appendage type	Density percentile (%)	Competition-free distance (m)	Competitive trees within 25m	Age threshold
> 15 cm diameter	10	21	1	105
	25	17	2	124
	50	12	5	157
	75	5	13	205
	90	4	16	223
> 20 cm diameter	10	21	1	113
	25	17	2	143
	50	12	5	196
	75	5	13	273
	90	4	16	301

Table 2.10. Development of large appendages with tree age is demonstrated by predicting the mean and 90th percentile appendage diameter (cm) given different neighborhood densities with models in **Table 2.7**. Density is represented as the proportion of maximum density.

	Density = 0		Density = 0.5		Density = 1	
Age	90th percentile	mean	90th percentile	mean	90th percentile	mean
100	14.9	10.0	10.3	7.5	5.8	5.0
150	16.5	10.9	11.9	8.4	7.4	5.9
200	18.1	11.8	13.5	9.3	9.1	6.8
250	19.7	12.7	15.1	10.2	10.7	7.6
300	21.3	13.6	16.7	11.1	12.3	8.5
350	23.0	14.5	18.3	12.0	13.9	9.4
400	24.6	15.3	19.9	12.9	15.5	10.3

Larger and more complex crown structure in less-dense neighborhoods may have as much to do with appendage longevity as with increases in branch diameter and mass growth (Kramer et al., 2014; Maguire et al., 1999). The largest branches are located 10 to 30% into the crown above CBH; these are not, however, the fastest-growing branches (Ishii et al., 2017; Maguire et al., 1999; Weiskittel et al., 2007). Almost paradoxically, we expect the highest branches in a dense neighborhood to grow faster than branches at the same height in a low-density neighborhood due to preferential allocation of trunk resources to the most vigorous branches in spring (Sprugel, 2002). The advantage low and slow-growing branches have over high and fast-growing branches is two-fold. First, they accumulate wood on structures that are already large, and second, they have a higher probability of having been injured because of their age and lower position in the crown. Each injury-recovery iteration is an opportunity to create more complexity via reiteration (Kramer et al., 2014). Crown base height increases 2.2 m with each 10% increase in neighborhood density (**Appendix 2.C**), and it is unlikely dead lower branches can be replaced in the upper crown, which is already densely occupied. Crown lift truncates the old and large ends of the appendage distribution, thus increasing the age at which certain large and complex appendages appear and decreasing their average size. It takes at least a century to produce a 15-cm-diameter branch (**Table 2.10**), so when large low branches die it takes a long time replace them.

Another demographic consequence of neighborhood density may be creation of clustered appendages through a delayed shift from density-dependent to density-independent branch mortality. Appendage numbers decrease and foliage aggregates at 4-m scales as trees age due to both of these processes (Ishii and McDowell, 2002; Van Pelt and Sillett, 2008), but the dominant process at a particular tree age may be modified by neighborhood density. Analogous to dense

forests and tree mortality, a dense neighborhood may prolong the period of density-dependent mortality among appendages that sustains relatively uniform spacing (Larson et al., 2015). In a less-dense neighborhood, the period dominated by density-dependent mortality may be shorter, allowing density-independent processes such as wind damage and decay to dominate. These processes typically lead to more aggregated spatial patterns in forests (Franklin and Van Pelt, 2004) and probably also do within tree crowns.

Quantities and sizes of limbs, reiterated trunks, and fans (**Table 2.6**) are more closely associated with trunk and appendage injury than neighborhood density, because trees utilize these structures to recover leaf area and canopy dominance despite neighborhood conditions. Although all injuries stimulate such reiterated structures, replacement of broken trunks is a higher priority and thus is better predicted than the others. TDI is indicative of trunk diameter and number of breaks, which explains why 54% and 73% of the variability in abundance and surface area of trunks is explained by TDI and ADI alone. Trunk reiteration from branches—limb formation—is dependent on status of the treetop for disruption of apical control, severity of damage, and light environment of the branch when it breaks (Sillett et al., 2018a). Therefore, although the numerical response of limbs is moderately well-predicted (R^2 = 0.39), the surface area is not (R^2 = 0.17). Higher levels of TDI invariably lead to more fans (**Table 2.6**), and thus these structures represent an important means to recover leaf area. An interaction between neighborhood density and TDI also appears to increase large appendages at neighborhood density above 25% and fewer below 25%. In reality, the numbers of all large appendages are so depressed at high neighborhood densities that this effect makes little difference. However, at low neighborhood densities where abundance of large appendages is high, severe damage decreases their expected numbers (**Appendix 2.C**). This is similar to the interaction between ADI and TDI

for numbers of reiterated trunks, in which more damage leads to more trunk reiterations except at high levels where there combined effect slows (but does not reverse) the increase in reiterated trunk abundance (**Appendix 2.C**). Both cases are attributable to the fact that severe injuries physically remove appendages (and their photosynthetic capacity).

2.4.2 *A modified conceptual framework for crown development*

Incorporating neighborhood density into a conceptual framework of crown development demonstrates extreme reductions in the surface area of live model-conforming branches, dead appendages, and, to some degree, type B segments with increased density. As trees approach maximum height, their structural potential has been modified by prior conditions. Less-dense neighborhoods equate to lower mean structure heights, more appendages of all types (**Figure 2.6a**, **Appendix 2.C**), and larger-diameter appendages at younger ages (**Table 2.9**, **Table 2.10**). The difference between 20 and 80% of maximum density is stark, at all ages reducing surface area of all but type L and T segments by more than half (**Figure 2.6b**). However, trees in high- and low-density neighborhoods have all types of appendages (**Figure 2.6a**), demonstrating that density alone does not limit which types of appendages are present.

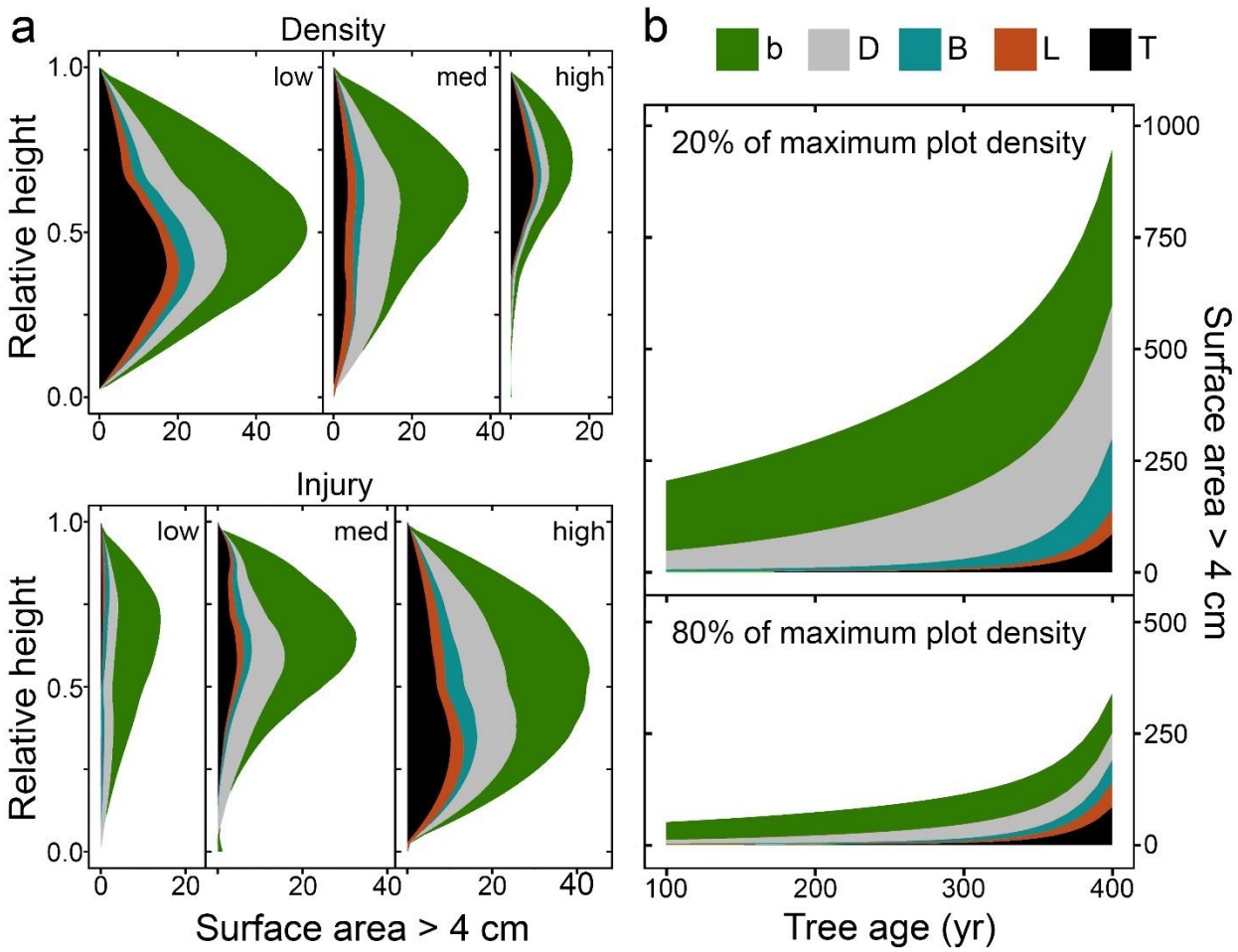

Figure 2.6. Conceptual model of conifer development including neighborhood density. Side (**a**) is appendage summary for three classes of increasing density and tree injury (**low-high**) with 12 trees per class. Injury here is represented as the average of standardized TDI and ADI (**Table 2.2**). Surface areas of > 4 cm diameter are averages within 20 relative height (appendage height/tree height) bins by type. Averages are loess-smoothed with span parameter of 0.6 in R to better illustrate vertical distributions. Side (**b**) is model of neighborhood density effects on total crown complexity for trees in upper range of expected damage given tree age (see text). Surface area of each appendage type is predicted from models using density, age, and damage indices (ADI and TDI, **Table 2.8**). Reasonable values for ADI and TDI predictors are estimated as upper 95% confidence intervals based on age (R^2 = 0.48 and 0.20, respectively, see results). Appendage types are coded by color with b = model-conforming branch, D = dead, B = segmented appendage, L = limb, and T = reiterated trunk.

Injury is the other determinant surface area in each appendage type and with various combinations of density, time, and injury trees exhibit highly contrasting structure. Because trees are injured in low- and high-density neighborhoods, all appendage types are present across different densities (**Figure 2.6a top**), and because trees accrue injury with age, all appendage types appear to increase with injury (**Figure 2.6a bottom**). However, only type B, L, and T segments statistically increase with injury not accounted for by age (**Table 2.8**). Type B appendages are intermediate with surface area being regulated by neighborhood density and tree injury, while L and T segments respond to injury alone. Effects of density and injury are separated by modeling the monotonic increase of injury with age at different densities (**Figure 2.6b**). This shows that densely-grown and open-grown trees develop vastly different crown forms and surface areas in type b, B, D appendages while acquiring similar levels of complex structure in limbs and reiterated trunks (**Figure 2.6b**, **2.7**).

It must be noted that the relationship between age and injury is highly variable so we show injury as increasing with age independent of density. In fact, trees in high density neighborhoods exhibit "crown shyness" (Rouvinen and Kuuluvainen, 1997) due to interacting branches, and those in more open conditions are likely more prone to wind damage (Aubry et al., 2009). Our data show no correlation of density with TDI ($P = 0.128$) and a weak negative correlation with ADI ($R^2 = 0.15$, $P = 0.011$), the opposite expectation if branches from opposing trees are breaking each other. This is not conclusive given our sample size and more realistically reflects high variability and that our data do not have the resolution to distinguish between types of injury at different densities. Therefore, the model presented is necessarily general to avoid over interpreting the data and can certainly be updated with future work.

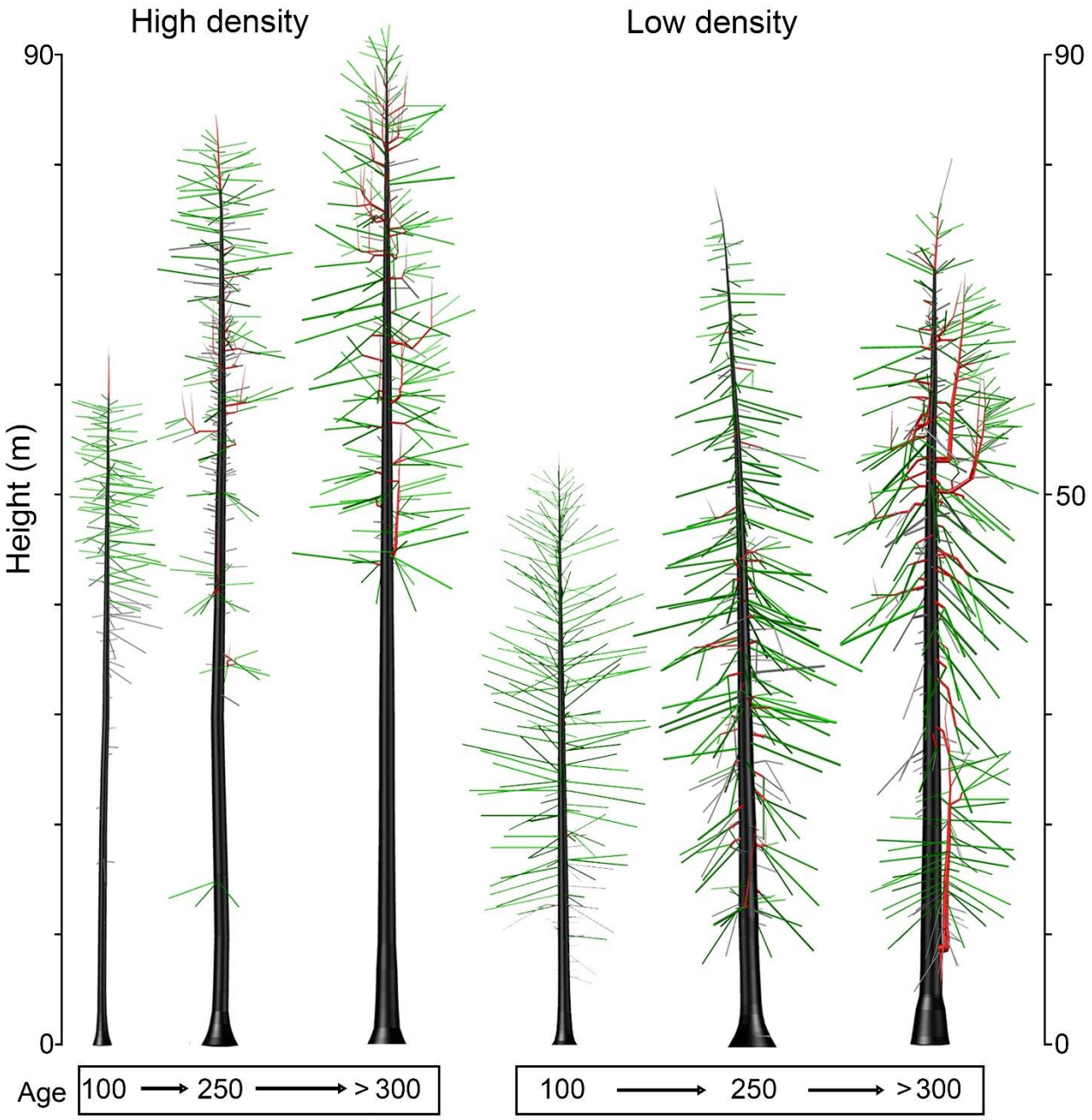

Figure 2.7. Maps of trees from contrasting neighborhood density and similar tree ages demonstrate the potential to produce various crown structure over time. These trees are selected to show maximum expression of within-crown structure excluding those subjected to major trunk-break events and alteration of neighborhood density during development as in **Appendix 2.D**. Black = main trunk, red = segmented appendages including trunk reiterations, green = model-conforming branches, gray = dead.

We recognize that our interpretation is based on neighborhood conditions at the time of measurement and do not necessarily reflect conditions each tree experienced throughout its lifetime. For this reason, the conceptual framework represents trees experiencing relatively consistent neighborhood densities and without unusually severe injuries. We can assume that a dense neighborhood with similarly sized trees likely reflects continuously dense conditions. However, we cannot assume that a low-density neighborhood has always been low-density, or that a moderate-density neighborhood was not less dense in the past. We accounted for the first exception by selecting study trees with few substantial recent neighborhood disturbances, but we did not control for the second possibility. Even without accounting for forest dynamics it is encouraging that we are able to account for 41 to 73% of the variability in macro-crown characteristics and 32 to 62% in appendage abundance and diameter. To explore the potential effects of changing neighborhood conditions over time we present our interpretations of six case study trees in **Appendix 2.D**.

2.4.3 *Management for large complex trees*

Crown development of *P. sitchensis* and *P. menziesii* are compared first to illustrate the unique role that *P. sitchensis* can play in management of temperate conifer forests in the Pacific Northwest. A standard of comparison is based on *P. menziesii* since it is the best-studied as well as being the most commonly managed species in the region. *Picea sitchensis* accumulates twice the crown mass as *P. menziesii* by age 200 and thrice the crown mass by age 300 (**Table 1.7**). The transition out of the model-conforming phase occurs at approximately 300 yr in *P. menziesii* from the Cascade Mountains compared to 200 yr in *P. sitchensis* studied here, before which there are few (if any) reiterated trunks and nearly twice the branch density (# m^{-1}) of older trees (Van Pelt and Sillett, 2008). Since *P. menziesii* from the Olympics develop biomass and leaf area

faster than in the Cascades (Sillett et al., 2018b), we included crown mapping data from 15 *P. menziesii* aged 81 to 624 yr from Olympic rainforests (Sillett et al., 2018b) to afford a direct comparison of specific crown structures (**Figure 2.8**).

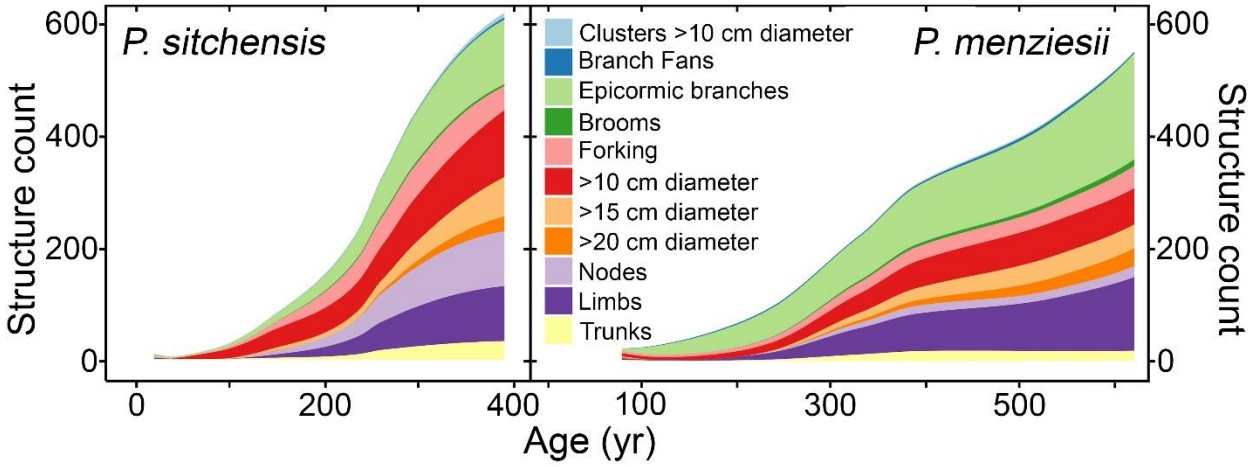

Figure 2.8. Structural quantities from 36 *P. sitchensis* and 15 *P. menziesii* trees quantified using the same techniques from this study are loess-smoothed with a span parameter of 0.8 in statistical program R to compare development. The x-axis scale on both graphs is the same.

The most obvious difference between the species is the more rapid accumulation of crown structures in *P. sitchensis*. In just over 200 yr, *P. sitchensis* develops the same number of structures as a 400-yr-old *P. menziesii*, and in 400 yr has more structures than *P. menziesii* accumulates in 600 yr (**Figure 2.8**). Three major within-crown differences between the species are higher number of epicormic branches earlier in life, fewer large appendages, and fewer appendage nodes in *P. menziesii*. Greater abundance of epicormic branches suggests that *P. menziesii* is better able to lengthen its crown following reductions in neighborhood density, while smaller numbers of large appendages suggests slower appendage growth than *P. sitchensis*. Enhanced ability to produce new branches would seemingly enable *P. menziesii* to respond more to neighborhood density reductions than *P. sitchensis*, but this advantage does not translate to growth; *P. sitchensis* carries 38% more leaves for a given crown volume, allowing it to produce

roughly twice the basal area of *P. menziesii* after thinning (Kramer et al., 2018; Roberts and Harrington, 2008). Recall that a node is a term used during crown mapping to denote abrupt changes in diameter or direction. The discrepancy in node abundance may have more to do with relative developmental stage than with tree age. Rainforest *P. menziesii* typically establish in dense cohorts (Franklin et al., 2002; Sillett et al., 2018b), while the *P. sitchensis* of this study occupy a wide range of forest conditions. Low-density neighborhoods support many long-lived branches in *P. sitchensis* and develop larger, more complex appendages than similarly aged *P. menziesii*. Although *P. sitchensis* develops faster than *P. menziesii*, maximum realized complexity is probably somewhat less due to a shorter lifespan. *Pseudotsuga menziesii* can approach 1000 yr in rainforests (Carder, 1995; Sillett et al., 2018b). Accumulation of damage and reiterated structure during longer lifespans allows *P. menziesii* to develop more complex crowns than *P. sitchensis* in the same way that *S. sempervirens*, which can live more than twice as long as *P. menziesii*, develops the most complex crowns of all (Sillett et al., 2015b; Sillett and Van Pelt, 2001).

Effective strategies to increase crown-level complexity will focus on retaining the oldest appendages to reduce the time for trees to acquire large structure, on accelerating their growth, and on promoting specific structures such as limbs and reiterated trunks (Sillett et al., 2018a). All three management objectives related to development of crown complexity can be assisted by the information provided here on crown development in *P. sitchensis*. First, based on our data, individual *P. sitchensis* produce appendages > 15 cm diameter at heights as low as 13 m and on average as low as 29 m. These heights are reached—and by extension *P. sitchensis's* oldest appendages initiated—in as few as 18 and 46 yr, respectively. Therefore, density delays large appendage formation by killing low branches that would otherwise become large much sooner.

Second, we now have empirical estimates of appendage sizes at particular tree ages and neighborhood densities (**Table 2.10**), but managers tend to understand trunk diameter responses to thinning better than branch diameter responses (Cochran et al., 1994; Maguire et al., 1991; Weiskittel et al., 2007). To aid interpretation of our results, we present predicted mean appendage diameters and DTB at varying neighborhood densities and tree ages (**Table 2.7**) and the change relative to that expected in the highest density (**Figure 2.9**). Decreasing density nearly equally increases trunk and appendage diameters by a maximum of 60 to 150% in 100- to 400-yr-old trees, respectively. Although the effect appears small in older trees, it is quite large considering that older trees typically have larger appendage and trunk diameters. Third, limbs are unequivocally associated with injury (**Table 2.6**) and are the largest horizontal appendages. In *P. sitchensis* the average diameter of the three largest appendages by type b, B, and L are 15, 18, and 21 cm, respectively (all $P < 0.001$), and the maximum are 28, 60, and 92 cm, emphasizing that limbs are the largest horizontal appendages in conifers (Kramer et al., 2018; Sillett et al., 2015b; Van Pelt and Sillett, 2008).

General guidelines for the scale and intensity with which to accelerate development of large trees through silvicultural manipulations can also be inferred from this study. Neighborhoods of 25-m radius influence crown characteristics of large *P. sitchensis* trees, and some evidence indicates that the azimuth of tree competition is important (Rouvinen and Kuuluvainen, 1997, **Table 2.5**), likely due to low southerly sun angles in the Pacific Northwest. This is somewhat larger than neighborhoods of smaller trees of other species (Coates et al., 2009; Roberts and Harrington, 2008) but is not surprising given the light sensitivity of *P. sitchensis*, its leaf-dense crowns, and its tall stature. If a manager is focused on an individual tree, a treatment radius of ~25 m might be considered and weighted to the south or southwest (in northern

latitudes). Within this radius, each 25% reduction in neighborhood density increases crown volume roughly 20% and after 100 yr can more than double appendage diameter (**Figure 2.9**). However, different neighborhood densities also create trees with distinctly different character (**Figure 2.7**). A large open-grown tree provides more habitat within its crown, while narrow complex trees surrounded by similar neighbors may provide comparable amounts of habitat on a per-area basis. Given that there are few explicit links between different types of crown structure and its use as habitat (but see Watson, 2001), tree density should vary across an ecological treatment to include open-grown trees with many large appendages as well as clumps of densely-grown trees. These recommendations are easy to incorporate into ecological forest management that specifically calls for leaving individuals, clusters, and openings (Churchill et al., 2013; Franklin et al., 2018; Franklin and Johnson, 2012).

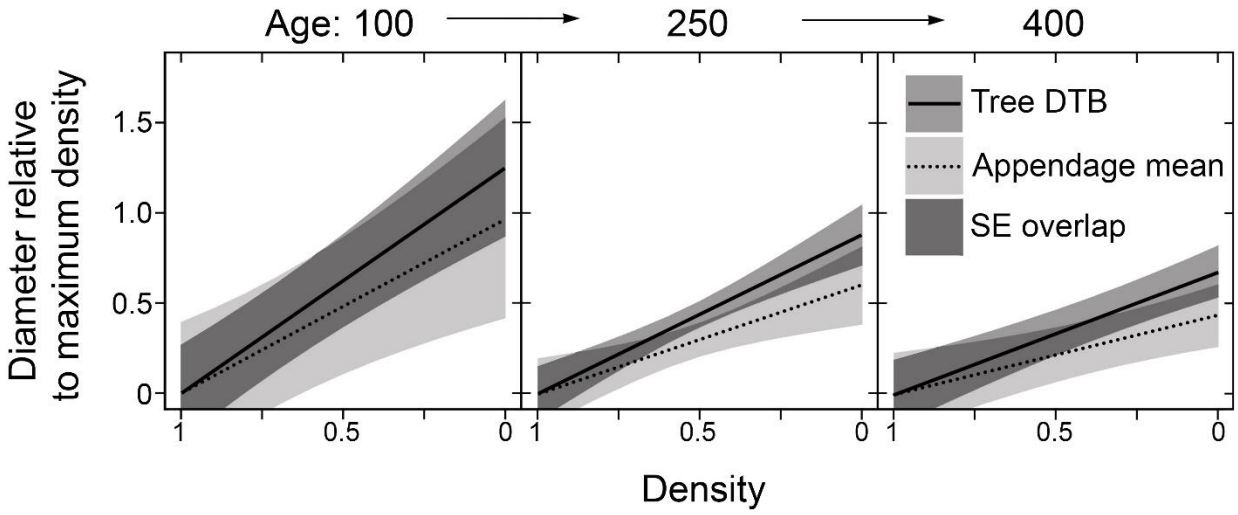

Figure 2.9. Predicted diameter based on models of age and neighborhood density (**Table 2.7**) is expressed relative to expected diameter at maximum density for DTB and mean appendage diameter of 36 trees to show relative diameter increase at lower densities. Tree age used for prediction is shown above each plot. Shaded areas are ± 1 standard error (SE), and dark shaded area is overlapping SE.

In addition to manipulating neighborhood density by removing trees, managers can injure trees by blasting or cutting off treetops, tipping branches, and falling trees into each other to promote crown complexity (Brandeis et al., 2002; Sillett et al., 2018a). These methods are expensive and dangerous so should only be applied if the resulting crown response will last a long time. Limbs are inhibited if trees are in the model-conforming stage of development, are in a dense neighborhood, or subsequently die as the crown lifts. Purposefully injuring trees should follow slowing of rapid height growth at ~50 m (~150 yr), be above average crown base height of ~30 m, or if earlier and lower, must insure that the neighborhood is free of competition within ~25 m.

The management implication for promoting structurally complex crowns is to leave dominant trees that are primed with larger crowns to respond more rapidly to decreased neighborhood density. In forests managed for old-growth characteristics, such as in Late Successional Reserves under the Northwest Forest Plan, there may be limited opportunities to manipulate forest structure before such treatment becomes socially unacceptable (Franklin et al., 2018). In such situations it is judicious to retain and thin around trees that already have large complex features and rely on natural disturbances to promote more. Reducing stand density intensifies wind exposure, which in turn increases wind damage and branch diameters (Watt et al., 2005). Furthermore, pre-treatment crown form may limit or delay the structural response to density manipulation. Crown size is shaped by forest density and is a good predictor of growth (Binging and Dobbertin, 1995; Cole and Lorimer, 1994; Sumida et al., 2013), thus crown form sculpted by past conditions can delay future growth responses (Sorrensen-Cothern et al., 1993). Growth response lags can be quite long in older forests, up to 25 yr in 160- to 650-yr-old *P. menziesii* (Latham and Tappeiner, 2002). We propose that these lags are because pre-treatment

crown structure is not yet optimized for a new light environment, and older trees have longer lags because their crowns—with fewer and larger appendages—have more structural inertia.

The concepts developed here are applicable to other temperate forests dominated by large conifers, but have limited transferability to angiosperm-dominated forests. In well-watered systems neighborhood size is most likely a function of tree size because of shading by tall neighbors. Any comparable-statured tree to *P. sitchensis* and *P. menziesii* will probably benefit from density reductions within 25 m. There are also parallels between the traits of *P. sitchensis* and *P. menziesii* and other forests. Anytime there is a mix of a faster-growing shorter-lived tree and a slower-growing longer-lived tree, forest-level crown complexity benefits from the inclusion of both. The concepts do not apply well to angiosperms because most conifer architecture is tall and narrow with minimal horizontal surfaces, while most angiosperms have naturally spreading architecture with many horizontal surfaces (Tomlinson, 1983). There is no clear distinction between type B, L, and T segments in many angiosperms, so while density reductions will certainly increase appendage sizes, injury may not produce predictable responses.

2.5 CONCLUSION

Picea sitchensis is a rapidly growing tree that is highly responsive in structural development to its largest neighbors. Variable neighborhood density in rainforests allows *P. sitchensis* to express a 4-fold difference in crown volume after 300 yr and does so much more quickly than associated tree species. A 300-yr-old *P. sitchensis* accumulates three times the crown mass of other tall conifers with which it associates—*P. menziesii* and *S. sempervirens*—in the same amount of time (Kramer et al., 2018). Within the crown, appendage diameters of a given aged tree vary over 100%, and appearance of large appendages (> 15 cm diameter) are delayed by over a century due to high neighborhood density. Silviculturally, *P. sitchensis* could

be effectively deployed to produce trees with large appendages much more rapidly than slower-growing species. This large canopy-dominant tree is ultimately limited by its relatively short lifespan (compared to *P. menziesii, S. sempervirens, and T. plicata*), which constrains maximum appendage size and complexity, and thus should be considered an integral but dynamic component of rainforest ecosystems.

Three related research directions extend from this study of *P. sitchensis* crown development. The first is to combine allometric relationships of *P. sitchensis* with knowledge of its response to neighborhood density for quantifying biomass increments and carbon stores at a landscape scale. Such an investigation will integrate accurate estimates of wood volume increment from tree cores along the trunk, tree height and crown size, and spatial patterns of density. The tree cores we obtained, while tree dimensions and forest canopy structure can be determined from currently available LiDAR acquisitions. Our core samples contain one of the wettest and one of the driest years on record (2011 and 2015 respectively, https://wrcc.dri.edu/wwdt/time/), providing an opportunity to assess sensitivity of tall *P. sitchensis* to drought stress. A second line of investigation is understanding how changes (either reductions or increases) in neighborhood density alter the trajectory of crown development. When does starting down one developmental trajectory preclude a tree from attaining other potential forms? We can target trees where neighborhood density changed substantially, use tree-ring records to reconstruct time series of growth increments as well as trees ages, and evaluate their potential to accumulate more structure before death. A third line of investigation is to explicitly relate crown structures to specific uses by arboreal animals. For example, do large open-grown crowns attract different organisms than complex crowns in dense neighborhoods? A systematic deployment of

automated cameras at different locations is one approach, while another is to affix tracking devices to arboreal animals to examine their use patterns.

Chapter 3. WATERSHED SCALE

Effects of disturbance and species composition on canopy structure of Olympic rainforests

Formatted for submission to Landscape Ecology June 30th 2019.

3.1 INTRODUCTION

Interplay between disturbance and plant succession over space and time creates observable vegetative patterns at large scales. Early ideas of plant succession (Clements, 1936), how individual plants compete with each other after random dispersal (Gleason, 1926), and how plant communities organize as a mosaic of patches, each in a unique phase of development (Watt, 1947), provide the groundwork for modern landscape ecology. One central contemporary theme in this field is understanding reciprocal effects of composition and spatial arrangement of vegetation patches —referred to as pattern— on ecological processes. Examples of such processes include provision of habitat for specific species of interest and flux of materials and energy (Risser, 1995; Turner, 1989). Another theme in landscape ecology is that there are few meaningful universal principals. Each ecosystem has so many unique contingencies that principals general enough to encompass them are often "trite or useless" (Wiens, 2008). The inapplicability of general concepts to specific ecosystems necessitates developing principals applying to a suite of landscapes sharing common features or domains of scale, called contingent principals (Hobbs and Lindenmayer, 2007). We cannot develop contingent principals for every context, but we can describe contexts with disproportionate ecological value that share characteristic features with other ecosystems.

One disproportionally important ecosystem is represented by alluvial valleys along the northwest coast of North America and best represented on the Olympic Peninsula in Washington State, USA and Vancouver Island, Canada. Valley bottoms are dominated by *Picea sitchensis* (hereafter *P. sitchensis*) and contain some of Earth's largest and tallest trees in open-canopy forests, supporting herds of large undulates, productive side channels with rearing salmonids, and endangered pelagic birds and owls (Elk-schwartz and Service, 1945; Lehmkuhl and Raphael, 1993; Raphael et al. 1995; Sedell et al., 1982). The openness of such conifer forests allows ample light to reach understory herbs and shrubs (Alaback, 1982), providing nutritious foliage, fruits, and seeds to insects, birds, and mammals. Open forests also promote development of big trees with more numerous large appendages (Kramer et al., 2019). Large appendages in turn, support canopy epiphytes, soils, and arboreal creatures such as squirrels and bats (Carey, 1996; Gorman et al., 2019; Sillett and Van Pelt, 2007).

An intriguing pattern evident in the Olympic Mountains is the structural difference between valley-bottom forests and their upland counterparts. Upon visiting these forests, the open canopy of valley-bottom relative to upland forests is immediately apparent (**Figure 3.1**). Whereas the former are open-canopied and "fine-textured" at large scale, the latter are closed-canopied and patchy (**Figure 3.2**). These forests have a similar seasonal-rainforest climate regime but, because of contrasting geomorphology, are subject to distinct disturbance agents. Fire predominantly affects upland forests, and alluvial processes rework valley bottoms (Henderson et al., 1989; Huff, 1995; Latterell et al., 2006). Additionally, the dominant overstory tree species in valley bottoms, *P. sitchensis*, is shade-tolerant, moisture-loving, and able to establish on rotten wood—characteristics allowing it to persist as a late successional species in old-growth forests (Minore, 1979; Van Pelt, 2007). In contrast, the dominant upland species, *P.*

menziesii is a long lived shade-intolerant pioneer requiring mineral soil and ample sun to establish (Franklin et al., 2002; Minore, 1979). These two factors—contrasting disturbances and dominant species composition—provide the context for contingent principals shaping vegetative pattern. Here we explore relationships between disturbance and species dominance on canopy structure by examining the spatial distribution of large trees across the landscape.

Figure 3.1. Examples of canopy structure in valley-bottom *P. sitchensis* forests (**top**), valley-bottom *P. menziesii* cohorts (**middle**), and upland *P. menziesii* forests (**bottom**). Above-canopy views are on the **left**, and understory views are on the **right**.

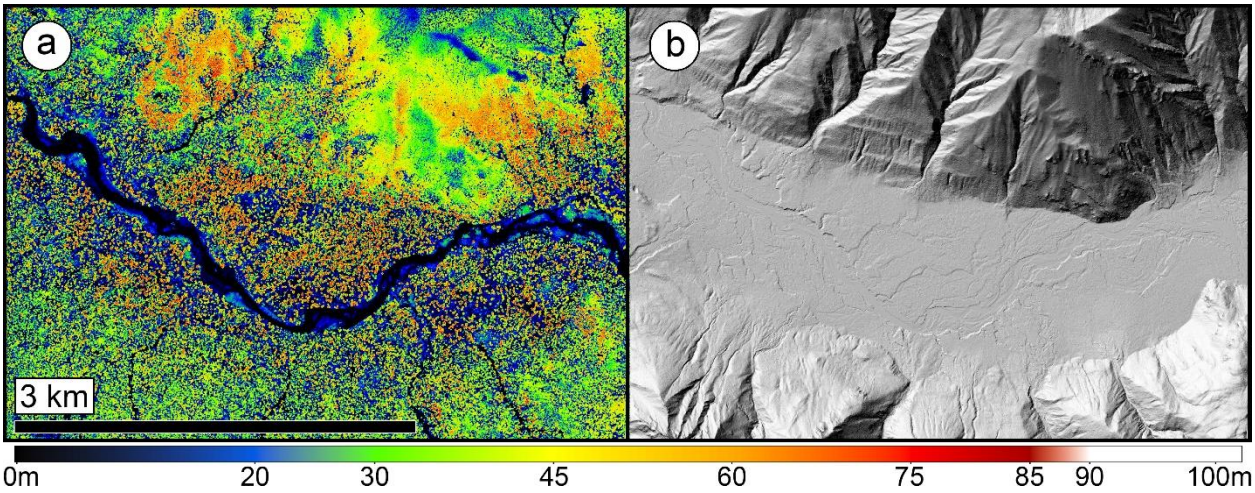

Figure 3.2. Normalized canopy height model (CHM, **a**) of the South Fork Hoh River highlighting canopy structure in relation to topography (**b**). Color bar shows canopy height above ground.

By contrasting disturbance agents and successional processes in valley bottoms and upland positions, we can deduce expected patterns of canopy structure. Upland positions subject to large (1000s of ha) infrequent high severity fires (Henderson et al., 1989), such as those on north and east aspects, likely establish as contiguous cohorts of Douglas-fir, some of which reach advanced stages of succession before the next fire. Because cohort-forming disturbances are likely larger and occur at timescales sometimes longer than maximum tree age on northeast-facing slopes, they should have a finer patch grain reflecting small-scale, agent-based mortality of canopy dominants and shade-tolerant understory trees like *Tsuga heterophylla* and *Abies amabilis* (hereafter *T. heterophylla* and *A. amabilis*). Within this broader context, southwest slopes are exposed to both cyclonic winds and more frequent smaller (100s of ha) fires (Gavin et al., 2003; Huff, 1995). These events should lead to mixed patches with those affected by wind being more variable because they regrow from residual understory trees, and those affected by fire being more homogeneous because they represent cohorts of *P. menziesii* in various stages of succession. In valley bottoms, the dominant disturbance agent is lateral river movement in the

flood plain (Latterell et al., 2006). Areas recently reworked by the river should consist of structural patches produced by many small "islands" of structure in different stages of riparian forest development, most of which are relatively short because of frequent disturbance and rapid colonization of gravel bars by *Alnus rubra* (hereafter *Alnus*, Balian and Naiman, 2005; Van Pelt et al., 2006). Areas less-visited by the river, especially on terraces, should exhibit forests progressing far enough through succession that fungi are actively killing trees in small groups. This may be similar to processes on northeast slopes but may result in more open structure because of dominance by shorter-lived *P. sitchensis* (Kramer et al., 2018). Cohorts of *P. menziesii* can also (rarely) establish in valley bottoms (**Figure 3.1**), likely following fire or floods that expose mineral soil (Cordes, 1972; Sillett et al., 2018b). In such cases the effects of dominant species can be isolated by comparing to *P. sitchensis* forests to those containing similarly aged *P. menziesii*. A valley-bottom *P. menziesii* forest that has not yet developed horizontal diversity through small-scale mortality should be more homogeneous than a valley-bottom *P. sitchensis* forest unless external disturbance agents overwhelm biological processes.

Canopy structure contributes to many landscape functions, and one of the most important is provision of critical habitat. Especially large and old trees are disproportionally important in this regard (Lindenmayer, 2016; Lindenmayer et al., 2014; Lutz et al., 2012). For example, living trees with decayed wood, large appendages, and well-developed epiphyte communities provide refugia that lifeboat species from one disturbance to the next (Ishii et al., 2018). In 1-ha of old-growth redwood forest, the 3 largest of 113 trees provide 30 % of epiphyte mass, 54 % of canopy soil, and 50 % of arboreal water storage (Sillett and Van Pelt, 2007). This is due to the amount of complex appendages, decayed wood, and bark characteristics that provide micro-habitats in large trees (Michel and Winter, 2009). In old oak forests where microhabitats like dead wood, fungal

fruiting bodies, and loose bark are quantified, they are better predictors of bird and bat diversity than stand characteristics like basal area and diameter distribution (Regnery et al., 2013). Single large *P. sitchensis* trees can host > 68 species of bryophytes, lichens, and ferns (Gorman et al., 2019). Thus, especially rare, large, old, and complex trees—hereafter referred to as "elite" trees—provide the vast majority of critical habitat. In *P. sitchensis* forests, trees crown size increases nearly proportionally to the openness of the forest (Kramer et al., 2019), so valley-bottom forests may contain more elite trees given their openness.

Canopy structure of *P. sitchensis*-dominated forest has been described in limited areas from plots confined mostly to valley bottoms (Cordes, 1972; Fonda, 1974; Mckee et al., 1982; Van Pelt et al., 2006), likely because steep slopes were difficult to sample (but see, Huff, 1995). Here we analyze wall-to-wall light detection and ranging (LiDAR) data of an old-growth watershed, overcoming access limitations and allowing a complete description of canopy structure. We extend this analysis by extrapolating detailed measurements of *P. sitchensis* and *P. menziesii* trees to map locations of elite individuals across the landscape and quantify how disturbance and species composition relate to provision of critical habitat. Our purpose is to describe and propose possible reasons for striking differences between structure of valley-bottom and upland forests. To accomplish this we have four specific objectives: 1) contrast composition and canopy structure in upland versus valley-bottom forests as evidence for or against expectations due to geomorphology, 2) contrast the same metrics of canopy structure in a valley-bottom *P. menziesii* forest with those in upland *P. menziesii* and valley-bottom *P. sitchensis* forests to elucidate overriding effects of species composition, 3) discuss further steps needed to validate our conclusions, and 4) assess influence of canopy pattern on function by examining the distribution of elite trees across the landscape.

3.2 METHODS

3.2.1 *Site-based disturbances and dominant species*

The study site is the Main and South Fork Hoh Rivers in Olympic National Park, WA, USA. Glacier- and rain-fed rivers create a meandering to island-braided structure (Beechie et al., 2006) including overflow channels cutting through forest and old abandoned routes (Abbe and Montgomery, 2003; O'Connor et al., 2003). Ancient glacial terraces and debris fans in valley-bottoms create moist areas of forest protected from river movement (Thackray, 2001), geomorphically dividing valley bottom forest into valley alluvial and terrace forests (Fonda, 1974). Upland tributaries enter the flood plain then parallel slopes before joining the main river, creating extensive off-channel water courses (Sedell et al., 1982; Swanson and Lienkaemper, 1982). The Olympic Peninsula and Vancouver Island are hit roughly every 15–30 yr by brief, intense (gusts > 60 m s^{-1}), and highly localized cyclones from the southwest (Mass and Dotson, 2010). Blowdown concentrates on upper southwest slopes, ridges, and isolated areas of turbulence behind ridges (Ruth and Yoder, 1953), knocking down overstory trees, but leaving the understory largely intact. Although these forests can receive more than 300 cm of precipitation, only 10 % falls during summer months (PRISM, 2018), and steep canyon walls become dry in summer. Isolated small (150–600 ha) fires recur more frequently (~400-750 yr return interval) on southwest slopes during normal summer fire weather (Gavin et al., 2003; Huff, 1995), but fires exceeding 13,000 ha occur on all slopes during synoptic dry east winds (Henderson et al., 1989). These are heavily fuel-loaded, burning intensely, and exposing mineral soil. Wind in valley bottoms is less intense due to flat topography and low elevation (Ruth and Yoder, 1953), and fires typically dwindle when moving from upslope, not recurring with substantial intensity for > 1,400 yr (Gavin et al., 2003). Alongside fast-acting intense disturbances by water, wind, and fire

is the chronic progress of wood decay fungi in valley-bottom and upland forests. Slow-acting root and heart rot fungi take upwards of a century to kill significant portions of the overstory (Franklin et al., 2002), thus becoming dominant disturbance agents only when other severe disturbances have not "reset" the successional clock within a few centuries.

Valley bottom and upland forests are dominated by *P. sitchensis* and *P. menziesii*, respectively, which have distinct developmental trajectories. Forests dominated by *P. sitchensis* develop from a wide range of pathways because seedlings establish in dead wood or mineral soil and grow well in partial shade (Mckee et al., 1982; Minore, 1979). In consequence, it forms pioneer cohorts following floods, slowly infiltrates grassy meadows, gradually establishes as understory trees of pioneering *A. rubra* and *Populus trichocarpa* (Peterson et al., 1997; Van Pelt et al., 2006), and maintains presence in old-growth forests (Franklin et al., 1982; Taylor, 1990). *Pseudotsuga menziesii* is not shade-tolerant, and its seedlings require mineral soil to establish (Burns and Honkala, 1990; Minore, 1979). In rainforests *P. menziesii* typically establishes as a pioneering cohort following fire (Huff, 1995). In the absence of disturbance, a *P. menziesii* overstory gradually succumbs to decay and is slowly replaced by more shade-tolerant species (Franklin et al., 2002). In both valley-bottom and upland forests, *T. heterophylla* is the numerically dominant understory species and is more shade tolerant than either *P. sitchensis* or *P. menziesii* (Minore, 1979). Through time it occupies all size classes including the upper canopy alongside *P. sitchensis* in valley bottoms and can eventually replace *P. menziesii* cohorts. The time required for *T. heterophylla* to reach the overstory is highly variable, depending on sizes and survival post-disturbance, availability of log seedbeds (nurse logs), and overstory competition (Franklin et al., 2002). Shorter *P. sitchensis* compared to *P. menziesii* lifespan (~300 vs. ~800 yr) is likely due to its higher susceptibility to decay (Kramer et al., 2018; Van Pelt,

2007). At elevations from 600 to 900 m, dominance shifts to *A. amabilis* and *T. heterophylla*, which have a similar stand-replacing disturbance regime to *P. menziesii* (Henderson et al., 1989). Since we seek to describe the fundamental character of valley-bottom forests versus upland due to disturbance, we restrict contrasts to elevations < 900 m. Given disturbance patterns outlined above and species differences, expectations based on them are outlined in **Table 3.1** and **Table 3.2**.

Table 3.1. Expected forest structural patterns in two valley bottom and two upland positions are due to different species composition and disturbance agents.

Context	Expected canopy structure	Rationale
Valley alluvial	Large contiguous areas of short and open forest with small patches of taller trees in various stages of succession. Low levels of aggregation results in fine-texture mosaic.	Lateral river movement and migrating side channels create areas colonized by younger trees within forest, and where channel has not been for long periods, fungal decay of susceptible *P. sitchensis* and *T. heterophylla* creates additional gaps.
Valley terrace	Structure will be similar to valley bottoms but have larger patches of mid-canopy trees and more aggregated gap and open conditions.	No contemporary river disturbance and last glaciers visited > 10,000 year ago, so canopy structure driven primarily by interaction of fungal decay with *P. sitchensis* and *T. heterophylla* species. More mid-story *T. heterophylla* establishment than on valley alluvial because fallen trees provide more nurse logs than alluvial disturbance.
Southwest slope	High percentage of closed-canopy forests in large patches representing establishment cohorts. Relatively few gaps far apart.	Long-lived *P. menziesii* cohorts maintain a closed canopy after fire by outliving natural fire return interval. Wind disturbed forest rebounds densely with surviving understory *T. heterophylla*.
Other upland	Smaller less aggregated patches of overstory trees and more open forest conditions than southwest slopes but less than either valley position. More gaps, further apart than in valleys but closer than on southwest slopes.	Disturbances less frequent than southwest slopes so forest may be more open as overstory trees decay and collapse, obscuring patches from large-scale fires and wind events.

Table 3.2. Expected canopy structure in valley-bottom forests dominated by *P. sitchensis* or *P. menziesii* and upland forest dominated by *P. menziesii*. Names used in figures and tables for each context are in parentheses.

Context	Expected canopy structure	Rationale
Valley *P. sitchensis* (*Picea* lowland)	Structure similar to overall valley bottoms except for a larger percent area and larger patches of tall trees.	Area selected for 300-350 yr trees will have more tall structure than valley bottoms overall but is still subject to processes leading to open-canopy structure such as decay and water channels.
Valley *P. menziesii* (Jackson Creek)	Higher percent land and more aggregated larger patches of tall structure than typical valley *P. sitchensis* but with more open canopy than upland. Less patchiness due to homogeneous topography.	Fewer longer lived *P. menziesii* will have died after 350 years than *P. sitchensis*, and *P. menziesii* tends to establish in dense cohorts, while *P. sitchensis* has more varied developmental pathways. Continually wet edaphic conditions promoting fungi will kill trees faster and fluvial disturbances will create more open conditions than drier upland forest.
Upland *P. menziesii* (Tall upland)	Similar to overall upland forest but having higher percent area in tall structure. Still with larger and more aggregated patches of closed-canopy structure classes. Fewer open-canopy classes than valley *P. menziesii*.	Site selected to have similar-aged trees to valley *P. menziesii* so will have more tall closed-canopy structure representing a dense cohort that has not seen subsequent disturbance. The undisturbed cohort will result in fewer and smaller gaps.

3.2.2 *Data preparation*

Data were obtained from three sources: (1) an aerial LiDAR acquisition, (2) three-dimensional mapping of 36 *P. sitchensis* trees and 30-m-plots around them across the western Olympic Peninsula (Kramer et al., 2019), and (3) similar mapping of 12 *P. menziesii* trees from the same region (Sillett et al., 2018b). LiDAR data for the Hoh river watershed were acquired in 2013 and accessed through the Puget Sound LiDAR Consortium (PSLC, 2016) along with a vendor-created 1-m-resolution digital elevation model (DEM). The original point data were processed in FUSION (McGaughey, 2009) to output 30-m-resolution raster images of various canopy structure metrics, vector shapefiles of high points and tree-approximate objects (TAOs), and a 0.75-m-resolution canopy height model (CHM, see **Table 3.3**). Additional metrics of tall TAOs and basal area per hectare (**Table 3.3, Table 3.4**) were computed by predicting diameter at top of buttress (DTB, see Kramer et al., 2018) based on TAO height from plot data (DTB =

0.624 x height$^{1.25}$, N = 488, R^2 = 0.795), then summarizing the number of TAOs and cumulative basal area in each 30-m-pixel or within each geomorphic or structural class (see below). All non-conifers and broken-top trees were excluded from the DTB equation because we applied it to trees > 55-m-tall. Both exclusions were conservative choices because angiosperms and larger broken-top trees have larger diameters for a given height. Species included in the equation were *P. sitchensis*, *P. menziesii*, *T. heterophylla*, and *A. amabilis*.

Table 3.3. Variables for classifying landform and canopy structure with categories highlighted in gray. All references to "returns" are to laser pulse returns from aerial LiDAR. Most rasters are summarized at 30 x 30-m-cell resolution.

Variable	Unit	Definition
General definitions		
CHM – Canopy height model	m	0.75-m resolution raster of canopy surface elevation normalized by subtracting ground elevation
DEM – Digital elevation model	m	10-m resolution raster of land surface elevation above sea level
Tree high points	m	Local maximum return heights representing upper canopy treetop locations
TAO – Tree-approximate object	Attributes: height (m) and area (m^2)	Either pixel (raster) or vector (polygon) shape representing crown area associated with tree high point. Delineation from LiDAR point cloud based on inflection of canopy surface, thus each TAO may include subordinate trees, and trees with multiple tops may be represented my multiple TAOs. Calculated with standard output of FUSION software.
Geomorphic class	—	Classified 30-m-pixel raster delineating forest by valley alluvial, valley terrace, southwest-facing upland, and other (**Figure 3.3c**).
Geomorphic classification		
Slope	°	Slope raster calculated from 100-m-smoothed 1-m DEM and then itself smoothed by the mean of all cells within a 100-m radius
Aspect	°	Azimuth in degrees calculated from 300-m-smoothed DEM
Canopy structure classification		
Mean return height	m	Mean of all return heights
Cover above 3 m	%	Returns above 3 m / total returns * 100, measure of canopy cover
Cover above mean return	%	Returns above mean height / total returns * 100
Basal area	m^2 ha^{-1}	Diameter above buttress predicted from tree height (see text) and used to summarize tree basal area.
95th percentile height	m	95th percentile return height
Return height deviation	m	Sum(|each return – mean return|)/number of returns
Percent canopy 10-30m	%	Percent of TAO area associated with high points 10 - 30 m tall within a 30-m cell

3.2.3 *Landscape classification*

Because canopy structure varied with landform (**Figure 3.2**), and different disturbance regimes were expected on southwest versus other upland positions, the landscape was classified into two valley-bottom and two upland classes based on geomorphology. In addition, one area of valley bottom containing a known *P. menziesii*-dominated forest along Jackson Creek was outlined (**Figure 3.3c**) based on aerial photographs, the CHM, and first-hand knowledge of the site. Areas excluded from analysis prior to classification included the active river channel, areas adjacent to the active river channel with trees < 20 m tall representing *Salix spp.* and young *A. rubra* stands, and elevations > 900 m or exposed ridges which both contained non-forested terrain. This step reduced the analysis area to 9,700 of 11,840 ha. Valley bottoms were first delineated by eye where slope exceeded roughly 20° along the edge of the characteristic U-shaped glacial valley (**Figure 3.3**). Within valley bottoms, terraces created by landslides or glaciers unaffected by river channel migration were visually outlined. These were discernable as sloping cone-shaped deposits originating from side canyons or flat regions with an abrupt scarp connecting them to the floodplain (**Figure 3.3**). For upland positions, thresholding based on slope, and aspect (**Table 3.3**) was performed in ArcMap 10.3 (ESRI, 2014) to delineate exposed southwest-facing aspects from others. These had slopes > 20° and aspects between 135 and 315° (180° centered on southwest). The resulting classification was post-processed to remove areas < 0.8 ha by reclassifying them to the nearest larger group (**Figure 3.3**). All rasters were then consolidated in a data matrix for further analysis in R (R Core Team, 2018).

Table 3.4. Variables describing canopy and tree-crown structure within geomorphic classifications and used in specific stand-scale analyses. All metrics calculated from 30-m resolution rasters or from TAO polygon and high point vector shapes (see **Table 3.3**).

Variable	Unit	Definition
General definitions		
Structure class	—	30-m raster of four structure classes based on hierarchical clustering of variables in **Table 3.3**.
Patch	—	30-m pixels sharing an edge and structure class are in the same patch. Minimum patch size is one pixel.
Canopy structure		
Percent area	%	Percent area within specific canopy structure classes.
Mean and CV patch area	ha	Mean and coefficient of variation of patch area within structure classes.
Aggregation	—	Clumpiness index (McGarigal et al., 2012), -1 = uniform, 0 = random, 1 = maximally aggregated, based on like adjacencies.
Mean and CV nearest patch distance	m	Mean and coefficient of variation of nearest-neighbor Euclidean distance to a patch of the same structure class.
Elite trees		
95^{th} percentile diameter	cm	95^{th} percentile appendage diameter per tree, measured at attachment to trunk.
TPH –TAOs per ha	# ha^{-1}	Count of high points in a geomorphic class. TPH is summarized for subsets of largest and tall trees.
CRR – Canopy relief ratio	—	(mean return – min return) / (max return – min return), measure of canopy density.
Polygon crown area	m	Area of polygon TAO (North et al., 2017)
Raster crown area	m	Area of raster, usually larger than polygon crown radius because a different algorithm is used to make raster TOAs.

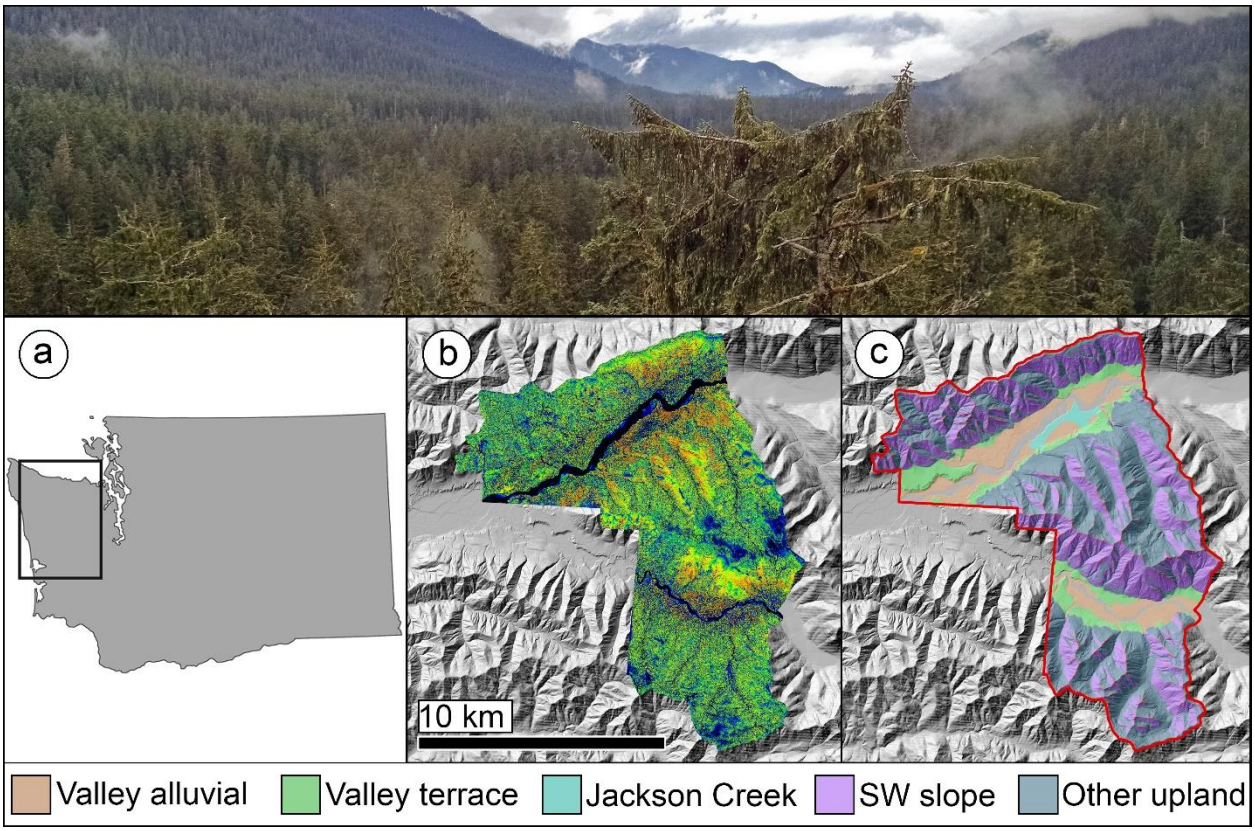

Figure 3.3. Olympic rainforest valleys in western Washington State, USA (**a**) are typically flat with steep walls (**top**). LiDAR-derived images of topography and normalized canopy height (**b**) and land classifications (**c**) are in the lower panel. Red border is an 11,840 ha LiDAR acquisition in the Hoh river watershed within Olympic National Park. See text for description of land classification.

In addition to classifying the study area by landform, canopy structure was classified into two open-canopy and two closed-canopy categories based on LiDAR metrics. This served two purposes: (1) to integrate diverse LiDAR-metrics into intuitive categories of structure and (2) to facilitate description of spatial variability of canopy structure based on size and juxtaposition of like patches (see below). After a preliminary discriminant analysis of 17 LiDAR metrics (**Appendix 1**), percent cover above 3 m, percent cover above mean return height, percent canopy in 10- to 30-m tall trees, 95th percentile return height, return height deviation, basal area ha^{-1}, and mean return height (**Table 3.4**) were chosen to classify canopy structure. Of these, cover above 3

m, and canopy in 10- to 30-m tall trees were arcsin-square-root-transformed, and basal area ha^{-1} was square-root-transformed, then all seven metrics were scaled and centered to conform to assumptions of principal components analysis (PCA, **Appendix 1**). A random sample of 20,000 of > 200,000 data rows with each metric quantified were decomposed into Eigenvectors and Eigenvalues using PCA. A Euclidean distance matrix of principal component scores weighted by Eigenvalue were used to hierarchically cluster the data using Ward's distance in the hclust function in R and specifying for four structural classes (Murtagh and Legendre, 2014). Structure classes were then imputed across unsampled data using Random Forests (Breiman, 2001) with the randomForests function in R. Structure classes represented short and open (short), medium height and open (medium-open), medium height and dense (medium-dense), and tall and dense (tall) 30-m scale structural neighborhoods (**Figure 3.4**). At opposite ends of the classification, short had relatively low percent cover, basal area, return height deviation, and height, and the highest canopy cover in 10–30 m tall trees, while tall was characterized by the highest percent cover, basal area, height deviation, maximum height, and lowest percent canopy in 10–30-m tall trees (**Figure 3.4**). Medium-open and -dense were distinguished from short and tall by having intermediate mean return height, but both had tall trees. Medium-open was distinct from medium-dense by having less basal area and percent cover as well as greater variation in height and cover at 10–30 m (**Figure 3.4**). These classes became the basis for later geomorphic comparisons based on patch characteristics.

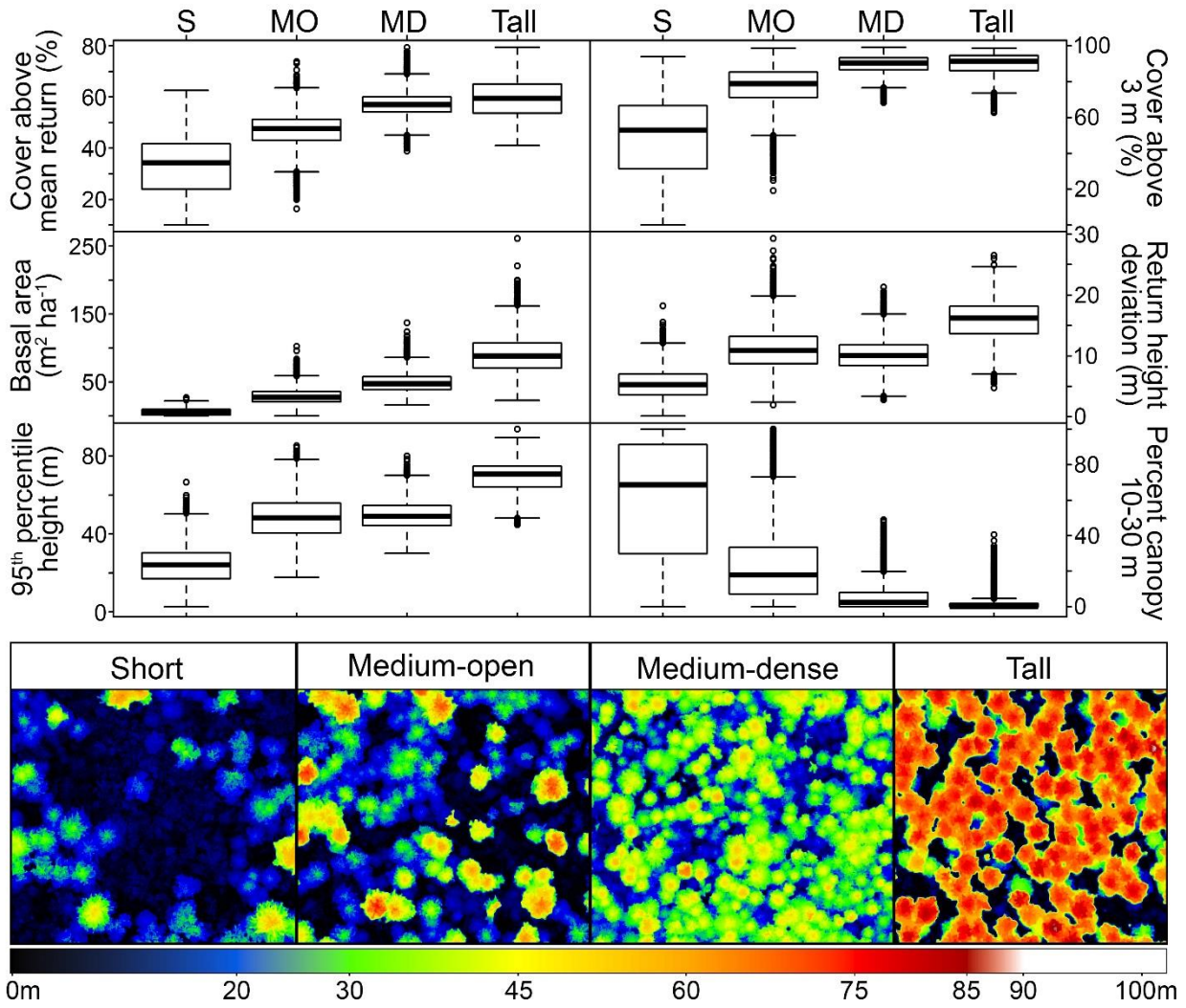

Figure 3.4. Hierarchical clustering of neighborhood-scale (30 m) structure is based on principal components of seven LiDAR-derived forest metrics (**top**). The seventh metric, mean return height, is not shown because it strongly correlates with 95th height (*Pearson's r* = 0.69). Letters above box plots correspond to four structural classes (**bottom**) selected from the CHM from areas dominated by each class. Each selection is approximately 130 x 130 m.

3.2.4 *Assessing effects of geomorphic context on canopy structure*

Describing forests among geomorphic classes was accomplished with metrics representing composition and configuration structural patches. Percent land area, mean and coefficient of variation of patch area, aggregation, and mean and coefficient of variation of nearest patch distance (**Table 3.4**) were computed for each structure class separately within each

geomorphic class using the landscapemetrics package in R. Percent area was a simple measure of structural dominance, while patch area, aggregation, and nearest patch-patch distance together described patch configuration. For example, small patches with high aggreataion and short patch-patch distances signifed spatially correlated and widely dispersed patches, whereas the same situation but with high patch-patch distances signified rare spatially correlated clusters of small pathches. Evidence for or against expected patterns (**Table 3.1**) of canopy structure was based on comparisons of these structural metrics across geomorphic contexts.

3.2.5 *Assessing effects of dominant species on canopy structure*

Because species dominance must also influence canopy structure, *P. menziesii* valley-bottom canopy structure was compard to valley-bottom *P. sitchensis* and upland *P. menziesii* areas using the same patch-scale metrics just described. Valley-bottom *P. menziesii* in Jackson Creek established as a cohort ~350 yr ago (Sillett et al., 2018b). Using CHM heights and ages of four cored trees (340, 353, 294 and 300 yr) from the 36-tree *P. sitchensis* dataset, two similar forested benches in close proximity to each other were located. An tall upland area of *P. menziesii* was selected based on relatively gentle homogeneous topography, similar tree heights, and because it was only 0.4 km from Jackson Creek. Although we did not have ages of any of its trees, the proximity to Jackson Creek and typical establishment of *P. menziesii* cohorts after severe fire in western Olympic forests (Huff, 1995) implied that they were of similar age. Expected patterns compared against are summarized in **Table 3.2**.

3.2.6 *Assessing spatial distribution of elite trees*

The last analysis was performed to integrate contributions of each structural class in different geomorphic contexts to provision of elite trees using detailed crown maps of 36 *P.*

sitchensis and 12 *P. menziesii* in combination with LiDAR data. Crown maps represented trees as coninc frusta where each frustum end was denoted with a node signifying abrupt changes in direction or diameter and giving rise to typical branches represented as cylinders (**Figure 3.5**). These maps allowed tree-level summarization of number of appendages > 20 cm diameter, number of nodes, 95th percentile appendage diameter, and crown volume to represent tree size and complexity. The summed per tree rank of each of these variables was used to rank all trees, then the top 10th percentile trees were isolated and used to define thresholds of LiDAR-derived height, crown area (mean of polygon and raster crown area, **Table 3.4**), and forest density using CRR. Thresholds were validated by applying them back to the 48 trees and examing which were selected. Identified trees from the validation were coded as complex and others as not complex and predicted with stepwise logistic regression using species, height, raster crown area, and polygon crown area as possible predictors. Probability of all trees across the study region were then predicted for all high points > 55-m tall and coded as complex if their probability was > 50 %. Number and density of trees in each structural and geomorphic class were then summarized and compared to examine where elite trees were in relation to geomorphic and forest structural contexts. Elevations > 600 m were excluded from elite tree density calculations because this elevation is the lower transition limit from dominance by *P. menziesii* to dominance by smaller *T. heterophylla* and *A. amabilis* species (Henderson et al., 1989) and would otherwise have artificially reduced elite tree density. Elite tree densities were then compared across geomorphic and structural contexts to describe how these classes differentially contribute to the distribution of such critically important habitat.

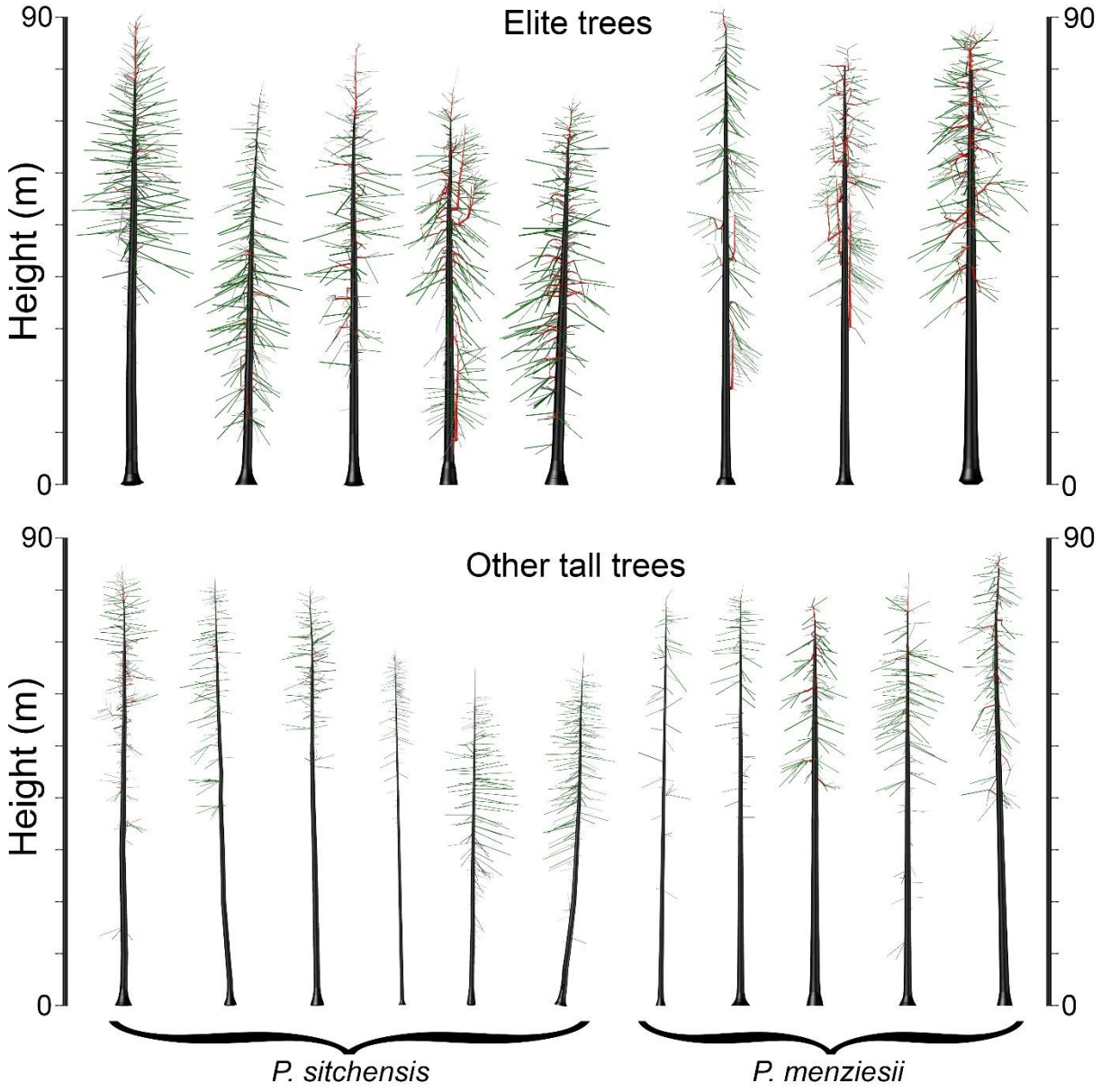

Figure 3.5. Models of crown-mapped trees are a collection of conic frusta representing main trunk (black), complex appendages (red), and branches (green). These are examples of *P. sitchensis* (**left**) and *P. menziesii* (**right**). **Top** shows trees selected from LiDAR-based thresholds crown area (165 m^2), height (72.1 m), and CRR (0.42) extracted from top 10 % of all 48 trees ranked by within-crown characteristics (see text). Trees arranged within species and left to right from lower to higher rank. **Bottom** shows examples of other tall trees not considered elite.

3.3 RESULTS

3.3.1 *Canopy structure differs across geomorphic context*

Watershed-scale canopy structure reflected expectations based on prevailing disturbances and overstory species in valley-bottom versus upland contexts (**Table 3.1**). Valley bottoms had more open-canopy interspersed with smaller patches of closed-canopy forest, while upland had more aggregated closed-canopy forest (**Figure 3.6**). In the following examples, all numbers are drawn from **Table 3.5**. Medium-open structure in valley bottoms was interpreted as background matrix because of its high land percentage (59–67 %) and large (1–2 ha) and highly variable patches reaching more than five times average area (CV = 4.9–5.6). Upland medium-dense structure dominated a patchy matrix with similar percent land area (55–60 %), patch size (0.8–1.1 ha), and patch size variability (CV= 3.8–5.0), but with more aggregation than medium-open structure in valley bottoms (0.21–0.34 vs 0.14–0.26). Characteristics of non-matrix patches in valley bottoms suggested dispersed fine-grain texture. These were roughly an order of magnitude smaller than for medium-open matrix, ranging from 0.13–0.29 ha with less variation (CV = 1.0–3.8 vs. 4.9–5.6) and less aggregation of closed-canopy classes (tall and medium-dense) than upland (0.1–0.4 vs. 0.3–0.6, respectively). Upland non-matrix patches suggested a coarse tall texture alongside more fine-grain and medium-open texture. For example, tall upland patches were relatively rare (12–20 %), large (0.38–0.63 ha) and aggregated (0.55–0.60), while more common medium-open structure (20–30 %) was evenly and widely dispersed given its smaller patch sizes (0.25–0.27 ha) and lower aggregation (0.23–0.29). Lastly, short classes were rare and small in valley-bottom (3–11 % and 0.13–0.21 ha) and upland forests (0.7–0.9 % and 0.16–0.17 ha) but more widely spaced in upland (229 vs 89 m), suggesting fewer gaps. In summary, valley bottoms consisted of a matrix of medium-open forest with dispersed small patches of remaining

structure classes, while upland areas consisted mostly of medium-dense forest with large aggregated tall classes interspersed with small patches of open and short structure (**Figure 3.6**).

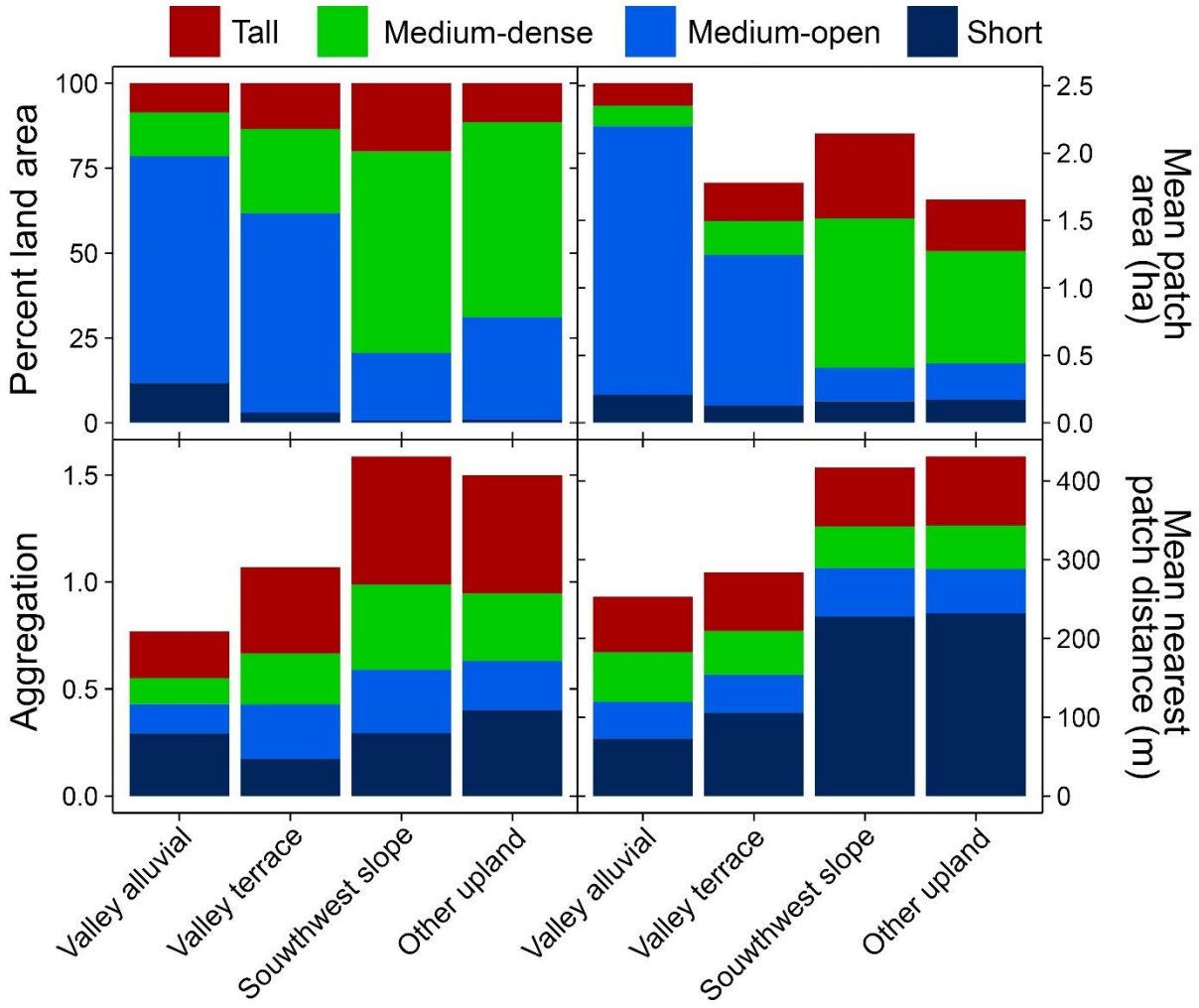

Figure 3.6. Patch characteristics of forests in different geomorphic contexts. Metrics are defined in **Table 3.4** and examples of structure classes are presented in **Figure 3.4**.

Table 3.5. Summary metrics of classified canopy structure within geomorphic class. Metrics are defined in **Table 3.4**. CV = coefficient of variation calculated as standard deviation / mean.

Geomorphic class	Structure class	Percent area (%)	Mean patch area (ha)	CV patch area	Aggregation	Mean nearest patch distance (m)	CV nearest patch distance
Valley alluvial	Tall	8.5	0.17	1.52	0.22	70.2	0.61
(1,220 ha)	Medium-dense	12.9	0.15	1.11	0.12	63.1	0.49
	Medium-open	66.8	1.99	5.64	0.14	47.1	0.42
	Short	11.7	0.21	2.14	0.29	72.5	0.59
Valley terrace	Tall	13.4	0.29	3.14	0.40	74.3	0.87
(910 ha)	Medium-dense	24.8	0.25	3.77	0.24	55.4	0.37
	Medium-open	58.7	1.12	4.91	0.26	48.6	0.45
	Short	3.0	0.13	1.04	0.17	105.6	0.88
Southwest slope	Tall	20.0	0.63	4.72	0.60	74.8	0.97
(3,830 ha)	Medium-dense	59.4	1.10	4.61	0.40	52.3	0.53
	Medium-open	19.8	0.25	2.08	0.30	61.9	0.63
	Short	0.7	0.16	1.08	0.29	227.8	1.09
Other upland	Tall	11.5	0.38	3.25	0.55	87.3	1.11
(4,090 ha)	Medium-dense	57.3	0.83	5.00	0.31	55.6	0.53
	Medium-open	30.2	0.27	2.24	0.23	56.1	0.50
	Short	0.9	0.17	3.88	0.40	232.0	0.90

Valley and upland comparisons were intended to separate effects of different disturbances given the same dominant species. Comparing valley alluvial to valley terraces eliminated effects of alluvial disturbance in *P. sitchensis* forests, while comparing southwest slopes to other upland area intensified effects of high-severity wind and fire in *P. menziesii* forests. Alluvial disturbance increased continuity of medium-open and amount of short forest, because valley terraces had smaller and less variable patch areas (mean = 1.1 vs 2.0; CV = 49 vs 56) and more dispersed (aggregation = 0.17 vs 0.29) short structure located further apart (106 vs. 73 m) than valley bottoms (**Table 3.5**). Absence of alluvial processes also increased the amount of medium-dense structure on terraces (25 vs 13 %) and increased aggregation of all but short structure (**Figure 3.6**). More frequent disturbance on *P. menziesii* southwest slopes increased percent land in tall structure (from 12 to 20 %), mean and variation of patch area in tall structure (mean from 0.38 to 0.63 and CV from 32.5 to 47.2), and aggregation in all but short structure

relative to other slopes (**Table 3.5, Figure 3.6**). Gaps-size variability on southwest slopes was 28 % less than other slopes (CV = 1.1 vs 3.9, **Table 3.5**).

3.3.2 *Disturbance versus species effects on structure in valley-bottom forests*

Valley bottoms dominated by *P. sitchensis* (*Picea* lowland) and *P. menziesii* (Jackson Creek) were compared to upland *P. menziesii* (tall upland) to separate effects of species composition and disturbance. Amount and patch size of tall forest increased with dominance by *P. menziesii*, amount and size of medium-open and short forest increased with dominance by *P. sitchensis*, while upland processes increased aggregation, amount, and size of medium-dense forest relative to alluvial processes. Effects common to tall upland and Jackson Creek were attributed to disturbance, while those common to *Picea* lowland and Jackson Creek were attributed to species composition. Alluvial processes increased medium-open forest in *Picea* lowland (54 %) and Jackson Creek (46 %) relative to tall upland (23 %, **Table 3.6**). In addition, both valley-bottom forests had from 74 to 80 % less medium-dense forest, resulting in shared dominance of tall and medium-open classes. In no case did composition of tall or medium-open forest fall below 33 % in *Picea* lowland or Jackson Creek. Valley-bottom processes also had a dispersing effect on tall, medium-dense, and medium-open structure, evidenced by lower aggregation of these classes in *Picea* lowland and Jackson Creek (**Figure 3.7**). Forests of *P. menziesii* had more tall structure than *P. sitchensis* (46-47 vs 33) in larger patches (0.7–1.0 ha vs 0.4 ha) regardless of geomorphic position (**Table 3.6**). Presence of *P. sitchensis* compounds effects of valley-bottom processes on open canopy structure. For example, percent land and patch size of medium-open forest increased from tall upland to Jackson Creek to *Picea* lowland, while distance between short structure patches decreased (**Figure 3.7**).

Table 3.6. Summary metrics of classified canopy structure for comparing valley-bottom *P. sitchensis* (*Picea* lowland), valley-bottom *P. menziesii* (Jackson Creek), and upland *P. menziesii* (tall upland) canopy structure. Metrics are defined in **Table 3.4**. CV = coefficient of variation calculated as standard deviation / mean.

Geomorphic class	Structure class	Percent area (%)	Mean patch area (ha)	CV patch area (%)	Aggregation	Mean nearest patch distance (m)	CV nearest patch distance (%)
Picea lowland	Tall	32.6	0.39	293	0.27	50.1	24
(138 ha)	Medium-dense	8.0	0.11	61	0.05	69.2	42
	Medium-open	54.3	0.85	436	0.16	45.3	17
	Short	5.1	0.12	57	0.12	86.0	72
Jackson Creek	Tall	47.0	0.74	397	0.29	50.0	23
(117 ha)	Medium-dense	5.3	0.11	49	0.09	84.9	82
	Medium-open	46.4	0.51	286	0.20	46.4	18
	Short	1.3	0.10	24	0.04	144.1	96
Tall upland	Tall	45.7	0.96	362	0.43	46.9	22
(128 ha)	Medium-dense	31.1	0.36	162	0.25	49.6	26
	Medium-open	22.9	0.30	235	0.28	57.2	48
	Short	0.2	0.09	0	-1.00	260.8	30

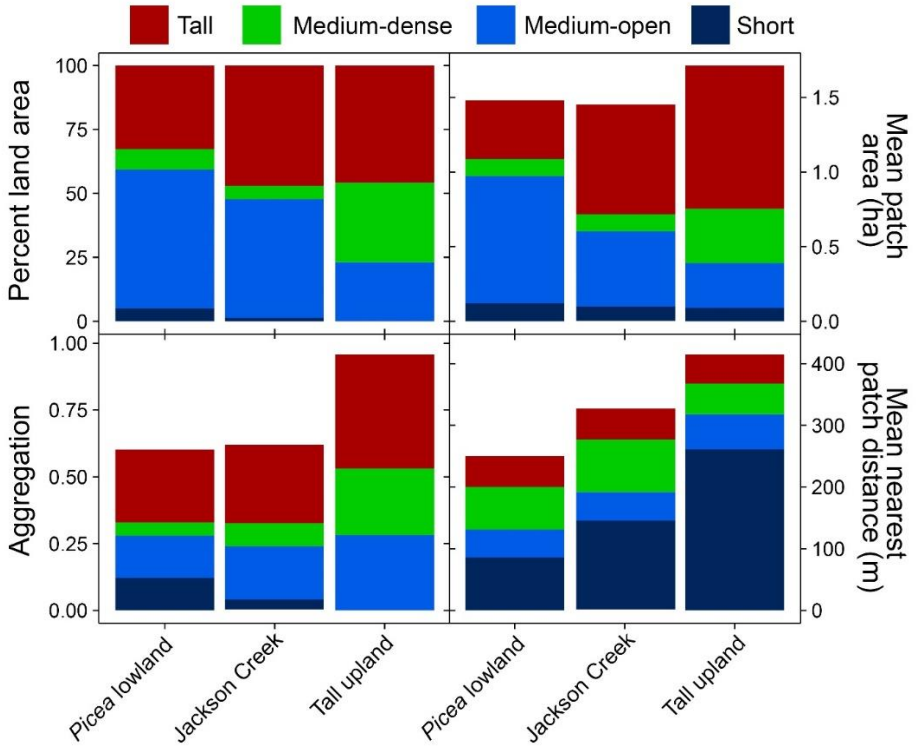

Figure 3.7. Patch characteristics of *Picea* lowland, Jackson Creek, and tall upland forests. Metrics are defined in **Table 3.4** and examples of structure classes are presented in **Figure 3.4**.

3.3.3 *Spatial distribution of elite trees*

Elite trees—defined based on within-crown structure ranking—were significantly predicted by CRR, height, and crown area, while species had no effect (**Table 3.7**). Not surprisingly, wider-crowned and taller trees in less dense forest were more likely to be classified as large and complex (**Table 3.7**). Across the study area, elite trees were exceedingly rare and included only 180 individuals identified across 5,500 ha < 600 m elevation (and only 3 above 600 m). Valley bottoms had the highest density of such trees with 0.05 ha^{-1} in *P. sitchensis* forests collectively, and 0.07 ha^{-1} in Jackson Creek (**Table 3.8**). Upland positions had less than half the density of such trees as valley bottoms (0.02 ha^{-1}), likely due to high percent of land area in medium-dense forest (57–59 %, **Table 3.8**). Approximately 55 % of these trees in valley-bottom *P. sitchensis* were in medium-open forest that covered 67 % of land area. However, elite trees were particularly dense in tall structure class which was only 11 % of land area yet accounted for 37 % of their numbers (**Table 3.8**).

Table 3.7. Logistic regression of largest 10 % of individuals from 36 crown-mapped *P. sitchensis* and 12 *P. menziesii* trees. Only significant predictors at alpha = 0.05 are shown and listed in order of importance. Models fit with logit link function and binomial distribution.

Dependent variable	Intercept	CRR	Polygon area (m^2)	Height (m)	*N*
Elite tree probability	-10.33	-44.7	0.051	0.247	48

Table 3.8. Within geomorphic classes, elite trees predicted from LiDAR metrics are summarized by percent within each structure class. Area and tree density within each geomorphic class are listed below labels. All valley alluvial and valley terraces are consolidated into valley bottom and southwest and other slopes into upland. Representative elite trees are shown in **Figure 3.5**.

Geomorphic class	Structure class	Percent of elite trees	Percent land
Valley bottom	Tall	36.5	11.0
(2126 ha)	Medium-dense	8.7	18.9
0.049 TPH	Medium-open	54.8	62.7
	Short	0.0	7.4
Upland	Tall	66.2	15.8
(3256 ha)	Medium-dense	7.4	58.4
0.0201 TPH	Medium-open	26.5	25.0
	Short	0.0	0.8
Jackson Creek	Tall	62.8	47.0
(118 ha)	Medium-dense	0.0	5.3
0.068 TPH	Medium-open	37.5	46.4
	Short	0.0	1.3

3.4 DISCUSSION

3.4.1 *Effects of disturbance and species on canopy structure in Olympic Forests*

Patterns of canopy structure in valley-bottom *P. sitchensis* forests largely agree with expectations based on context-specific disturbance processes. Valley bottoms exhibit characteristics of shifting steady-state mosaics (Oldeman, 1990; Bormann and Likens, 1979) where small dispersed patches cycle to create large-scale stability. Action of the main river channel, overflow channels, and terrace tributaries (Sedell et al., 1982) form connected areas of low canopy cover, and their movement over time creates large areas of open canopy structure interspersed with islands and dissected forest patches (Beechie et al., 2006; Latterell et al., 2006). Red alder commonly colonizes such areas, creating areas of relatively diminutive forest. After 40 yr stands dominated by *A. rubra* have basal area ~28 m^2 ha^{-1} (Balian and Naiman, 2005) and height ~20 m (Van Pelt et al., 2006), which classifies them as short structure in this study

(**Figure 3.4**). Gravel bars establishing simultaneously with *A. rubra* and *P. sitchensis* likely fall into the medium-open category within 90 yr when maximum heights exceed 50 m and angiosperm trees begin to decline (Van Pelt et al., 2006). Medium-open forest occupies > 50 % of valley terraces despite lacking the river disturbance creating this condition in valley alluvial. One ill-described agent contributing to open structure is migration of outflow from steep ephemeral upland tributaries as they reach the valley floor. These shallow corridors are easily deflected by fallen trees (*personal observation*) and evident as pathways of cobble through the forest and in DEM imagery (**Figure 3.8**). In addition to this disturbance, with enough time, contagious processes of fungal decay and wind create expanding gaps (Hennon, 1995; Taylor, 1990) and infilling of younger generations of trees reflected in larger medium-dense components on terraces (**Figure 3.9**). Together, openness and clusters of medium-dense forest signal late-successional *P. sitchensis-T. heterophylla* forests (Franklin and Dyrness, 1988). These patterns confirm plot-based observations of more open alluvial- versus dense *T. heterophylla*-rich terrace forests (Fonda, 1974; Mckee et al., 1982) and generalize them across the watershed.

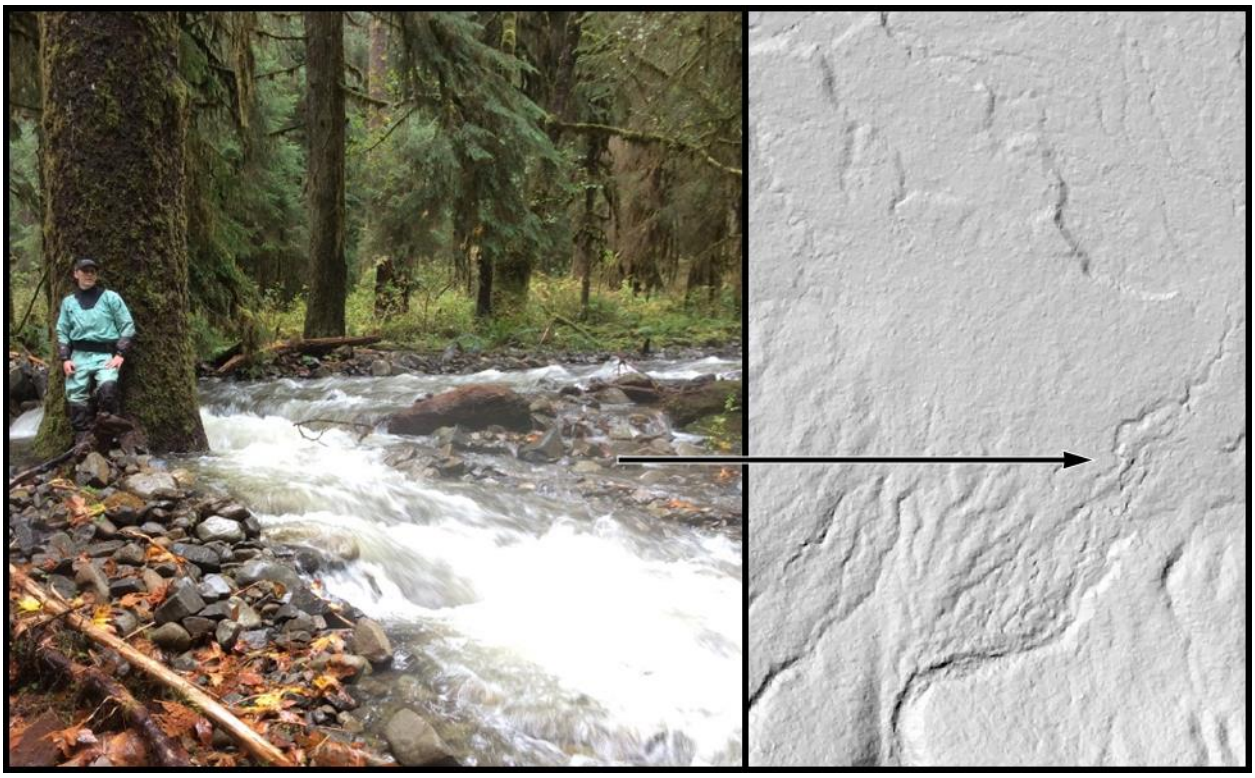

Figure 3.8. During hard rains, ephemeral drainages migrate through forests. **Left** shows water creating a new channel and splitting around a tree. **Right** shows evidence of this phenomenon at the base of a slope debris fan.

Like in valley bottoms, structure of upland forests reflects strong effects of disturbance. Fire and wind appear to result in cohorts of dense closed-canopy structure. Both slopes exhibited a coarser-grained appearance than valley bottoms (**Figure 3.9**). Differences between southwest and other slopes are not as distinct as expected, but southwest slopes do have more and larger patches of aggregated medium-dense and tall forest (**Figure 3.6**). Many, but not all, southwest aspects have distinctive patchy structure (**Figure 3.3b** and **c**); thus, a clear disturbance signal specific to southwest slopes is diluted by less patchy regions. Such inconsistency in patchiness is expected with highly variable localized wind effects (Knapp and Hadley, 2012; Ruth and Yoder, 1953) and low fire frequency (Huff, 1995). Interplay between *P. menziesii* lifespan and disturbance interval likely also makes northeast and southwest aspects less distinct. Northeast

aspects would show more difference in structure if disturbance intervals were significantly longer than tree lifespan and allowed non-competitive overstory mortality to become a dominant process. The concept of tree lifespan relative to disturbance has been applied to community organization (e.g. Jackson and Brown, 1999) and applies equally well to forest structural development.

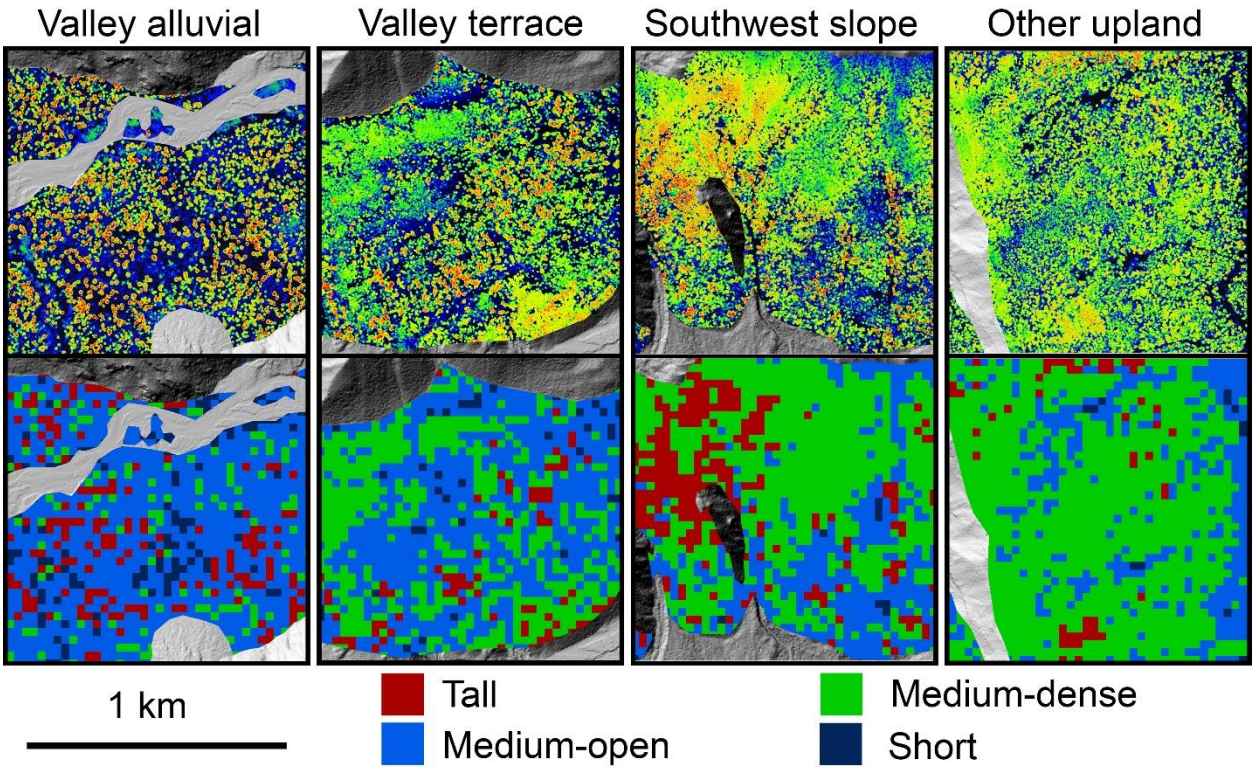

Figure 3.9. Paired clips of CHM and classified canopy structure raster demonstrating some characteristic features of forests in each geomorphic class.

Processes in valley bottoms interact with species dominance to produce alternate patterns of canopy structure. Ability of water channel movement and fungi to modify overstory structure is dampened by *P. menziesii*. In valley bottoms these two agents create more open canopy, but when *P. menziesii* is present, more area and larger patches of tall forest exist with fewer, less

aggregated, and more widely spaced short structure (**Figure 3.10**). *Pseudotsuga menziesii* is less flood-tolerant than *P. sitchensis* (Minore, 1979), so the increased number of tall trees is probably due to lower susceptibility of *P. menziesii* to decay. Although the characteristic signature of valley-bottom forest with high percentage of medium-open forest remains in Jackson Creek, it appears to be concentrated peripherally, perhaps representing a gradation with adjacent *P. sitchensis* (**Figure 3.10**). Alluvial processes are able to overcome the effects of *P. menziesii* by decreasing percentage of medium-dense structure in forests of this age (**Figure 3.10**). Two explanations are worthy of consideration. First, although comparable tall upland forest was selected based partially on evenness of slope and aspect, upland topography varies more than in Jackson Creek and may result in differential disturbance intensity, tree establishment, and subsequent growth. Second, if medium-dense forest is primarily represented by *T. heterophylla*, then lack of *T. heterophylla* in Jackson Creek (Sillett et al., 2018b) and in alluvial relative to upland forests in general (Fonda, 1974; Mckee et al., 1982) may explain this pattern. Although the orogeny of Jackson Creek is unknown, if it established after a flood rather than fire as the upland forest presumably did, there would be few nurse logs on which *T. heterophylla* depends for recruitment (Harmon and Franklin, 1989).

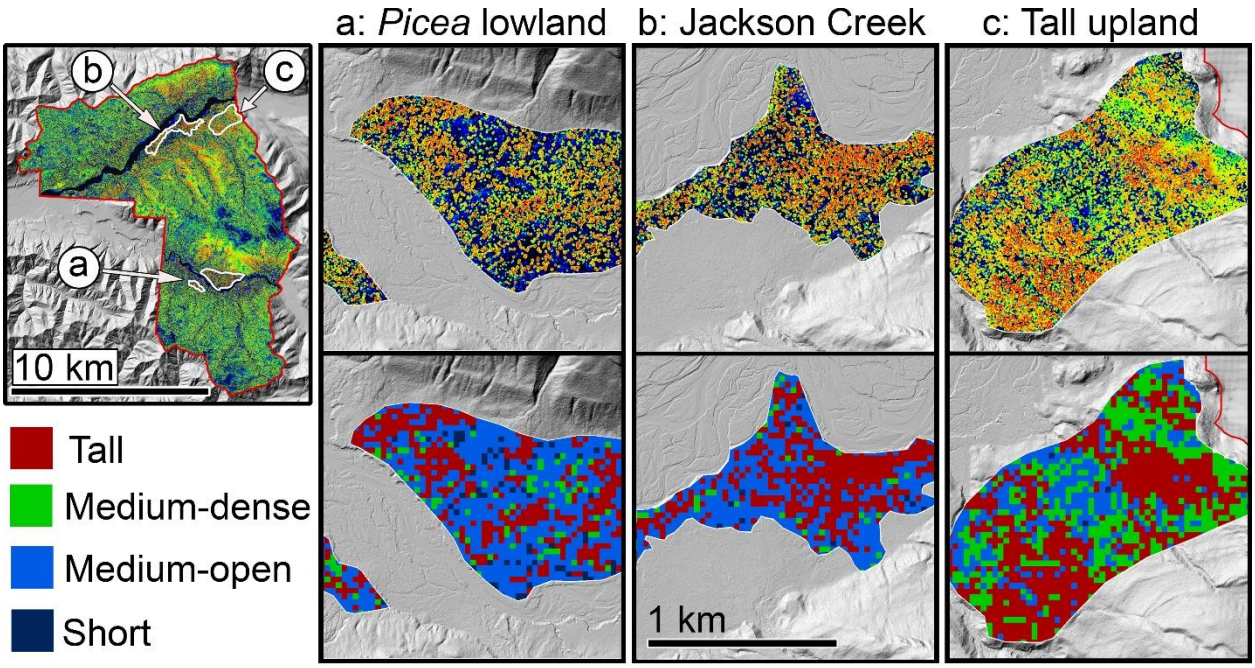

Figure 3.10. Map of locations of three (**a**) Spruce lowland, (**b**) Jackson Creek, and (**c**) Tall upland *P. menziesii* showing comparison of CHM (**top**) and classified canopy structure raster (**bottom**) isolated from surrounding forest. Grey surrounding clips indicate topography as shade-relief DEM.

3.4.2 *Proposed mechanisms for canopy structure pattern*

We propose structure in western Olympic forests is controlled by the presence or absence of either *P. sitchensis* or *P. menziesii* through mechanisms of establishment and survival followed by interaction of these species with intensity and frequency of disturbance. In valley bottoms *P. menziesii* grows well, but cohorts are rare, suggesting recruitment limitation. Either competition after valley disturbances is too strong, or mineral soil is limited given that adjacent upland seed source is abundant. Successful *P. menziesii* establishment may require a narrower suite of initial conditions that leads to a narrower set of outcomes. If establishment conditions are met, *P. menziesii* prolongs the closed-canopy phase, growing into tall dense stands seen upland and in Jackson Creek. When *P. menziesii* fails to establish, *P. sitchensis* is free to develop via a wide range of pathways ranging from dense cohort establishment to sparse invasion of meadows

and alder groves (Cordes, 1972; Peterson et al., 1997; Van Pelt et al., 2006). In addition, because *P. sitchensis* is widely distributed in valley bottoms and more susceptible to decay, greater proportions are subject to river migration and fungi. Upland, *P. sitchensis* is excluded because it cannot survive drier conditions. Here dominant *P. menziesii* and abundant *T. heterophylla* interact with disturbance processes. When disturbances are more intense and recur more frequently than overstory species lifetimes, large homogeneous patches develop. If disturbance is less intense and frequent, a more fine-grained mosaic emerges as forests develop vertical and horizontal spatial variability (Franklin et al., 2002).

Testing these ideas will require further study from several different approaches. To better understand how *P. menziesii* establishment in valley bottoms alters canopy structure, a wider range of *P. menziesii* cohorts compared to *P. sitchensis* forests with trees of similar age. At least two terrace *P. menziesii* cohorts, one ~200 and ~650 yr, exist (Sillett et al., 2018b) as well as terrace *P. sitchensis* forests with 200 yr trees (Kramer et al., 2019) making such a study potentially feasible. Further study of direct causes of medium-open forests will determine how much of this forest condition is due to past channel movements and how much is due to decay. Visiting specific forest openings in valley alluvial and terrace contexts and deducing their cause from current conditions will isolate the relative importance of these to disturbance agents. In upland forests, one avenue for testing the importance of species lifespan versus time since disturbance is relevant. Using data from this study, upland forests in both patchy and fine-grained mosaics can be located and compared against the hypothesis that patchy forests are dominated by longer-lived species experiencing more severe disturbance at higher frequencies than relatively homogeneous forests. In total, such information would provide better estimates of background sizes and frequencies of disturbance agents and enable description of expected

landscapes under alternate scenarios. One promising method of spatial inference requires assumptions of both forest susceptibility and disturbance probability, frequency, and intensity to create "neutral" landscapes for comparison (Gardner et al., 1987). For example, a neutral landscape could be modeled using known disturbance patterns in valley-bottom *P. sitchensis* forests and compare them with actual valley-bottom *P. menziesii* forests to isolate effects of species composition.

3.4.3 *Effects of canopy structure on locations of elite trees*

Valley-bottom forests are widely recognized as important habitat for charismatic species like elk, salmon, and the endangered marbled murrelet. Processes creating favorable conditions for these creatures, such as open-canopy forests with diverse understory plants as well as productive off-channel pools, are the same that grow the vast majority of elite trees (**Figure 3.11**). These trees are rare; on average, one would have to search 20 ha of valley-bottom and 50 ha of upland forest just to find one. A small minority of elite trees provide the vast majority of arboreal habitats (Sillett and Van Pelt, 2007), so although rare, these trees are critically important. Open forest clearly grows larger trees (Kramer et al., 2019), but open forests have fewer trees. This relationship opens questions of the relative ability of valley-bottom and upland forests to produce elite trees. Elite tree density is higher in the tall structure class of this study (which is also dense), a fact evident when comparing the percent of these trees to area of each structure class (**Table 3.8**), yet upland forest with the highest percent of tall trees has half the tree density of valley-bottom forest. How can forests with more tall structure—the class with higher percentage of tall trees—have fewer of them overall? The key is that elite trees are not found within large blocks of tall structure but rather in tall structure interfacing with medium-open structure and gaps (**Figure 3.11**, **Figure 3.12**). Spatial patterns of structural classes in relation to

each other are more important than how much of a structural class exists. The relatively fine-textured pattern of small areas of tall forests embedded in a matrix of medium-open structure is more influential for growing the most important habitat trees then the total amount of tall trees on the landscape.

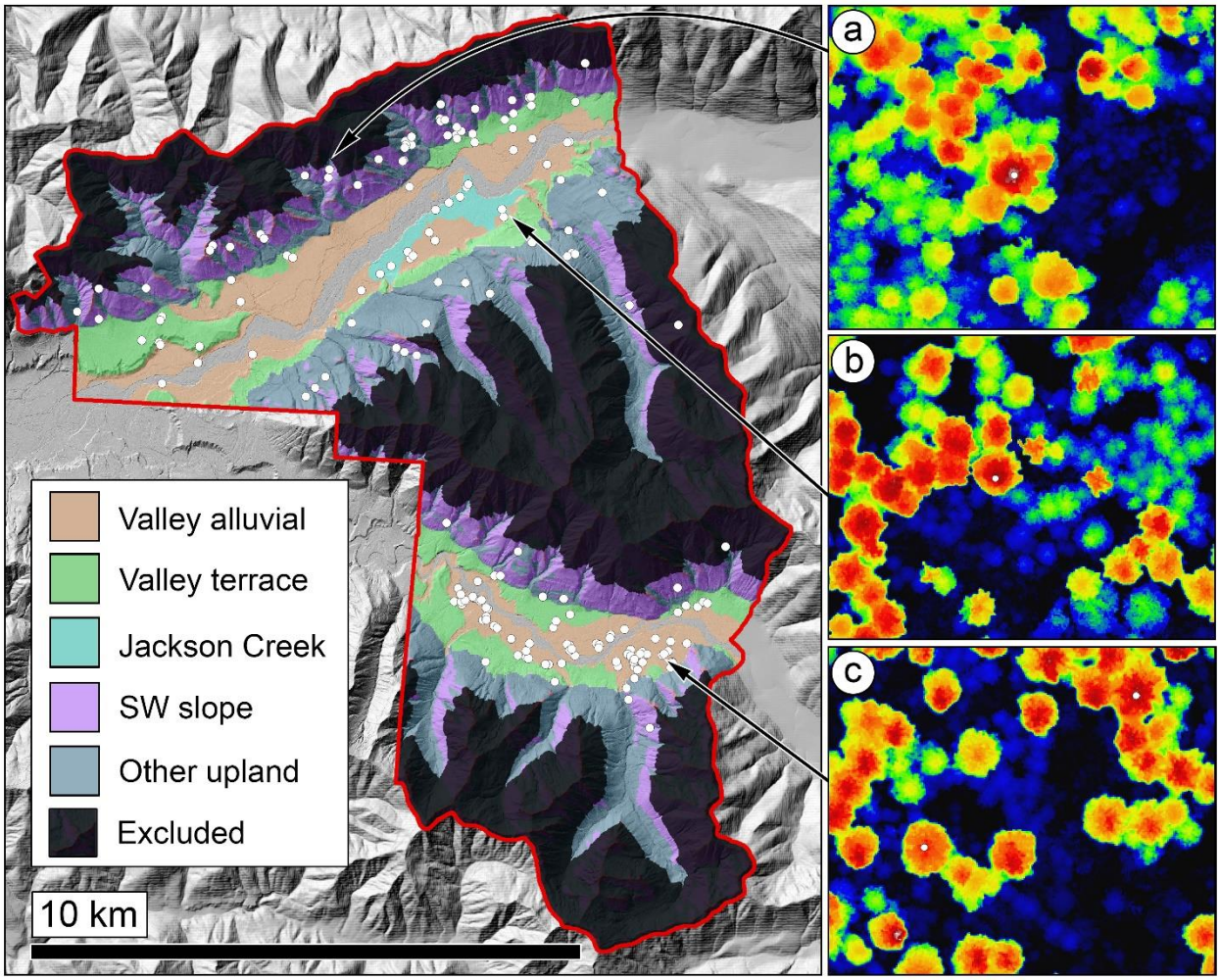

Figure 3.11. On **left**, map of study area showing locations of elite trees (white circles) based on logistic regression of CRR, crown area, and height. Excluded area exceeds 600 m elevation. On **right**, LiDAR CHM indicating locations of elite trees bordering a gap in an upland forest (**a**), between dense edge and gap bordering Jackson Creek (**b**), and in clumps of tall trees bordering open conditions characteristic of valley-bottom forest (**c**). Note three elite trees identified in areas excluded from analysis of tree density > 600 m elevation.

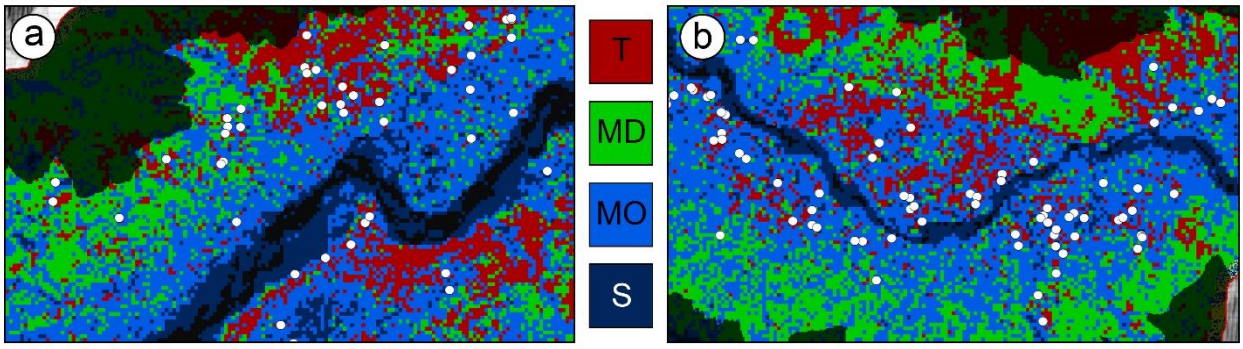

Figure 3.12. Locations of elite trees (white circles) along the Hoh (**a**) and South Fork Hoh (**b**) Rivers with respect to tall (**T**), medium-dense (**MD**), medium-open (**MO**), and short (**S**) canopy structure classes. Dark area is excluded from analysis of tree density.

3.5 CONCLUSION

This study builds upon previous work examining allometry, growth, and development of *P. sitchensis* in alluvial valleys of the Olympic Peninsula in relationship to *Psuedotsuga* (Kramer et al., 2019, 2018). *Picea sitchensis* is probably the fastest-growing conifer in the Pacific Northwest and attains proportions comparable to any of the largest species, sometimes at nearly twice the rate (Kramer et al., 2018; Van Pelt, 2001). We also know that forest density affects the development of complex crowns by delaying formation of large appendages for over 100 yr and reducing crown dimensions by > 80 % (Kramer et al., 2019). Here we describe patterns of open- and closed-canopy forest in valley bottoms and upland positions in the context of disturbance and species dominance. We integrate relationships of tree complexity based on detailed within tree measurement, crown size, and forest density to examine the effects of forest pattern on the distribution of elite individuals.

Valley-bottom forests in the Olympic Mountains are distinct from upland forests due to interaction between disturbance agents and characteristics of the dominant species. Because of anastomosing rivers and susceptibility of *P. sitchensis* to fungi, the forest canopy is a relatively open matrix with high height variability and scattered tall, medium-dense, and short patches.

This structural pattern promotes elite individuals at twice the density of upland forests. Upland forests can provide similar individuals when canopy structure more closely resembles that in valley bottoms. Crucially, it is the interface of tall dense structure with open-canopy forest that provides perfect conditions for growing the most important habitat trees.

FINAL SUMMARY

The most important aspects of *P. sitchensis* development from the three preceding chapters can be incorporated into a cohesive management framework. From chapter one: Because *P. sitchensis's* growth rate is faster than either *P. menziesii* or *S. sempervirens*, its crown is nearly twice as heavy in 200 yr and five times heavier in 500 yr. Forsaking decay resistance for rapid growth, *P. sitchensis* survives a maximum of 500 yr while rainforest *P. menziesii* may live another 300 yr (Carder, 1995) and *S. sempervirens* another millennium (Sillett et al., 2010). From chapter two: Neighborhood density causes nearly 4-fold differences in crown volume in trees over 60-m tall, crown volume decreasing 20 % for each 25 % increase in neighborhood density. Mean appendage diameters vary by > 100 % after 100 yr and age when > 15-cm diameter appendages first appear ranges from 100 to 220 yr. Specific habitat-related appendages develop nearly 100 % faster in *P. sitchensis* than *P. menziesii* and some, like reiterated trunks and limbs, are closely associated with appendage and trunk injury. From chapter three: Valley-bottom forests contrast sharply with denser more aggregated upland forests by having small patches of gap, medium-height dense, and tall patches in a matrix of variable but generally open-canopy forest. Valley-specific disturbances and *P. sitchensis* ecology create optimal conditions to growing elite trees in this context. Valley-bottoms have twice the density of these trees compared to upland forests due to extensive interface between tall-dense and open-canopy forest.

What emerges is a uniquely important species producing enormous crowns in short periods, while being a dynamic yet stable component of the ecosystem. *Picea sitchensis* invests more in crown building than co-occurring dominant species. Crown mass reaches 15 % of total mass compared to 9 % in *P. menziesii* and *S. sempervirens* (Kramer et al., 2018). Given its live-fast-die-young strategy, the forests *P. sitchensis* inhabits change rapidly. Fallen trees increase

light for understory vegetation and are replaced by understory seedlings on decaying logs. The ability to regenerate in shade combined with attainment of great size, insures constancy of *P. sitchensis* as an overstory community member through time. The most unique contribution of *P. sitchensis* is probably the range of dominant tree density in such forests. On average they are more open, but they contain patches as dense as any forest, translating to wide ranges in tree structure and subsequent habitat for different organisms. Dense trees produce groves with high biomass and productivity, while unencumbered crowns with hundreds of large appendages draped with mosses create homes for arboreal creatures.

Guidelines for ecological forest management of *P. sitchensis* presented here are associated specifically with accelerating development of large and complex trees so they can be more easily incorporated into existing restoration frameworks. Forests moist enough to support *P. sitchensis* should include it if goals are to create large trees quickly; *P. sitchensis* grows nearly 100 cm diameter per century and relatively early death insures contribution of large logs, gaps, and regenerative capacity in the future forest. Competitive interactions within a 25–30-m radius constrain crown development of *P. sitchensis*, thus some trees should be left with at least this much competition-free space. But how many trees? In valley alluvial sites and terraces short structure is 11.7 and 3 % of forest, respectively, and many open-grown trees are in medium-open matrix forest structure (66.8 and 58.7 % respectively), suggesting an absolute minimum of 3 % of land area in such condition and perhaps as highs as 30 %. Appendages large enough for marbled murrelet nesting can be attained in 100 yr with 30-m of competition-free space, while leaving only 12-m increases this time to 150 yr. To emulate natural conditions, it is worthwhile to manage differently in areas affected by rivers. Valley alluvial sites and terraces average only 16–17 dominant trees per ha (**Table 4.1**), however their spatial distribution varies. Alluvial sites

have 8.5 % in tall, 13 % in medium-dense, 66.8 % in medium open and 11.7 % in gap, while terraces have 13.4 % in tall, 24.8 % in medium dense, 58.7 % in medium open, and 3 % in gap, and each structural class has specific densities of dominant trees (**Table 4.1**). Lastly, encouraging injury in some trees enhances production of reiterated trunk and the largest appendages (limbs). Retention trees with broken tops should be left with a minimum of 12-m radius of growing space to allow crowns to rebuild. These guidelines should be easy to incorporate into existing variable density practices which already leave individuals, clumps of various sizes, and openings.

Table 4.1. Canopy structural attributes in geomorphic classes showing percent area, basal area, and trees per hectare in each neighborhood structure class for trees > 55-m tall. Parentheses are ± 1 standard deviation. Mean basal area and trees per hectare weighted by percent area for each geomorphic class are presented below underlined labels. Basal area based on diameter predicted from height (N = 488, R^2 = 0.75).

Geomorphic class	Structure class	Percent area (%)	Basal area (m^2 ha^{-1})		Mean TPH (# ha^{-1})	
Valley alluvial	Tall	8.5	68.3	(22.3)	49	(18)
BA: 19.3	Medium dense	12.9	32.1	(19.7)	30	(19)
TPH: 16	Medium open	66.8	13.9	(14.5)	13	(13)
	Short	11.7	0.1	(1.2)	0	(1)
Valley terrace	Tall	13.4	75.8	(27.7)	53	(36)
BA: 17.6	Medium dense	24.8	22.2	(20.0)	21	(18)
TPH: 17	Medium open	58.7	12.2	(14.0)	11	(11)
	Short	3.0	0.3	(1.5)	0	(1)
Southwest slope	Tall	20.0	78.6	(38.7)	71	(36)
BA: 28.9	Medium dense	59.4	14.1	(17.0)	16	(19)
TPH: 24	Medium open	19.8	8.9	(12.1)	9	(12)
	Short	0.7	0.2	(1.4)	0	(2)
Other upland	Tall	11.5	78.0	(33.25)	63	(29)
BA: 19.8	Medium dense	57.3	18.1	(16.9)	21	(19)
TPH: 20	Medium open	30.2	11.1	(12.2)	12	(12)
	Short	0.9	0.3	(1.5)	0	(2)

Several obvious questions present themselves due to the inferred linkages of crown structure with canopy ecology and in successfully utilizing *P. sitchensis* for restoration. While this dissertation focuses on crown structure underlying canopy biodiversity and abundance of epiphytes, it does not make more than circumstantial links (**Appendix 2.C**) between specific structures, their crown location, what density of forest they occur in, and their importance to arboreal organisms. A systematic study of which organisms benefit from which structures is the next step, possibly accomplished with remote cameras and direct survey. An example research question is: Are large appendages in dense forests similarly important to epiphyte composition and biomass as in open forests? In addition, comparisons of structure between species largely assume that crown structure in *P. sitchensis* is equally important to similar structure in *P. menziesii* and *S. sempervirens.* In reality, different bark texture, litter fall structure, species chemistry, and ability to adventitiously root into canopy soil likely alter the relative importance us such appendages. Studying differences in canopy moss- and fern-mat structure on similarly sized appendages in different species will illuminate such contrasts. Lastly, I strongly assert *P. sitchensis* should be included in restoration treatments while completely ignoring well-documented silvicultural problems related to the white pine weevil (*Pissodes strobi*). Weevils kill the uppermost treetop (leader), causing trunk defects (Lysak et al., 2006). In an ecological setting, this is not necessarily a problem so long as the tree survives, nonetheless leader death may impair the ability of *P. sitchensis* to become a canopy dominant tree. There is evidence that weevils prefer leaders heated for long periods during the day to those growing in the shade of other trees (Spittenhouse et al., 1994; Taylor et al., 1996). Of special interest regarding restoration treatments would be effects of multi-species silviculture on the incidence of this insect.

REFERENCES

Abbe, T.B., Montgomery, D.R., 2003. Patterns and processes of wood debris accumulation in the Queets river basin, Washington. Geomorphology 51, 81–107.

Abràmoff, M.D., Hospitals, I., Magalhães, P.J., Abràmoff, M., 2004. Image processing with ImageJ. Biophotonics Int. 11, 36–42.

Alaback, P.B., 1982. Dynamics and understory biomass in Sitka spruce-western henlock forests of southeast Alaska. Ecology 63, 1932-1948.

Anderson, D.L., Koomjian, W., French, B., Altenhoff, S.R., Luce, J., 2015. Review of rope-based access methods for the forest canopy: Safe and unsafe practices in published information sources and a summary of current methods. Methods Ecol. Evol. 6, 865–872.

Aubry, K.B., Halpern, C.B., Peterson, C.E., 2009. Variable-retention harvests in the Pacific Northwest: A review of short-term findings from the DEMO study. For. Ecol. Manage. 258, 398–408.

Balian, E. V, Naiman, R.J., 2005. Abundance and production of riparian trees in the lowland floodplain of the Queets River, Washington. Ecosystems 8, 841–861.

Bastin, J.-F., Barbier, N., Réjou-Méchain, M., Fayolle, a., Gourlet-Fleury, S., Maniatis, D., de Haulleville, T., Baya, F., Beeckman, H., Beina, D., Couteron, P., Chuyong, G., Dauby, G., Doucet, J.-L., Droissart, V., Dufrêne, M., Ewango, C., Gillet, J.F., Gonmadje, C.H., Hart, T., Kavali, T., Kenfack, D., Libalah, M., Malhi, Y., Makana, J.-R., Pélissier, R., Ploton, P., Serckx, a., Sonké, B., Stevart, T., Thomas, D.W., De Cannière, C., Bogaert, J., 2015. Seeing central African forests through their largest trees. Sci. Rep. 5, 13156.

Bauhus, J., Puettmann, K., Messier, C., 2009. Silviculture for old-growth attributes. For. Ecol. Manage. 258, 525–537.

Beechie, T.J., Liermann, M., Pollock, M.M., Baker, S., Davies, J., 2006. Channel pattern and river-floodplain dynamics in forested mountain river systems. Geomorphology 78, 124–141.

Binging, G., Dobbertin, M., 1995. Evaluation of competition indices in individual tree growth models. For. Sci. 41, 360–377.

Bormann, B.T., 1990. Diameter-based biomass regression model ignore large sapwood-related variation in Sitka spruce. Candian J. For. Res. 20, 1098–1104.

Bormann, F.H., Likens, G.E., 1979. Pattern and process in a forested ecosystem. Springer-Verlag, New York, USA.

Brandeis, T.J., Newton, M., Filip, G.M., Cole, E.C., 2002. Cavity-nester habitat in artificially made Douglas-fir snags. J. Wildl. Manage. 66, 625–633.

Breiman, L., 2001. Random forests. Mach. Learn. 45, 5–32.

Brown, C.E., Campbell-Spickler, J., Marks, S.B., Reiss, J.O., 2018. *Aneides vagrans* is absent from angiosperm crowns in an old-growth redwood forest. Herpetol. Conserv. Biol. 13, 533–538.

Burger, A.E., Ronconi, R. A., Silvergieter, M.P., Conroy, C., Bahn, V., Manley, I. A., Cober, A., Lank, D.B., 2010. Factors affecting the availability of thick epiphyte mats and other potential nest platforms for Marbled Murrelets in British Columbia. Can. J. For. Res. 40, 727–746.

Burnham, K.P., Anderson, D.R., 2002. Model selection and multi-model inference: A practical information-theoretic approach.

Burns, R.M., Honkala, B.H., 1990. R.M. Burns, B.H. Honkala (Eds.) Silvics of North America: 1. Conifers. USDA For. Serv., Washington, DC. (Agricultural Handbook 654).

Carder, A.C., 1995. Forest Giants of the World Past and Present. Fitzhenry and Whiteside, Markham, Ont.

Carey, A.B., Wilson, S., 2001. Induced spatial heterogeneity in forest canopies: Responses of small mammals. J. Wildl. Manage. 65, 1014-1027.

Carey, A.B., 1996. Interactions of northwest forest canopies and arboreal mammals. Northwest Sci. 70, 72-78.

Carey, A.B., 2007. AIMing for healthy forests: Active, Intentional Management of multiple values. USDA Forest Service, Gen. Tech. Rep. No. PNW-GTR-721.

Chin, A.R.O., Sillett, S.C., 2017. Leaf acclimation to light availability supports rapid growth in tall *Picea sitchensis* trees. Tree Physiol. 37, 1352–1366.

Chojnacky, D.C., Heath, L.S., Jenkins, J.C., 2014. Updated generalized biomass equations for North American tree species. Forestry. 87, 129-151.

Churchill, D.J., Larson, A.J., Dahlgreen, M.C., Franklin, J.F., Hessburg, P.F., Lutz, J.A., 2013. Restoring forest resilience: From reference spatial patterns to silvicultural prescriptions and monitoring. For. Ecol. Manage. 291, 442–457.

Cissel, J.H., Swanson, F.J., Weisberg, P.J., 1999. Landscape management using historical fire regimes: Blue River, Oregon. Ecol. Appl. Appl. 9, 1217–1231.

Clements, F.E., 1936. Nature and structure of the climax. J. Ecol. 24, 252–284.

Cline, M.G., 1997. Concepts and terminology of apical dominance. Am. J. Bot. 84, 1064–1069.

Coates, K.D., Canham, C.D., Lepage, P.T., 2009. Above- versus below-ground competitive effects and responses of a guild of temperate tree species. J. Ecol. 97, 118–130.

Cochran, P.H., Geist, J.M., Clemens, D.L., Rodrick, R., Powell, D.C., 1994. Suggested stocking levels for forest stands in northeastern Oregon and outheastern Washington, USDA, Forest

Service PNW Res. Stat. PNW-RN-513.

Cole, W.G., Lorimer, C.G., 1994. Predicting tree growth from crown variables in managed northern hardwood stands. For. Ecol. Manage. 67, 159–175.

Contreras, M.A., Affleck, D., Chung, W., 2011. Evaluating tree competition indices as predictors of basal area increment in western Montana forests. For. Ecol. Manage. 262, 1939–1949.

Coonen, E.J., Sillett, S.C., 2015. Separating effects of crown structure and competition for light on trunk growth of *Sequoia sempervirens*. For. Ecol. Manage. 358, 26–40.

Cordes, 1972. An ecological study of the Stika spruce forest on the west coast of Vancouver Island. Doctoral Dissertation, University of British Columbia.

Côté, J.-F., Fournier, R. a., Egli, R., 2011. An architectural model of trees to estimate forest structural attributes using terrestrial LiDAR. Environ. Model. Softw. 26, 761–777.

Crook, M.J., Ennos, A.R., Banks, J.R., 1997. The function of buttress roots : A comparative study of the anchorage systems of buttressed (*Aglaia* and *Nephelium ramboutan* species) and non-buttressed (*Mallotus wrayi*) tropical trees. J. Exp. Bot. 48, 1703–1716.

Deal, R.L., Hennon, P., O'Hanlon, R., D'Amore, D.D., 2014. Lessons from native spruce forests in Alaska: managing Sitka spruce plantations worldwide to benefit biodiversity and ecosystem services. Forestry 87, 193–208.

Dean, C., Kirkpatrick, J.B., Osborn, J., Doyle, R.B., Fitzgerald, N.B., Roxburgh, S.H., 2018. Novel 3D geometry and models of the lower regions of large trees for use in carbon accounting of primary forests. AoB plants 10, 1–20.

Ellyson, W.J.T, Sillett, S.C. 2003. Epiphyte communities on Sitka spruce in an old-growth redwood forest. Bryologist 106, 197-211.

England, J.R., Attiwill, P.M., 2006. Changes in leaf morphology and anatomy with tree age and

height in the broadleaved evergreen species , *Eucalyptus regnans* F . Muell. Trees 20, 79–90.

Ennos, A.R., 1993. The function and formation of buttresses. Tree 8, 350–351.

Esau, K., 1965. Plant Anatomy, 2nd ed. John Wiley and Sons, New York., pp.2-10

ESRI, 2014. ArcGIS Desktop: Release 10.3.

Fahey, T.J., Woodbury, P.B., Battles, J.J., Goodale, C.L., Hamburg, S.P., Ollinger, S. V, Woodall, C.W., 2010. Forest carbon storage : ecology, management, and policy. Front. Ecol. Environ. 8, 245–252.

Fajardo, A., Mcintire, E.J.B., Olson, M.E., 2018. When short stature is an asset in trees. Trends Ecol. Evol. 34, 193–199.

Farr, W.A., Harris, A.S., 1979. Site index of Sitka spruce along the Pacific coast related to latitude and temperatures. For. Sci. 25, 145–153.

Fonda, R.W., 1974. Forest succession in relation to river terrace development in Olympic National Park, Washington. Ecology 55, 927–942.

Ford, E.D., 1982. High productivity in a polestage Sitka spruce stand and its relation to canopy structure. Forestry 55, 1–17.

Forsman, E.D., Swingle, J.K., 2007. Use of arboreal nests of tree voles (*Arborimus* spp.) by amphibians. Herpetol. Conserv. Biol. 2, 113–118.

Franklin, J.F., Dyrness, C.T., 1988. Natural vegetation of Oregon and Washington. Oregon State University Press, Corvallis, OR., pp.58-69.

Franklin, J.F., Johnson, K.N., 2012. A restoration framework for federal forests in the Pacific Northwest. J. For. 110, 429–439.

Franklin, J.F., Johnson, N.K., Johnson, D.L., 2018. Ecological Forest Management. Waveland

Press, Long Grove, IL.

Franklin, J.F., Spies, T.A., Van Pelt, R., Carey, A.B., Thornburgh, D.A., Berg, D.R., Lindenmayer, D.B., Harmon, M.E., Keeton, W.S., Shaw, D.C., Bible, K., Chen, J., 2002. Disturbances and structural development of natural forest ecosystems with silvicultural implications, using Douglas-fir forests as an example. For. Ecol. Manage. 155, 399–423.

Franklin, J.F., Swanson, F.J., Sedell, J.R., 1982. Relationships within the valley floor ecosystems of western Olympic National Park: A Summary, in: Ecological Research in National Parks of the Pacific Northwest. Oregon State University Forest Research Laboratory, Corvallis, OR, pp. 43–45.

Franklin, J.F., Van Pelt, R., 2004. Spatial aspects of structural complexity in old-growth forests. J. For. 22–28.

Gardner, R.H., Milne, B.T., Turner, M.G., O'Neill, R.V., 1987. Neutral models for the analysis of broad-scale landscape pattern. Landsc. Ecol. 1, 19–28.

Gavin, D.G., Brubaker, L.B., Lertzman, K.P., 2003. Holocene fire history of a coastal temperate rain forest based on soil charcoal radiocarbon dates. Ecology 84, 186–201.

Gleason, H.A., 1926. The individualistic concept of the plant association. Bull. Torrey Bot. Club 53, 7–26.

Goetz, S.J., Baccini, A., Laporte, N.T., Johns, T., Walker, W., Kellndorfer, J., Houghton, R.A., Sun, M., 2009. Mapping and monitoring carbon stocks with satellite observations: a comparison of methods. Carbon Balance Manag. 4, 1-7.

Gorman, A.A.J., Kerhoulas, L.P., Polda, W.T., Kerhoulas, N.J., 2019. Epiphyte diversity, abundance, and distribution in an old Sitka spruce crown. Evansia 36, 12–22.

Greene, S.E., Harcombe, P.A., Harmon, M.E., Spycher, G., 1992. Patterns of growth, mortality

and biomass change in a coastal *Picea sitchensis-Tsuga heterophylla* forest. J. Veg. Sci. 3, 697–706.

Grissino-Mayer, H.D., 2001. Evaluating crossdating accuracy: A manual and tutorial for the computer program COFFECHA. Tree-Ring Res. 57, 205–221.

Hackenberg, J., Morhart, C., Sheppard, J., Spiecker, H., Disney, M., 2014. Highly accurate tree models derived from terrestrial laser scan data: A method description. Forests 5, 1069–1105.

Hallé, F., Oldeman, R.A.A., Tomlinson, P.B., 1978. Tropical trees and forests: an architectural analysis. Springer-Verlag, New York, New York, USA.

Hamer, T.E., Nelson, S.K., 1995. Characteristics of marbled murrelet nest trees and nesting stands, in: C. J. Ralph Jr., M. Raphael, and J. F. Piatt, G.L.H. (Ed.), Ecology and Conservation of the Marbled Murrelet. USDA, Forest Service, Albany, California, USA, pp. 69–82.

Harcombe, P.A., Greene, S.E., Kramer, M.G., Acker, S.A., Spies, T.A., Valentine, T., 2004. The influence of fire and windthrow dynamics on a coastal spruce-hemlock forest in Oregon, USA, based on aerial photographs spanning 40 years. For. Ecol. Manage. 194, 71–82.

Harmon, M.E., Franklin, J.F., 1989. Tree seedlings on logs in *Picae-Tsuga* forests of Oregon and Washington. Ecology 70, 48–59.

Harmon, M.E., Woodall, C.W., Fasth, B., Sexton, J., 2008. Woody detritus density and density reduction factors for tree species in the United States: A synthesis. USDA, For. Serv. Gen. Tech. Rep. NRS-29.

Harrison, R.B., Terry, T.A., Licata, C.W., Flaming, B.L., Meade, R., Guerrini, I.A., Strahm, B.D., Xue, D., Lolley, M.R., Sidell, A.R., Wagoner, G.L., Briggs, D., Turnblom, E.C.,

2009. Biomass and stand characteristics of a highly productive mixed Douglas-fir and western hemlock pantation in coastal Washington. West. J. Appl. For. 24, 180–186.

Harvey, G.M., 1962. Heart rots of Douglas-fir. USDA, For. Serv., Forest Pest Leaflet 73.

Henderson, J.A., Peter, D.H., Lesher, R.D., Shaw, D.C., 1989. Forested plant association of the Olympic National Forest. USDA, Forest Service. R6 Ecol. Tech. Paper 001-88.

Hennon, P.E., 1995. Are heart rot fungi major factors of disturbance in gap-dynamic forests? Northwest Sci. 69, 284–293.

Hershey, K.T., Meslow, E.C., Ramsey, F.L., Ramsey, F.L., 1998. Characteristics of forests at spotted owl nest sites in the Pacific Northwest. J. Wildl. Manage. 62, 1398–1410.

Hobbs, R.J., Lindenmayer, D.B., 2007. From perspectives to principals: Where to from here?, in Lindenmayer, D.B., Hobbs, R.J. (Eds.), Managing and Designing Landscapes for Conservation: Moving from Perspectives to Principals. Blackwell, Oxford., pp. 561-568.

Huff, M.H., 1995. Forest age structure and development following wildfires in the western Olympic Mountains, Washington. Ecol. Appl. 5, 471–483.

Ishii, H., Ford, D.E., Dinnie, E.C., Ford, E.D., Dinnie, C.E., 2002. The role of epicormic shoot production in maintaining foliage in old *Pseudotsuga menziesii* (Douglas-fir) trees II. Basal reiteration from older branch axes. Can. J. Bot. 80, 916–926.

Ishii, H., Ford, E.D., 2001. The role of epicormic shoot production in maintaining foliage in old *Pseudotsuga menziesii* (Douglas-fir) trees. Can. J. Bot. 79, 251–264.

Ishii, H., McDowell, N., 2002. Age-related development of crown structure in coastal Douglas-fir trees. For. Ecol. Manage. 169, 257–270.

Ishii, H., Sillett, S.C., Carroll, A.L., 2017. Crown dynamics and wood production of Douglas-fir trees in an old-growth forest. For. Ecol. Manage. 384, 157–168.

Ishii, H., Ford, E.D., Kennedy, M.C., 2007. Physiological and ecological implications of adaptive reiteration as a mechanism for crown maintenance and longevity. Tree Physiol. 27, 455–462.

Ishii, H., Jennings, G.M., Sillett, S.C., Koch, G.W., 2008. Hydrostatic constraints on morphological exploitation of light in tall *Sequoia sempervirens* trees. Oecologia 156, 751–763.

Ishii, H., Minamino, T., Azuma, W., Hotta, K., Nakanishi, A., 2018. Large, retained trees of *Cryptomeria japonica* functioned as refugia for canopy woody plants after logging 350 years ago in Yakushima , Japan. For. Ecol. Manage. 409, 457–467.

Jackson, W.D., Brown, M.J., 1999. Pattern and process in the vegetation, in: Reid, J.B., Hill, R.S., Brown, Michael J., Hovenden, M.J. (Eds.), Vegetation of Tasmania. Australian Biological Resources Study, Hobart, pp. 359–365.

Jenkins, J.C., Chojnacky, D.C., Heath, L.S., Birdsey, R.A., 2004. Comprehensive database of diameter-based biomass regressions for North American tree species. USDA For. Serv. Gen. Tech. Rep. NE-319.

Jenkins, J.C., Chojnacky, D.C., Heath, L.S., Birdsey, R.A., 2003. National-scale biomass estimators for United States tree species. For. Sci. 49, 12–35.

Jepson, J., 2000. The tree climber's companion: A reference and training manual for proffesional tree climbers, 2nd ed. Beaver Tree Publishing, Longville, MN.

Jeronimo, S.M.A., Kane, V.R., Churchill, D.J., Mcgaughey, R.J., Franklin, J.F., 2018. Applying LiDAR individual tree detection to management of structurally diverse forest landscapes. J. For. 116, 336–346.

Kane, V.R., McGaughey, R.J., Bakker, J.D., Gersonde, R.F., Lutz, J. a., Franklin, J.F., 2010.

Comparisons between field- and LiDAR-based measures of stand structural complexity. Can. J. For. Res. 40, 761–773.

Kimmey, J.W., 1956. Cull factors for Sitka spruce, western hemlock and western redcedar in Southesat Alaska. USDA For. Serv., Alaska For. Res. Center Station Paper No. 6.

Kimmey, J.W., 1958. The heart rots of redwood. USDA, For. Serv., California For. and Range Exp. Stat. Forest Pest Leaflet 25.

Kimmey, J.W., Hornibrook, E.M., 1952. Cull and breakage factors and other tree measurement tables for redwood. USDA, For. Serv. For. Surv., California For. and Range Exp. Stat. Release No. 13.

Kluyver, T., Ragan-Kelley, B., Pérez, F., Granger, B., Bussonnier, M., Frederic, J., Kelly, K., Hamrick, J., Grout, J., Corlay, S., Ivanov, P., Avila, D., Abdalla, S., Willing, C., Development Team, J., 2016. Jupyter Notebooks — a publishing format for reproducible computational workflows, in: Loizides, F., Schmidt, B. (Eds.), Positioning and Power in Academic Publishing: Players, Agents and Agendas. IOS Press, pp. 87–90.

Knapp, P.A., Hadley, K.S., 2012. A 300-year history of Pacific Northwest windstorms inferred from tree rings. Glob. Planet. Change 92–93, 257–266.

Koch, G.W., Sillett, S.C., Jennings, G.M., Davis, S.D., 2004. The limits to tree height. Nature 428, 851–854.

Kramer, R.D., Sillett, S.C., Carroll, A.L., 2014. Structural development of redwood branches and its effects on wood growth. Tree Physiol. 34, 314–330.

Kramer, R.D., Sillett, S.C., Van Pelt, R., Franklin, J.F., 2019. Neighborhood competition mediates crown development of Picea sitchensis in Olympic rainforests: Implications for restoration management. For. Ecol. Manage. 441, 127–143.

Kramer, R.D., Sillett, S.C., Van Pelt, R., 2018. Quantifying aboveground components of *Picea sitchensis* for allometric comparisons among tall conifers in North American rainforests. For. Ecol. Manage. 430, 59–77.

Lamb, S.M., MacLean, D.A., Hennigar, C.R., Pitt, D.G., 2017. Imputing tree lists for New Brunswick spruce plantations through nearest-neighbor matching of airborne laser scan and inventory plot data. Can. J. Remote Sens. 43, 269–285.

Lanner, R.M., Connor, K.F., 2001. Does bristlecone pine senesce? Exp. Gerontol. 36, 675–85.

Larson, A.J., Lutz, J.A., Donato, D.C., Freund, J.A., Swanson, M.E., HilleRisLambers, J., Sprugel, D.G., Franklin, J.F., 2015. Spatial aspects of tree mortality strongly differ between young and old-growth. Ecology.

Latham, P., Tappeiner, J., 2002. Response of old-growth conifers to reduction in stand density in western Oregon forests. Tree Physiol. 22, 137–146.

Latterell, J.J., Scott Bechtold, J., O'keefe, T.C., Van Pelt, R., Naiman, R.J., 2006. Dynamic patch mosaics and channel movement in an unconfined river valley of the Olympic Mountains. Freshw. Biol. 51, 523–544.

Lefsky, M.A., Cohen, W.B., Acker, S.A., Parker, G.G., Spies, T.A., Harding, D., 1999. LiDAR remote sensing of canopy structure and biophysical properties of Dougals-fir western hemlock forests. Remote Sens. Environ. 70, 339–361.

Lehmkuhl, J.F., Raphael, M.G., 1993. Habitat pattern around northern spotted owl location on the Olympic Peninsula, Washington. J. Wildl. Manage. 57, 302–315.

Lindenmayer, D.B., 2016. The importance of managing and conserving large old trees: A case study from Victorian mountain ash forests. Proc. R. Soc. Victoria 128, 64–70.

Lindenmayer, D.B., Laurance, W.F., Franklin, J.F., Likens, G.E., Banks, S.C., Blanchard, W.,

Gibbons, P., Ikin, K., Blair, D., Mcburney, L., Manning, A.D., Stein, J.A.R., 2014. New policies for old trees : Averting a global crisis in a keystone ecological structure. Conserv. Lett. 7, 61–69.

Lisein, J., Pierrot-Deseilligny, M., Bonnet, S., Lejeune, P., 2013. A photogrammetric workflow for the creation of a forest canopy height model from small unmanned aerial system imagery. Forests 4, 922–944.

Looney, C.E., Amato, A.W.D., Palik, B.J., Fraver, S., Kastendick, D.N., 2018. Size-growth relationship, tree spatial patterns, and tree-tree competition influence tree growth and stand complexity in a 160-year red pine chronosequence. For. Ecol. Manage. 424, 85–94.

Lutz, J.A., Larson, A.J., Swanson, M.E., Freund, J. a., 2012. Ecological importance of large-diameter trees in a temperate mixed-conifer forest. PLoS One 7, 1-15.

Lutz, J.A., Furniss, T.J., Johnson, D.J., Davies, S.J., Allen, D., Alonso, A., Anderson-Teixeira, K.J., Becker, K.M.L., Andrade, A., Baltzer, J., Blomdahl, E.M., Bourg, N.A., Bunyavejchewin, S., Burslem, D.F.R.P., Cansler, A.C., Fischer, G.A., Fletcher, C., Freund, J.A., Giardina, C., Germain, S.J., 2018. Global importance of large-diameter trees. Glob. Ecol. Biogeogr. 1–16.

Luyssaert, S., Schulze, E.-D., Börner, A., Knohl, A., Hessenmöller, D., Law, B.E., Ciais, P., Grace, J., 2008. Old-growth forests as global carbon sinks. Nature 455, 213–215.

Lysak, T., Ross, D.W., Maguire, D.A., Overhulser, D.L., 2006. Predicting spruce weevil damage in Sitka spruce in the northern Oregon Coast Range. West. J. Appl. For. 21, 159–164.

Maas-Hebner, K.G., Emmingham, W.H., Larson, D.J., Chan, S.S., 2005. Establishment and growth of native hardwood and conifer seedlings underplanted in thinned Douglas-fir stands. For. Ecol. Manage. 208, 331–345.

Maguire, D.A., Johnston, S.R., Cahill, J., 1999. Predicting branch diameters on second-growth Douglas-fir from tree-level descriptors. Can. J. For. Res. 29, 1829–1840.

Maguire, D.A., Kershaw, J.A., Hann, D.W., 1991. Predicting the effects of silvicultural regime on branch size and crown wood core in douglas-fir. For. Sci. 37, 1409–1428.

Mass, C.F., Dotson, B., 2010. Major extratropical cyclones of the Northwest United States: Historical review, climatology, and synoptic environment. Mon. Weather Rev. 138, 2499–2527.

McCune, B., Rosentreter, R., Ponzetti, J.M., Shaw, D.C., 2000. Epiphyte habitats in an old conifer forest in western Washington, U.S.A. Bryologist 103, 417–427.

McGarigal, K., Cushman, S.A., Ene, E., 2012. FRAGSTATS v4: Spatial pattern analysis program for categorical and continuous maps. University of Amherst. http://www.umass.edu/landeco/research/fragstats/fragstats.html.

McGaughey, R.J., 2009. FUSION/LDV:software for LiDAR data analysis and visualization.

Mckee, A., Laroi, G., Franklin, J.F., 1982. Structure, composition, and reproductive behavior of terrace forests, South Fork Hoh River, Olympic National Park, in: Starkey, E.E., Franklin, J.F., Mathews, J.W. (Eds.), Ecological Research in National Parks of the Pacific Northwest. National Park Service Cooperative Studies Unit, Corvallis, OR, pp. 22–29.

Means, J.E., Hansen, H.A., Koerper, G.J., Alaback, P.B., Klopsch, M.W., 1994. Software for computing plant biomass- BIOPAK users guide. USDA For. Serv., Gen.Tech. Rep. No. PNW-GTR-340.

Mencuccini, M., Martínez-Vilalta, J., Hamid, H.A., Korakaki, E., Vanderklein, D., 2007. Evidence for age- and size-mediated controls of tree growth from grafting studies. Tree Physiol. 27, 463–473.

Mencuccini, M., Martínez-Vilalta, J., Vanderklein, D., Hamid, H. a, Korakaki, E., Lee, S., Michiels, B., 2005. Size-mediated ageing reduces vigour in trees. Ecol. Lett. 8, 1183–90.

Michel, A.K., Winter, S., 2009. Tree microhabitat structures as indicators of biodiversity in Douglas-fir forests of different stand ages and management histories in the Pacific Northwest, U.S.A. For. Ecol. Manage. 257, 1453–1464.

Minore, D., 1979. Comparative autecological characteristics of northwestern tree species: A literature review. USDA Forest Service, PNW For. and Ran. Exp. Stat., Portland, Oregon, Gen. Tech. Rep. PNW-87.

Murtagh, F., Legendre, P., 2014. Ward's hierarchical agglomerative clustering method: Which algorithms implement Ward's Criterion? J. Classif. 31, 274–295.

Nadkarni, N.M., 1981. Canopy roots: Convergent evolution in rainforest nutrient cycles. Science 214, 2–4.

Nakanishi, A., Sungpalee, W., Sri-ngernyuang, K., Kanzaki, M., 2016. Large variations in composition and spatial distribution of epiphyte biomass on large trees in a tropical montane forest of northern Thailand. Plant Ecol. 217, 1157–1169.

Nakanishi, A., Sungpalee, W., Sri-ngernyuang, K., Kanzaki, M., 2013. Determination of epiphyte biomass composition and distribution with a three-dimensional mapping method in a tropical montane forest in northern Thailand. Tropics 22, 27–37.

Nelson, R., Margolis, H., Montesano, P., Sun, G., Cook, B., Corp, L., Andersen, H-E., deJong, B., Pellat, F.P., Fickel, T., Kauffman, J., Prisley, S., 2017. LiDAR-based estimates of aboveground biomass in the continental US and Mexico using ground, airborne, and satellite observations. Remote Sens. Environ. 188, 127–140.

Newton, M., Cole, L., 2015. Overstory development in Douglas-fir-dominant forests thinned to

enhance late-seral features. For. Sci. 61, 809–816. doi:10.5849/forsci.14-194

Nölke, N., Fehrmann, L., Jaya, I.N.S., Tiryana, T., Seidel, D., Kleinn, C., 2015. On the geometry and allometry of big- buttressed trees - a challenge for forest monitoring : new insights from 3D-modeling with terrestrial laser scanning. iForest 8, 574–581.

North, M.P., Kane, J.T., Kane, V.R., Asner, G.P., Berigan, W., Churchill, D.J., Conway, S., Gutiérrez, R.J., Jeronimo, S., Keane, J., Koltunov, A., Mark, T., Moskal, M., Munton, T., Peery, Z., Ramirez, C., Sollmann, R., White, A., Whitmore, S., 2017. Cover of tall trees best predicts California spotted owl habitat. For. Ecol. Manage. 405, 166–178.

O'Connor, J.E., Jones, M.A., Haluska, T.L., 2003. Flood plain and channel dynamics of the Quinault and Queets Rivers, Washington, USA. Geomorphology 51, 31–59.

Oldeman, R.A., 1990. Forests: Elements of silvology. Springer-Verlag.

Palik, B.J., Montgomery, R.A., Reich, P.B., Boyden, S.B., 2014. Biomass growth response to spatial pattern of variable-retention harvesting in a northern Minnesota pine ecosystem. Ecol. Appl. 24, 2078–2088.

Perry, T.D., Jones, J.A., 2016. Summer streamflow deficits from regenerating Douglas-fir forest in the Pacific Northwest , USA. Ecohydrology 10, 1–13.

Peterson, E.B., Peterson, N.M., Weetman, G.F., Martin, P.J., 1997. Ecology and management of Sitka spruce: Emphasizing its natural range in British Columbia. UBC Press, Vancouver, BC. pp. 336

Pike, L.H., Rydell, R.A., Denison, W.C., 1977. A 400-year-old Douglas-fir tree and its epiphytes: biomass, surface area, and their distributions. Can. J. For. Res. 7, 680–699.

Poorter, L., Bongers, F., Aide, T.M., Almeyda Zambrano, A.M., Balvanera, P., Becknell, J.M., Boukili, V., Brancalion, P.H.S., Broadbent, E.N., Chazdon, R.L., Craven, D., de Almeida-

Cortez, J.S., Cabral, G.A.L., de Jong, B.H.J., Denslow, J.S., Dent, D.H., Dewalt, S.J., Dupuy, J.M., Duran, S.M., Espirito-Santo, M.M., Fandino, M.C., Cesar, R.G., Hall, J.S., Hernandez-Stefanoni, J.L., Jakovac, C.C., Junqueira, A.B., Kennard, D., Letcher, S.G., Licona, J.-C., Lohbeck, M., Marín-Spiotta, E., Martínez-Ramos, M., Massoca, P., Meave, J.A., Mesquita, R., Mora, F., Muñoz, R., Muscarella, R., Nunes, Y.R.F., Ochoa-Gaona, S., de Oliveira, A.A., Orihuela-Belmonte, E., Peña-Claros, M., Pérez-García, E.A., Piotto, D., Powers, J.S., Rodríguez-Velázquez, J., Romero-Pérez, I.E., Ruíz, J., Saldarriaga, J.G., Sanchez-Azofeifa, A., Schwartz, N.B., Steininger, M.K., Swenson, N.G., Toledo, M., Uriarte, M., van Breugel, M., van der Wal, H., Veloso, M.D.M., Vester, H.F.M., Vicentini, A., Vieira, I.C.G., Vizcarra Bentos, T., Williamson, G.B., Rozendaal, D.M.A., 2016. Biomass resilience of Neotropical secondary forests. Nature 530, 211–214.

PRISM, 2018. PRISM Climate Group. Gridded Climate Data for the Contiguous USA. http://prism.oregonstat.edu. Accessed 12 April 2018.

Progar, R.A., Schowalter, T.D., 2002. Canopy arthropod assemblages along a precipitation and latitudinal gradient among Douglas-fir *Pseudotsuga menziesii* forests in the Pacific Northwest of the United States. Ecography (Cop.). 25, 129–138.

PSLC, 2018. Pudget Sound LiDAR Consortium. <http://pugetsoundlidar.ess.washington.edu/> Accessed 6 July 2016.

Raphael, M.G., Young, J.A., Galleher, B.M., 1995. A landscape analysis of marbled murrelet habitat in western Washington. in: Ralph, J.C., Hunt, G.L., Raphael, M.G., Piatt, J.F. (Eds.) Ecology and Conservation of the marbled murrelet. USDA, Forest Service. Pac. Soutwest Res. Sta., Gen. Tech. Rep. PSW-GTR-152.

Regnery, B., Couvet, D., Kubarek, L., Kerbiriou, C., 2013. Tree microhabitats as indicators of

bird and bat communities in Mediterranean forests. Ecol. Indic. 34, 221–230. doi:10.1016/j.ecolind.2013.05.003

Risser, P.G., 1995. The Allerton Park workshop revisited - A commentary. Landsc. Ecol. 10, 129–130.

Roberts, S.D., Harrington, C.A., 2008. Individual tree growth response to variable-density thinning in coastal Pacific Northwest forests. For. Ecol. Manage. 255, 2771–2781.

Rouvinen, S., Kuuluvainen, T., 1997. Structure and asymmetry of tree crowns in relation to local competition in a natural mature Scots pine forest. Can. J. For. Res. 27, 890–902.

R Core Team, 2018. R: A language and environment for statistical computing. R Foundation for Statistical Computing, Vienna, Austria. https://www.R-project.org/.

Ruth, R.H., Yoder, R.A., 1953. Reducing wind damage in the forests of the Oregon Coast Range. USDA, Forest Service, PNW For.and Ran. Exp. Stat., Portland, Oregon. Research Paper No. 7.

Ryan, K.C., Reinhardt, E.D., 1988. Predicting postfire mortality of seven western conifers. Can. J. For. Res. 18, 1291–1297.

Schwartz, J.E., Mitchell, G.E., 1945. The Roosevelt Elk on the Olympic Peninsula. J. Wildl. Manage. 9, 295–319.

Sedell, J.R., Bisson, P.A., June, J.A., Speaker, R.W., 1982. Ecology and habitat requirements of fish populations in South Fork Hoh River, Olympic National Park.pdf, in: Starkey, E.E., Franklin, J.F., Matthews, J.W. (Eds.), Ecological Research in National Parks of the Pacific Northwest. Oregon State University Research Laboratory, Corvallis, OR, pp. 35–42.

Sheil, D., Eastaugh, C.S., Vlam, M., Zuidema, P.A., Groenendijk, P., van der Sleen, P., Jay, A., Vanclay, J., 2017. Does biomass growth increase in the largest trees? Flaws, fallacies and

alternative analyses. Funct. Ecol. 31, 568–581.

Sheridan, C.D., Puettmann, K.J., Huso, M.M.P., Hagar, J.C., Falk, K.R., 2013. Management, morphological, and environmental factors influencing Douglas-fir bark furrows in the Oregon Coast Range. West. J. Appl. For. 28, 97–106.

Sillett, S.C., 1999. Tree crown structure and vascular epiphyte distribution in *Sequoia sempervirens* rain forest canopies. Selbyana 20, 76–91.

Sillett, S.C., Antoine, M.E., Campbell-Spickler, J., Carroll, A.L., Coonen, E.J., Kramer, R.D., Scarla, K.H., 2018a. Manipulating tree crown structure to promote old-growth characteristics in second-growth redwood forest canopies. For. Ecol. Manage. 417, 77–89.

Sillett, S.C., McCune, B., Peck, J.E., Rambo, T.R., Ruchty, A., 2000. Dispersal limitations of epiphytic lichens result in species dependent on old-growth forests. Ecol. Appl. 10, 789–799.

Sillett, S.C., Spickler, J.C., Van Pelt, R., 2000. Crown structure of the world's second largest tree. Madroño 47, 127–133.

Sillett, S.C., Van Pelt, R., 2007. Trunk reiteration promotes epiphytes and water storage in an old-growth redwood forest canopy. Ecol. Monogr. 77, 335–359.

Sillett, S.C., Van Pelt, R., 2001. A redwood tree whose crown may be the most complex on earth, in: Labrecque, M. (Ed.), L'Arbre. Montreal, Quebec, Canada, pp. 11–18.

Sillett, S.C., Van Pelt, R., Carroll, A.L., Kramer, R.D., Ambrose, A.R., Trask, D., 2015b. How do tree structure and old age affect growth potential of California redwoods? Ecol. Monogr. 85, 181–212.

Sillett, S.C., Van Pelt, R., Freund, J.A., Campbell-Spickler, J., Carroll, A.L., Kramer, R.D., 2018b. Development and dominance of Douglas-fir in North American rainforests. For.

Ecol. Manage. 429, 93–114.

Sillett, S.C., Van Pelt, R., Koch, G.W., Ambrose, A.R., Carroll, A.L., Antoine, M.E., Mifsud, B.M., 2010. Increasing wood production through old age in tall trees. For. Ecol. Manage. 259, 976–994.

Sillett, S.C., Van Pelt, R., Kramer, R.D., Carroll, A.L., Koch, G.W., 2015a. Biomass and growth potential of Eucalyptus regnans up to 100 m tall. For. Ecol. Manage. 348, 78–91.

Skillen, J.R., 2015. Federal ecosystem management: Its rise, fall, and afterlife. University of Kansas Press, Lawrence, KS. 348 pp.

Smith, F.W., Long, J.N., 2001. Age-related decline in forest growth: an emergent property. For. Ecol. Manage. 144, 175–181.

Sorrensen-Cothern, Ford, E.D., Sprugel, D.G., 1993. A model of competition incorporating plasticity through modular foliage and crown development. Ecol. Mongraphs 63, 277–304.

Spickler, J.C., Sillett, S.C., Marks, S.B., Welsh Jr., H.H., 2006. Evidence of a new niche for a North American salamander: *Aneides vagrans* residing in the canopy of old-growth redwood forest. Herpetol. Conserv. Biol. 1, 16–26.

Spittenhouse, D.L., Sieben, B.G., Taylor, S.P., 1994. Spruce weevil hazard mapping based on climate and ground survey data, in: Alfaro, R.I., Kiss, G., Fraser, R.G. (Eds.), The White Pine Weevil. FRDA, Richmond, British Columbia, p. 311.

Sprugel, D.G., 2002. When branch autonomy fails: Milton's law of resource availability and allocation. Tree Physiol. 22, 1119–1124.

Starker, T.J., 1934. Fire resistance in the forest. J. For. 32, 462–467.

Sumida, A., Miyaura, T., Torii, H., 2013. Relationships of tree height and diameter at breast height revisited: analyses of stem growth using 20-year data of an even-aged

Chamaecyparis obtusa stand. Tree Physiol. 33, 106–18.

Swanson, M.E., Lienkaemper, G.W., 1982. Interactions among flucial processes, forest vegetation, and aquatic ecosystems, South Fork Hoh River, Olympic National Park, in: Starkey, E., Franklin, J.F., Matthews, J.W. (Eds.), Ecological Research in National Parks of the Pacific Northwest. Oregon State University, Forest Research laboratory, Corvallis, OR, pp. 30–34.

Tanago, J.G. De, Lau, A., Bartholomeus, H., Herold, M., Avitabile, V., Raumonen, P., Martius, C., Goodman, R.C., Disney, M., Manuri, S., Burt, A., Calders, K., 2017. Estimation of above-ground biomass of large tropical trees with terrestrial LiDAR. Methods Ecol. Evol. 9, 223–234.

Taylor, A.H., 1990. Disturbance and persistence of Sitka spruce (*Picea sitchensis* (Bong) Carr.) in coastal forests of the Pacific Northwest , North America. J. Biogeogr. 17, 47–58.

Taylor, S.P., Delong, C., Alfaro, R.I., L., R., 1996. The effects of overstory shading on white pine weevil damage to white spruce and its effects on spruce growth rates. Can. J. For. Res. 26, 306–312.

Thackray, G.D., 2001. Extensive early and middle Wisconsin glaciation on the western Olympic Peninsula, Washington, and the variability of Pacific moisture delivery to the northwestern United States. Quat. Res. 55, 257–270.

Thorpe, H.C., Astrup, R., Trowbridge, A., Coates, K.D., 2010. Competition and tree crowns: A neighborhood analysis of three boreal tree species. For. Ecol. Manage. 259, 1586–1596.

Tomlinson, P.B., 1983. Tree architecture: New approaches help to define the elusive biological property of tree form. Am. Sci. 71, 141–149.

Turner, M.G., 1989. Landscape ecology: The effect of pattern on process. Annu. Rev. Ecol. Syst.

20, 171–197.

Van Pelt, R., 2007. Identifying mature and old forests in western Washington. Washington State Department of Natural Resources, Olympia, WA, pp.104

Van Pelt, R., 2001. Forest giants of the Pacific coast. University of Washington Press, Seattle, WA.

Van Pelt, R., O'Keefe, T.C., Latterell, J.J., Naiman, R.J., 2006. Riparian forest stand development along the Queets River in Olympic National Park, Washington. Ecol. Monogr. 76, 277–298.

Van Pelt, R., Sillett, S.C., 2008. Crown development of coastal *Pseudotsuga menziesii*, including a conceptual model for tall conifers. Ecol. Monogr. 78, 283–311.

Van Pelt, R., Sillett, S.C., Kruse, W.A., Freund, J.A., Kramer, R.D., 2016. Emergent crowns and light-use complementarity lead to global maximum biomass and leaf area in *Sequoia sempervirens* forests. For. Ecol. Manage. 375, 279–308.

Wagener, W.W., Davidson, R.W., 1954. Heart rots in living trees. Bot. Rev. 20, 61–134.

Wassenberg, M., Chiu, H-S., Guo, W., Spiecker, H., 2015. Analysis of wood density profiles of tree stems : Incorporating vertical variations to optimize wood sampling strategies for density and biomass estimations. Trees 29, 551–561.

Watson, D.M., 2001. Mistletoe– A keystone resource in forests and woodlands worldwide. Annu. Rev. Ecol. Syst. 32, 219–249.

Watt, A.S., 1947. Pattern and process in the plant community. J. Ecol. 35, 1–22.

Watt, M.S., Moore, J.R., McKinlay, B., 2005. The influence of wind on branch characteristics of *Pinus radiata*. Trees 19, 58–65.

Weiskittel, A.R., Maguire, D. a., Monserud, R. a., 2007. Response of branch growth and

mortality to silvicultural treatments in coastal Douglas-fir plantations: Implications for predicting tree growth. For. Ecol. Manage. 251, 182–194.

Wiens, J.A., 2008. Allerton Park 1983: The beginnings of a paradigm for landscape ecology? Landsc. Ecol. 23, 125–128.

Williams, C.B., Sillett, S.C., 2007. Epiphyte communities on redwood (*Sequoia sempervirens*) in Northwestern California. Bryologist 110, 420–452.

Winter, L.E., Brubaker, L.B., Franklin, J.F., Miller, E.A., Dewitt, D.Q., 2002. Initiation of an old-growth Douglas-fir stand in the Pacific Northwest: a reconstruction from tree-ring records. Can. J. For. Res. 32, 1039–1056.

Wunder, L., Carey, A.B., Northwest, P., 1996. Use of the forest canopy by bats. Northwest Sci. 70, 79–85.

Yao, T., Yang, X., Zhao, F., Wang, Z., Zhang, Q., Jupp, D., Lovell, J., Culvenor, D., Newnham, G., Ni-meister, W., Schaaf, C., Woodcock, C., Wang, J., Li, X., Strahler, A., 2011. Measuring forest structure and biomass in New England forest stands using Echidna ground-based LiDAR. Remote Sens. Environ. 115, 2965–2974.

Zhu, J., Lu, D., Zhang, W., 2014. Effects of gaps on regeneration of woody plants: a meta-analysis. J. For. Res. 25, 501–510. doi:10.1007/s11676-014-0489-3

Zolkos, S.G., Goetz, S.J., Dubayah, R., 2013. A meta-analysis of terrestrial aboveground biomass estimation using LiDAR remote sensing. Remote Sens. Environ. 128, 289–298.

APPENDIX 1.A

Table 1. Studies utilizing crown mapping in chronological order from first inception to current methodology are provided as a reference for locating species-specific protocols, data, and equations. Methods and trees sample sizes presented here only indicate those used in crown mapping.

Reference	Methods	Application	Trees	Tree species	Tree heights (m)	Notes
Pike et al. 1975	Trunk measured at 5 m intervals except (~6m of top), hierarchical appendage mapping with systems of axes (>4cm) and branchlets (<4 cm)	Floristic lichen and bryophyte survey	20	*Pseudotsuga menziesii, Tsuga heterophylla, Pinus lambertiana, Taxus brevifolia, Acer circinatum*	25-85	9 *P. menziesii*, 1 *P. sitchensis*, remaining 10 not clear
Pike et al. 1977	Same as above	Tree and epiphyte biomass, epiphyte volume and surface area	1	*Pseudotsuga menziesii*	77	Good methods flow chart, data from one tree presented, 9 total mapped trees
Massman 1982	Same as above	Modeling vertical tree foliage distribution	10	*Pseudotsuga menziesii, Pinus lambertiana*	44-77	same trees as above, 9 PSME, 1 PILA
Sillett 1995	Sketch of all living branches, estimated axis length	Lichen, bryophyte, and fern sampling for community analysis	4	*Pseudotsuga menziesii*	55-68	
Sillett 1999	Main trunk and reiterations mapped at 5-m vertical resolution and distances from main trunk, sketches of smaller structure from large reiterations. Rudimentary visualizations	Relating complex tree structure to epiphyte distributions	8	*Sequoia sempervirens*	82-97	First attempt to map *S. sempervirens* and epiphyte distributions
Sillett et al. 2000	Same as above	Quantifying volume, mass, and structure of 2nd largest tree, including decay	1	*Sequoiadendron giganteum*	77	First attempt to map *S. giganteum*
Sillett and Van Pelt 2000	Same as above	Quantifying reiterated structure in very complex tree and documenting epiphyte occurrence	1	*Sequoia sempervirens*	110	

Appendix 1.A. Table continued

Reference	Methods	Application	Trees	Tree species	Tree heights (m)	Notes
Sillett and Van Pelt 2001	Same as above	Same as above, documents arboreal plants and animals.	1	*Sequoia sempervirens*	92	Arboreal salamander, canopy soils, and 6th order reiterations noted
Ishii and Wilson 2001	Light measured every 5 m. Branch height, diameter, angle, and length. Trunk diameters	Branch population dynamics	6	*Pseudotsuga menziesii*	50-62	
Ishii and McDowell 2002	Branch heights and diameters measured. No segmentation of larger appendages	Branch demographics and crown development processes	16	*Pseudotsuga menziesii*	14-62	Access via scaffolding in smaller trees and rope in larger trees, 20-, 40-, and 450-yr-old trees
Sillett and Bailey 2003	Main trunk, trunk segments, and connecting limb segments mapped. No appendages measured other than those giving rise to a trunk, dimensions of fern mats measured	Associating crown structure with canopy fern mat biomass, predictive equations for fern mats based on dimensional measurements	32	*Sequoia sempervirens, Picea sitchensis*	77-101	27 SESE, 5 PISI
Ellyson and Sillett 2003	Main trunk and branch mapping using foliar units (**Table 1.2**). Branch height and size measured but not direction. Large appendages not segmented.	Substrate quantification and sampling design for epiphyte communities	5	*Picea sitchensis*	83 - 92	
Van Pelt et al. 2004	As presented in this study, more rudimentary data visualization and naming scheme	Methods description, proof of concept with case study	26	*Pseudotsuga menziesii, Eucalyptus regnans, Thuja plicata, Tsuga heterophylla*	43-92	Methods description with case study, few illustrations, in niche text
Sillett and Van Pelt 2007	As above with additional measurements of water storage, canopy soil volumes and epiphyte biomass. Only mapped trees with reiterations, no branches.	Explicit links of complex structure, canopy habitat, soil, water storage, and diversity in a population of trees.	27	*Sequoia sempervirens*	40-101	Seminal work linking structure, habitat, plot measurements, and canopy ecology
Williams and Sillett 2007	Main trunk, trunk and connecting limb segments mapped, all epiphyte species surveyed from treetop to ground	Epiphyte community structure and habitat associations, vascular epiphyte biomass	9	*Sequoia sempervirens*	80 - 113	

Appendix 1.A. Table continued

Reference	Methods	Application	Trees	Tree species	Tree heights (m)	Notes
Van Pelt and Sillett 2008	Similar to methods in this study, used foliar unit protocol. More complex hierarchical naming system.	Tree crown structural development	70	*Pseudotsuga menziesii*	18-87	Good flow chart
Sillett et al. 2010	Modern mapping methods, use of current segment naming system	Tree-level component biomass and area. Structure, age, and wood production.	43	*Sequoia sempervirens Eucalyptus regnans*	29 - 113	Comprehensive flow chart, 22 EURE and 21 SESE, re-mapped trees for aboveground growth increments
Oldham et al. 2010	Used trees from Sillett et al. 2010	Sampling design for leaf anatomy study	5	*Sequoia sempervirens*	108 - 113	
Bar-Ness et al. 2012	Similar to methods in this paper with additional measurements for foliar envelope around branch axis. Used foliar units, rudimentary visualizations	Structural differences between young and old tree crowns	16	*Eucalyptus obliqua*	35-75	
Nakanishi et al. 2013	Points on tree surveyed with laser from ground or within tree, segments modeled as frusta between. Diameters measured via stadia hairs from range-finding laser or with tape. Nothing <10 cm diameter was segmented. Branches modeled as cones and predicted with equations.	Case study demonstrating methods for quantifying epiphytes by crown mapping trees	1	*Mastixia euonymoides*	47	One branch dissected for predictive equations
Sillett et al. 2015a	As described in this study	Tree structure and age effects on growth increments, species comparison, long-term growth analysis	140	*Sequoia sempervirens, Sequoiadendron giganteum*	9 - 116	97 SESE, 43 SEGI, DTB equations applied to estimate whole-tree biomass increments
Sillett et al. 2015b	As described in this study	Allometric equations, growth analysis, tree ages, quantifying plot-level biomass of a tall forest	27	*Eucalyptus regnans*	61 - 100	case study

Appendix 1.A. Table continued

Reference	Methods	Application	Trees	Tree species	Tree heights (m)	Notes
Coonen and Sillett 2015	As described in this study, except smaller branch cutoff (2 cm diameter)	Crown structure and light availability relating to trunk wood production	24	*Sequoia sempervirens*	23-72	
Nakanishi et al. 2016	As in Nakanishi et al. 2013	Quantifying mass, distribution, and composition of epiphytes	3	*Mastixia euonymoides*	39-48	
Ishii et al. 2017	As in Ishii and Wilson 2001	10 tree growth in trunk and branch components, branch demography	6	*Pseudotsuga menziesii*	51-63	remeasurement of trees from Ishii and Wilson 2001
Sillett et al. 2018a	As described in this study	Experimental manipulation to promote structural complexity	24	*Sequoia sempervirens*	59-75	re-mapped trees to determine changes after manipulations
Sillett et al. 2018b	As described in this study	Allometric equations, growth analysis, tree ages, quantifying plot-level biomass	60	*Pseudotsuga menziesii*	35-97	

References

Bar-Ness, Y.D., Kirkpatrick, J.B., Mcquillan, P.B., 2012. Crown structure differences and dynamics in 100-year-old and old-growth *Eucalyptus obliqua*. Aust. For. 75, 120–129. doi:10.1080/00049158.2012.10676393

Coonen, E.J., Sillett, S.C., 2015. Separating effects of crown structure and competition for light on trunk growth of *Sequoia sempervirens*. For. Ecol. Manage. 358, 26–40. doi:10.1016/j.foreco.2015.08.035

Ellyson, W.J.T., Sillett, S.C., 2003. Epiphyte communities on Sitka spruce in an old-growth redwood forest. Bryologist 106, 197–211.

Ishii, H., McDowell, N., 2002. Age-related development of crown structure in coastal Douglas-fir trees. For. Ecol. Manage. 169, 257–270. doi:10.1016/S0378-1127(01)00751-4

Ishii, H.R., Sillett, S.C., Carroll, A.L., 2017. Crown dynamics and wood production of Douglas-fir trees in an old-growth forest. For. Ecol. Manage. 384, 157–168. https://doi.org/10.1016/j.foreco.2016.10.047

Ishii, H., Wilson, M.E., 2001. Crown structure of old-growth Douglas-fir in the western Cascade Range, Washington. Can. J. For. Res. 31, 1250–1261. doi:10.1139/cjfr-31-7-1250

Massman, W., 1982. Foliage distribution in old-growth coniferous tree canopies. Can. J. For. Res. 12, 10–17. doi:10.1139/x82-002

Nakanishi, A., Sungpalee, W., Sri-ngernyuang, K., Kanzaki, M., 2016. Large variations in composition and spatial distribution of epiphyte biomass on large trees in a tropical montane forest of northern Thailand. Plant Ecol. 217, 1157–1169. doi:10.1007/s11258-016-0640-7

Nakanishi, A., Sungpalee, W., Sri-ngernyuang, K., Kanzaki, M., 2013. Determination of epiphyte biomass composition and distribution with a three-dimensional mapping method in a tropical montane forest in northern Thailand. Tropics 22, 27–37.

Oldham, A.R., Sillett, S.C., Tomescu, A.M.F., Koch, G.W., 2010. The hydrostatic gradient, not light availability, drives height-related variation in *Sequoia sempervirens* (Cupressaceae) leaf anatomy. Am. J. Bot. 97, 1–15. doi:10.3732/ajb.0900214

Pike, L.H., Denison, W.C., Tracy, D.M., Sherwood, M.A., Rhoades, F.M., 1975. Floristic survey of epiphytic lichens and bryophytes growing on old-growth conifers in Western Oregon. Bryologist 78, 389–402.

Pike, L.H., Rydell, R.A., Denison, W.C., 1977. A 400-year-old Douglas-fir tree and its epiphytes: biomass, surface area, and their distributions. Can. J. For. Res. 7, 680–699.

Sillett, S.C., 1995. Branch epiphyte assemblages in the forest interior and on the clearcut edge of a 700-year-old Douglas fir canopy in Western Washington. Bryologist 98, 301–312.

Sillett, S.C., 1999. Tree crown structure and vascular epiphyte distribution in Sequoia sempervirens rain forest canopies. Selbyana 20, 76–91.

Sillett, S.C., Antoine, M.E., Campbell-spickler, J., Carroll, A.L., Coonen, E.J., Kramer, R.D., Scarla, K.H., 2018a. Manipulating tree crown structure to promote old-growth characteristics in second-growth redwood forest canopies. For. Ecol. Manage. 417, 77–89.

Sillett, S.C., Bailey, M.G., 2003. Effects of tree crown structure on biomass of the epiphytic fern *Polypodium scouleri* in redwood forests. Am. J. Bot. 90, 255–261.

Sillett, S.C., Spickler, J.C., Van Pelt, R., 2000a. Crown structure of the world's second largest tree. Madroño 47, 127–133.

Sillett, S.C., Van Pelt, R., 2000b. A redwood tree whos crown is a forest canopy. Northwest Sci. 74, 34–43.

Sillett, S.C., Van Pelt, R., 2001. A redwood tree whose crown may be the most complex on earth, in: Labrecque, M. (Ed.), L'Arbre. Montreal, Quebec, Canada, pp. 11–18.

Sillett, S.C., Van Pelt, R., 2007. Trunk reiteration promotes epiphytes and water storage in an old-growth redwood forest canopy. Ecol. Monogr. 77, 335–359.

Sillett, S.C., Van Pelt, R., Carroll, A.L., Kramer, R.D., Ambrose, A.R., Trask, D., 2015a. How do tree structure and old age affect growth potential of California redwoods? Ecol. Monogr. 85, 181–212.

Sillett, S.C., Van Pelt, R., Freund, J.A., Campbell-Spickler, J., Carroll, A.L., Kramer, R.D., 2018b. Development and dominance of Douglas-fir in North American rainforests. For. Ecol. Manage. 429, 93–114. doi:10.1016/j.foreco.2018.07.006

Sillett, S.C., Van Pelt, R., Koch, G.W., Ambrose, A.R., Carroll, A.L., Antoine, M.E., Mifsud, B.M., 2010. Increasing wood production through old age in tall trees. For. Ecol. Manage. 259, 976–994.

Sillett, S.C., Van Pelt, R., Kramer, R.D., Carroll, A.L., Koch, G.W., 2015b. Biomass and growth potential of *Eucalyptus regnans* up to 100 m tall. For. Ecol. Manage. 348, 78–91. doi:10.1016/j.foreco.2015.03.046

Van Pelt, R., Sillett, S.C., 2008. Crown development of coastal *Pseudotsuga menziesii*, including a conceptual model for tall conifers. Ecol. Monogr. 78, 283–311.

Van Pelt, R., Sillett, S.C., Nadkarni, N.M., 2004. Quantifying and visualizing canopy structure in tall forests: methods and a case study, in: Lowman, M.D., Rinker, B.H. (Eds.), Forest Canopies. Elsevier, pp. 49–72.

Williams, C.B., Sillett, S.C., 2007. Epiphyte communities on redwood (*Sequoia sempervirens*) in Northwestern California. Bryologist 110, 420–452.

APPENDIX 1.B

Applying the methodology in divergent tree species

Picea sitchensis and *Eucalyptus globulus* are quite different structurally, so comparing them helps to demonstrate the generalized nature of crown mapping to quantify aboveground quantities. *Picea sitchensis* (hereafter *P. sitchensis*) is native to the northwest coast of North America from northern California to Alaska, where mild wet winters and relatively cool foggy summers maintain high moisture. It is relatively shade tolerant, reproducing in gaps under its own canopy (Taylor, 1990), fast growing (Ford, 1982) and can live upwards of 400 years (Van Pelt, 2007). *Picea sitchensis* routinely germinates on logs and then extends roots to the soil creating widely buttressed bases (Taylor, 1990; Van Pelt, 2007). Although it conforms to the same architectural model of a monopodial trunk with radially oriented branches of generally increasing size with decreasing height as other *Pisca* trees, it is unlike them in that it is one of the world's tallest (up to 97 m) and largest trees. Due to its rapid production of light but strong wood and potential for immense size, *P. sitchensis* is heavily used by humans. During WWI a whole army division was appointed to extracting its wood for airplanes (Crosman, 2011), and it is now widely planted for timber in Great Britain, Ireland, Scotland, Denmark, and Iceland (Deal et al., 2014).

Eucalyptus globulus (hereafter *E. globulus*) is native to Tasmania, Victoria, and New South Wales in Australia (Potts and Reid, 2003). Like *P. sitchensis*, it thrives in a temperate climate with upwards of 90 cm of precipitation, although it can thrive with less in climates ameliorated by fog (Burns and Honkala, 1990). It is intolerant of shade, fast growing, and able to dominate competing vegetation (e.g., Forrester et al., 2005). *Eucalyptus* species generally do not produce easily discernable boundaries between early- and late-wood, so is difficult to age with ring analysis (Ogden, 1978; Wood et al., 2010), but *E. globulus* certainly becomes centuries old (Platen et al., 2011). In Tasmanian rainforests, it becomes a canopy dominant reaching heights > 90 m and trunk volumes > 360 m^3, making it one of the largest angiosperms (S.C. Sillett and R. Van Pelt *unpublished data*). Like *P. sitchensis*, it produces large basal buttresses (**Figure 1**). *Eucalyptus globulus* has the structure of a single dominant stem that forks into a spreading crown with leaves arrayed on dimensionally similar small branches (Tomlinson, 1983). Although it twists and cracks when dried, properly cured *E. globulus* wood was used for mining timbers, pier

pilings, and shipbuilding in the 1800s (Potts and Reid, 2003). *Eucalyptus globulus* is planted worldwide and common in California, Spain, Portugal, and Chile, where it is primarily used as a windbreak and for pulp, poles, small lumber, and fuel (Burns and Honkala, 1990).

Visualization as demonstration of generalizability

The utility of the mapping method to span divergent taxa is demonstrated on four of eight crown mapped *E. globulus* trees measured from 2010 to 2013 in California and Tasmania. They span the full range in size and height of *E. globulus* from 10 to 470 cm *f*-DBH and 12.2 to 90.4 m tall. The protocol is not limited only to trees and can be usefully applied to all manner of woody plants due to its modular structure and hierarchical naming system. The modularity allows researchers to augment specific portions of the protocol to suit their needs. For example, in *E. globulus* versus *P. sitchensis*, foliage is quantified either by counting foliar units or by creating whole-branch equations based on a stratified random selection and dissection of branches. Likewise, the leaves of other species with novel architecture can be quantified in different ways not yet conceived.

The rendering of crown structure of both species based on the methodology is reasonably realistic (**Figure 1**) and allows quantitative descriptions of basic structure. *Picea sitchensis* maintains a single dominant central trunk for most of its height and expresses structural complexity with large reiterating appendages. In contrast, *E. globulus* exhibits a common spreading angiosperm architecture, and expresses structural complexity with large up-tending forked limb systems. In both cases the dominant structure and complexity is captured via segmentation. *Picea sitchensis* branches are densely arrayed around the trunks and generally have up-sloping branches in the upper crown, grading to down-sloping branches in the lower crown. *Eucalyptus globulus* crowns are dominated more by larger segments with sparser and invariably up-sloping branches than in *P. sitchensis*. The visualization offers an orthographic view of the trees from any direction that cannot be obtained any other way. In addition, it can be applied to large as well as small trees in various growing conditions (**Figure 1**).

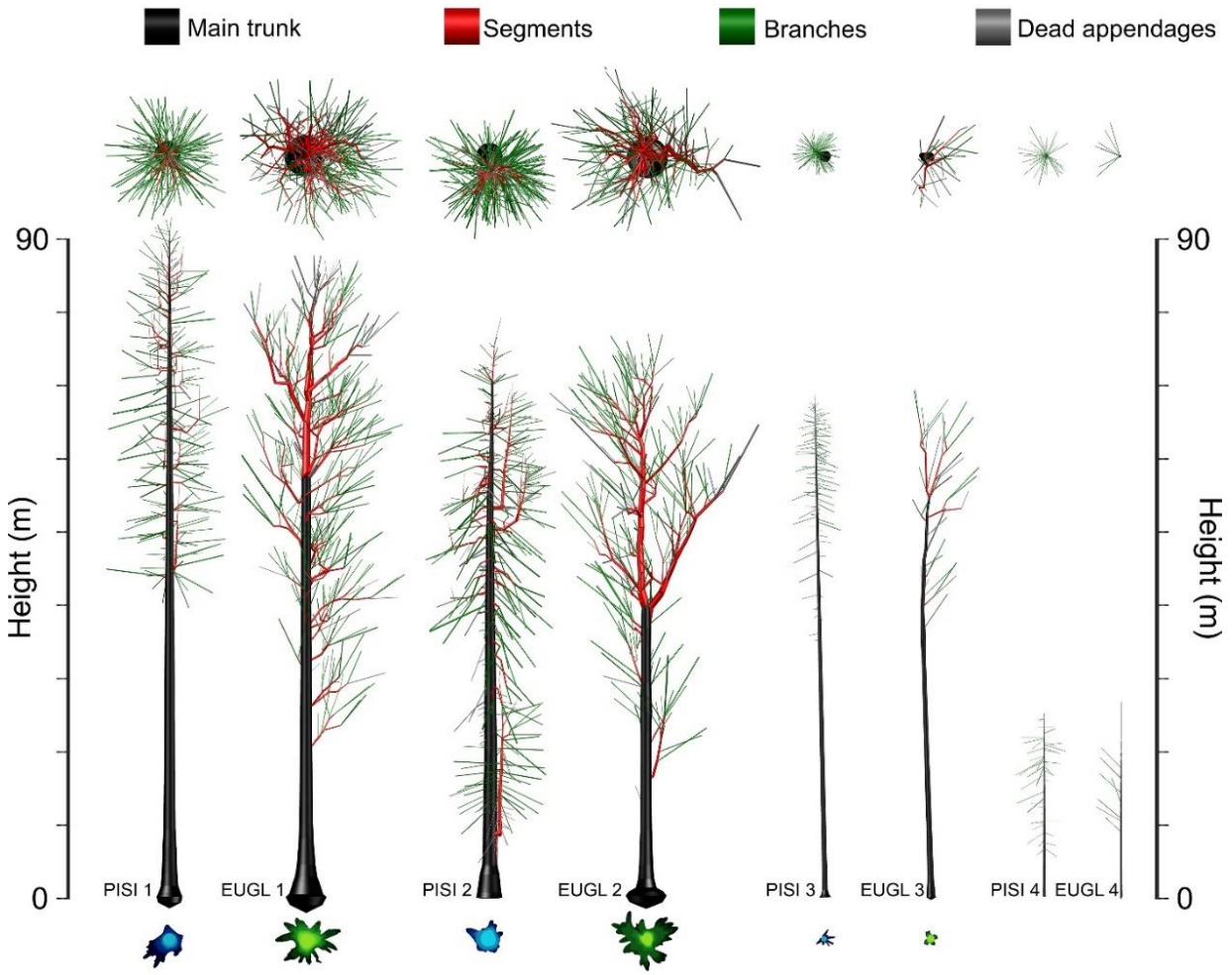

Figure 1. Scaled 3D models of tallest (1), dominant-complex (2), suppressed (3), and young (4) P. sitchensis (PISI) and E. globulus (EUGL) trees. A top view is shown above, profile view center, and footprint map, if applicable, below. Crown mapping quantifies trees of divergent structure of all sizes. Orthographic projections can be shown from any view angle. 3D measurements are combined with sampling of internal tree structure to calculate aboveground quantities. Approximate times to crown map from left to right in people-days are 6, 8, 6, 7, 1.5, 2, 0.5, 0.2.

References

Burns, R.M., Honkala, B.H., 1990. Silvics of North America. Agricultural Handbook 654.

Chin, A.R.O., Sillett, S.C., 2017. Leaf acclimation to light availability supports rapid growth in tall Picea sitchensis trees. Tree Physiol. 37, 1352–1366. doi:10.1093/treephys/tpx027

Crosman, 2011. The army in the woods: Spruce Production Division records at the National

Archives. Oregon Hist. Q. 112, 100–106.

Deal, R.L., Hennon, P., O'Hanlon, R., D'Amore, D.D., 2014. Lessons from native spruce forests in Alaska: managing Sitka spruce plantations worldwide to benefit biodiversity and ecosystem services. Forestry 87, 193–208. doi:10.1093/forestry/cpt055

Ford, E.D., 1982. High productivity in a polestage Sitka spruce stand and its relation to canopy structure. Forestry 55, 1–17.

Forrester, D.I., Bauhus, J., Cowie, A.L., 2005. On the success and failure of mixed-species tree plantations : Lessons learned from a model system of *Eucalyptus globulus* and *Acacia mearnsii*. For. Ecol. Manage. 209, 147–155. doi:10.1016/j.foreco.2005.01.012

Ogden, J., 1978. On the dendrochronological potential of Australian trees. Aust. J. Ecol. 3, 339–356.

Platen, J. Von, Kirkpatrick, J.B., Allen, K.J., 2011. Fire frequency variation in south-eastern Tasmanian dry eucalypt forest 1740 – 2004 from fire scars. Aust. For. 74, 180–189. doi:10.1080/00049158.2011.10676361

Potts, B.M., Reid, J.B., 2003. Tasmania's Eucalypts: Their place in science. Pap. Proc. R. Soc. Tasmania 137, 21–37.

Taylor, A.H., 1990. Disturbance and persistence of Sitka Spruce (*Picea sitchensis* (Bong) Carr.) in coastal forests of the Pacific Northwest , North America. J. Biogeogr. 17, 47–58.

Tomlinson, P.B., 1983. Tree architecture: New approaches help to define the elusive biological property of tree form. Am. Sci. 71, 141–149.

Van Pelt, R., 2007. Identifying mature and old forests in western Washington.

Wood, S.W., Hua, Q., Allen, K.J., Bowman, D.M.J.S., 2010. Age and growth of a fire prone Tasmanian temperate old-growth forest stand dominated by *Eucalyptus regnans*, the world's tallest angiosperm. For. Ecol. Manage. 260, 438–447. doi:10.1016/j.foreco.2010.04.037

APPENDIX 1.C

Tree rigging, coring, and branch removal tips

Tree rigging

The initial scaling and rigging of a tree is arguably the most dangerous step during crown mapping. Although there are institutions, techniques, and tools dedicated to accessing trees safely, these are mostly confined to the arboriculture or industrial climbing industry. Many of the techniques used in those industries are applicable to climbing larger trees, but there are nuances unique to accessing tall trees that we address here.

One such nuance is setting a line in the tree for the first time, which we call pioneering. When a line is shot into a tall tree, it is often hard or impossible to see the supporting branch. It is also difficult to see what dead and hanging branches await during the first ascent. The primary danger when climbing a tree for the first time is a branch breaking and dropping climber some distance, or a falling branch impacting the climber.

There are necessary tools and precautions to take when pioneering a tree. Essential tools include an impact-rated helmet, binoculars, a 3-mm diameter bright orange line for pulling ropes into trees, a projectile device capable of launching a weighted line as high as possible into the tree, two-way radios, and ground personnel. Before taking any shots into the tree, take extra time to scan the crown, noting dead and hanging wood, the lean of the trunk, and possible openings in the foliage to shoot a line through the crown. Aim as close as possible to the trunk and over large branches on the uphill side of the lean. Ideally a shot is arched through a window in the foliage and returns close to the trunk on the opposite side. A high shot allows a climber to access the top of the tree without disrupting the sensitive epiphytic communities while ascending. Take as much time as needed to confirm what the shot is over with binoculars. Sometimes it is helpful to pull in a thicker climbing rope to see what it is over with the knowledge that you may need to pull it down and reshoot the line.

The most time-consuming aspect of rigging is returning the projectile to the ground after the shot. To speed this process, attach the projectile with neon colored 20 lb. test fishing filament on a reel. This is strong enough to pull up the 3 mm cord and easy enough to break if the projectile is snagged and will not move. Tie a figure-8 follow-through knot in the end of the fishing line to create a loop (this and subsequent knots are described here:

www.animatedknots.com). Because there are so many branches the initial cord touches, the cumulative friction often does not allow the projectile to return. This is compounded in wet mossy conditions and with thicker cord. It is sometimes more efficient to use the heaviest projectile possible at the cost of some height on the shot to insure its return. Plucking and systematically bouncing the projectile aids its descent. Once the projectile reaches the ground, tie the cord into a loop of line and haul it up with the reel.

Often the climbing rope snags when pulling it into the tree, and there are several techniques to reduce this problem. Use a low-profile knot such as one side of a triple fisherman's knot around the rope tip to reduce snags. We recommend a 3-mm haul cord that is dynamic (can stretch and recover in length), as opposed to common static arborist haul lines made from tech materials such as Dyneema®. The stretch allows one person to hold the cord while another pulls down on the rope so it pulls below the snag but with tension on the cord. Pulling down on the cord at the same time as releasing the rope "slingshots" it over the obstruction with the recovering length of the cord aiding the process. If this technique fails, it is worthwhile to lower the rope, tie into the opposite side of the haul cord and pull in the opposite direction. If this too fails, then try pulling on the haul line with multiple people with the knowledge that a branch may break and drop from the tree. Realize that despite your best efforts you may have to reshoot the line.

Once a line is pulled into the tree with a suitable high point, tie off one end to a neighboring tree with a running bowline and enough tail to back it up with a double overhand stopper knot or Yosemite finish. Before climbing you must test the high point in the tree. Make sure other people are clear from the fall zone, and clip into the rope with a single ascension device. Be prepared to unclip and get out of the way in case something breaks. Weight the rope and slowly increase the amount of force on the rope by bouncing to test the high point. If the rope feels solid it is time to climb. It is a good idea to clear precarious dead wood that other climbers may encounter during the first ascent, but realize that dead wood is important for canopy organisms and should be left intact if it is not dangerous.

The next step is to advance the high point of the rope to the top of the tree and set it up for efficient mapping. Extra attention to detail in this step pays off handsomely for the remainder of the mapping effort. It is best to carry two 20' lengths of rope set up for positioning (Jepson, 2000), at least three small weighted (10-12oz.) bags, a pulley with a quick-link and 1 inch

tubular webbing, and a fiberglass measuring-tape as long as the tree is tall. Once at the high point of the shot, clip into the tree with a positioning line, have a ground person untie the anchor knot and lower climbed end until the anchored end is ~5 m below you. This is a critical step because it halves the weight the climber experiences while advancing the rope to the top of the tree, but it is risky because dropping the rope will strand the climber. Tie the rope into your harness with a bite knot and climb as high as safely possible alternating clipping in with the 2 20' positioner lines. Attempt to climb up the most suitable path without winding back and forth or ascending between tight spaces so subsequent climbers will have a carefree ascent. Once at an appropriate anchor location, tie the webbing around the trunk with a water knot and attach the pulley to this with a hand-tightened quick-link. Insure there are branches shortly below the pulley in case the webbing fails during subsequent ascents. Run the free end rope through the pulley, clip a weighted bag into the rope end and lower it to the opposite side that was climbed. Use a two-way radio to make sure a ground person has eyes on the rope as it lowers. Once the rope touches the ground on both ends, tie it off at the top with an appropriate anchor knot to allow both lines to be climbed at the same time.

The above step warrants extra time and care to do properly. When the end with the weighted bag is being lowered for the first time, it is common for it to perch on a branch and get stranded. As the climber continues to lower the rope it forms a loop. The extra rope taken up in the loop insures that it will not reach the ground. When lowering the climber needs to periodically lift the rope to feel for the weight of the bag as well as be in contact with a ground person who can see if the bag is hung up on a branch.

The last two steps when setting up a tree are to hang a vertical fiberglass measuring tape from the top to the bottom of the tree, and to insure the lowered end of the rope goes down a suitable climbing path. Lower the tape measure from the treetop and secure it when a ground person verifies that the zero mark on the tape is aligned with the average ground level around the tree (**Figure 1.3** of main text). Use two-way radios so a person on the ground can communicate this to the climber. In particularly large trees it can be difficult and time consuming to find the tape measure while taking height measurements when it is on the opposite side of the trunk. In these cases it is well worth the effort to hang an additional tape measure aligned to the first one on the opposite side of the trunk. Once the tape measures as set, have a ground person secure the

end of the rope that was initially climbed and descend the end that was lowered, rerouting as necessary to assure a clear climbing path.

When you are done climbing, never leave the rope in the tree for long periods. It is best to replace the rope with 3 mm black cord that is nearly invisible once secured. Position this cord close to the trunk in case of falling debris, tie it in a loop and secure it near the ground before leaving the tree. It is helpful to gently spiral it around the trunk to keep it close, especially in leaning trees. When it is time to enter the tree in the future, run the loop one full rotation through the pulley to check for any wear spots in the black cord before pulling in the main climbing line. Fix any wear spots by cutting and tying the cord back together with a single fisherman's knot. This ensures that you do not have to re-rig the tree if the line snaps while pulling up the main climbing rope.

Core sampling

Coring a tree along the trunk is much different from coring a tree on the ground. Consequently, we developed a few techniques that make this process easier. First you will need a small kit with appropriate tools to carry with you in the tree. This includes: beeswax, WD-40, 90% rubbing alcohol, a rifle cleaning "bore snake," a wooden golf tee, indelible markers, and scotch tape. It is also good to have a 20' positioning rope and a companion climber. In addition, bring a sturdy long, narrow bag in which to carry borers and core mounts. The mounts are simply slats of wood with a groove for taping in extracted cores. We have found taping cores directly into labelled mounts after extraction is the most secure and efficient way to carry long cores from the field. Always secure the borers with a tether to your harness.

The basic process is to locate where you want to core, extract the core, tape the core onto a mount and drop this into the core bag, then extract the borer. Core above buttressing on the main trunk and avoid anomalous swellings near large appendages. Always wax the coring bit between cores and spray a little WD-40 through the bit between cores. If you hit decay or pitch, clean the bit using the bore snake and rubbing alcohol. **Table 1** reviews potential problems and gives simple tips to fix them.

Table 1. Coring problems and solutions

Problem	Solution
Two borers being used on opposite sides of trunk collide in the middle	This is uncommon but disastrous. Always have one person start coring ≥10 cm above the other.
Not enough room between branches to spin handle	Bring an additional short borer and use its handle.
Not enough leverage to start borer, especially in leaning trees	Use a positioning rope attached to another climber or around the tree to provide purchase.
Nowhere to safely support the core mount when moving the core to the mount	Use foot loops on an ascender to support legs and provide flat surface on top of thighs.
Core does not come out	Extract spoon, rotate corer 180° counter clockwise, try again, and repeat using different rotations.
Cores twisted	Inspect bit for cleanliness and chips in blade, clean, lube, and sharpen if necessary.
Borer spins but does not come out (may be loud)	This happens with decay or when the bit is clogged with pitch and wood dust. Pull hard each half turn of the corer, and do not spin without pulling.
Core piece stuck in bit	Use spoon to extract it. If just a small piece is stuck in tip, slam spoon in many times rotating between attempts, being careful not to damage spoon or detach it from holder. Use wooden golf tee to push it deeper into bit and extract with spoon.
Losing pieces of core	Cores shrink ~2% in length and may crack as they dry. Tape onto core mount at least every 5 cm. Be careful with bag containing mounted cores at all times.

Branch sampling

Safely sampling branches up to the largest in the tree for dissection while retaining all material is a critically important yet difficult task. It is best to do this with a team of at least two in the tree and two on the ground well out of the fall zone. We have found that a large heavy-duty bag (Google search “1000kg bulk bag”) suspended from four points below the target branch is the best way to collect large samples. The overall process is to use a haul line (haul line 1) suspended from a pulley above the branch to secure and move sequentially excised branch

pieces, starting at the tip and working toward the trunk, into the bag. Once the bag is loaded to a heavy but manageable weight, lower it to the ground using a separate haul-line system (haul line 2). Many branches are large enough to require multiple loads. Use an approved (CE or UIAA) auto-locking friction device to lower the payload to the ground. Secure and move sequentially excised branch pieces, starting at the tip and working toward the trunk, into the bag. Once the bag is loaded to a heavy but manageable weight, lower it to the ground using a separate haul-line system (haul line 2). Many branches are large enough to require multiple loads. Use an approved (CE or UIAA) auto-locking friction device to lower the payload to the ground.

When making cuts, climbers need to take a few extra precautions for themselves as well as the tree. It is best to utilize a high point for independent climbing ropes to allow for the most freedom of movement. Attach the haul line 1 to the distal-most piece of branch to be excised. Before starting a cut, spend some time to make sure the cut piece and rope is not going to swing into the climber or the saw. Also make sure the swing-path of ropes supporting the branch and climbers are not encumbered by dead or hanging branches. Make a shallow cut under the branch to slice the bark, then begin to cut directly above this cut to meet it. The shallow undercut prevents the bark from stripping down the underside of the branch and possibly damaging trunk cambium. Making cuts at 1-cm diameter intervals where the branch stem will be cut for dissection later will save the ground crew from having to make extra cuts. Once a piece is cut a second climber can work it into the bag while the first repositions haul line 1 for another cut. When the branch base is reached, take extra care not to cut the branch collar, which will facilitate wound compartmentalization. When lowering the heavy duty bag, do so slowly and move it when necessary to avoid perching on branches. Stop it just above the ground and allow a ground person to swing it as far as they can from the tree while the weight is still mostly on the rope. This will make it easy for them to clear the branch from the drop zone. They can then attach a new bag to the rope and send it up to the climbers.

APPENDIX 1.D

Calculating whole-tree quantities requires many supporting equations and multipliers. These are presented below for *Picea sitchensis* in the order in which they appear in the manuscript. The table of contents supplies descriptions of how to use each table, click on the table names to quickly link to relevant tables. Trunk densities were obtained from small cores using the Archimedes principal. Appendage cross-sections were measured for average length and diameter, and bark and sapwood thickness. They were then debarked, and weighed by component after drying.

Table 1. Variable codes, definitions, and units used in this appendix. Variable codes referred to in tables for brevity. Predictors are independent variables used to predict dependent variables.

Variable code	Description	Variable type	Units
DBH	tape wrap diameter at 1.37 m	predictor	cm
f-DBH	diameter of circle with same area of trunk cross section at 1.37 m	predictor	cm
DTB	diameter above basal butressing where trunk becomes round	predictor	cm
diam	basal diameter of tree element	predictor	cm
CV	volume of paraboloid defined by crown depth and crown radius	predictor	m^3
mainTrnkVol	volume of main trunk, based on total diameter and height measurements	predictor	m^3
mainTrnkArea	Volume of main trunk, based on total diameter and height measurements	predictor	m^2
relHt	height of tree element divided by total tree height, ranges from 0-1	predictor	unitless
ht	height of tree element of height of tree	predictor	m
totRadius	total radius including bark of branch or trunk component	predictor	m
SD	slope distance, straight line distance from brach base to tip	predictor	m
density	density for volume to mass and mass to volume converstions	dependent	Kg m^{-2}
LMA	leaf mass to projected area ratio	dependent	g m^{-2}
barkThick	thickness of bark for calculating type "B" conic frusta	dependent	mm
woodRad	wood radius of tree component for calculating conic frusta	dependent	m
heartRad	heartwood radius of tree component for calculating conic frusta	dependent	m
totMass	aboveground dry mass of whole tree or branch	dependent	kg
totVol	aboveground wood and bark volume including appendages	dependent	kg
woodVol	aboveground wood volume	dependent	m^3
heartVol	aboveground heartwood volume including appendages	dependent	m^3
camArea	surface area of the cambium	dependent	m^2
leafMass	dry mass of leaves	dependent	kg
leafArea	projected sillhouette area of leaves	dependent	m^2
millLeaves	millions of leaves	dependent	count

Table 2. Equations for predicting wood and heartwood radius for trunk components and bark thickness or heartwood radius for branch or limb type segments. Predicted radii used to calculate bark, sapwood, and heartwood volumes of trunk sections and appendage segments. All units in meters except relative height (**Table 1**).

Component	DV	Form	***a***	***b***	***c***	***d***	***e***	*N*	R^2	RMSE
trunk	woodRad	***a****totRadius + ***b***	9.753E-01	-8.245E-03				268	0.9996	8.13E-17
trunk	heartRad	***a****totRadius + ***b****relHt + ***c****ht + ***d****refHt*ht + ***e***	9.731E-01	-3.923E-02	2.153E-05	8.433E-04	-4.963E-02	268	0.998	7.33E-17
branch	barkThick	$a*totRadius^{b} * e^{relht*c} * e^{ht*d}$	-3.723E+00	5.690E-01	-2.340E-01	5.575E-03		241	0.789	5.43E-05
branch	heartRadius	***a****totRadius + ***b****relHt + ***c****ht + ***d****refHt*ht + ***e***	8.820E-01	-7.426E-03	-2.701E-04	3.203E-04	-5.174E-03	146	0.903	7.83E-17

Table 3. Whole-branch equations for predicting branch tissue fractions using diameter (cm) at branch base. Min, mean, and max refer to the dependent variable.

Dependent variable	Form	***a***	***b***	*N*	R^2	RMSE	min	mean	max
total mass (kg)	$a*diam^{b}$	6.983E-02	2.503E+00	48	0.984	1.57E+01	8.00E-01	6.13E+01	6.50E+02
total volume (m^3)	$a*diam^{b}$	1.468E-04	2.416E+00	48	0.985	2.31E-02	1.00E-03	1.00E-01	1.00E+00
wood volume (m^3)	$a*diam^{b}$	6.033E-05	2.598E+00	48	0.985	1.84E-02	1.00E-03	7.20E-02	8.04E-01
heartwood volume (m^3)	$a*diam^{b}$	1.108E-05	2.9186E+00	48	0.981	1.22E-02	0.00E+00	3.50E-02	4.76E-01
bark area (m^2)	$a*diam^{b}$	3.770E-01	1.548E+00	48	0.906	7.19E+00	6.01E-01	1.92E+01	1.07E+02
cambium area (m^2)	$a*diam^{b}$	2.212E-01	1.585E+00	48	0.913	4.61E+00	3.84E-01	1.26E+01	7.13E+01
leaf mass (kg)	$a*diam^{b}$	1.126E-01	1.484E+00	64	0.919	1.44E+00	1.06E-01	3.87E+00	2.58E+01
leaf area (m^2)	$a*diam^{b}$	4.892E-01	1.508E+00	64	0.922	6.72E+00	2.66E-01	1.79E+01	1.22E+02
millions of leaves	$a*diam^{b}$	2.483E-02	1.519E+00	64	0.915	3.73E-01	9.00E-03	9.31E-01	6.45E+00

Table 4. *Picea sitchensis* multipliers for counts of small (0-2 cm) and large (2-4 cm) branchlets ± 1 standard error.

Dependent vaeriable	0-2 cm diameter			2-4 cm diameter			*N*
total mass (kg)	4.32E-02	±	3.18E-02	9.26E-01	±	2.38E-01	16
total volume (m^3)	6.74E-05	±	7.59E-05	1.60E-03	±	6.31E-04	16
wood volume (m^3)	1.76E-05	±	2.05E-05	6.81E-04	±	2.80E-04	16
bark area (m^2)	1.19E-01	±	1.56E-01	1.08E+00	±	4.82E-01	16
cambium area (m^2)	6.52E-02	±	8.31E-02	6.52E-01	±	2.83E-01	16
leaf mass (kg)	2.91E-02	±	2.07E-02	3.41E-01	±	8.36E-02	31
leaf area (m^2)	6.06E-02	±	4.33E-02	1.13E+00	±	2.82E-01	31
millions of leaves	1.67E-03	±	1.23E-03	4.53E-02	±	1.18E-02	31

Table 5. Density equations for Picea sitchensis components. See **Table 1** for variable codes and units on predictor variables.

Component	Dependent variable	Form	***a***	***b***	***c***	*N*	R^2
trunk	sapwood density (kg m^{-3})	a*relHt^b + c	1.865E+02	2.947E+00	3.690E+02	33	0.724
trunk	heartwood density (kg m^{-3})	a*relHt^b + c	3.123E+02	5.178E+00	3.947E+02	33	0.734
>1cm branches	wood and bark density (kg m^{-3})	a*diam + b* ht + c	1.464E+01	8.972E-01	4.976E+02	102	0.423
<1cm twigs	total density (kg m^{-3})	a*ln(SD) + b	-9.760E+01	2.745E+02		40	0.745
leaves	LMA (g m^{-2})	a*ln(relHt) + b*ln(ht) + c	1.435E+02	-8.724E+01	6.231E+02	28	0.490
single leaf	mass (g)	a*ln(relHt) + b*ln(ht) + c	5.246E-03	-3.801E-03	2.142E-02	28	0.396

Table 6. Mean density and water content of *Picea sitchensis* components and tissues. Trunk bark assumed same density as branch bark in publication.

component	tissue	mean density (kg/m^3)			water content (%)			*N*	notes
all	bark	404	±	14				42	
branch	wood+bark	620	±	8				115	
branch	sapwood	730	±	15				42	
branch	heartwood	778	±	16				33	trunk heart/sap density ratio (1.065) applied to branch wood density
trunk	sapwood	412	±	10	49	±	22	33	
trunk	heartwood	439	±	14	2	±	0	33	

Table 7. Equations for predicting whole-tree tissue fractions of *Picea sitchensis* trees from main trunk volume or surface area. Predictors are listed in order of importance. These equations are applied to 5 trees of dataset four from the study which are then included into the whole dataset. Note the two equations using **main trunk area** rather than **main trunk volume**. Suggested use: Predict total, bark, heart, and leaves then calculate sapwood by subtraction. For crown components subtract "allTrunks" values from total. See **Table 1** for predictor variable codes and units.

Dependent variable	Form	***a***	***b***	***c***	***d***	*N*	R^2	RMSE
total mass (kg)	$\boldsymbol{a}$*mainTrnkVol$^{\boldsymbol{b}}$ + $\boldsymbol{c}$*CV	3.464E+02	1.049E+00	5.427E-01	—	55	0.994	1.700E+03
bark mass (kg)	$\boldsymbol{a}$*mainTrnkVol$^{\boldsymbol{b}}$ + $\boldsymbol{c}$*CV	3.540E+01	9.391E-01	1.992E-01	—	55	0.945	4.146E+02
wood mass (kg)	$\boldsymbol{a}$*mainTrnkVol$^{\boldsymbol{b}}$ + $\boldsymbol{c}$*CV	3.080E+02	1.055E+00	2.917E-01	—	55	0.997	1.104E+03
sapwood mass (kg)	$\boldsymbol{a}$*mainTrnkVol$^{\boldsymbol{b}}$ + $\boldsymbol{c}$*CV	1.424E+02	7.516E-01	3.465E-01	—	55	0.950	6.177E+02
heartwood mass (kg)	$\boldsymbol{a}$*mainTrnkVol$^{\boldsymbol{b}}$	2.062E+02	1.113E+00	—	—	55	0.996	1.112E+03
all trunks wood mass (kg)	$\boldsymbol{a}$*mainTrnkVol$^{\boldsymbol{b}}$	3.428E+02	1.018E+00	—	—	55	0.999	4.678E+02
all trunks sapwood mass (kg)	$\boldsymbol{a}$*mainTrnkArea$^{\boldsymbol{b}}$	1.839E+01	9.693E-01	—	—	55	0.906	5.267E+02
all trunks heartwood mass (kg)	$\boldsymbol{a}$*mainTrnkVol$^{\boldsymbol{b}}$	2.204E+02	1.086E+00	—	—	55	0.997	9.093E+02
wood volume (m^3)	$\boldsymbol{a}$*mainTrnkVol$^{\boldsymbol{b}}$ + $\boldsymbol{c}$*DTB$^{\boldsymbol{d}}$	7.558E-01	1.037E+00	1.392E-04	2.149E+00	55	0.999	1.577E+00
total volume (m^3)	$\boldsymbol{a}$*mainTrnkVol$^{\boldsymbol{b}}$ + $\boldsymbol{c}$*DTB$^{\boldsymbol{d}}$	8.245E-01	1.033E+00	2.089E-04	2.149E+00	55	0.998	2.534E+00
bark volume (m^3)	$\boldsymbol{a}$*mainTrnkVol$^{\boldsymbol{b}}$ + $\boldsymbol{c}$*CV	9.638E-02	9.245E-01	1.788E-03	8.657E-01	55	0.945	1.083E+00
sapwood volume (m^3)	$\boldsymbol{a}$*mainTrnkVol$^{\boldsymbol{b}}$	6.258E-01	6.898E-01	—	—	55	0.914	1.764E+00
heartwood volume (m^3)	$\boldsymbol{a}$*mainTrnkVol$^{\boldsymbol{b}}$	5.312E-01	1.101E+00	—	—	55	0.997	2.376E+00
all trunks wood volume (m^3)	$\boldsymbol{a}$*mainTrnkVol$^{\boldsymbol{b}}$	8.632E-01	1.018E+00	—	—	55	0.999	1.042E+00
all trunks sapwood volume (m^3)	$\boldsymbol{a}$*mainTrnkArea$^{\boldsymbol{b}}$	4.589E-02	9.764E-01	—	—	55	0.906	1.374E+00
all trunks heartwood volume (m^3)	$\boldsymbol{a}$*mainTrnkVol$^{\boldsymbol{b}}$	5.483E-01	1.087E+00	—	—	55	0.997	2.156E+00
cambium (m^2)	$\boldsymbol{a}$*CV$^{\boldsymbol{b}}$ + $\boldsymbol{c}$*mainTrnkVol$^{\boldsymbol{d}}$	1.383E+00	7.702E-01	2.086E+01	7.567E-01	55	0.923	2.105E+02
leaf mass (kg)	$\boldsymbol{a}$*CV$^{\boldsymbol{b}}$ + $\boldsymbol{c}$*mainTrnkVol$^{\boldsymbol{d}}$	5.473E-01	7.696E-01	5.337E+00	7.311E-01	55	0.892	8.315E+01
leaf area (m^2)	$\boldsymbol{a}$*CV$^{\boldsymbol{b}}$ + $\boldsymbol{c}$*mainTrnkVol$^{\boldsymbol{d}}$	2.304E+00	7.789E-01	2.203E+01	7.440E-01	55	0.892	3.799E+02
millions of leaves	$\boldsymbol{a}$*CV$^{\boldsymbol{b}}$ + $\boldsymbol{c}$*mainTrnkVol$^{\boldsymbol{d}}$	1.149E-01	7.835E-01	1.086E+00	7.506E-01	55	0.891	1.982E+01

Table 8. Equations for predicting whole-tree tissue fractions in *Picea sitchensis* based on simple field measurements of DTB and *f*-DBH. Variables listed in order of importance. Suggested use: Predict total, bark, heart, and leaves then calculate sap by subtraction so total = sum of parts. For crown components, subtract "allTrunks" values from total. See **Table 1** for predictor variable codes and units. RMSE in units of dependent variable.

Dependent variable	Form	***a***	***b***	***c***	***d***	*N*	R^2	RMSE
total mass (kg)	$\boldsymbol{a}$*DTB$^{\boldsymbol{b}}$ + $\boldsymbol{c}$*f-DBH$^{\boldsymbol{d}}$	2.818E-01	2.256E+00	2.279E-01	1.917E+00	60	0.983	4.55E+03
bark mass (kg)	$\boldsymbol{a}$*DTB$^{\boldsymbol{b}}$ + $\boldsymbol{c}$*f-DBH$^{\boldsymbol{d}}$	9.201E-02	1.965E+00	9.317E-02	1.696E+00	60	0.956	5.23E+02
wood mass (kg)	$\boldsymbol{a}$*DTB$^{\boldsymbol{b}}$ + $\boldsymbol{c}$*f-DBH$^{\boldsymbol{d}}$	2.245E-01	2.278E+00	1.813E-01	1.932E+00	60	0.982	4.23E+03
sapwood mass (kg)	$\boldsymbol{a}$*DTB$^{\boldsymbol{b}}$ + $\boldsymbol{c}$*f-DBH$^{\boldsymbol{d}}$	7.697E-01	1.650E+00	8.388E-01	1.419E+00	60	0.954	7.77E+02
heartwood mass (kg)	$\boldsymbol{a}$*DTB$^{\boldsymbol{b}}$ + $\boldsymbol{c}$*f-DBH$^{\boldsymbol{d}}$	9.182E-02	2.421E+00	7.243E-02	2.048E+00	60	0.979	4.06E+03
all trunks wood mass (kg)	$\boldsymbol{a}$*DTB$^{\boldsymbol{b}}$ + $\boldsymbol{c}$*f-DBH$^{\boldsymbol{d}}$	2.814E-01	2.216E+00	2.278E-01	1.871E+00	60	0.976	4.22E+03
all trunks sapwood mass (kg)	$\boldsymbol{a}$*DTB$^{\boldsymbol{b}}$ + $\boldsymbol{c}$*f-DBH$^{\boldsymbol{d}}$	6.037E+00	1.154E+00	7.728E+00	9.795E-01	60	0.882	6.74E+02
all trunks heartwood mass (kg)	$\boldsymbol{a}$*DTB$^{\boldsymbol{b}}$ + $\boldsymbol{c}$*f-DBH$^{\boldsymbol{d}}$	1.179E-01	2.360E+00	9.477E-02	1.995E+00	60	0.976	4.01E+03
wood volume (m3)	$\boldsymbol{a}$*DTB$^{\boldsymbol{b}}$ + $\boldsymbol{c}$*f-DBH$^{\boldsymbol{d}}$	6.407E-04	2.250E+00	4.918E-04	1.897E+00	60	0.980	1.04E+01
total volume (m3)	$\boldsymbol{a}$*DTB$^{\boldsymbol{b}}$ + $\boldsymbol{c}$*f-DBH$^{\boldsymbol{d}}$	7.536E-04	2.240E+00	5.648E-04	1.888E+00	60	0.981	1.12E+01
bark volume (m3)	$\boldsymbol{a}$*DTB$^{\boldsymbol{b}}$ + $\boldsymbol{c}$*f-DBH$^{\boldsymbol{d}}$	3.372E-04	1.901E+00	3.344E-04	1.636E+00	60	0.955	1.33E+00
sapwood volume (m3)	$\boldsymbol{a}$*DTB$^{\boldsymbol{b}}$ + $\boldsymbol{c}$*f-DBH$^{\boldsymbol{d}}$	3.820E-03	1.525E+00	3.148E-03	1.280E+00	60	0.943	1.85E+00
heartwood volume (m3)	$\boldsymbol{a}$*DTB$^{\boldsymbol{b}}$ + $\boldsymbol{c}$*f-DBH$^{\boldsymbol{d}}$	2.555E-04	2.395E+00	2.034E-04	2.026E+00	60	0.979	9.92E+00
all trunks wood volume (m3)	$\boldsymbol{a}$*DTB$^{\boldsymbol{b}}$ + $\boldsymbol{c}$*f-DBH$^{\boldsymbol{d}}$	7.101E-04	2.214E+00	5.770E-04	1.870E+00	60	0.977	1.04E+01
all trunks sapwood volume (m3)	$\boldsymbol{a}$*DTB$^{\boldsymbol{b}}$ + $\boldsymbol{c}$*f-DBH$^{\boldsymbol{d}}$	1.497E-02	1.162E+00	1.938E-02	9.869E-01	60	0.883	1.75E+00
all trunks heartwood volume (m3)	$\boldsymbol{a}$*DTB$^{\boldsymbol{b}}$ + $\boldsymbol{c}$*f-DBH$^{\boldsymbol{d}}$	2.909E-04	2.362E+00	2.345E-04	1.997E+00	60	0.977	9.88E+00
cambium (m2)	$\boldsymbol{a}$*DTB$^{\boldsymbol{b}}$ + $\boldsymbol{c}$*f-DBH$^{\boldsymbol{d}}$	3.688E-01	1.546E+00	3.336E-01	1.332E+00	60	0.927	2.51E+02
leaf mass (kg)	$\boldsymbol{a}$*DTB$^{\boldsymbol{b}}$ + $\boldsymbol{c}$*f-DBH$^{\boldsymbol{d}}$	1.511E-01	1.495E+00	1.504E-01	1.293E+00	60	0.891	1.00E+02
leaf area (m2)	$\boldsymbol{a}$*DTB$^{\boldsymbol{b}}$ + $\boldsymbol{c}$*f-DBH$^{\boldsymbol{d}}$	6.107E-01	1.514E+00	6.221E-01	1.313E+00	60	0.891	4.59E+02
millions of leaves	$\boldsymbol{a}$*DTB$^{\boldsymbol{b}}$ + $\boldsymbol{c}$*f-DBH$^{\boldsymbol{d}}$	2.986E-02	1.523E+00	3.077E-02	1.323E+00	60	0.890	2.39E+01

Table 9. Equations for converting between DBH, DBH, and *f*-DBH (see **Table 1**) for *Picea sitchensis*. DV is dependent variable, RMSE is root mean squared error in cm, and AICc is Akaike's information criterion corrected for small sample sizes. AICc are only comparable between models with the same dependent variable. DTB.ht is the height of the DTB measurement above average ground level

DV	Form	***a***	***b***	***c***	*N*	R^2	RMSE	AICc
f-DBH	***a****DBH + ***b****DTB	6.617E-01	4.024E-01	-	44	0.979	12.6	354
f-DBH	***a****DBH	9.151E-01	0.000E+00	-	44	0.968	15.8	372
f-DBH	***a****DTB + ***b****DTB.ht + ***c****DTB*DTB.ht	1.155E+00	1.107E+00	5.402E-02	44	0.936	22.3	407
DTB	***a*****f*-DBH + ***b****DTB.ht + ***c*****f*-DBH*DTB.ht	7.750E-01	3.904E+00	-3.118E-02	44	0.916	15.0	372
DTB	***a****DBH + ***b****DTB.ht + ***c****DBH*DTB.ht	6.997E-01	6.434E+00	-3.462E-02	44	0.870	18.7	391

Table 10. Equations used to evaluate mass versus are relationships between tree species and to predict the age of the largest trees in dataset 4 and standard error around age estimates of uncored trees.

Species	Dependent variable	V1	*a*	*b*	*N*	R^2	RMSE	Mean	Form of equation
PISI	Total mass (Mg)	Age (yr)	7.071E-05	2.351E+00	60	0.824	1.46E+01	3.53E+01	$aV1^b$
PISI	Main trunk mass (Mg)	Age (yr)	9.473E-05	2.273E+00	60	0.827	1.20E+01	3.01E+01	$aV1^b$
PISI	Crown mass (Mg)	Age (yr)	9.335E-07	2.766E+00	60	0.740	3.12E+00	5.18E+00	$aV1^b$
PISI	Leaf mass (kg)	Age (yr)	5.775E-01	1.213E+00	60	0.613	1.90E+02	4.35E+02	$aV1^b$
PISI	Age (yr)	Total mass (Mg)	5.083E+01	4.464E-01	55	0.817	4.51E+01	2.01E+02	$aV1^b$
PSME	Total mass (Mg)	Age (yr)	7.220E-03	1.447E+00	15	0.758	1.55E+01	3.75E+01	$aV1^b$
PSME	Main trunk mass (Mg)	Age (yr)	7.065E-03	1.436E+00	15	0.774	1.35E+01	3.43E+01	$aV1^b$
PSME	Crown mass (Mg)	Age (yr)	2.977E-04	1.564E+00	15	0.554	2.18E+00	3.19E+00	$aV1^b$
PSME	Leaf mass (kg)	Age (yr)	1.280E+00	9.034E-01	15	0.424	1.41E+02	2.52E+02	$aV1^b$
SESE	Total mass (Mg)	Age (yr)	3.610E-02	1.188E+00	93	0.721	5.87E+01	1.29E+02	$aV1^b$
SESE	Main trunk mass (Mg)	Age (yr)	3.833E-02	1.164E+00	93	0.739	4.93E+01	1.16E+02	$aV1^b$
SESE	Crown mass (Mg)	Age (yr)	9.030E-04	1.392E+00	93	0.390	1.42E+01	1.37E+01	$aV1^b$
SESE	Leaf mass (kg)	Age (yr)	2.646E+00	7.924E-01	93	0.629	2.28E+02	5.92E+02	$aV1^b$

APPENDIX 1.E

Core processing and determining tree age

Developing age estimates for trees that are too large to core to the center or to calculate main trunk growth requires coring the trunk at multiple heights, measuring and crossdating cores, and estimating tree age based on an iterative routine utilizing ring width relationships to wood radius at multiple heights. This appendix details that process as done for *Picea sitchensis* in the current study. For information about best techniques for extracting cores at multiple heights along a trunk see **Appendix C**.

After extracting and measuring the fresh length of cores in the field they were taken to the lab and allowed to dry before processing. They were mounted with Elmers™ white glue (so they can be removed if needed) into grooves in specially made wooden slats. After the glue dried, we measured dry wood length of each core to develop a scalar of dry wood radius to fresh (fresh = dry * 1.02501, R^2 = 0.9998, N = 154). Cores were then sanded with progressively finer sandpaper (80-1100 grit) until the rings were easily distinguishable. The cores were cross-dated and marked under a dissection scope by hand so that each calendar decade received one dot, every half-century two dots, and every century three dots. The marked cores were scanned at 600-1200 dpi depending on the tightness of the rings and measured with CooRecorder (Cybis Dendrochronology) and WinDendro (Régent Instruments) software. Crossdating was confirmed using detrended ringwidth plots in CDendro (Cybis Dendrochronology) and COFFECHA (Grissino-Mayer, 2001). This was first done within each tree before checking trees against and then adding them to a cumulative master chronology. Ring widths were then consolidated into one file and output for further analysis.

Ages of all but the three largest trees (**Appendix G**, and main text **Figure 10**, Trees 58-60) were estimated using the full population of core samples at multiple heights as described previously (Sillett et al., 2018, 2015). The basic principal was to estimate trunk age at different heights and then to fit a linear model for trunk age by height, where the *y*-intercept is trunk age at 0 m height (i.e., ground level). First, ring widths from cores of the same tree and height were averaged. Dry ring widths were then scaled to fresh using the equation above and paired with calculated wood radius for each year ($\text{wood radius}_{(t-1)} = \text{wood radius}_{(t)} - \text{ring width}_{(t)}$). Each series was divided into quartiles and mean ring width in relation to mean wood radius for each

quartile were treated as independent measurements for each series. Nine suppressed or recently damaged trees with unusually small rings were excluded from the analysis to insure equations were conservative. At standard lower trunk heights (diameter at top of buttress (DTB), 10, 30, 50 m) a power equation (**Table 1**) was created to predict ring width based on wood radius and height using all cores within 1 m of each height. For averaged ring-width series that did not reach pith (tree center), trunk age at series height was estimated by iteratively decrementing the remaining unaged wood radius by its predicted ring width until the radius equaled zero, counting the iterations, and then adding this to the number of rings in the series. Final tree ages and their uncertainty were the intercept and its standard error from a linear model of height to predict age (average R^2 for all trees = 0.966). This process was repeated for uncored trees using their full wood radii.

Table 1. Power equations used to predict ring width from wood radius. DV is dependent variable, IV is independent variable. DTB is diameter at the top of buttress, which varied in height from 2.4-7.0 m. This equation was only applied to improve age estimates for trees where predictions were unrealistically close to the oldest verified year of any core.

Height (m)	DV	IV	Form	***a***	***b***	R^2	*N*
DTB	ring width (mm)	wood radius (m)	$\boldsymbol{a}IV^{\boldsymbol{b}}$	2.003E+00	-5.115E-01	0.291	104
10	ring width (mm)	wood radius (m)	$\boldsymbol{a}IV^{\boldsymbol{b}}$	1.583E+00	-6.142E-01	0.413	112
30	ring width (mm)	wood radius (m)	$\boldsymbol{a}IV^{\boldsymbol{b}}$	1.085E+00	-7.627E-01	0.560	108
50	ring width (mm)	wood radius (m)	$\boldsymbol{a}IV^{\boldsymbol{b}}$	9.003E-01	-4.345E-01	0.334	116

To assess if age estimates were reasonable for uncored trees and to estimate the age of the three largest three trees, which averaged 70% more massive than the next largest tree (**Appendix G**), we utilized models of age and total dry mass. Log-log equations of age from biomass fit with an interaction term cored vs. uncored trees that had neither a different intercept nor slope (P = 0.197, P =0.986, R^2 = 0.77), so these data were pooled to create a final equation to predict ages of the largest trees. Before pooling we *a priori* removed two trees that had severe damage causing major growth setbacks as evidenced by their crown structure (see main text **Figure 10**, trees 25 and 33), because the three largest trees clearly had not been subjected to such drastic setbacks. Using all 55 remaining trees, the total mass predicted 0.812 % of the variability in age

($Age = 5.083 * r^{0.446}$). The standard error of the mean was used for the ages of the uncored trees, while the standard error of individual predictions for the three largest trees was used to reflect increased uncertainty due to extrapolation. These ages were carried forward for the final comparison of *P. sitchensis*, *Pseudotsuga menziesii*, and *Sequoia sempervirens* by comparing the best fitted models of age to total, crown, and leaf mass.

References

Grissino-Mayer, H.D., 2001. Evaluating crossdating accuracy: A manual and tutorial for the computer program COFFECHA. Tree-Ring Res. 57, 205–221.

Sillett, S.C., Van Pelt, R., Carroll, A.L., Kramer, R.D., Ambrose, A.R., Trask, D., 2015. How do tree structure and old age affect growth potential of California redwoods? Ecol. Monogr. 85, 181–212.

Sillett, S.C., Ven Pelt, R., Freund, J.A., Campbell-spickler, J., Carroll, A.L., Kramer, R.D., 2018. Development and dominance of Douglas-fir in North American rainforests. For. Ecol. Manage. 429, 93–114. doi:10.1016/j.foreco.2018.07.006

APPENDIX 2.A

Additional Methods

This appendix details additional methods necessary for repeatability of results from field measurements. The first section elaborates on sampling design methodology, the second on plot design, the third on specific variable calculations used in each analysis, and the fourth on calculating appendage ages.

Sampling design

The tree sample was designed to be as objective as possible while including wide ranges of complex crown structure, neighborhood forest density, and ages near or after the transition from model-conforming development to crown building. The first goal was accomplished by opportunistically selecting trees with multiple tops and especially large limbs as encountered in the field (N = 5). Most trees in the forest were not complex, so trees selected via random sampling other than these complex individuals were relatively simple. The remaining trees were sampled with a stratified random approach, dividing the sampling space by five levels of neighborhood density and four levels of height.

The scale at which to quantify neighborhood density was established using light detection and ranging (LiDAR) data in a preliminary analysis. Forests of the Olympic Peninsula have been extensively mapped with aerial LiDAR (www.pudgetsoundlidar.ess.washington.edu), which can identify tree spatial patterns and heights. Additional algorithms approximately distinguish foliage associated with each treetop from the surrounding forest into polygons called tree approximate objects (TAOs, Jeronimo et al., 2018). The area of TAOs in 25 ha of forest (N = 1762 TAOs) was modeled using various combinations of forest density (**Table**) calculated at 5-m increments from 10 to 35 m. The lower bound of 10 m was within the distance that two large tree crowns physically interact given that the 95% quantile radius of a TAO is 6.57 m. The upper bound was 35 m because a tree would have to be taller than the maximum theoretical tree height (Koch et al., 2004) to cast shade on another's lower-crown foliage assuming an average tree crown height of 30 m from the ground (this study) and a minimum growing season sun angle of 60° above the horizon. Various models of the predictors (**Table**) were compared with AIC_c model weights (Wagenmakers and Farrell, 2004), which gave the most important radius of 30 m (**Table**).

Table 1. Covariates calculated for modeling TAO area. All variables are summaries for neighborhood plots and are calculated for radii of 10 to 35 m radius incremented by 5 m.

Variable	Formula	Description
Ht	Local maxima of (CSM – DEM)	Height of focal treetop above ground level
RelHt	$\sum_i^n \left({focal\ tree\ height}/{height_i} \right)$	Sum of focal tree height relative to all plot tree heights
InvDist	$\sum_i^n \left({1}/{dist_i^2} \right)$	Cumulative inverse square weighted distance of neighborhood trees to central tree
AziDist	$\sum_i^n \left({\cos(dist_i - \pi) + 1.5}/{2.5 * {1}/{dist_i^2}} \right)$	Azimuth-weighted inverse distance. Weighted so south = 1, north = 0.2, and cos smoothing between.
HorAng	$\sum_i^n \tan^{-1} \left({TAO\ diam_i}/{dist_i} \right)$	Amount of 360 degrees around focal tree occupied by neighbor tree crowns
Count	Total trees within plot radius	Number of trees >30 m tall in each plot
RipK	See (Ripley, 1977)	Ripley's K function evaluated at each plot r using border correction to evaluate neighborhood clustering

Table 2. Models fit for three calibration datasets. All models are fit for each plot radius ranging from 10 to 35 m in increments of 5 m. Y is the response variable of the log of TAO area. A Moran's I test is used on the residuals of each model to determine if there was spatial dependence. All models are fit using a normal distribution. An x indicates an interaction term between parameters.

Model	Form	Hypothesis
Null	y ~ Ht x RelHt	Null model: TAO area depends only on absolute tree height and height relative to neighbor trees.
aMod	y ~ Ht x RelHt + InvDist	These four models test for an effect of neighborhood density in addition to the null. Each of the last variables in the model is a different neighborhood density metric (Table 1).
bMod	y ~ Ht x RelHt + AziDist	
cMod	y ~ Ht x RelHt + HorAng	
dMod	y ~ Ht x RelHt + Count	
eMod	y ~ Ht x RelHt + RipK x InvDist	These four models test for an effect of an interaction between clustering and the four different measures of neighborhood density.
fMod	y ~ Ht x RelHt + RipK x AziDist	
gMod	y ~ Ht x RelHt + RipK x HorAng	
hMod	y ~ Ht x RelHt + RipK x Count	

Table 3. Top 6 models in the candidate set. Numbers trailing each model name refer to the neighborhood radius used to calculate covariates. Model refers to models in **Table** , parameters is the parameters count, LogLik is the log likelihood, deltaAIC$_c$ is the change in AIC$_c$ relative to the top-ranked model, weight is the likelihood of each model divided by the likelihood of all models, and CumWt is the cumulative model weight.

Model	Parameters	LogLik	AICc	deltaAIC*c*	Weight	CumWt
gMod30	8	-10605	21227	0.0	0.98	0.98
gMod35	8	-10610	21235	8.2	0.02	1.00
hMod30	8	-10611	21238	11.5	0.00	1.00
gMod25	8	-10615	21247	19.7	0.00	1.00
hMod35	8	-10616	21248	20.9	0.00	1.00
hMod25	8	-10618	21253	25.8	0.00	1.00

Once an appropriate radius was determined, a metric of neighborhood density was selected from LiDAR data by visually comparing point clouds clipped at a 30-m-radius scale

(**Figure**) to various calculated metrics output from the cloud metrics function of FUSION (McGaughey, 2009) software. The best metric was canopy relief ratio, which was calculated as (mean return height – min return height)/(max return height – min return height). This metric was calculated for a random sample of ~12,000 trees > 60 m tall used to represent the full population of trees in the study region. These were then stratified by 5 even intervals for random sub-selection of target trees based on neighborhood density.

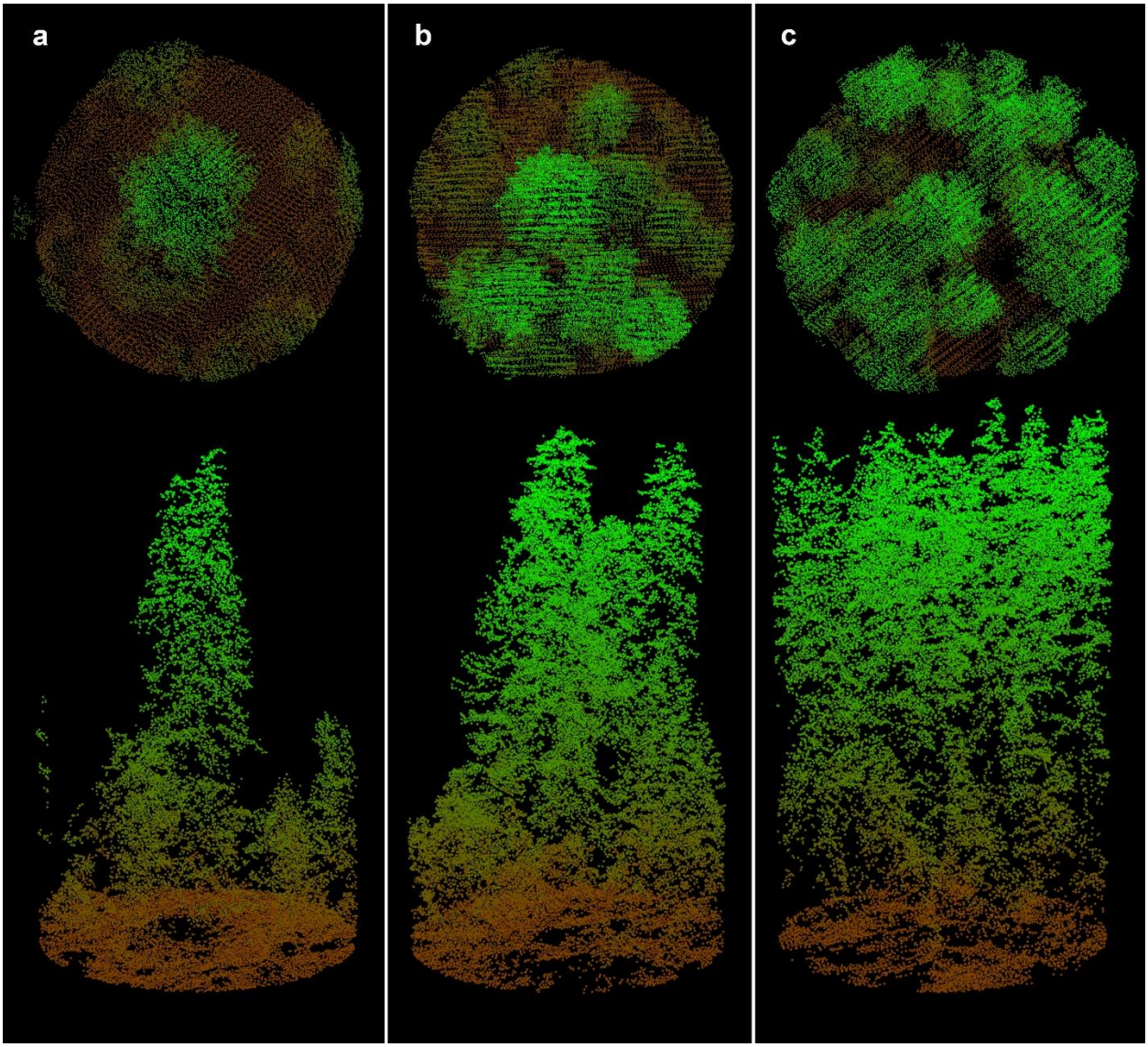

Figure 1. Clips of 30 m radius plots from the LiDAR point cloud showing minimum (**a**), mean (**b**), and maximum (**c**) canopy relief ratio.

The second layer of stratification was tree age, which was substituted by tree height. To create reasonable height surrogates for age, ring-width data extracted from multiple heights and reconstructed height growth of five tall *Pica sitchensis* trees (49.6 to 90.6 m) in Del Norte County, California were used to create a height-growth curve. Two curves were created by shifting the years of different tree series to align their curvature so that either 1) the last year's height of the shortest series from the tallest tree matched with corresponding year's height of the next tallest tree, thus creating an upper bound, or 2) the first year's height of a tree was matched to the corresponding year's height on the next tallest tree, thus creating a lower bound (**Figure**). In either case the tallest tree was anchored at the year of the last ring it produced (2016). These individual curves were fit with a third order polynomial equation and then averaged to generate the curve used to stratify the sampling effort. Three even-age strata were bounded between ages associated with 60 and 90 m, 60 m being the lower limit of the study and 90 m being close to the expected maximum tree height for *P. sitchensis* (most of the > 90 m LiDAR returns were from *Pseudotsuga menziesii*). The height corresponding with each age stratum was averaged with uniform height stratifications of 60, 70, 80, and 90 m, thus creating cutoffs at 60, 74, 83, and 90 m. These age classes resulted in uneven height strata that were wider for shorter trees, resulting in more concentrated sampling of taller trees. This sampling more accurately reflected the fact that as trees approached maximum height, they exhibited a wider range of ages. Combined, the forest density and height strata filled the sampling space with 13 bins. With a target of 36 trees, this allowed for up to three trees in densely populated strata and two in peripheral strata with enough leeway to map additional trees > 90 m tall if they were found (**Figure**).

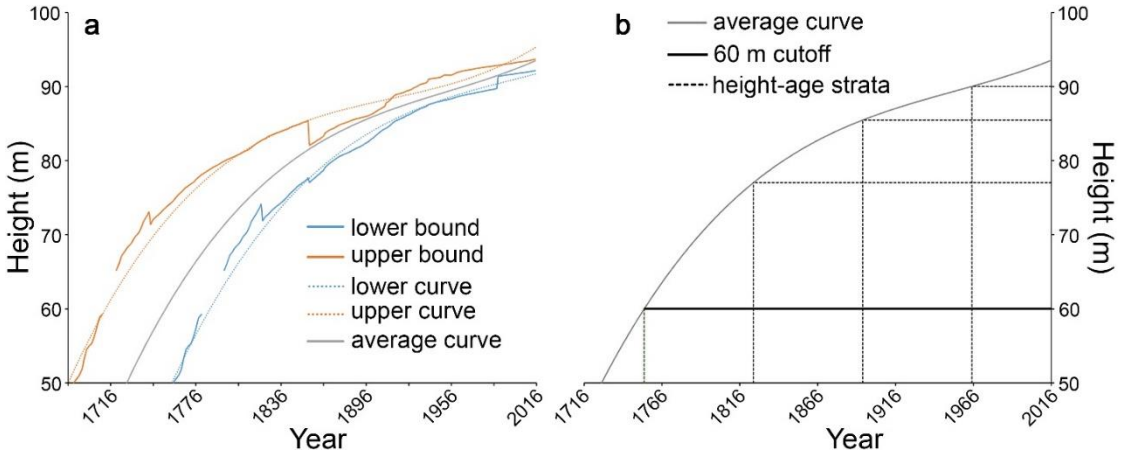

Figure 2. Height growth curve using ring-width data (**a**) to develop height stratifications reflecting uniform age strata (**b**).

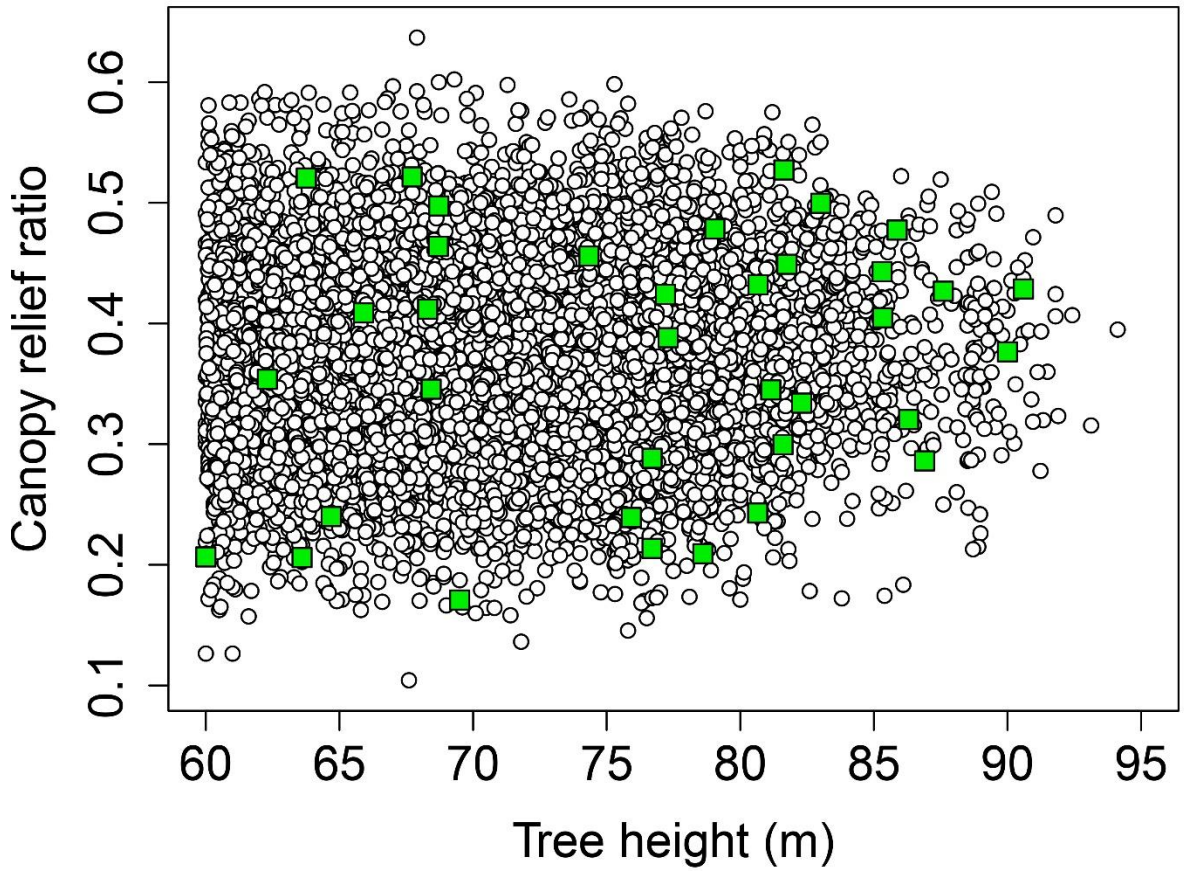

Figure 3. Final tree sample (green squares) within point cloud of > 12,000 randomly sampled trees > 60 m tall.

Plot design

Plots were designed to sample trees capable of shading up to the average crown base (~30 m) of a tree in plot center assuming a minimum sun angle of 60° above horizontal for the months of June to August at 48° latitude. Because we did not have data for *P. sitchensis* forests in the study region, we used data from three nearby *P. menziesii* forests recently measured (Sillett et al., 2018). From these data, average crown-base-height (CBH) for trees > 60 m tall and diameter-to-height relationships were extracted. The height a tree had to be at any given distance from the center tree to be able to cast shade above the average CBH (~30 m) on a hypothetical central tree was calculated. Shadow length was based on minimum solar angle during the prime growing months from May-September of 60° above the horizon. Heights tall enough to shade the

tree were converted back to diameter using the earlier-extracted relationship. These relationships were used to determine reasonable cutoffs for which diameters to sample and at what distances. Trees that met the distance and diameter thresholds received trunk measurements of diameter and height as well as crown measurements of radius and base height to calculate crown volume (**Figure**). Crown base was defined as where foliage extended 1/3 the way around the trunk and radius as the distance between points directly beneath the crown edge in cardinal directions and trunk pith at ground level. Additionally, we wanted to quantify possible root competition, so all trees within ≤ 10 m from the center and ≥ 5 cm diameter were measured.

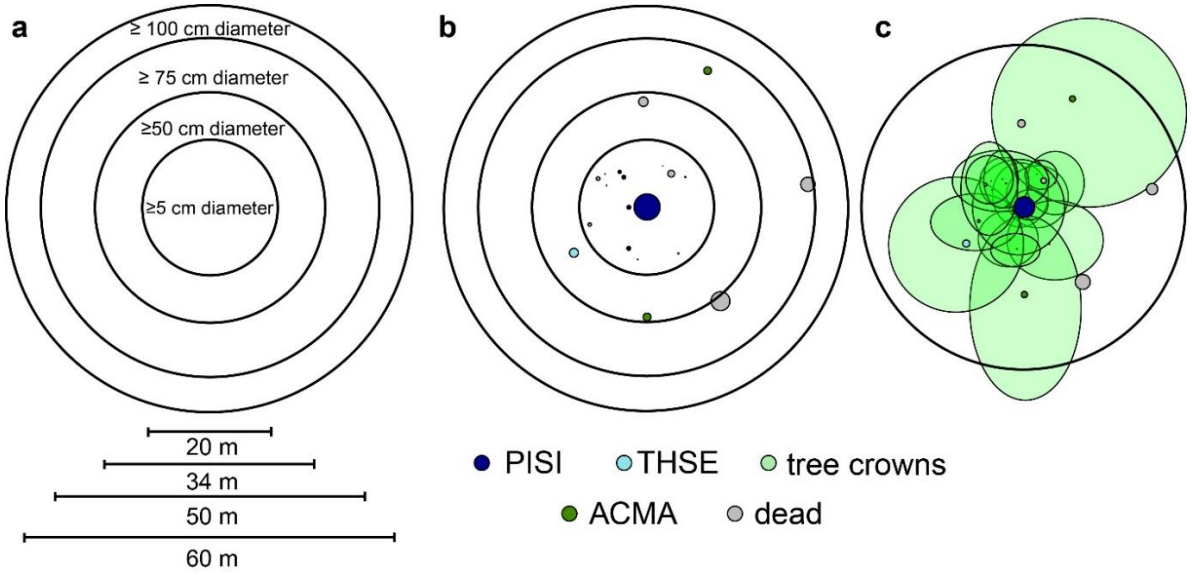

Figure 4. Diagram of plot design showing distance and diameter cutoffs for which trees were measured. **(a)** shows diameter cutoffs, **(b)** is an example of tree diameters and species in one plot, and **(c)** illustrates projected crown shapes based on crown radii taken in four cardinal directions showing only outer plot radius.

Variable calculations

Plot summary variables

Tree-level data within each neighborhood were summarized at the plot scale to use as predictors of macro-characteristics (e.g., horizontal surfaces, crown volume, height) and specific within-crown structures. Before any plot-level summaries were completed, Cartesian coordinate of all trees were calculated based on field-measured distances and azimuths from plot center.

Ultimately 20 variables were chosen based on previously published neighborhood variables (horizontal angle and distance-dependent crown volume, Contreras et al., 2011; Coonen and Sillett, 2015), metrics related to the azimuth of competing trees based on crown asymmetry weighted towards the southwest in northern latitudes (Rouvinen and Kuuluvainen, 1997), and intuitive yet simplified metrics representing tree density for easy measurement and interpretation by managers. These were described in **Table** , but one of them deserves more description.

Distance-dependent crown volume is the volume of all neighboring tree crowns that intersect the cone of influence around a center (**Figure**). This cone was defined with the same inverted cone used to design the plot except that the lowest point of reference was at crown base height of each study tree rather than 30 m (**Figure**). From this shape and the positions of neighboring trees, the intersection height of this cone with each neighbor was calculated. If the intersection height was below the crown base of a neighbor tree, the full crown volume of that tree was included in the calculation, whereas if it was above the crown base a partial crown volume was included based on the depth above the crown intersection. To estimate the partial crown volume, estimated radius and crown depth above the intersection were used to compute volume as a paraboloid. Crown radius at the intersection was estimated based on crown radius to crown depth relationships for all 729 live trees in all 36 plots predicted separately for conifer and hardwood species by including an interaction between tree lineage and crown depth (**Table**).

Table 4. Plot-level independent variables for identifying determinants of neighborhood structure and scale on *Pica* trunk form, crown radius, and crown ratio (main text Table 2). These are designed to

test the ability of simple metrics against standard forestry metrics and proven neighborhood competition indices.

Variable	Description
Competitive trees	Count of trees ≥ 60% of diameter of study tree
Tall trees	Count of trees ≥ 80% as tall as study tree
Horizontal angle (°)	Sum of (study tree diameter/plot tree diameter) x atan(plot tree diameter/plot tree distance), metric C11 in Contreras et al. 2011
Southwest-weighted horizontal angle	Horizontal angle x azimuth weight, azimuth weight sequence from 0–1 by increments of 1/180 so that 45°=0 and 225°= 1
South-weighted horizontal angle	See above, but weighted so that 0 or 360°= 0 and 180° = 1
Trees per hectare (TPH)	Count of trees within limiting distance, note that plot design excludes smaller trees at further distances
Basal area (m^2)	Total basal area of all neighbor trees
Basal area of large trees (m^2)	Total basal area of neighbor trees ≥ 80% of the diameter of the study tree
Basal area of *Tsuga heterophylla* (m^2)	Basal area of the most shade tolerant and abundant conifer
Mean distance of large trees (m)	Mean distance of all trees ≥ 80% of the diameter of the study tree
Mean distance of very large trees (m)	Mean distance of all trees ≥ 90% of the diameter of the study tree
Competition-free distance (m)	Distance to the nearest competitive tree, if none encountered then given a distance of 31 m (N = 2)
Crown volume of medium-sized trees (m^3)	Crown volume of all trees ≥ 50 cm diameter
Distance-dependent crown volume (m^3)	Volume occupied by neighbor tree crowns in a 60° inverted cone from crown base of study tree (Coonen and Sillett 2015)
Basal area of trees within 60° of south	Plot trees within 120° arc centered on south
Basal area of trees within 80° of south	Plot trees within 160° arc centered on south
Basal area of trees within 100° of south	Plot trees within 200° arc centered on south
Count of trees within 60° of south	Plot trees within 120° arc centered on south
Count of trees within 80° of south	Plot trees within 160° arc centered on south
Count of trees within 100° of south	Plot trees within 200° arc centered on south

Table 5. Equations for modeling crown radius at partial crown depths. Two equations were fit with one model by specifying an interaction term with lineage and crown depth. DV = dependent variable, IV = independent variable.

Lineage	DV	IV	*a*	*b*	Form	*N*	*P*	R^2
Hardwood	Crown radius	Crown depth	8.61E-01	6.29E-01	a x IV^b	729	< 0.001	0.60
Conifer			9.75E-01	4.62E-01				

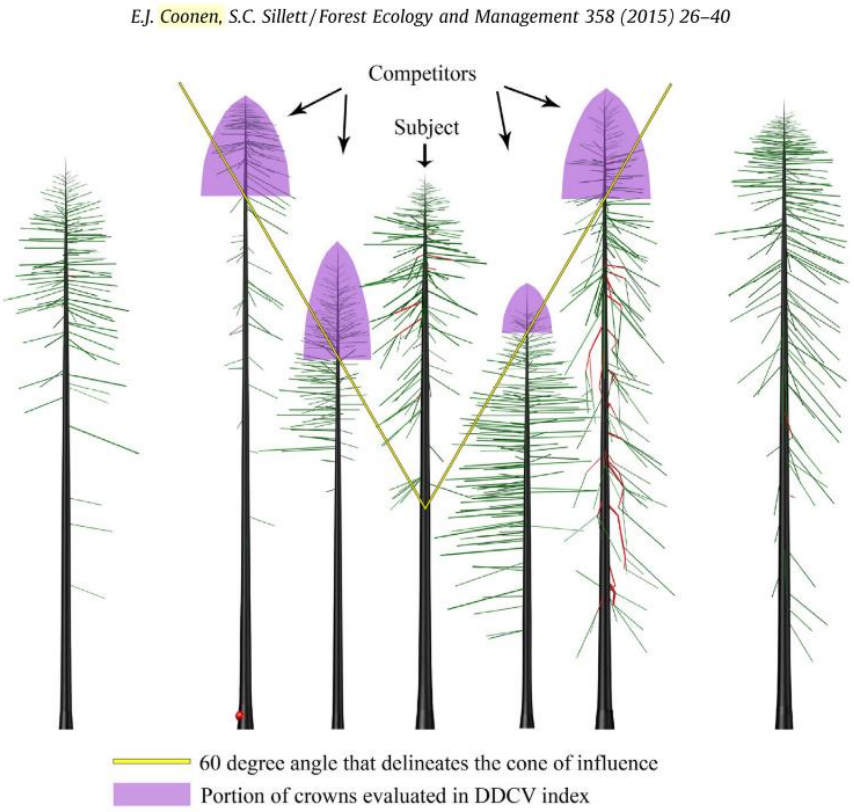

Figure 5. Figure from Coonen and Sillett (2015) reprinted to show the representation of distance-dependent crown volume.

Tree summary variables

The tree-level variables were based on mapping every appendage in the crown. Some appendages fit the model-conforming branching architecture of a simple axis or axes populated with small clusters of shoots. These were termed **model-conforming branches** and received simple measurements of diameter, height, horizontal extension, azimuth, slope, and notes on

damage and forking. Other appendages had clearly been injured, exhibiting abrupt changes in direction or diameter, and sometimes giving rise to reiterated trunks resembling the main tree trunk and having its own branches. These were segmented at locations best capturing their direction or diameter changes (**Figure**). Segments were represented as different types. Branch segments (B) were sloped ≤ 45° from horizontal and had no reiterated trunk distal to them (**Figure** segment 120-122), limb segments (L) were the same as B but with a reiterated trunk distal to them (**Figure** segment 111-120), and trunk type (T) segment sloped were >45° above horizontal (**Figure** segment 120-123). These could all give rise to model-conforming branches along their length or from distal ends. Thus all crown structures were summarized hierarchically either by individual segments and model-conforming branches or by appendages as single model-conforming branches and collections of segments and branches with one attachment point to the main trunk.

Counts and diameters of specific within-tree structures were based on summarizations at the appendage scale before calculation. This means certain values were smaller than they would have been if using all segments and model-conforming branches. For example, a tree's count of epicormic appendages was much less than the count of all epicormic branches because an original appendage could have given rise to multiple epicormic branches but was summarized as a single appendage. Summarizing by appendage also increased the mean diameter and 90^{th} percentile diameter for the same reason (i.e., smaller connections to basal segment of an appendage were ignored).

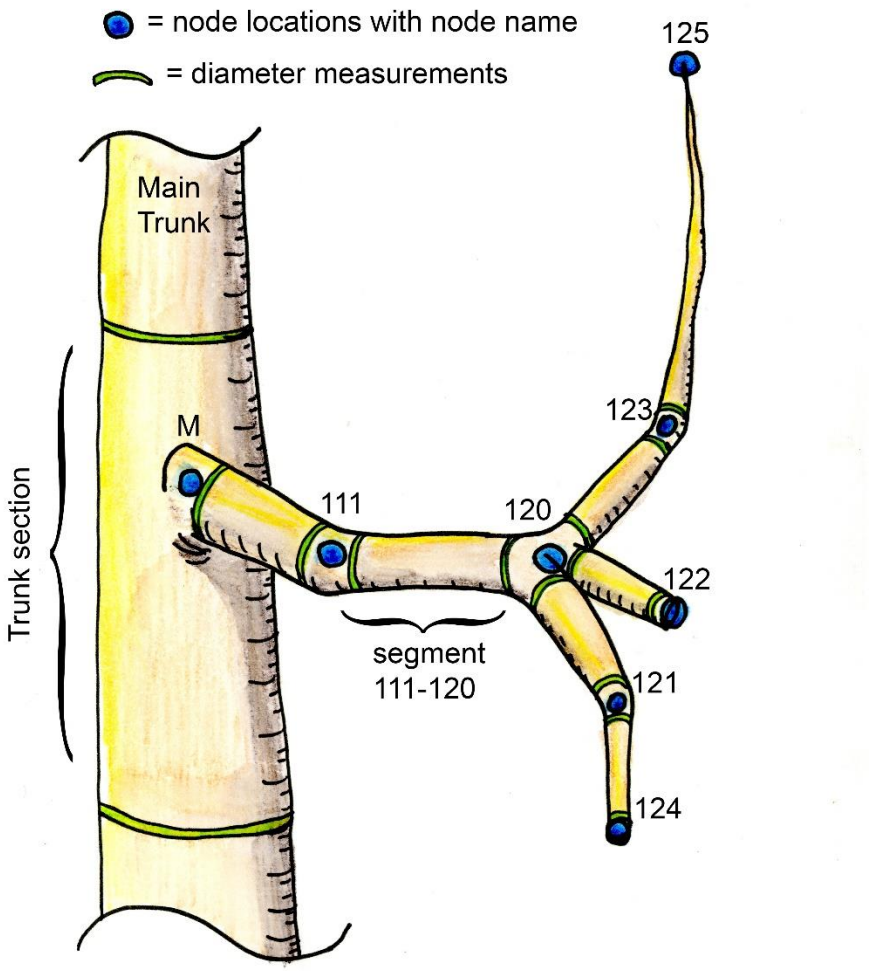

Figure 6. Reprint of figure from Kramer et al. (2018) showing appendage segmentation at changes in diameter or direction. Note that segment name is hyphenation of base and top node names.

All of within-crown variables were described in Table 2 of the main text, but definitions of forking and clusters of large appendages needed further qualification. Forking was a score based on the notes of individual branches and on the 3D structure of segmented appendages. Notes for branches were parsed into a forking column with the following rule: forked = 1, highly forked = 2, very highly forked = 3. As appendages were summarized, a fork count was calculated based on its segments as the number of distal ends minus 1. For, example, in **Figure** , there are three unique distal nodes (122, 124, and 125), so that appendage would receive a forking score of 2. A tree's total forking score was the sum of scores for all branches and segments. Clusters were defined after consideration of a particular concentration of appendages located in one of the trees (far right in Figure 1 of Appendix 4) that was covered in moss and had ample evidence of squirrel use. The minimum vertical, horizontal, and angular difference (0.8 m, 0.4 m, and 45°)

that identified this cluster was used to identify other clusters. The minimum diameter of appendages in each cluster was set at 10 cm because these are large and old enough to support abundant epiphytes, but also because small, young, model-conforming branches are often so densely distributed along trunks as to be lumped in clusters at this spatial scale. Thus, our algorithm was intended to consider clustering of appendages after substantial branch self-thinning had occurred.

The appendage damage index (ADI) was based both on appendage structure and parsed notes on each live crown component, while top damage index (TDI) was based on obvious breaks exhibited by the main trunk (and reiterated trunks) and notes on possible past top breaks. Within segmented systems, each distal segment (e.g. 121-124, 120-122, 123-125 in **Figure**) was first classified as injured or not, and if injured it was given a score based on the ratio of distal and basal diameters (**Table**). Likewise, injured branches were scores based on the ratio of their distal to branch basal diameter (**Table**). To quantify TDI, all main trunks and reiterated continuations were identified by visually inspecting the 3D models. Damage exhibited by their structure was quantified as the sum of ratio of break diameters (segment boundaries) to tree diameter at the top of buttressing (DTB). Noted but unmapped old breaks or what looked like could have been old breaks were also included in a similar way, but “possible” breaks were weighted by 0.5 (**Table**).

Table 5. Heuristic for classifying appendage and top break damage for the purpose of calculating ADI and TDI. Notes were parsed and scored using regular expression in R.

Tree component	Damage Criteria	Score
Appendage damage index: sum of structure and notes scores for all segments and branches		
Segment	Distal diameter >4 cm and ≤1 branch with an angular trajectory >50° from the segment azimuth	Injured = 1, otherwise 0
	Distal diameter/appendage basal diameter ≥1/3 and <1/2	2
	Distal diameter/appendage basal diameter ≥1/2	3
Branch	Distal diameter >4 cm	Injured = 1, otherwise 0
	Distal diameter/branch basal diameter ≥1/3 and <1/2	2
	Distal diameter/branch basal diameter ≥1/2	3
Structural total	sum(segment injured x score) + (Branch injured x score)) for all branches and segments	
Segment and branch notes	interacting with neighbor, rub	1
	spiral fracture, cracked, fractured, swollen, kinked, scarred, split	2
	broke and recovered, broken, hanging, pull out	3
Top damage index: sum of structure and notes ratios for main trunk and reiterated continuations of main trunk		
Main or reiterated trunk	Segmented because of obvious kink or diameter change	diameter at break/DTB
Main trunk notes	old break, old top break	diameter at break/DTB
	possible old break, possible old top break, possible break	0.5*diameter at break/DTB

Appendage ages

Discussion in the main text refers to ages of original appendages (i.e., those initiated by the treetop apical meristem at height of origin), so age of the trunk at the origin height of each appendage is a good approximation its age. Ages of the main trunk at core locations were estimated using the method described in the main text and elsewhere (Sillett et al., 2015). Ages of original appendages were then estimated by interpolating between aged trunk locations. Trunk age at each cored height except DTB was modeled with a second order polynomial using an interaction between tree and height (36 equations from one model, $N = 172$, $R^2 = 0.97$), and the age of each original appendage below the highest core was estimated with this model. To reconstruct treetop heights, height increments above the highest core were estimated by assuming they were proportional to the ring widths of the highest core. After developing an age

vs. top height relationship for each tree, original branches above the highest core were given the estimated age of the treetop when it was at their height.

APPENDIX 2.B

Evidence of canopy habitat

Large appendages and accumulations of soil and epiphytes provide structure, nesting sites, and food for arboreal organisms (Brown et al., 2018; Burger et al., 2010; Carey, 1996; Sillett and Van Pelt, 2007). During crown mapping we encountered enormous quantities of moss mats and along with evidence of animal activity. Moss mats were conglomerate communities of mosses, liverworts, lichens, and vascular plants often strengthened by roots of the fern *Polypodium glycyrrhiza* and sometimes with adventitious roots of *P. sitchensis* growing from the appendage (**Figure 1**). While mapping tree crowns, we recorded random paired measurements of diameters around appendages both including epiphytes and underneath against bark. We also took notes when we encountered evidence of arboreal vertebrates.

The paired moss-wrap and underlying diameter data were used to determine the smallest branch that could support a moss mat large enough for a *Brachyramphus marmoratus* nesting site (~14 cm, Hamer and Nelson, 1995). *Brachyramphus* is a threatened bird that lays a single egg every 1-2 years on moss mats in the canopy. Equations to convert appendage diameter to moss diameter and the reverse were fit using log-log linear regression (**Table 1**). Animal use of within crown structures was summarized by decoding notes from within tree data collection using R string matching functions, where each note was associated with a specific appendage. Notes included the terms mouse and squirrel feces, dissected cones, seed caches, nest, and tunnel.

Table 1. Equations for modeling moss and supporting appendage diameter. All $P < 0.001$.

Dependent variable	Independent variable	*a*	*b*	Form	*N*	R^2
Moss + Branch diameter	Branch diameter	1.60E+00	9.39E-01	$a \times IV^b$	332	0.73
Branch diameter	Moss + Branch diameter	1.37E+00	7.48E-01	$a \times IV^b$	332	0.71

Thick moss mats were found abundantly throughout the crown. The 332 moss-mat measurements varied from 5 to 80 m in height and on appendages from 4 to 55 cm diameter. While their median and mean thickness (moss diameter – appendage diameter) were 2.9 and 4.7 cm, respectively, they attained a maximum thickness of 35.6 cm. Based on the second equation in **Table 1**, a 14-cm-diameter moss mat was supported on average by an appendage 9.89 cm diameter, so a diameter of 10 cm was set as the lower limit for large appendages. On younger branches, moss mats were generally loosely attached and dominated by *Antitrichia gigantea* (**Figure 1**). As they aged, moss mats develop a firmly attached dense steel-wool-like under layer of dead moss and vascular plant roots (**Figure 1**). Adventitious *P. sitchensis* roots from the parent tree were rarely encountered, constituting only 14 observations on 6 trees. Although use of moss mats by insects and other animals was not quantified, many pupating insects, centipedes, millipedes, spiders, and even worms were encountered during canopy data collection (**Figure 1**). If the supporting appendage died, the moss mat would often slough off with the bark as underlying bark and sapwood decayed, and moss growth would commence anew (**Figure 1**). Despite this observation, a live versus dead categorical variable was not significant for predicting moss diameter ($P = 0.94$), so there was no difference, on average, between moss thickness of live and dead appendages.

Most arboreal evidence of vertebrate animal use was from rodents in the live crown. Evidence consisted of dissected cones, nests, and tunnels in moss mats, feces, seed caches, and animal sightings. There was no evidence on any appendage < 6 cm diameter, while the median appendage diameter (data were right skewed) for any animal sign was 14.2 ± 1.1 cm ($N = 62$). These appendages were on average at 45 ± 3 % relative crown height. While one observation occurred well below the live crown (on an isolated branch), all others were confined between 0 and 83 % relative crown height. Lack of observations in the upper crown (top 17 %) may be because young branches had not yet developed robust moss mats. Only 8 of 54 observations were on dead appendages. A few especially high concentrations of rodent activity, including tunnels, nests, and feeding platforms were observed on clustered and damaged appendages with deep cracks and moss mats spanning small gaps between them, on epicormic sprays of branches in the low crown, and on individual appendages that had broken away from the trunk and recovered by producing multiple branches at the distal break to form brooms (**Figure 2**).

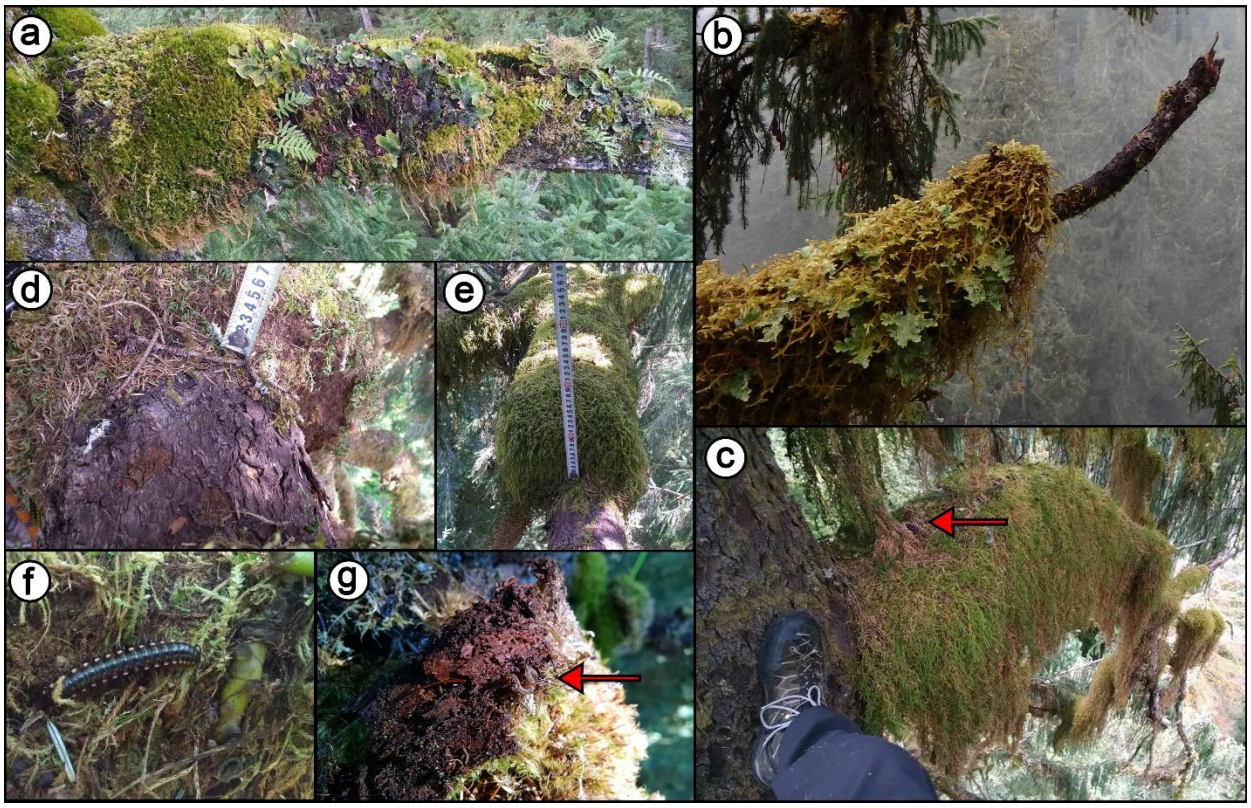

Figure 1. Photographs of moss mats showing diversity and structure. (**a**) Rich community of mosses, liverworts, lichens, ferns grows on a long-dead lower crown branch. (**b**) In this loosely attached *Antitrichia*- and *Lobaria*-dominated mat on a dead branch, note epiphytes sloughed off the distal end. **c**) This thick moss mat on a large low-crown branch is dominated by the vascular plant *Selaginella oregana.* Note *P. sitchensis* cones on mat near trunk placed by a feeding squirrel (arrow). (**d**) Underlying structure of epiphytes, including roots, are firmly attaching this moss mat to branch bark (tape scale in cm). (**e**) Thickness and extent of this well-developed moss mat in the mid-crown are emphasized by tape measure (red marks at 10-cm intervals). (**f**) *Harpaphe* millipedes live among rhizomes of *Polypodium glycyrrhiza* growing in a moss mat. (**g**) Earthworms live amidst epiphytes and decaying bark in moss mats (arrow). Photos by Russell Kramer.

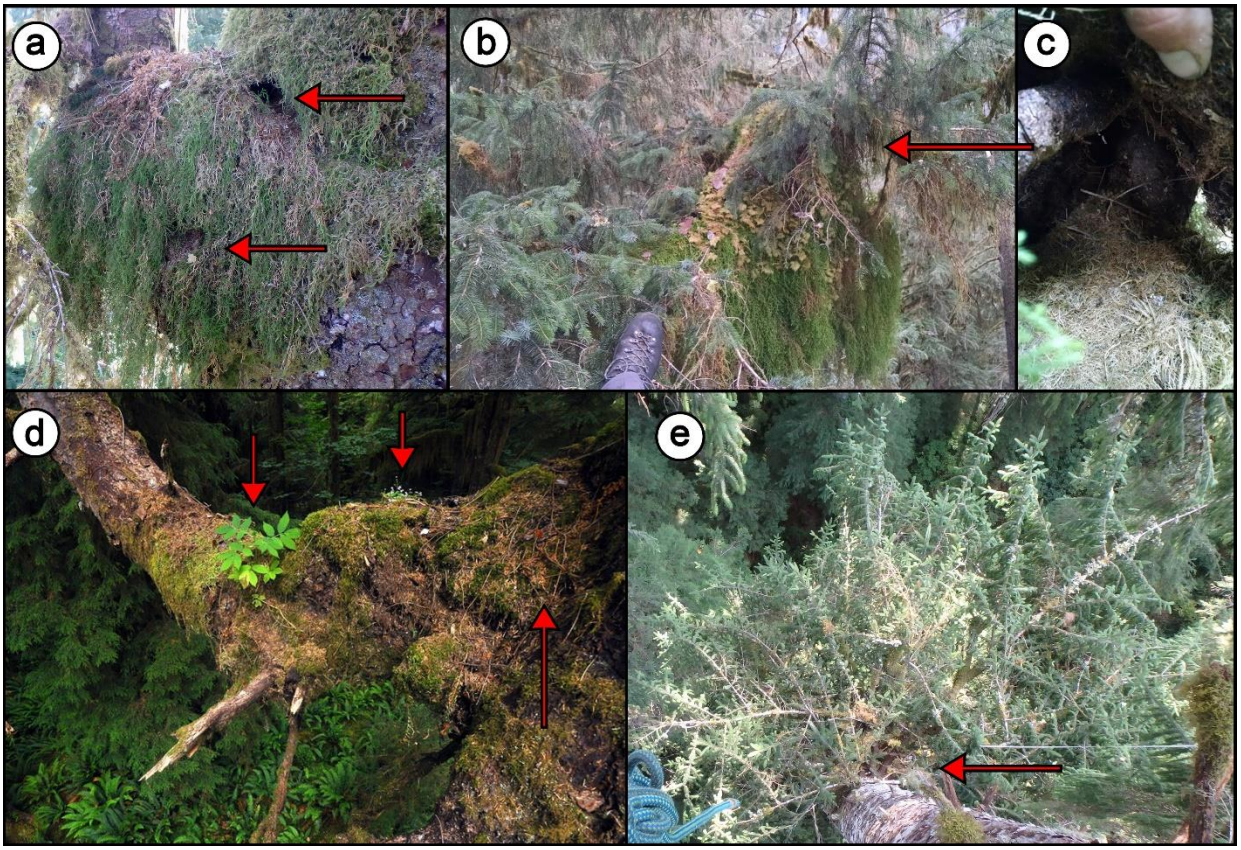

Figure 2. Photographs of habitat-related structures. (**a**) This squirrel tunnel occurs in a large moss mat with *Selaginella*. The upper arrow shows entrance hole, while lower shows a gap in epiphytes spanning space between two vertically clustered 24-cm-diameter appendages used as cover. (**b**) This broomed appendage that broke at the arrow and recovered with epicormic branches at the break is the location of a large moss mat with *Hylocomium* and *Selaginella*. (**c**) This tunnel leads to a squirrel nest within the moss mat on broomed appendage shown in (**b)**. (**d**) *Sambucus* (left arrow) and flowering *Claytonia* (middle arrow) live on a 61-cm-diameter limb 9 m above the ground. A large *P. sitchensis* seed cache (multiple handfuls) likely from a *Peromyscus* mouse is located under the moss mat against the trunk (right arrow). (**e**) This epicormic branch spray has a profusion of overlapping stems from a single location on the trunk. Older branch sprays accumulate detritus and moss, creating substrates for animal use. Photo (**d)** by Jessica Jemison, others by Russell Kramer.

References

Brown, C.E., Campbell-Spickler, J., Marks, S.B., Reiss, J.O., 2018. *Aneides vagrans* is absent from angiosperm crowns in an old-growth redwood forest. Herpetol. Conserv. Biol. 13, 533–538.

Burger, A.E., Ronconi, R. a., Silvergieter, M.P., Conroy, C., Bahn, V., Manley, I. a., Cober, A., Lank, D.B., 2010. Factors affecting the availability of thick epiphyte mats and other potential nest platforms for Marbled Murrelets in British Columbia. Can. J. For. Res. 40, 727–746. doi:10.1139/X10-034

Carey, A.B., 1996. Interactions of northwest forest canopies and arboreal mammals. Northwest Sci. 70, 72–78.

Hamer, T.E., Nelson, S.K., 1995. Characteristics of marbled murrelet nest trees and nesting stands, in: C. J. Ralph Jr., M. Raphael, and J. F. Piatt, G.L.H. (Ed.), Ecology and Conservation of the Marbled Murrelet. USDA, Forest Service, Albany, California, USA, pp. 69–82.

Sillett, S.C., Van Pelt, R., 2007. Trunk reiteration promotes epiphytes and water storage in an old-growth redwood forest canopy. Ecol. Monogr. 77, 335–359.

APPENDIX 2.C

Additional modeling

To refrain from overburdening the main text, supporting models not directly relevant to the primary objectives of the study were omitted, and some models were presented in a concise format without coefficient estimates and their standard errors. This appendix contains modeling that supported the main analyses and a full report of model coefficients that were not included. The last section also includes predicted outputs from macro- and within-crown characteristics. All references to tables are within this appendix unless explicitly stated as from the main text.

Neighborhood modeling

This section presents two analyses of three sets of models for determining the best neighborhood predictors of trunk form (DTB/tree height), crown radius, and crown ratio ((tree height – crown base height)/tree height). The first three model sets compared 20 plot-level metrics calculated at a 30-m scale with AIC_c model weights. The top five metrics common to two of the tree sets were selected and used in the second analysis. In the second analysis, these metrics were calculated at 5-m intervals from 10 to 30 m and ranked to determine the most appropriate scale for neighborhood analysis. The common model form for each is simply:

$$Z \sim Norm(\mu, \sigma^2): \mu = \boldsymbol{a} + \boldsymbol{b}X,$$

where Z is either trunk form, crown radius, or crown ratio for each model set, X is the plot-level predictor (**Table**), $\boldsymbol{a}$ is the intercept, and $\boldsymbol{b}$ is the slope.

Table 1. Plot-level independent variables for identifying determinants of neighborhood structure and scale on *Pica* trunk form, crown radius, and crown ratio. This is reprinted from Table 4 of Appendix 1 for interpretation of neighborhood models. These are designed to test the ability of simple intuitive metrics against standard forestry metrics and proven neighborhood competition variables.

Variable	Description
Competitive trees	Count of trees ≥ 60% of diameter of study tree
Tall trees	Count of trees ≥ 80% as tall as study tree
Horizontal angle (°)	Sum of (study tree diameter/plot tree diameter) x atan(plot tree diameter/plot tree distance), metric C11 in Contreras et al. 2011
Southwest-weighted horizontal angle	Horizontal angle x azimuth weight, azimuth weight sequence from 0–1 by increments of 1/180 so that 45°=0 and 225°= 1
South-weighted horizontal angle	See above, but weighted so that 0 or 360°= 0 and 180° = 1
Trees per hectare (TPH)	Count of trees within limiting distance, note that plot design excludes smaller trees at further distances
Basal area (m^2)	Total basal area of all neighbor trees
Basal area of large trees (m^2)	Total basal area of neighbor trees ≥ 80% of the diameter of the study tree
Basal area of *Tsuga heterophylla* (m^2)	Basal area of the most shade tolerant and abundant conifer
Mean distance of large trees (m)	Mean distance of all trees ≥ 80% of the diameter of the study tree
Mean distance of very large trees (m)	Mean distance of all trees ≥ 90% of the diameter of the study tree
Competition-free distance (m)	Distance to the nearest competitive tree, if none encountered then given a distance of 31 m (N = 2)
Crown volume of medium-sized trees (m^3)	Crown volume of all trees ≥ 50 cm diameter
Distance-dependent crown volume (m^3)	Volume occupied by neighbor tree crowns in a 60° inverted cone from crown base of study tree (Coonen and Sillett 2015)
Basal area of trees within 60° of south	Plot trees within 120° arc centered on south
Basal area of trees within 80° of south	Plot trees within 160° arc centered on south
Basal area of trees within 100° of south	Plot trees within 200° arc centered on south
Count of trees within 60° of south	Plot trees within 120° arc centered on south
Count of trees within 80° of south	Plot trees within 160° arc centered on south
Count of trees within 100° of south	Plot trees within 200° arc centered on south

Neighborhood analysis 1: Best metrics

Table 2. Model rankings using 20 dependent variables calculated at a 30-m scale (**Table**) to predict trunk form, crown radius, and crown ratio. Models are sorted by model weight within each set, and sets are distinguished by a header row. DV = dependent variable, LL = log likelihood, AIC_c = Akaike's Information Criterion corrected for small sample sizes, Weight is likelihood of each model divided by likelihood of all models, CumWt is cumulative model weight, and R^2 is adjusted R^2. All N = 36.

DV	Independent variable	LL	AIC_c	Weight	CumWt	R^2
Trunk form	Competitive trees	-11.24	29.23	0.57	0.57	0.60
Trunk form	Horizontal angle	-12.22	31.20	0.21	0.78	0.57
Trunk form	Southwest-weighted horizontal angle	-12.54	31.83	0.15	0.93	0.57
Trunk form	South-weighted horizontal angle	-13.69	34.13	0.05	0.98	0.54
Trunk form	Competition-free distance	-14.90	36.56	0.01	0.99	0.50
Trunk form	Count of trees within 100° of south	-16.26	39.28	0.00	1.00	0.47
Trunk form	Tall trees	-17.91	42.58	0.00	1.00	0.41
Trunk form	Count of trees within 60° of south	-18.57	43.90	0.00	1.00	0.39
Trunk form	Count of trees within 80° of south	-18.89	44.54	0.00	1.00	0.38
Trunk form	Basal area of large trees	-19.69	46.13	0.00	1.00	0.35
Trunk form	Mean distance of large trees	-20.91	48.57	0.00	1.00	0.31
Trunk form	Tree per hectare	-21.93	50.61	0.00	1.00	0.27
Trunk form	Mean distance of very large trees	-22.37	51.48	0.00	1.00	0.25
Trunk form	Basal area of trees within 60° of south	-23.36	53.48	0.00	1.00	0.21
Trunk form	Basal area of trees within 80° of south	-23.56	53.86	0.00	1.00	0.20
Trunk form	Basal area of trees within 100° of south	-24.00	54.75	0.00	1.00	0.18
Trunk form	Basal area of *Tsuga heterophylla*	-24.94	56.63	0.00	1.00	0.13
Trunk form	Basal area	-24.98	56.71	0.00	1.00	0.13
Trunk form	Crown volume of medium-sized trees	-26.45	59.66	0.00	1.00	0.06
Trunk form	Distance-dependent crown volume	-26.96	60.66	0.00	1.00	0.03
DV	Independent variable	LL	AIC*c*	Weight	CumWt	R^2
Crown radius	Competition-free distance	-56.34	119.43	0.86	0.86	0.53
Crown radius	Southwest-weighted horizontal angle	-59.30	125.35	0.04	0.91	0.44
Crown radius	Horizontal angle	-59.58	125.91	0.03	0.94	0.43
Crown radius	Competitive trees	-59.71	126.16	0.03	0.97	0.43
Crown radius	South-weighted horizontal angle	-60.18	127.11	0.02	0.99	0.41
Crown radius	Mean distance of large trees	-62.01	130.77	0.00	0.99	0.35

Crown radius	Tall trees	-62.60	131.95	0.00	1.00	0.33
Crown radius	Mean distance of very large trees	-62.66	132.07	0.00	1.00	0.33
Crown radius	Count of trees within 100° of south	-62.80	132.35	0.00	1.00	0.32
Crown radius	Basal area of large trees	-64.24	135.23	0.00	1.00	0.26
Crown radius	Count of trees within 60° of south	-64.40	135.55	0.00	1.00	0.26
Crown radius	Count of trees within 80° of south	-64.94	136.63	0.00	1.00	0.23
Crown radius	Basal area of trees within 60° of south	-66.61	139.97	0.00	1.00	0.16
Crown radius	Basal area of trees within 80° of south	-66.95	140.65	0.00	1.00	0.14
Crown radius	Tree per hectare	-67.09	140.93	0.00	1.00	0.14
Crown radius	Basal area of trees within 100° of south	-67.16	141.07	0.00	1.00	0.13
Crown radius	Distance-dependent crown volume	-67.20	141.15	0.00	1.00	0.13
Crown radius	Basal area	-68.12	142.98	0.00	1.00	0.09
Crown radius	Crown volume of medium-sized trees	-69.60	145.94	0.00	1.00	0.01
Crown radius	Basal area of *Tsuga heterophylla*	-69.62	145.99	0.00	1.00	0.01

DV	Independent variable	LL	AIC_c	Weight	CumWt	R^2
Crown ratio	Tall trees	33.78	-60.81	0.60	0.60	0.46
Crown ratio	Horizontal angle	32.81	-58.86	0.23	0.83	0.43
Crown ratio	Competitive trees	31.50	-56.25	0.06	0.89	0.39
Crown ratio	Southwest-weighted horizontal angle	31.39	-56.04	0.06	0.95	0.39
Crown ratio	South-weighted horizontal angle	30.28	-53.81	0.02	0.97	0.35
Crown ratio	Tree per hectare	29.66	-52.56	0.01	0.98	0.32
Crown ratio	Basal area of large trees	29.38	-52.01	0.01	0.99	0.31
Crown ratio	Crown volume of medium-sized trees	29.13	-51.52	0.01	0.99	0.30
Crown ratio	Basal area	28.50	-50.24	0.00	0.99	0.28
Crown ratio	Count of trees within 100° of south	28.48	-50.20	0.00	1.00	0.28
Crown ratio	Competition-free distance	27.25	-47.76	0.00	1.00	0.23
Crown ratio	Basal area of trees within 60° of south	26.84	-46.94	0.00	1.00	0.21
Crown ratio	Count of trees within 60° of south	26.71	-46.68	0.00	1.00	0.20
Crown ratio	Basal area of trees within 100° of south	26.64	-46.53	0.00	1.00	0.20
Crown ratio	Count of trees within 80° of south	26.36	-45.98	0.00	1.00	0.19
Crown ratio	Basal area of trees within 80° of south	25.44	-44.13	0.00	1.00	0.14
Crown ratio	Basal area of *Tsuga heterophylla*	23.40	-40.05	0.00	1.00	0.04
Crown ratio	Mean distance of large trees	23.31	-39.86	0.00	1.00	0.04
Crown ratio	Mean distance of very large trees	22.85	-38.95	0.00	1.00	0.01
Crown ratio	Distance-dependent crown volume	22.69	-38.64	0.00	1.00	0.00

Neighborhood analysis 2: Plot scale

Table 3. Model rankings using four dependent variables calculated at a 10- to 30-m scales at 5-m intervals to predict trunk form, crown radius, and crown ratio. Models are sorted by weight within each set, and sets are distinguished by a header row. Competition-free distance produced too many zeros at small scales to be meaningful, so it was left at the full scale of 30 m. DV = dependent variable, LL = log likelihood, AIC_c = Akaike's Information Criterion corrected for small sample sizes, Weight is the likelihood of each model divided by the likelihood of all models, CumWt is the cumulative model weight, and R^2 is adjusted R^2. All N = 36.

DV	Independent variable	LL	AICc	Weight	CumWt	R^2
Trunk form	Competitive trees 30	-11.24	29.23	0.22	0.22	0.60
Trunk form	Competitive trees 25	-11.27	29.29	0.21	0.43	0.60
Trunk form	Horizontal angle 25	-11.75	30.24	0.13	0.56	0.58
Trunk form	Horizontal angle 15	-12.00	30.75	0.10	0.66	0.58
Trunk form	Horizontal angle 30	-12.22	31.20	0.08	0.74	0.57
Trunk form	Southwest-weighted horizontal angle 30	-12.54	31.83	0.06	0.80	0.57
Trunk form	Southwest-weighted horizontal angle 25	-12.61	31.98	0.05	0.85	0.56
Trunk form	Horizontal angle 20	-12.73	32.21	0.05	0.90	0.56
Trunk form	Southwest-weighted horizontal angle 15	-12.97	32.70	0.04	0.94	0.56
Trunk form	Competitive trees 20	-13.50	33.74	0.02	0.96	0.54
Trunk form	Competitive trees 15	-13.61	33.96	0.02	0.98	0.54
Trunk form	Southwest-weighted horizontal angle 20	-14.01	34.76	0.01	0.99	0.53
Trunk form	Competition-free distance	-14.90	36.56	0.01	1.00	0.50
Trunk form	Competitive trees 10	-17.63	42.01	0.00	1.00	0.42
Trunk form	Southwest-weighted horizontal angle 10	-17.64	42.03	0.00	1.00	0.42
Trunk form	Horizontal angle 10	-18.39	43.54	0.00	1.00	0.40
DV	Independent variable	LL	AICc	Weight	CumWt	R^2
Crown radius	Competition-free distance	-56.34	119.43	0.33	0.33	0.53
Crown radius	Competitive trees 15	-56.69	120.13	0.23	0.57	0.52
Crown radius	Horizontal angle 15	-57.97	122.70	0.06	0.63	0.48
Crown radius	Southwest-weighted horizontal angle 20	-58.08	122.92	0.06	0.69	0.48
Crown radius	Southwest-weighted horizontal angle 15	-58.19	123.14	0.05	0.74	0.47
Crown radius	Competitive trees 25	-58.24	123.23	0.05	0.79	0.47
Crown radius	Horizontal angle 25	-58.27	123.29	0.05	0.84	0.47
Crown radius	Competitive trees 20	-58.47	123.68	0.04	0.88	0.47
Crown radius	Horizontal angle 20	-58.73	124.21	0.03	0.91	0.46

Crown radius	Southwest-weighted horizontal angle 25	-58.86	124.48	0.03	0.94	0.45
Crown radius	Competitive trees 10	-59.15	125.05	0.02	0.96	0.45
Crown radius	Southwest-weighted horizontal angle 30	-59.30	125.35	0.02	0.97	0.44
Crown radius	Horizontal angle 30	-59.58	125.91	0.01	0.99	0.43
Crown radius	Competitive trees 30	-59.71	126.16	0.01	1.00	0.43
Crown radius	Southwest-weighted horizontal angle 10	-62.11	130.97	0.00	1.00	0.35
Crown radius	Horizontal angle 10	-62.11	130.97	0.00	1.00	0.35

DV	Independent variable	LL	AICc	Weight	CumWt	R^2
Crown ratio	Horizontal angle 30	32.81	-58.86	0.50	0.50	0.43
Crown ratio	Competitive trees 30	31.50	-56.25	0.14	0.64	0.39
Crown ratio	Southwest-weighted horizontal angle 30	31.39	-56.04	0.12	0.76	0.39
Crown ratio	Horizontal angle 25	31.33	-55.92	0.11	0.87	0.38
Crown ratio	Southwest-weighted horizontal angle 25	30.52	-54.29	0.05	0.92	0.36
Crown ratio	Competitive trees 25	29.72	-52.69	0.02	0.95	0.33
Crown ratio	Horizontal angle 20	29.31	-51.87	0.02	0.96	0.31
Crown ratio	Horizontal angle 15	29.00	-51.25	0.01	0.97	0.30
Crown ratio	Competitive trees 15	28.78	-50.80	0.01	0.98	0.29
Crown ratio	Competitive trees 20	28.38	-50.01	0.01	0.99	0.27
Crown ratio	Southwest-weighted horizontal angle 20	28.31	-49.86	0.01	0.99	0.27
Crown ratio	Southwest-weighted horizontal angle 15	27.65	-48.54	0.00	1.00	0.24
Crown ratio	Competition-free distance	27.25	-47.76	0.00	1.00	0.23
Crown ratio	Competitive trees 10	26.00	-45.26	0.00	1.00	0.17
Crown ratio	Horizontal angle 10	24.53	-42.31	0.00	1.00	0.10
Crown ratio	Southwest-weighted horizontal angle 10	24.46	-42.16	0.00	1.00	0.10

Selected metrics were consistently good from 15 to 30 m with the best scale varying among them. We chose to calculate plot density at a distance of 25 m for the count of competitive trees and both Southwest-weighted and unweighted horizontal angles. Additionally, we included the competition-free distance as a variable for the full plot radius, because when calculated at smaller scales it was meaningless if distance was greater than calculation radius. These were used in a principal components analysis to calculate a composite metric of density (main text Table 5). To reduce skew and kurtosis for the principal components analysis, the competition-free distance and count of competitive trees were square-root transformed. Later in

the main text, a conversion between density and the simplest metrics comprising it is provided. These conversions were based on equations in **Table** .

Table 4. Equations for converting the composite Density metric to two simple components presented in Table 9 of the main text. IV = independent variable.

Dependent variable	IV	*a*	*b*	Form	*P*	*N*	R^2
sqrt(Competition-free distance (m))	Density	5.424	-3.981	$a + b$IV	<0.001	36	0.81
sqrt(Competative trees 25m)	Density	-0.043	4.661	$a + b$IV	<0.001	36	0.92

Crown-level modeling

Whole tree macro-characteristics were modeled to infer how neighborhood density effect the size and shape of crown characteristics and to create Figure 6 of the main text. These were created with linear models of the natural-log of the dependent variables crown volume, total mass, both horizontal surface indices (> 4 and > 10 cm), percent crown mass, and height, and by the normal linear model of crown base height (CBH). All models used neighborhood density and age as predictors, while CBH also used tree height as a predictor. The full models are presented in **Table** .

Table 5. Models of tree macro-characteristics including neighborhood density, tree age, and height as predictors. HSI = horizontal surface index. Variable derivations are in main text Table 2. All p-values < 0.001.

Dependent Variable	V1	V2	*a*	*b*	*c*	Form	*N*	R^2
Crown volume (m^3)	Denisty	Age	5.49E+03	-1.68E+00	2.05E-03	$a \times e^{b\,V1} \times e^{c\,V2}$	36	0.73
Total mass (Mg)	Denisty	Age	3.14E+00	-1.23E+00	9.44E-01	$a \times e^{b\,V1} \times V2^{c}$	36	0.71
HSI > 4 cm	Denisty	Age	7.36E-03	-1.06E+00	7.68E-01	$a \times e^{b\,V1} \times V2^{c}$	36	0.41
HSI > 10 cm	Denisty	Age	7.35E-03	-1.90E+00	1.49E+00	$a \times e^{b\,V1} \times V2^{c}$	36	0.51
Percent crown mass	Denisty	—	2.16E-01	-1.14E+00	—	$100 \times (a \times e^{b\,V1})$	36	0.57
Height (m)	Age	Denisty	1.66E+01	2.64E-01	1.22E-01	$a \times V1^{b} \times e^{c\,V2}$	36	0.46
CBH (m)	Denisty	Tree ht (m)	-2.18E+01	2.19E+01	4.52E-01	$a + b\,V1 + c\,V2$	36	0.41

Specific within-crown appendages (**Table**) were modeled with hurdle models to predict thresholds for zero counts with a logistic function and a Poisson regression for positive counts.

Like the previous analysis, this was also done in two steps. The first fit logistic models using all possible combinations of age, density, ADI, and TDI (**Table**) without including interaction terms. The best model ranked by model weight (model likelihood/sum of all model likelihoods), where all coefficients were significant ($\alpha < 0.05$), was selected as the logistic portion of the hurdle model. The Poisson portion of the analysis considered all possible combinations of the same predictors while also including paired interaction terms between density, ADI, and TDI. Age was not included in interactions because we wanted age to represent the underlying developmental process modified by neighborhood density and tree injury. The final models and coefficients are presented in **Table** .

Table 6. Partial version of main text Table 2.2 describing modeled within-crown structures.

Variable	Units	Description
Dependent variables of within-tree structure		
Epicormic appendages	count	Branches arising from vascular cambium, younger than tree at branch height and often attached at acute angles to trunk (Ishii et al. 2002)
Forking	index	Forking score summed at appendage-level, based on notes for branches (forked = 1, highly forked = 2, very highly fored = 3) and structure for attached segments (# of unique distal nodes – 1)
Large appendages	count	Appendages from main trunk > 10, 15, and 20 cm diameter
Clusters	count	≥ 2 appendages from main trunk > 10 cm diameter, within 0.8 m vertical, 0.4 m horizontal, and 45° azimuth
Brooms	count	Appendages with ≥ 3 branches from a common point > 1 m from the trunk (**Figure 3**)
Fans	count	Clusters of ≥ 3 appendages, < 1 m from the trunk, < 5° apart, and within 0.3 m vertical distance
Reiterated trunks	count	Reiterated trunks from main trunk or from appendage
Limbs	count	Appendage giving rise to a reiterated trunk
Mean appendage diameter	cm	Mean diameter of all appendages for each tree
90th quantile appendage diameter	cm	Diameter of 90^{th} quantile diameter for each tree
Independent variables for describing tree development		
Age	years	Intercept of linear model of height and age for aged trunk heights using tree cores
Density	unitless	Linear combination of forest density metrics, scaled from 0–1 (**Table 6)**
Appendage damage index (ADI)	unitless	Sum of damage rating on each appendage, see **Appendix 1** for rating heuristic
Top damage index (TDI)	unitless	Sum of ratio of top break and tree DTB for all observed breaks

Table 7. Coefficient estimates for hurdle models predicting quantities of specific within-crown structures. Standard error is under each estimate in parentheses and an interactions are denoted with a colon. Descriptions of variables are in **Table** .

	Modeled appendage variables							
Variable	>10cm diam.	>15cm diam.	>20cm diam.	Clusters	Brooms	Fans	Limbs	Reiterated trunks
Intercept	1.45E+02	3.98E+00	2.63E+00	7.19E-01	2.02E+00	1.58E-01	1.72E+00	1.33E+00
	1.30E+01	2.42E-01	5.50E-01	5.70E-01	2.00E-01	3.32E-01	1.32E-01	1.40E-01
Age	—	4.19E-03	7.03E-03	4.85E-03	—	—	—	—
	—	6.43E-04	1.37E-03	1.75E-03	—	—	—	—
Density	-1.37E+02	-4.47E+00	-7.02E+00	-1.95E+00	-1.26E+00	—	—	—
	2.21E+01	3.15E-01	8.63E-01	5.03E-01	4.32E-01	—	—	—
TBI	—	-5.83E-01	-9.72E-01	—	—	1.08E+00	—	1.44E+00
	—	1.17E-01	2.39E-01	—	—	3.28E-01	—	1.77E-01
Density:TDI	—	2.00E+00	3.45E+00	—	—	—	—	—
	—	3.20E-01	7.38E-01	—	—	—	—	—
ADI	—	—	—	—	—	—	3.17E-02	4.49E-02
	—	—	—	—	—	—	3.48E-03	3.83E-03
TDI:ADI	—	—	—	—	—	—	—	-2.29E-02
	—	—	—	—	—	—	—	6.23E-03
link function	none	ln	ln	ln	ln	ln	ln	ln
		Logistic binomial hurdle model with logit link						
Intercept	—	-1.84E+00	-1.05E+00	3.68E+00	-5.66E+00	-2.87E+00	-5.95E+00	-1.84E-01
	—	2.37E+00	2.28E+00	1.30E+00	2.19E+00	1.52E+00	2.29E+00	6.59E-01
Age	—	2.83E-02	2.17E-02	—	2.88E-02	1.06E-02	2.52E-02	—
	—	1.16E-02	1.01E-02	—	9.35E-03	5.58E-03	8.75E-03	—
Density	—	-5.08E+00	-6.27E+00	-4.33E+00	—	—	—	—
	—	2.70E+00	2.37E+00	1.87E+00	—	—	—	—
ADI	—	—	—	—	—	—	—	1.48E-01
	—	—	—	—	—	—	—	7.20E-02
N	36	36	36	36	36	36	36	36
R^2	0.52	0.62	0.61	0.37	0.32	0.40	0.39	0.54

Additional height equation

In discussing the conceptual framework for *Picea sitchensis* development, an assertion is made that less-dense neighborhoods lead to lower structure heights. This assertion is based on the models in **Table** . The mean relative height (component height / tree height) of all live and dead mapped components within each tree was predicted based on density and age.

Table 8. Mean relative height of live and dead crown components. These two equations are based on a single model using an interaction between live versus dead and age. $N = 72$ because data included 36 live and 36 dead mean relative heights. $P < 0.001$.

Dependent variable	V1	V2	*a*	*b*	*c*	Form	*N*	R^2
Mean relative height dead	Density	Age	2.64E-01	1.77E-01	7.81E-04	$a + b\,V1 + c\,V2$	72	0.59
Mean relative height live	Density	Age	5.85E-01	1.77E-01	1.09E-04	$a + b\,V1 + c\,V2$		

Model outputs

For interpreting expected sizes and quantities of various tree and within-crown structures with changes in tree age, neighborhood density, and injury, we utilized model predictions. Tabular outputs were used to calculate relative responses such as percentage increase of one variable in response to changes in another. Those for age threshold and diameter changes with density were supplied in main text Tables 9 and 10 so they are not presented here. Tabular outputs were generated for macro-tree characteristics (e.g., crown volume) and within-tree structure quantities (see **Table 6**). Macro-characteristic predictions were produced at 100-year age intervals; 25 % density intervals; and minimum, mean, and maximum ADI and TDI. We did not follow this convention for counts, which utilized a negative exponential function, thus producing unreliable estimates near zero density. For counts, we predicted density at 10, 50, and 90 % of its maximum. Additionally, to interpret interaction terms in models of large appendage quantity (> 15 cm, > 20 cm) and numbers of reiterated trunks (main text Table 6), we produced graphs with the dominant predictor on the x-axis, and the modifying predictor as different line colors (**Figure**).

Macro-characteristics

Table 9. Model predictions of macro-tree characteristics, showing expected response of predicted variables to all combinations of 100-year age and 25 % density combinations. Density = principal component of neighborhood density, CV = crown volume, HIS = horizontal surface index. Note that 400 is 11 years older than our oldest tree (389).

Predictors		Predicted					
Age	Density	CV (m^3)	Total mass (Mg)	HSI > 4 cm	HSI > 10 cm	Crown mass (%)	Tree height (m)
100	0.00	6731	25	0.29	0.04	21.6	56.2

200	0.00	8259	47	0.41	0.12	21.6	67.5
300	0.00	10134	69	0.58	0.22	21.6	75.1
400	0.00	12435	91	0.82	0.35	21.6	81.0
100	0.25	4417	18	0.22	0.02	16.3	57.9
200	0.25	5420	35	0.31	0.07	16.3	69.6
300	0.25	6651	51	0.45	0.13	16.3	77.4
400	0.25	8161	67	0.64	0.21	16.3	83.5
100	0.50	2899	13	0.17	0.01	12.3	59.7
200	0.50	3557	26	0.24	0.04	12.3	71.7
300	0.50	4365	38	0.34	0.08	12.3	79.8
400	0.50	5356	49	0.49	0.13	12.3	86.1
100	0.75	1903	10	0.13	0.00	9.2	61.6
200	0.75	2335	19	0.19	0.02	9.2	73.9
300	0.75	2865	28	0.27	0.05	9.2	82.3
400	0.75	3515	36	0.38	0.08	9.2	88.8
100	1.00	1249	7	0.10	0.00	6.9	63.5
200	1.00	1532	14	0.14	0.01	6.9	76.2
300	1.00	1880	20	0.20	0.02	6.9	84.8
400	1.00	2307	27	0.29	0.04	6.9	91.5

Within-crown structure quantities

Table 10. Predictions from hurdle models of specific appendage quantities from **Table 7**, showing predictions for all possible combinations for minimum, mean, and maximum values of age, density, TDI, and ADI. The density minimum is shown at 0.1 because negative exponential equations produced unrealistic predictions below this point. Note that 400 is 11 years older than our oldest tree (389).

Predictors				Predicted							
Age	Density	TDI	ADI	> 10 cm	> 15 cm	> 20 cm	Clusters	Brooms	Sprays	Limbs	Trunks
100	0.1	0.0	0	131	121	69	4	4	0	0	2
250	0.1	0.0	0	131	121	69	17	20	1	1	2
400	0.1	0.0	0	131	121	69	70	29	1	1	2
100	0.5	0.0	0	77	15	2	1	1	0	0	2
250	0.5	0.0	0	77	15	2	3	4	1	1	2
400	0.5	0.0	0	77	15	2	14	6	1	1	2

100	0.9	0.0	0	22	1	0	0	0	0	0	2
250	0.9	0.0	0	22	1	0	0	1	1	1	2
400	0.9	0.0	0	22	1	0	1	2	1	1	2
100	0.1	0.8	0	131	92	40	4	4	0	0	5
250	0.1	0.8	0	131	92	40	17	20	1	1	5
400	0.1	0.8	0	131	92	40	70	29	2	2	5
100	0.5	0.8	0	77	26	5	1	1	0	0	5
250	0.5	0.8	0	77	26	5	3	4	1	1	5
400	0.5	0.8	0	77	26	5	14	6	2	2	5
100	0.9	0.8	0	22	4	0	0	0	0	0	5
250	0.9	0.8	0	22	4	0	0	1	1	1	5
400	0.9	0.8	0	22	4	0	1	2	2	2	5
100	0.1	1.6	0	131	70	23	4	4	1	1	17
250	0.1	1.6	0	131	70	23	17	20	3	3	17
400	0.1	1.6	0	131	70	23	70	29	5	5	17
100	0.5	1.6	0	77	44	14	1	1	1	1	17
250	0.5	1.6	0	77	44	14	3	4	3	3	17
400	0.5	1.6	0	77	44	14	14	6	5	5	17
100	0.9	1.6	0	22	16	3	0	0	1	1	17
250	0.9	1.6	0	22	16	3	0	1	3	3	17
400	0.9	1.6	0	22	16	3	1	2	5	5	17
100	0.1	0.0	31	131	121	69	4	4	0	0	15
250	0.1	0.0	31	131	121	69	17	20	1	1	15
400	0.1	0.0	31	131	121	69	70	29	1	1	15
100	0.5	0.0	31	77	15	2	1	1	0	0	15
250	0.5	0.0	31	77	15	2	3	4	1	1	15
400	0.5	0.0	31	77	15	2	14	6	1	1	15
100	0.9	0.0	31	22	1	0	0	0	0	0	15
250	0.9	0.0	31	22	1	0	0	1	1	1	15
400	0.9	0.0	31	22	1	0	1	2	1	1	15
100	0.1	0.8	31	131	92	40	4	4	0	0	26
250	0.1	0.8	31	131	92	40	17	20	1	1	26
400	0.1	0.8	31	131	92	40	70	29	2	2	26
100	0.5	0.8	31	77	26	5	1	1	0	0	26
250	0.5	0.8	31	77	26	5	3	4	1	1	26
400	0.5	0.8	31	77	26	5	14	6	2	2	26
100	0.9	0.8	31	22	4	0	0	0	0	0	26
250	0.9	0.8	31	22	4	0	0	1	1	1	26
400	0.9	0.8	31	22	4	0	1	2	2	2	26

100	0.1	1.6	31	131	70	23	4	4	1	1	48
250	0.1	1.6	31	131	70	23	17	20	3	3	48
400	0.1	1.6	31	131	70	23	70	29	5	5	48
100	0.5	1.6	31	77	44	14	1	1	1	1	48
250	0.5	1.6	31	77	44	14	3	4	3	3	48
400	0.5	1.6	31	77	44	14	14	6	5	5	48
100	0.9	1.6	31	22	16	3	0	0	1	1	48
250	0.9	1.6	31	22	16	3	0	1	3	3	48
400	0.9	1.6	31	22	16	3	1	2	5	5	48
100	0.1	0.0	61	131	121	69	4	4	0	0	58
250	0.1	0.0	61	131	121	69	17	20	1	1	58
400	0.1	0.0	61	131	121	69	70	29	1	1	58
100	0.5	0.0	61	77	15	2	1	1	0	0	58
250	0.5	0.0	61	77	15	2	3	4	1	1	58
400	0.5	0.0	61	77	15	2	14	6	1	1	58
100	0.9	0.0	61	22	1	0	0	0	0	0	58
250	0.9	0.0	61	22	1	0	0	1	1	1	58
400	0.9	0.0	61	22	1	0	1	2	1	1	58
100	0.1	0.8	61	131	92	40	4	4	0	0	60
250	0.1	0.8	61	131	92	40	17	20	1	1	60
400	0.1	0.8	61	131	92	40	70	29	2	2	60
100	0.5	0.8	61	77	26	5	1	1	0	0	60
250	0.5	0.8	61	77	26	5	3	4	1	1	60
400	0.5	0.8	61	77	26	5	14	6	2	2	60
100	0.9	0.8	61	22	4	0	0	0	0	0	60
250	0.9	0.8	61	22	4	0	0	1	1	1	60
400	0.9	0.8	61	22	4	0	1	2	2	2	60
100	0.1	1.6	61	131	70	23	4	4	1	1	62
250	0.1	1.6	61	131	70	23	17	20	3	3	62
400	0.1	1.6	61	131	70	23	70	29	5	5	62
100	0.5	1.6	61	77	44	14	1	1	1	1	62
250	0.5	1.6	61	77	44	14	3	4	3	3	62
400	0.5	1.6	61	77	44	14	14	6	5	5	62
100	0.9	1.6	61	22	16	3	0	0	1	1	62
250	0.9	1.6	61	22	16	3	0	1	3	3	62
400	0.9	1.6	61	22	16	3	1	2	5	5	62

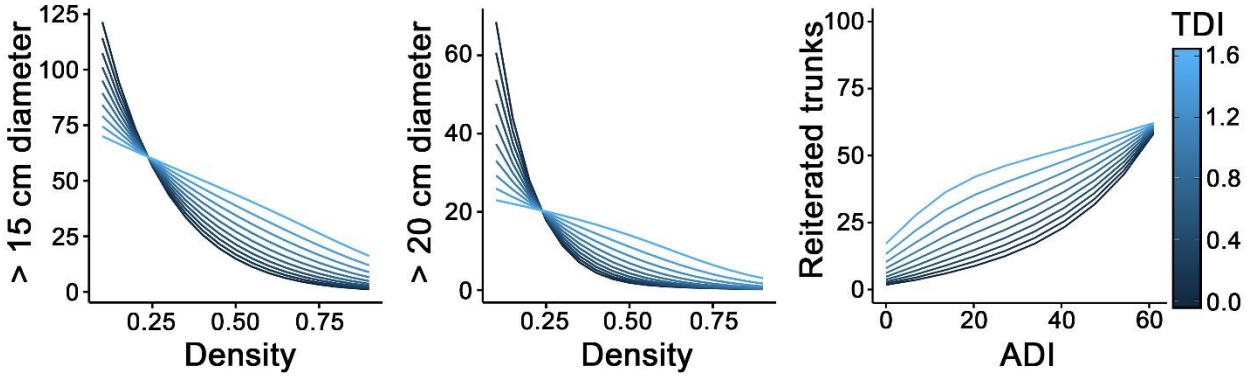

Figure 1. Model predictions for counts of variables, including an interaction term with TDI. Dominant predictor is plotted on x-axis, and modifying predictor is shown in shades of blue.

APPENDIX 2.D

Case study trees

Although we do not explicitly control for neighborhood density changes though time, five case-study trees illustrate possible effects these changes may have (**Figure**). These trees allow us to approximate how unusually large injuries or changes in neighborhood density alter the expression of crown structure. During plot installation, any recently fallen trees in the plot were mapped by location and diameter, and notes on presence of logs and suspected developmental history were recorded. Here we interpret the presence of large logs within plots as evidence of denser past conditions and presence of young but large competing trees with model-conforming crown structure as evidence of ingrowth.

The first tree (**Figure a**) is in a dense neighborhood that has always been dense and at one time had a co-dominant top. One top collapsed as evidenced by a large decayed wound at the junction with the remaining top just above 40 m and a lack of branches in the direction of the fallen trunk. The second (**Figure b**) is in a previously-dense neighborhood that had some nearby large trees blow down. The third (**Figure c**) is next to a swamp close to a few large old stumps and a cohort of rapidly growing young-but-large trees on a fallen log. It is also extensively damaged with a broken top and many injured appendages weeping pitch. The fourth (**Figure d**) is in an open neighborhood with no evidence of denser conditions. It exhibits a past break at 15 m that is 63% as large as its DTB. Based on the oldest trunk age (254 years) at 25 m and the average time to grow from 15 to 25 m computed from the 55-tree dataset (15 years), this break happened when the tree was only 34 years old. The last tree (**Figure e**) is the oldest in the dataset but ranks 9 out of 36 in total mass and now overtops a young forest of *A. rubra*. It was once a subordinate tree next to a large neighbor that collapsed, severely damaging but not killing it. Of the three prominent reiterated trunks, the lowest is 36 years old, 39.4 cm diameter, and 19.0 m tall; the middle is 59 years old, 39.5 cm diameter, and 19.2 m tall; and the continuation of the main trunk is 170 years old, 90.3 cm diameter, and 29.3 m tall.

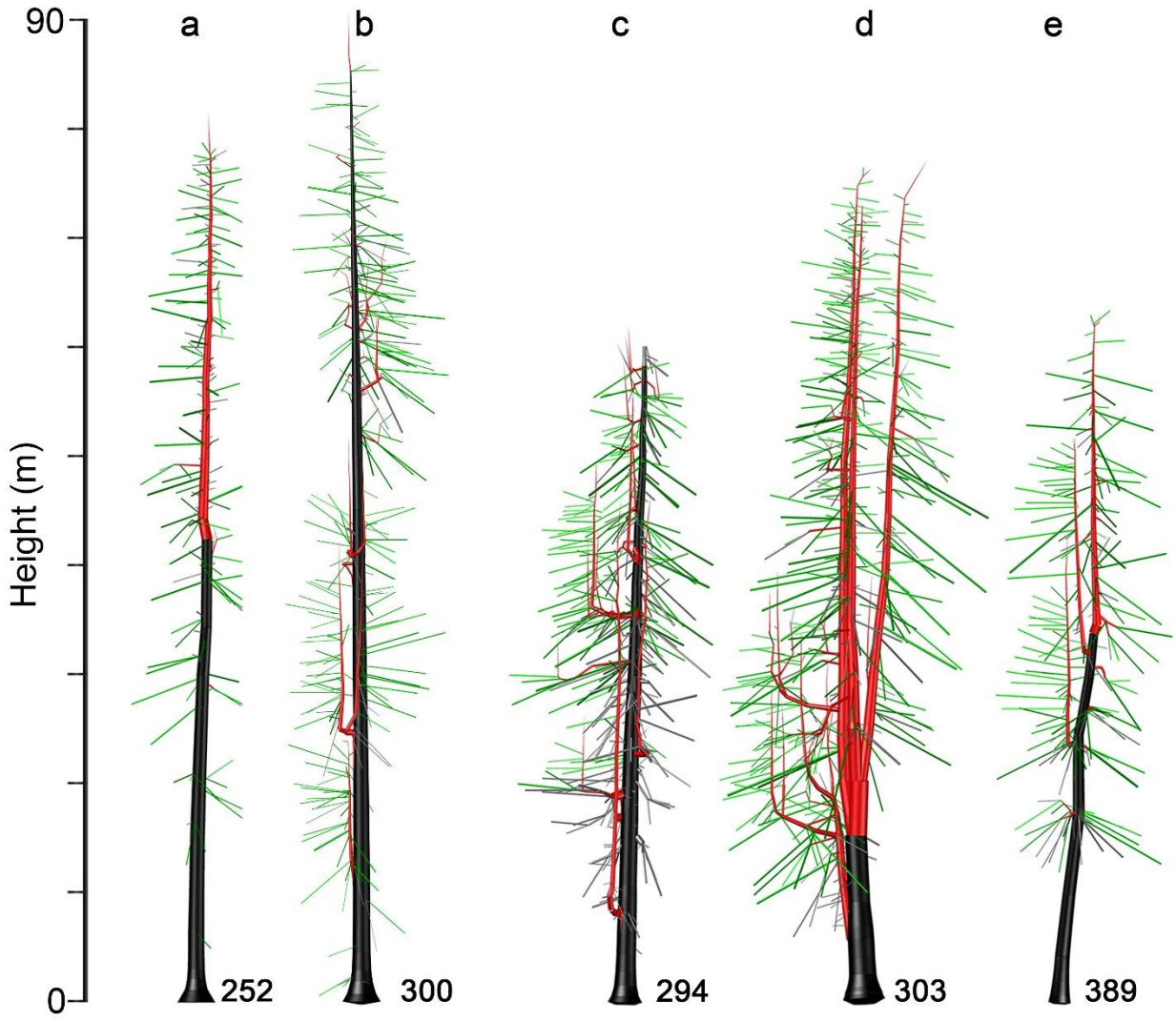

Figure 1. Five trees demonstrating crown characteristics due to large injuries and changes in neighborhood density. Within a relatively small age range (~140 years) these trees exhibit a wide range of structure. Tree ages are estimated from increment cores at multiple heights and displayed at the base of each tree. Black = main trunk, red = segmented appendages including reiterated trunks, green = model-conforming branches, gray = dead.

Considering each tree's unique structure and plot-based evidence of disturbance suggests that neighborhood conditions following injury have important consequences for crown development. Tree **a**, which stands in a dense neighborhood, was unable to respond vigorously to injury and retains a high-narrow crown. Tree **b** responded dramatically to a change in neighborhood density, because nearly all appendages below 50 m are epicormic and extend

nearly to the ground, but this response was recent because the epicormic crown is relatively narrow. Tree **c** is small for its age, possibly reflecting saturated soils on the edge of a swamp and recovery from repeated injuries. Because it stands in the open, trunk breakage and appendage damage allowed > 8 limb-trunk appendage complexes > 30 cm diameter to form. After breaking at 34 years, tree **d** recovered in full sun, producing an 81-cm-diameter limb-trunk complex at 6 m and three trunks > 1 m diameter above the break. In contrast to tree **a,** the response to severe injury in tree **d** was not dominated by treetop replacement and height growth or limited by shade from neighboring trees, allowing the crown to maintain low structure. Tree **e**, despite being nearly 400 years old, responded rapidly to injury and neighborhood density reduction. Nearly all its appendages are epicormic, and diameters and heights of the two younger reiterated trunks are increasing by an average of 1 cm yr^{-1} and 43 cm yr^{-1}, respectively. Note the large fan near the crown base of tree **e**, which is likely on its way to becoming an especially complex tree.

These trees suggest an additional layer of complexity added by the interaction between changing neighborhood density and severity of injury. This interaction creates trees of an even wider range in structural characteristics than the conceptual model would account for. For example, the creation of very complex narrow and wide trees (tree **b** and **d**) as well as complex small trees (tree **e**). Tree **b** probably could not have produced so much lower crown structure had some of its closest neighbors not fallen. Likewise, tree **d** could not have sustained such a severe top snap at 15 m had it not been unencumbered during its recovery. Trees **c** and **e** are near opposites where both were heavily injured but tree **c** has rapidly growing neighbors killing its lowest appendages, while close neighbors of tree **e** have fallen, allowing rapid growth of its relatively recent reiterations.

APPENDIX 3.A

Supporting Analyses

Random Forests discriminate analysis

Although forest structure differences between geomorphic positions on the landscape were apparent to the human eye, they were not so easy to distinguish using LiDAR-based summary metrics. A Random Forests discriminate analysis was performed to predict geomorphic classifications (i.e. valley flats and terraces, Southwest slopes, and remaining upland area) for two reasons. First, to determine which classes were more similar to each other and which were distinct, and second, to determine which metrics were most useful for making geomorphic distinctions. The best metrics were then used in future analyses described in the main text.

The set of metrics outlined in **Table 1** were chosen based on classification effectiveness in past research (Kane et al., 2010) as well as visual inspection in ArcMap 10.3 (ESRI, 2014) that appeared to differentiate between landscape contexts. Each metric was represented by a 30 x 30 m resolution raster image, which was uploaded into the statistical program R (R Core Team, 2018) to create a matrix of numbers that could be easily manipulated. To avoid oversampling large areas relative to smaller areas (e.g. upslope classification vs terraces), the number of cells in the smallest class (N = 1,429) was randomly divided into thirds. The first third was saved as a validation data set and the remainder was used for training the Random Forests model. Random Forests was run on the training data using 400 regression trees and 4 variables for each with the randomForest package in R (Breiman, 2001).

Table 1. All LiDAR-derived summary metrics of forest structure computed at 30 x 30-m-pixel resolution. Refer to main text Table 3 or (North et al., 2017) for definition of tree approximate object (TAO).

Variable	Unit	Description
Mean return height	m	Mean of all return heights
Cover above 3 m	%	Returns above 3 m / total returns * 100
Cover above mean return	%	Returns above mean height / total returns * 100
Basal area	m^2 ha^{-1}	Diameter above buttress predicted from tree height (see text) and used to summarize tree basal area.
Basal area of tall trees	m^2 ha^{-1}	Same as basal area but only includes trees > 55 m
95th percentile height	m	95th percentile return height
Return height deviation	m	$\sum_i^N \left(\lvert Y_i - \bar{Y} \rvert\right)/N$, where Y = return height
Percent canopy 5 – 9 m	%	Percent of TAO area associated with high points 5 – 10 m tall within a 30-m cell
Percent canopy 10 – 30m	%	Percent of TAO area associated with high points 10 – 30 m tall within a 30-m cell
Canopy relief ratio	—	(mean return – min return) / (max return – min return)
Percent canopy in single trees	%	Percent of total TAO area associated with isolated TAOs
Percent canopy in single trees > 55 m tall	%	Same as above but only for tall trees
Percent canopy in clumps of 5 – 9 trees	%	Clumps distinguished based on whether or not TAOs touch, then calculated as total clump area/total TAO area of all trees
Percent canopy in clumps of > 30 trees	%	Same as above but only clumps with > 30 trees area considered for numerator
Percent gap at 30 m	%	(Land area – Area of 30 m TAOs)/(Land area)
TAO per hectare	# ha^{-1}	Number of TAOs per hectare
Tall TAO per hectare	# ha^{-1}	Number of > 55-m-tall TAOs per hectare
Total canopy area at 30 m	m^2	Summed area of all 30-m-tall TAOs

Within-class error of the Random Forest model was similar between the training and validation data, so they were pooled and the model refit with all data. The model was not accurate predicting geomorphic class with an error rate of 49.1 %, but close examination the resulting confusion matrix (**Table 2**) was useful for determining which areas were more structurally related to each other than others. Valley flats were most commonly confused with terraces and valley terraces with flats (53 and 68 % respectively). Valley flats were also frequently (36 %) confused with Jackson Creek, itself a valley flat, but one dominated by *Pseudotsuga menziesii* rather than *Picea sitchensis*. Jackson Creek was the most-well classified with an error rate of only 28 %, but was confused with valley flats and terraces ~25 % of the time. Likewise, southwest aspects and upland were more frequently confused with each other (49 – 56 %) than with other classes (maximum of 14–33 % with valley terraces). The main conclusions of this analysis are that valley positions are more structurally related to each other in terms of LiDAR metrics (**Table 1**) than to upslope classes (i.e. southwest and upland), while terraces are somewhat of intermediate between the forest types, likely playing the role of an ecotone. Lastly, important variables identified by ranking them with two common metrics (Archer and Kimes, 2008) and the eight variables common among the top ten were retained for future analysis (**Table 3**).

Table 2. Confusion matrix from model based on random sample of raster cells (N = 1,429 per geomorphic class). A training model is fit to 2/3 of the sample and validated against the remaining 1/3, and the class error is shown for comparison (Validation error). Diagonal cells in gray represent correct predictions, cells to the upper right of diagonal are errors of commission, and to the lower left are errors of omission. Error for predicting data not used for each permutation of the random forest algorithm (out-of-bag error) is 49.09%.

	Cells predicted						
Cells observed	Valley flats	Valley terraces	Jackson creek	SW aspects	Upslope	Class error	Validation error
Valley flat	743	323	249	28	86	0.48	0.50
Valley terrace	398	476	245	117	193	0.67	0.70
Jackson Creek	271	118	1008	13	19	0.29	0.28
Southwest slope	44	152	45	855	333	0.40	0.37
Upland	157	195	69	422	586	0.59	0.59

Table 3. Eight variables common to top ten metrics using two measures of variable importance in discriminate analysis of geomorphic class (main text Table 3). Variables are sorted in decreasing order of mean accuracy decrease, which measures the difference in error of each random regression tree when prediction data not used to create it do not include each variable. Gini coefficient is the decrease in node impurity from splitting the tree at that variable (Archer and Kimes, 2008).

Variable	Units	Mean accuracy decrease	Mean decrease gini
Cover above 3 m	m	78.9	697.9
95th percentile return	m	57.9	506.1
Return height deviation	m	45.8	467.7
Cover above mean return	%	43.6	421.2
Basal area of tall trees	$m^2\ ha^{-1}$	41.0	223.0
Basal area per ha	$m^2\ ha^{-1}$	32.5	312.0
Average return height	m	32.4	319.1
Percent canopy 10-30 m	%	32.2	325.7

Principal components analysis for hierarchical clustering

The Random Forests algorithm was not good at prediction geomorphic class based on aggregate metrics of structure alone, so another approach was employed to better describe forest structure. To better assess the spatial heterogeneity in forest structure we needed a way to aggregate patches of similar forest and summarize the patterns of patchiness in each geomorphic context. A principal components analysis (PCA) was performed on the variables in **Table 3** and the Ward's distance (Murtagh and Legendre, 2014) was computed for each principal component. These distances were then used in a hierarchical clustering analysis to create 4 structural classes at 30-m resolution. This analysis is described in the main text, here we present steps taken to insure the assumptions of PCA were met (**Table 4**). These included transforming the input variables to minimize skew and kurtosis and to linearize them with respect to each other. All variables were centered by subtracting the mean and scaled by dividing by the standard deviation prior to PCA to eliminate effect of variable magnitude on the results.

Table 4. Variables are transformed to reduce skew and kurtosis, and to increases linearity between them before principal components analysis.

Metric	Skewness	Kurtosis	Transformation
Cover above 3 m	-0.83	1.12	asin(sqrt(x))
95th percentile return	0.28	-0.09	—
Return height deviation	0.66	0.31	—
Cover above mean return	-0.32	0.61	—
Basal area of tall trees	1.05	0.71	sqrt(x)
Basal area per ha	0.37	0.74	sqrt(x)
Average return height	0.28	0.37	—
Percent canopy 10-30 m	1.19	1.86	asin(sqrt(x))

Crown structure scaling

To scale crown structure from trees to forests, linear model in main text Table 5 were applied to each tree high point from the LiDAR data to predict the mean and 95 % confidence interval. The amount and uncertainty in crown structure was then taken as the mean for each of these values for all trees in each geomorphic class. In making claims about the magnitude of crown structure differences, references are made to precise numbers. These numbers are summarized below in **Table 5** below.

Table 5. Summarization of crown structure in different geomorphic classes underlying Figure 7 of the main text and references to specific values in the results and discussion. Diam90 = 90th percentile diameter, HSA = horizontal surface area (main text Table 2), HSI = Horizontal surface index (HSA in ha / land area in ha * 100), TPH = TOAs per ha > 55-m tall.

Geomorphic class	Structure class	Mean diam90	Lower diam90	Upper diam90	Mean HSA tree^{-1}	Lower HSA tree^{-1}	Upper HSA tree^{-1}	Mean HSI	Lower HSI	Upper HSI	TPH
Valley bottom	Gap	11.7	8.5	15.0	11.7	7.6	18.6	0.0	0.0	0.0	0.0
Valley bottom	MedOpen	12.9	10.2	15.7	24.3	17.3	34.6	2.9	2.1	4.1	2.4
Valley bottom	MedDense	11.8	8.6	15.0	19.1	13.2	28.1	4.7	3.2	6.9	4.9
Valley bottom	Tall	11.3	8.1	14.6	16.9	11.9	24.6	8.7	6.1	12.6	10.2
Valley bottom	Total	12.2	9.1	15.2	20.7	14.6	29.8	3.6	2.5	5.2	3.5
Southewest slope	Gap	26.1	21.8	30.4	18.2	9.9	34.1	0.2	0.1	0.3	0.2
Southewest slope	MedOpen	17.0	13.5	20.6	15.6	10.7	23.4	2.7	1.8	4.0	3.4
Southewest slope	MedDense	12.0	7.9	16.5	11.7	7.8	17.8	5.6	3.8	8.6	9.7
Southewest slope	Tall	6.8	3.4	12.5	8.0	5.2	12.7	12.9	8.4	20.5	32.3
Southewest slope	Total	9.5	5.8	14.6	9.9	6.6	15.4	6.4	4.2	9.9	12.9
Upland	Gap	19.4	16.1	22.8	11.4	7.2	18.5	0.1	0.0	0.1	0.1
Upland	MedOpen	16.3	12.8	19.9	15.5	10.7	22.8	3.1	2.2	4.6	4.0
Upland	MedDense	12.7	8.5	17.0	12.6	8.6	19.0	6.6	4.5	9.9	10.5
Upland	Tall	9.4	5.2	14.7	11.4	7.6	17.5	10.8	7.2	16.6	19.0
Upland	Total	12.4	8.3	16.8	12.8	8.7	19.2	5.6	3.8	8.4	8.8
Jackson Creek	Gap	0.0	0.0	0.0	0.0	0.0	0.0	0.0	0.0	0.0	0.0
Jackson Creek	MedOpen	18.3	14.6	22.1	20.5	14.9	28.8	3.9	2.8	5.4	3.8
Jackson Creek	MedDense	15.3	11.5	19.3	18.9	13.5	26.8	5.8	4.1	8.2	6.1
Jackson Creek	Tall	12.3	8.0	17.0	13.9	9.6	20.4	7.3	5.1	10.8	10.6
Jackson Creek	Total	14.1	10.0	18.5	15.9	11.3	23.0	5.4	3.8	7.7	6.7

References

Archer, K.J., Kimes, R. V, 2008. Empirical characterization of random forest variable importance measures. Comput. Stat. Data Anal. 52, 2249–2260. doi:10.1016/j.csda.2007.08.015

Breiman, L., 2001. Random Forests. Mach. Learn. 5–32. doi:10.1023/A:1010933404324

ESRI, 2014. ArcMap Desktop: Release 10.3.

Kane, V.R., McGaughey, R.J., Bakker, J.D., Gersonde, R.F., Lutz, J. a., Franklin, J.F., 2010. Comparisons between field- and LiDAR-based measures of stand structural complexity. Can. J. For. Res. 40, 761–773. doi:10.1139/X10-024

Murtagh, F., Legendre, P., 2014. Ward's hierarchical agglomerative clustering method: Which algorithms implement Ward's Criterion? J. Classif. 31, 274–295. doi:10.1007/s00357-

North, M.P., Kane, J.T., Kane, V.R., Asner, G.P., Berigan, W., Churchill, D.J., Conway, S., Gutiérrez, R.J., Jeronimo, S., Keane, J., Koltunov, A., Mark, T., Moskal, M., Munton, T., Peery, Z., Ramirez, C., Sollmann, R., White, A., Whitmore, S., 2017. Cover of tall trees best predicts California spotted owl habitat. For. Ecol. Manage. 405, 166–178. doi:10.1016/j.foreco.2017.09.019

R Core Team, 2019. R: A language and environment for statistical computing. R Foundation for Statistical Computing, Vienna, Austria. https://www.R-project.org/.

VITAE

Russell Kramer grew up in the central sierra foothills where his love of nature was inspired by the giant sequoias of Calaveras Big Trees State Park and abundant wilderness surrounding the Stanislaus River of his backyard. He first climbed into the conifer canopy as a student at Humboldt State University where he later earned his Masters Degree studying redwood canopy ecology. Since then he has traveled to Japan and Tasmania to study large trees. His PhD took him into the old-growth wilderness of the western Olympic Peninsula for 8 months of field work where he gained intimate knowledge of Sitka spruce dominated forests. Future plans include systematic study of Earths largest trees wherever they reside and a transition to studying reciprocal effects of riparian and forest ecosystems.